The Electrochemical Characterisation of Indole Based Conducting Polymers

Mark Thomas Robertson

Presented for the degree of Doctor of Philosophy

University of Edinburgh

1998

"Rabbit's clever," said Pooh thoughtfully.

"Yes," said Piglet, "Rabbit's clever."

"And he has Brain."

"Yes," said Piglet, "Rabbit has Brain."

There was a long silence.

"I suppose," said Pooh, "that that's why he never understands anything."

- A.A. Milne

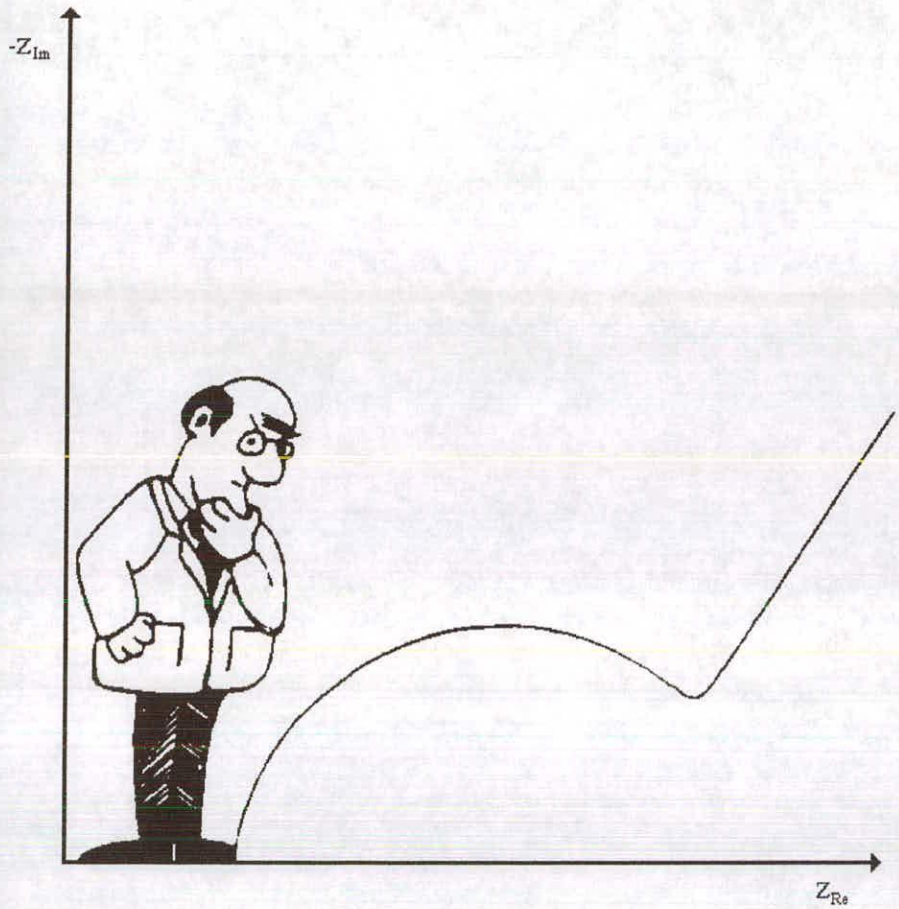
$-Z_{Im}$
Z_{Re}

For Mum and Dad

Declaration

I hereby declare that the work presented in this thesis is my own unless otherwise stated by reference

Mark Thomas Robertson

September 1998

Abstract

Conducting polymers based on heterocyclic organic systems have found a wide and varied number of applications from fast pH sensors to stealth coatings and drub delivery systems. What is surprising, however, is that very little is known about the actual mechanism by which electrical conduction through these systems occurs.

Ac impedance spectroscopy was used along with cyclic voltammetry and rotating disc electrode techniques, to electrochemically characterise polymers formed from indole-5-carboxylic acid (I5CA), 5-cyanoindole (5CI) and copolymer formed from a combination of the two. Physical parameters were obtained from the ac spectra by mathematically modelling the results to a novel transmission line developed during the course of the thesis.

Investigations of poly(I5CA) have shown that the polymer film undergoes substantial morphological changes on extensive cycling over the course of a number of weeks. It has been found that, on electropolymerisation, the polymer is deposited in compact trimer stacks with extensive π delocalisation occurring between the trimer units. This allows the polymer metallic like conduction with fast electron transfer between the polymer/electrolyte interface and the electrode/polymer interface. A kinetic barrier to cation insertion into the film is observed at relatively high potentials. It has been found that there is very little solvent/electrolyte in the film initially. On extensive cycling the coat is found to become less compact allowing the entry of solvent and electrolyte. This opening of the polymer film has the effect of buckling the trimer stacks and removing the π delocalisation. Instead of fast

electron transfer, the coat is observed to now conduct via a redox hopping mechanism with a large kinetic barrier at the electrode/polymer interface. At potentials away from the trimer E°, this kinetic barrier is the rate determining step for conduction in the polymer. However, near E° the cation insertion process once more becomes dominant though it is found that this barrier is independent of potential and electrolyte concentration (except at very low concentrations) indicating that the coat has become more solvated.

Polymer films formed from 5-cyanoindole are not observed to exhibit a gross morphological change on extensive cycling and instead remain in a compact, highly conducting, form similar to that of an uncycled poly(I5CA) coat. Studies have shown that in this compact form, only a small percentage of the film is available for redox activity. Such films are observed to have a strong anion dependence with the nature of the anion (i.e. shape) being an important factor.

Copolymer films formed from I5CA and 5CI show the behaviour of both monomer parents. CV and ac impedance data show the films to be cation influenced at low potentials and anion influenced at high potentials. The I5CA groups allow the film to become more open on cycling while the 5CI units seem to allow for the insertion of large organic cations. Changes in the pH response for different copolymer coat compositions can be correlated to the level if I5CA within the film.

The ac results for these very different films were found to fit well to the new transmission line model and the values and trends obtained showed good agreement with results from other techniques over a varied range of conditions. This proves the usefulness and power of the theory used.

Acknowledgements

This thesis could not have been accomplished without the help of certain people who provided me with the necessary guidance and friendship which kept me going through my years of study. I would like to express my profound gratitude and thanks to the following people:

Dr Andrew R Mount, my supervisor, for his excellent guidance and his infectious enthusiasm which helped me get through the long days and, in some cases, the even longer nights.

Dr Anita C. Jones, my second supervisor, for her support even though she hardly ever saw me and was never quite sure what I was still doing in the lab in the middle of the night.

Dr J. Gordon Mackintosh for showing me the ropes when I first started and encouraging me when nothing worked and Dr Alastair D. Thomson for continuing the work when Gordon graduated.

Peter Jennings and Lorna Kettle for their help with various aspects of this project as well as for valuable discussions.

The University of Edinburgh for funding this PhD.

Everyone at St Cuthbert's Company, St. Andrews Ambulance Corps for their friendship and for letting me watch the rugby for free.

Everyone at BBD Scotland for providing me with something/someone to hit when things didn't go according to plan.

My thanks also go to Kirsten Thomson for giving me her friendship and love when I needed it most.

Thanks also go to all the people I've had the good fortune to meet in my 8 years at Edinburgh University. Its been fun!

Conferences and Meetings

Butler Meeting '95, University of Strathclyde 1995

Butler Meeting '96, University of Edinburgh 1996

Electrochem '96, University of Bath, 1996

Butler Meeting '97, Caledonia University 1997

Butler Meeting '98, University of Newcastle, 1998

Firbush Physical Readings 1995-1998-09-27

Postgraduate Courses and Lectures

1. Physical colloquia
2. Electrochemical Analysis
3. Introduction to Patents
4. I.R. Spectroscopy
5. Computers in Chemistry
6. Modern Aspects of Electrochemistry
7. Non-Linear Optics
8. Introduction to C Programming
9. CV Writing Workshop

Contents

1. Introduction

Since their discovery in the first half of this century, polymeric material (matter composed of regularly repeating units known as monomers) has been the focus of gradually increasing level of study. In general, polymers can be categorised into one of two main groups[a]: natural (including such complex molecules as proteins and polysaccharides) and synthetic (usually simpler molecules with an organic or inorganic basis).

1.1. Conducting Polymers

1.1.1. Background

The observation that some synthetic polymers were able to carry a current when chemically or electrochemically oxidised has given rise to a great deal of interest in the past 30 years. The phenomenon was first observed in the inorganic polymer poly(sulphur nitride), $(SN)_x$, in the early 1970s[1]. This discovery caused a great deal of excitement with many groups looking to exploit this in, for example, the construction of molecular wires. However, even though it was later found that this

[a] *A third group exists known as elastomers which forms a sub-group of the other two.*

particular polymer is superconducting below 0.3K[2], the depth of study was limited due to the lack of any redox chemistry as well as the molecules' resistance to any form of functionalisation.

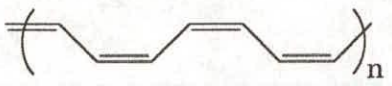

Figure 1.1: Structure of *cis*-Polyacetylene

In the later half of the decade, it was discovered that a polymer formed from the more reactive acetylene, poly(acetylene) (figure 1.1) changed from being electrically insulating to electrically conducting (a change in the conductivity of approximately 10^7-10^{10}) when oxidised by I_2 and other halogens[3]. Similar effects have also been seen while investigating systems which, like acetylene, have alternating single and double bonds such as heterocycles and benzoidal molecules. The chemistry of these molecules can easily be altered by the attachment of different functional groups. This gives rise to a wide variety of chemical and physical properties and has meant that the level of research into such organic conducting polymers has increased considerably over the past quarter of a century.

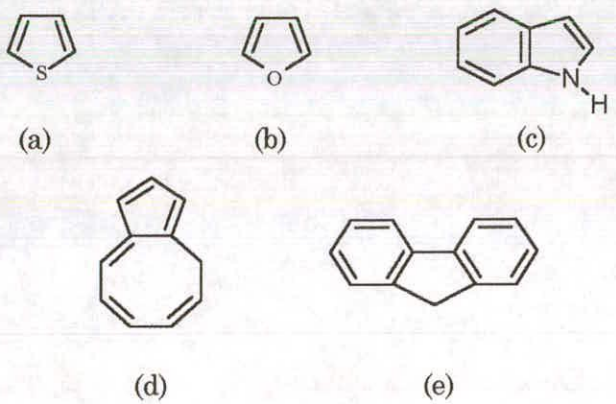

Figure 1.2: Monomers of conducting polymers with a similar structure to acetylene. (a) thiophene, (b) furan, (c) indole, (d) azulene, (e) fluorene

Research specifically into polymers formed from heterocyclics like thiophene - figure 1.2a - furan - figure 1.2b - and indole - figure 1.2c - and cyclic benzoidal molecules such as azulene - figure 1.2d - and fluorene - figure 1.2e - is of special interest since it is relatively easy to functionalise these systems by attaching different groups to the ring (by substitution). Such systems exhibit a large degree of delocalisation of π electrons over an extensive conjugated polymer system, enabling the material, in its most conducting form, to behave in a manner similar to a metal.

Research into such polymers first began around 1979 when it was reported by Diaz et al that the heterocyclic molecule pyrrole (figure 1.3) could, in the presence of a background electrolyte, be oxidised at the surface of a platinum electrode to produce a conducting poly(pyrrole) film[4] - figure 1.4 - (it can be seen that polypyrrole has a similar conjugated structure to cis-polyacetylene shown above).

Figure 1.3: Pyrrole

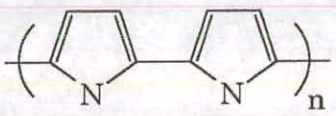

Figure 1.4: Structure of Polypyrrole

Since this discovery, electrochemical oxidation has become one of the main methods of preparation of organic conducting polymers from a wide range of monomeric material.

1.1.2. Preparation

Two main synthetic routes exist for the preparation of organic conducting polymers: chemical and electrochemical. Both methods involve the oxidation of the monomer species, producing a radical cation intermediate which can then go on to join with other nearby radicals resulting in chain growth. The only real difference is the method of radical generation.

1.1.2.1 Chemical Polymerisation

In chemical polymerisation this oxidation is accomplished using a strong chemical oxidising agent such as $FeCl_3$ or $CuCl_2$ or by exposing the monomer to various catalysts[5]. This process is often referred to as doping. However, unlike the doping of semi-conductor systems by replacement of atoms within the fixed lattice structure of a semi-conductor framework, this doping an example of a redox process where the oxidising agent removes electrons from the monomer, creating a dopant counteranion in the process. However, control over polymer growth and morphology is limited using this method (it will be shown in this thesis that polymer morphology is an important factor in the conductive properties of such molecules). It has also been found that a number of chemically polymerised materials such as polyacetylene exhibit a degree of air and moisture sensitivity resulting in a long term decrease in conductivity and therefore usefulness.

1.1.2.2 Electrochemical Polymerisation

Electropolymerisation of a conducting polymer takes place from a solution of the monomer in a suitable solvent (where the oxidation of the monomer is within the solvent limit) containing a background electrolyte in suitable excess to prevent the current passed to limit the process. The actual electropolymerisation mechanism is though to take place via a radical cation intermediate by a series of electrochemical (E) and chemical (C) steps[6,7,8] and is often referred to as an $E(CE)_n$ process. A representation of such a process is shown in figure 1.5 for the case of a general heterocycle.

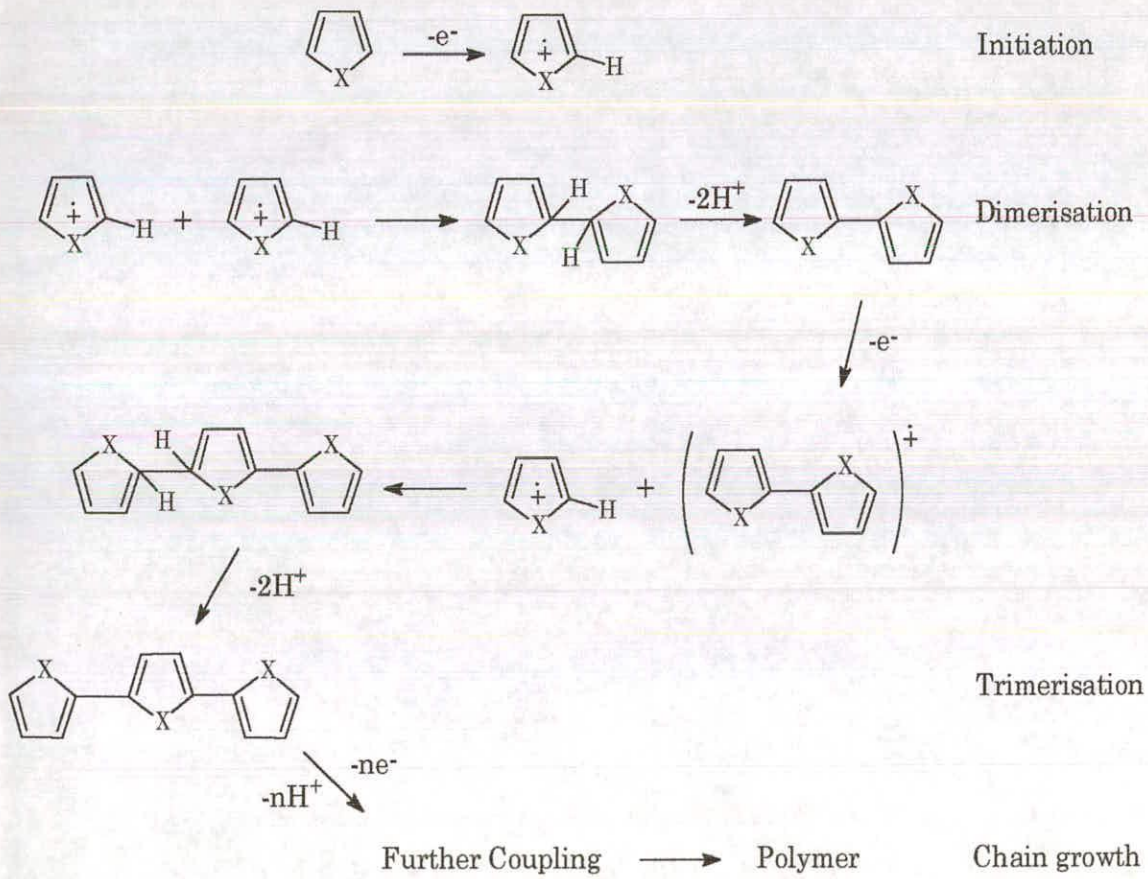

Figure 1.5: Polymerisation mechanism for a general heterocyclic monomer

Assuming that the electron transfer reaction is faster than the diffusion of the monomer from the bulk solution then a high concentration $[R^{+\bullet}]_{surface}$ of radicals is formed and maintained at the electrode surface. Once formed, the radical cations can follow one of several reaction pathways:

1. if the radical is stable then it can be transported (either by diffusion or convection) away from the electrode into the bulk solution where it can react to form a soluble species. Here,

$$\text{rate} \propto k_{MT}\left[R^{+\bullet}\right]_{surface}$$

where k_{MT} is the mass transfer rate constant.

2. if the radical is very unstable, it can react with the solvent molecules or the anions in the electrolyte to produce a soluble species. Here,

$$\text{rate} \propto k_{2}\left[R^{+\bullet}\right]_{surface}$$

3. if neither of these processes occur in a suitably fast timescale then the radicals can couple to give a dimer species where

$$\text{rate} \propto k_{3}\left[R^{+\bullet}\right]^{2}_{surface}$$

These dimers can then undergo further oxidation/radical coupling to give an insoluble polymer film which is deposited onto the surface of the electrode.

In general these processes compete for dominance. It is possible to introduce some selectivity into which of the three post-oxidation routes are followed by careful choice of substituent group and location. It is also possible to impart a 'pseudo-stability' to the radicals, and so favour the

third process above by increasing the radical concentration (by either increasing the concentration of the plating solution used or by increasing the polymerisation current) or by decreasing the value of k_{MT} (for example, by using a stagnant solution) thereby increasing the chance of film formation.

On electrodeposition, the polymer film is oxidised and to preserve electroneutrality a counterion from the bulk electrolyte must be included in the polymer matrix. The means that two mechanisms exist by which charge may be carried through the coat: either via the π electron system of the polymer backbone or via the movement of anions in the resulting pores in the film. This means that the choice of background electrolyte will have a pronounced effect on the polymer conductivity (this will be discussed in more detail in later chapters).

Polymerisation via electrochemical oxidation of the monomer has a number over advantages of chemical oxidation. These include increased control - the size of the polymer chains can easily be controlled by altering such parameters as monomer concentration and polymerisation time - and chemical specificity with a narrower spread in oligomer size and less chance of any side reactions. Electropolymerisation is also chemically easier without the need for extreme conditions or catalysts which are sometimes required for chemical polymerisation.

1.1.3 Applications

Organic based conducting polymers have a wide range of applications. Perhaps the most extensively researched is the use of conducting polymers to modify the surfaces of electrodes in order to increase reaction kinetics or electrode specificity. It is possible, for example, to introduce a

high degree of specificity into a conducting polymer by judicious choice of the functional groups present. Organic polymers, as mentioned previously, are very useful in this context due to the ease by which their functionality may be altered. In general, two routes exist towards this functionalisation; either before or after polymerisation has taken place. Both methods are chemically viable. However, in practice, the former route is used since the conditions necessary for substitution are sometimes too severe for the polymeric material, causing degradation before any work can be carried out[9]. Substitution before polymerisation also guarantees complete functionalisation whereas substitution afterwards does not. Such polymer modification enables the electrodes to act as a selective mediator to electron transfer between redox species in solution and the electrode surface. It can also, in some cases, allow certain electron transfer processes to occur which would be kinetically unfeasible at the bare, unmodified electrode. Polymer modified electrodes have found uses as biosensors[10] which use a chemical mediator, usually an enzyme, to facilitate electron transfer between the solution (and hence the analyte in question) and the modified electrode. A general schematic of this process is shown in figure 1.6. Probably one of the most important examples within this field is the use of a pyrrole-modified electrode as a glucose detector[11,12,13], enabling those suffering from *diabetes mellitus* to obtain fast and accurate measurements of their blood/glucose levels (something which they had been unable to do previously unless in a medical environment). Pyrrole is used here since polypyrrole can easily be produced in aqueous solutions of neutral pH. In a more chemical based application, modified electrodes have been used to acquire onsite information as to the concentration of heavy metals and other environmental pollutants in rivers and soils without the need for time consuming laboratory based analysis[14].

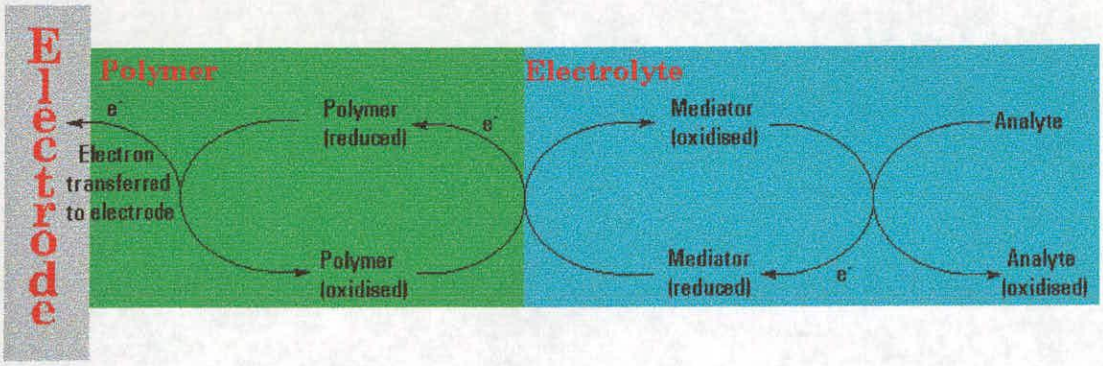

Figure 1.6: Electron transfer process for a bio-sensor based on a polymer modified electrode

As well as providing functionality by substitution onto the polymer molecule, it is also possible to obtain selectivity by incorporating known complexing agents into the polymer matrix as 'counterions'. For example, a range of sulphonated dyes, some of which are shown in figure 1.7, have been included in the polymer film to act as metal complexing agents and so develop new sensor strategies for metal ions such as copper[15] and aluminium[16]. Using such systems in combination with microelectrodes, sensitivities in the micromolar range have been obtained for copper and in the parts per billion range for aluminium. Similar dyes have also been found to undergo selective interactions with proteins and have been used in their detection in the low nanomolar range[17].

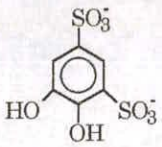

(a)

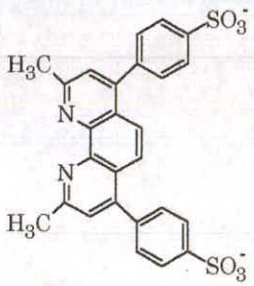

(b)

Figure 1.7: Examples of Sulphonated Dyes Incorporated into Conducting Polymers for Metal Sensing
(a) Tiron, (b) Bathocuproine disulphonate

As well as detecting redox species present in solution, polymer modified electrodes can also be used to sense gas phase species. It has been observed that the resistivity of polypyrrole exhibits a reversible increase when exposed to ammonia gas, hydrogen sulphide and many other organic vapours , the degree by which the conductivity changes being dependent on the concentration of gas present[18]. This application has found commercial applications in the brewing industries where an array of 12 polymers have been used to detect the presence of some of the 100+ different volatile products of the brewing process without being affected by common gases such as N_2. By comparing the data from these with those taken from an accepted brew it is possible to obtain a definite time at which to stop the brewing without the need to use time consuming and expensive processed such as gas chromatography - mass spectroscopy (GC-MS). Although such "electronic noses" are now a commercial reality - for example the 'Aromascan' system (Aromascan plc, UK) comprising of a polymer array along with the necessary pattern-recognition software - they cannot as yet remove the need of the human nose.

A number of organic conducting polymers exhibit a phenomenon known as electrochromism where the colour of the polymer shows a dependence on the oxidation level of the coat. In general (as will be discussed later), conducting polymers are dark when in there conducting oxidised state and become lighter in colour as they are reduced. Many polymers only show a small degree of electrochromism such as poly(indole-5-carboxylic acid) which changes colour from black to dark green. Others however are more striking - for example, polythiophene polymerised in the presence of BF_4^- undergoes a dramatic colour change during its redox switching from yellow to black[19]. The degree by which the colour changes is dependent upon the particular heterocycle/benzoidal system[20] (and, to a slight extent, on the nature of the substituent group if any) under study and the

counter-ion present in the coat[20]. The time taken to switch between the oxidation and reduction colour has been found to be dependent on the thickness of the polymer film[20]. Garnier et al. have found that this time is typically of the order of 10-50ms[20]. The potential applications of this particular phenomenon are obvious with such polymers being used in place of LCD screens as display units. The advantages of such displays over standard displays are numerous and include reduced power requirements since the polymer has no need of a continuous applied potential to hold the colour once the coat has been reduced/oxidised. This also gives a polymer display the added advantage of having a "built-in" memory capability.

Such systems have also found a use in the design of "smart windows". These consist of a thin layer of a suitable conducting polymer (i.e. one whose electrochromic colour change is between dark and colourless) sandwiched between two layers of a transparent conducting surface such as indium-tin oxide (ITO), along with a colourless electrolyte. By the application of a potential, the polymer layer within the window can be made to switch between its transparent state and its opaque state. The degree to which this switching takes place is dependent on the potential applied. If this set-up is linked to a bank of photo-detectors then it is possible to arrange for the window to automatically darken in accordance with the level of light present.

Organic conducting polymers are also used as materials for light emitting diodes/displays (L.E.D.s). Study into the fluorescent and electroluminescent properties of conducting polymers and their associated monomers is well advanced and has shown that it is possible, by judicious choice of polymer and polymerisation conditions, to obtain fluorescence over a wide range of the electromagnetic spectrum

encompassing the visible region[21]. It has also been shown that is possible to blend these polymers and, in doing so, to blend the colours emitted[21].

The dual nature of conducting polymers (i.e. having both insulating and semi-conducting/conducting states) have led to suggestions of possible applications in the microelectronics industry. At present, further miniaturisation of electronic devices has been restricted due to difficulties in growing suitably thin films of the more typical semi-conducting materials (e.g. silicon or GaAs) to form the different circuit components. However, no such problems exist for conducting polymers which can be electropolymerised onto microlithographically defined metallisation areas[22]. In fact, in this application, conducting polymers have a great advantage. As well as the possibility of controlling film thickness (by careful control of the polymerisation conditions), it is also possible to grow a film of any particular shape required by use of a suitable electrode.

Research is already underway into the possible application of conducting polymers in environmentally clean (i.e. containing no heavy metals), rechargeable batteries. So far most of the work carried out has been on the chemically polymerised poly(acetylene)[23,24] with very little study carried out on electropolymerised systems. Fortunately, the actual work on electrochemically synthesised polymers carried out so far as been promising. Polymer batteries consist of a neutral, reduced and an oxidised film of the conducting polymer (typically poly(thiophene) or poly(azulene)) in question on a metal support, as the cathode and anode respectively, surrounded by an electrolyte solution. Cells formed from poly(azulene) are found to compare well with those fabricated from poly(acetylene), giving a maximum open circuit voltage of over 2V and a short-circuit current of about 4mA[25]. (Polyacetylene batteries typically give an open circuit voltage of 1V and a short circuit current of 3mA

unless doped with a cation such as Li^+ [26]). Conducting polymer batteries are also found to be rechargeable over a number of discharge/charge cycles. These types of cells have a number of advantages over current acid batteries in that, as well as their low toxicity, they have a high charge to weight ratio allowing them a possible application in the next generation of electric vehicles.

It is also possible to use conducting polymer films in the production of high density information storage devices (figure 1.8). Work has been carried out in which thick films of polypyrrole have been grown on an electrode with a deliberately irregular surface[27]. Once electrodeposition is completed, these films can be peeled off the anode. It has been found that coats prepared in such a way exhibit an inverse surface relief pattern with very few defects. This surface can then be read capacitively using another electrode. Devices prepared from such polymers on a strengthening support have been shown to have a constant signal-to-noise ratio[27] and, due to the inherent stability of the polymer film, are expected to have a extensive life span both of the actual device and of the data contained on it.

The development of photovoltaic cells has been impeded due to the photocorrosion of small band gap semiconductors in the aqueous electrolyte used[28,29]. A number of possible protection routes has been proposed to prevent this process, one of these being to coat the photoanode with a conducting polymer, such as poly(3-methylthiophene)[30], due to their high conductivity and chemical stability as well as their ability to adhere to the actual cell[31,32]. The polymer coat acts as a barrier at the photoanode/electrolyte interface, preventing the electrolyte from reaching the susceptible photoanode.

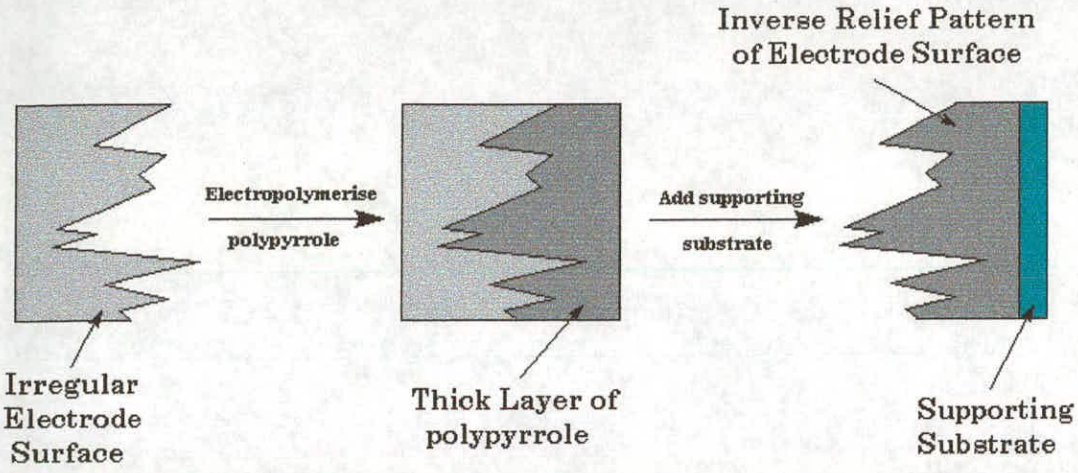

Figure 1.8: Basic schematic showing the use of a conducting polymer as a memory storage device

It has been found that certain conducting polymers (such as polypyrrole) exhibit low friction coefficients and low wear rates with values similar to PTFE[22] as well as having high electrical and thermal conductivities compared to standard bearing materials used in microengineering[33] (such as Si, SiO_2 or Si_3N_4). Conducting polymers also have the advantage of being easy to deposite evenly (through electropolymerisation), even on such irregularly shaped micromechanical structures as micromotors and microturbines.

A further proposed use for conducting polymer films is as a source of protection for sensitive electronics against EM radiation. Such films have already found a use in, for example, the stealth coatings of the F117 Nighthawk fighter[34] and other anti-radar materials, such as camouflage netting, for military application[35,36].

1.1.4 Conduction in Conducting Polymers

Although there has been a significant amount of research into the properties of electrically conducting polymer systems, there is surprisingly little consensus as to the actual mechanism by which such polymers conduct. At present, a number of models exist to describe the method of charge transport. Perhaps the two main models which exist to describe charge conduction through the polymer matrix are the delocalised band model[37] and the redox chemical model[38].

1.1.4.1 Delocalised Band Model

The delocalised band model makes use of a modified version of the band theory used to describe the electrical properties of a number of solids such as metals and semi-conductors. In "normal" band theory, movement of charge can be described in terms of electrons/holes moving between the highest occupied π electron band (the valence band) and the lowest unoccupied band (the conduction band); the energy gap between these bands being responsible for the electrical properties. Typically, conducting polymers, in their neutral state, have a band gap of the order 1-4eV[37] and so are electrically insulating. In semi-conductor technology, such large band gaps can be altered by a process known as doping which introduces holes into the (full) valence band or electrons into the (empty) conduction band. However, this is not possible in conducting polymers due to the fixed nature of the charge sites. There must, therefore, be another form a charge carrier.

In this particular model, oxidation of the polymer involves the loss of an electron from a monomer unit to form a radical cation (also referred to as a polaron). This causes the polymer chain to distort from its more stable

benzoidal form to a quinoid structure which is more able to accommodate the charge. Further oxidation of the polymer results in the loss of a second electron from the same chain forming a dication (or bipolaron – a doubly charged, spinless species similar to a phonon). This redox rearrangement is shown in figure 1.9 for the case of a general heterocyclic polymer.

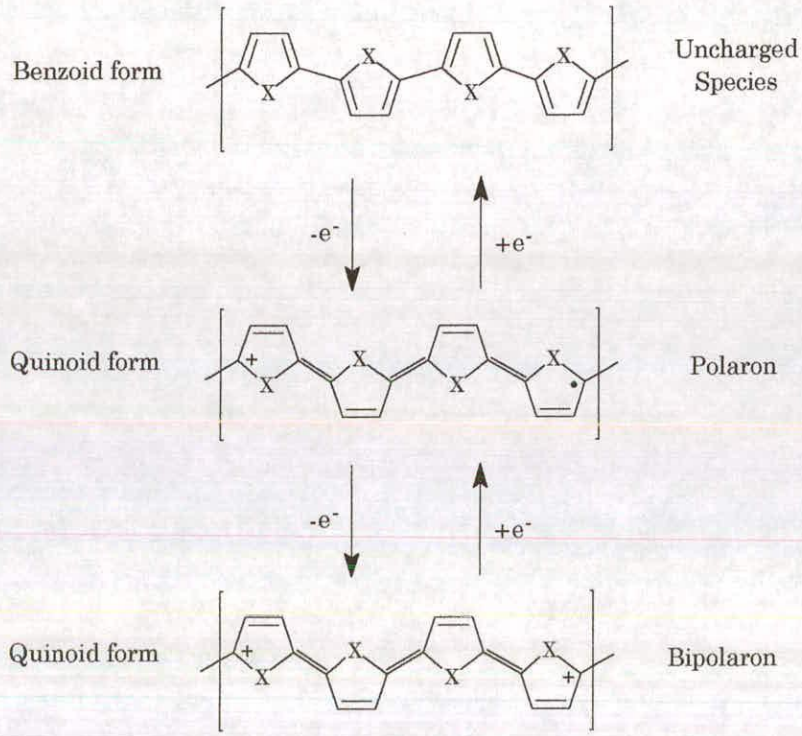

Figure 1.9: Benzoid-quinoid rearrangement of a general heterocycle

The formation of the bipolaron is energetically more favourable than the loss of an electron from a second polymer chain to form another polaron. It is believed that the transformation of the polymer from its benzoidal to quinoidal form causes new bands to form which reduces the band gap, allowing conduction to take place.

The validity of this model has been verified by electron spin resonance (ESR) measurements which have shown[39] the presence of polarons and, at higher oxidation states, bipolarons. It has been found that for

poly(pyrrole), no ESR spectrum is observed in the fully conducting state suggesting that the charge carriers are bipolarons. This model is also supported by optical measurements[40].

Although this is a good model for describing charge transport within a conducting polymer strand, it is a widely accepted fact that a given polymer will exist as a number of chains of various lengths. It is also accepted that these chains will be randomly orientated and so it is unlikely that they will be fully conjugated along their full length. Therefore it is necessary that there exists some mechanism by which intra-chain and inter-chain charge transfer can occur. This has led to the development of the redox chemical model.

1.1.4.2 Redox Chemical Model

The redox chemical model proposes that charge is transferred along the polymer chain by electrons "hopping" between neighbouring oxidised and reduced sites on the polymer chain. Albery et al.[41] have used this model to propose a two electron redox model for poly(pyrrole) detailed in figure 1.10 although they argue that, from experimental results, the model is applicable to several other conducting polymer systems[42]. Indeed this model have been used by a number of other groups[43,44,45,46].

In figure 1.10, the reduced (neutral) form of the polymer is represented by structure A, the intermediate radical cation (or polaron) by B and the fully oxidised form of the polymer (or bipolaron) by structure C.

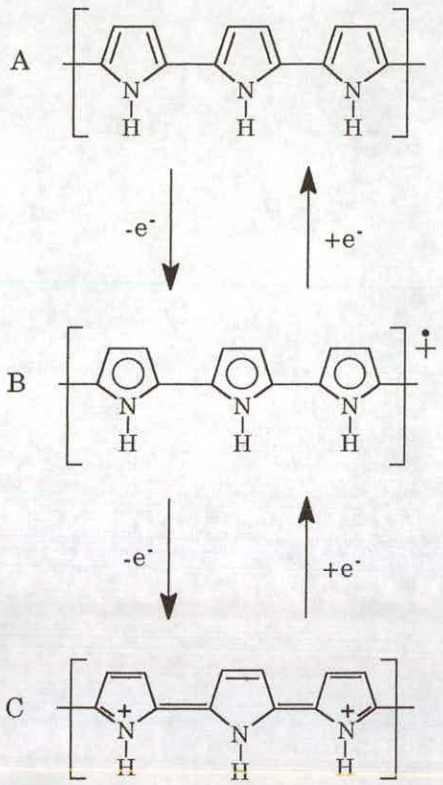

Figure 1.10: Reduced (A), intermediate (B) and fully oxidised (C) structures of poly(pyrrole)

Albery et al. have proposed that this redox reaction is accompanied by a change of state from a compact, lyophobic form (the α form) which is stable at reducing potentials to a more open lyophilic state (the β form) which is stable at oxidising potentials i.e. when the coat is conducting. This conducting state involves the incorporation of counterions from the supporting electrolyte and it has been suggested that these ions enter into pores around which the polymer is arranged in a helix structure[47,48]. Albery et al. have measured the rate of these phase changes and have observed them to be of the of the order of minutes to hours, dependent on the potential applied.

It is very probable that an all-encompassing general model to explain the conduction of charge within all conducting polymer matrices cannot be

found. Instead, it is more likely that a combination of charge transport mechanism occurs in many of them and so each polymer system will have to be described individually.

1.2 Indole

A large percentage of this thesis is based on study into conducting polymers based on 5-substituted indole derivatives. Indole (figure 1.11) was first shown to polymerise in 1982 by Tourillon and Garnier[49] and, along with a number of indole derivatives, was studied at length by Waltman and co-workers[50].

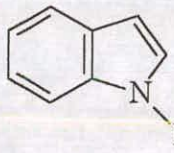

Figure 1.11: Indole

Indole is a logical choice for study in that it consists of a pyrrole ring (which has itself been extensively studied) fused to a benzene molecule. Work on polyindole by Tourillon[49] has shown that it has a conductivity which approximately 100 times less than polymer systems such as polypyrrole and polythiophene - putting polyindole into the semi-conductor range. The main difficulty in studying indole systems is the large amount of discussion and disagreement as to the actual mechanism, and therefore products, of this polymerisation process. This problem is compounded by the fact that unlike the majority of the previously studied polymer systems which all undergo α-α linking (as shown in figure 1.5) indole cannot due to the presence of the benzoidal ring. The asymmetric nature of the indole monomer also encourages the debate about the nature of the products. The main area of discord is the location of the actual linking sites in the actual monomer. A number of mechanisms

have been proposed, each suggesting different polymerisation product. Some of these products are shown in figure 1.12. Although there is still a large degree of discussion current on this topic, all recent work has come to the conclusion that, from spin density calculations, coupling must take place mainly through the 5-membered ring, not the benzoidal system. This, of course, discredits the structure proposed by Tourillon et al (figure 1.12a).

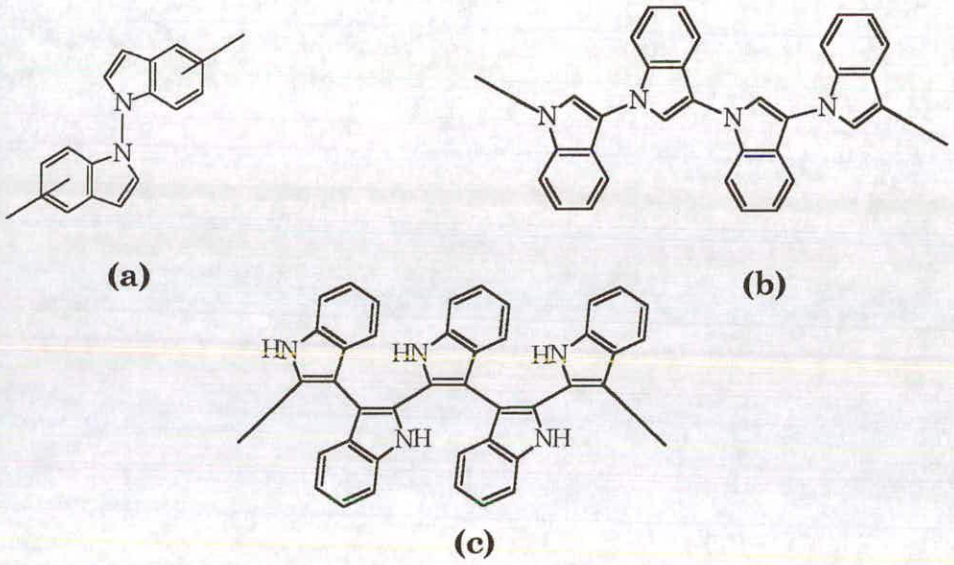

Figure 1.12: Structures of Polyindole Proposed By (a) Tourillon and Garnier[49], (b) Waltman et al[50], (c) Zotti et al[51]

Work by Waltman et al has attempted to solve this puzzle by examining the effect of changing the substituent position of an indole derivative (in this case methylindole) on the formation of an electropolymerised film[50]. On investigation of indoles which had electron-withdrawing substituents at the 2 or 3 positions i.e. on the pyrrole ring, it was found that no polymer film was synthesised on the working electrode even though the nature of the substituent should have encouraged electrophilic substitution on the neighbouring benzene. This suggested that the benzene ring played no part in linking and so any substituents on the benzene ring would only provide an electronic influence, not a steric one.

Electron spin density calculations on 5-substituted indoles carried out by Waltman[50] have shown that, in the initially produced radical cation, there is high spin density in the 1 and 3 positions which are of the order of 2 to 6 times greater than those at other positions in the molecule, including the benzene ring. This would then seem to suggest that linking takes place through these positions (figure 1.13).

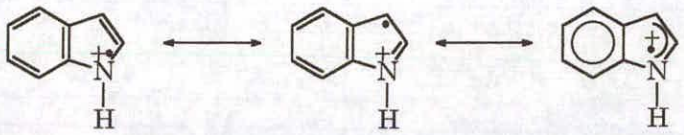

Figure 1.13: Resonance Structures of the Indole Radical

Work carried out on 5-substituted indoles seem, in the main, to bear this hypothesis out. It has been found that the existence of electron withdrawing (such as -CN or -COOH) groups on the 5 position can encourage film formation whereas electron donating groups reduce the likelihood of any film growth (table 1.1)[50].

monomer	film formed?	monomer	film formed?
indole	yes	5-aminoindole	no
1-methylindole	no	5-hydroxyindole	no
2-methylindole	no	5methoxyindole	no
3-methylindole	no	5-bromoindole	yes
4-methylindole	yes	5-chloroindole	yes
5-methylindole	no	5-fluoroindole	yes
6-methylindole	yes	indole-5-carboxylic acid	yes
7-methyindole	yes	5-cyanoindole	yes
3-cyanoindole	no	5-nitroindole	no

Table 1.1: Results from Waltman's study into the substituent effect on film growth

It has been postulated by Waltman[50] that the reason behind this can be easily understood by considering how the substituent groups affect the spin densities within the indole molecule/radical. As discussed previously, after the electrooxidation of the monomer to the radical cation, three different routes may be followed depending on the relative stability of the radical. In this case, the presence of an electron-withdrawing substituent such as -CN in the 5 position does little to change the spin density of the cation and so the substituted monomer behaves like the parent indole molecule i.e. a film is produced. With strongly electron-withdrawing side groups, the spin density at the reactive 3 position is decreased slightly but not enough to prevent polymerisation. On the other hand, with electron donating groups such as -OH, the spin density at the 3 position (as well as the 1 position) is dramatically reduced and delocalisation begins to be significant. This stabilises the radical, enabling it to diffuse into the bulk electrolyte instead of forming polymer.

More recently, work by Mount et al has agreed with this hypothesis that substituents on the benzene ring, although not an important factor sterically, exert a substantial electronic influence. Research by this group has shown that there are in fact 2 polymerisation products from the electro-oxidation of indole as well as a number of its 5-substituted derivatives[52]. Of these two products, it was found that one was soluble in DMF while the other was soluble in DMSO. The DMF-soluble fraction was characterised using cyclic voltammetry, NMR[53,54] and MALDI and L^{2}TOF[54,55] mass spectrometry and, from the results obtained, Mount has proposed it has an asymmetric trimer structure (figure 1.14) while the DMF-insoluble fraction was found to comprise of polymer made up of linked trimer units.

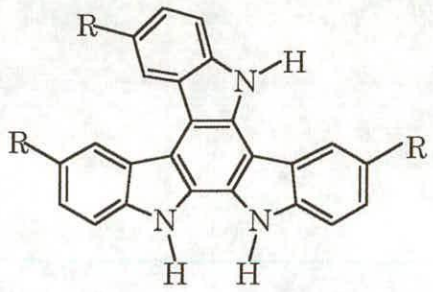

Figure 1.14: Trimer Structure Proposed by Mount et al as a polymerisation product for indole and its 5-substituted derivatives (R = H, CN, COOH)

From this work, it seems that indole and its 5-substituted derivatives polymerise first to form the cyclic trimer which then deposits on the anodic material where it can further link to form polymer. This polymerisation mechanism is summarised in figure 1.15

$$3nIn_{(aq)} \xrightarrow{-7ne^-,-6nH^+} nIn^+_{3\,(s)}$$

$$nIn^+_{3\,(s)} \xrightarrow{-2ne^-,-2nH^+} -(In^+_3)-_{(s)}$$

Figure 1.15: Polymerisation Mechanism Proposed for Indole by Mount et al. In, In_3^+, and In_n represent monomer, trimer and polymer respectively

Current-time transients taken during polymerisation all show constant current during the process showing that the films have good conductivity independent of film thickness (indeed, it is possible to produce layers which are millimetres thick without any significant loss in conduction). The transients also display a Koutecky-Levich dependence upon electrode rotation speed which, suggests the Mount group, indicates that after the deposition of the first monolayer of polymer, the monomer is first adsorbed onto the modified electrode surface before electrooxidation

occurs i.e. coupling occurs on the actual surface of the electrode and so the formation of the film becomes first order in monomer[52].

Studies by the same group have shown that it is possible to control the relative amounts of the two polymerisation products by altering the polymerisation conditions, most notably the monomer concentration (high concentrations lead to a greater percentage of trimer), the rotation speed of the anode (the faster the angular frequency, the greater the concentration of free trimer in the coat) and the time allowed for polymerisation (the greater the amount of time the more chance that free trimer in the coat will link to form polymer)[52]. This, of course, means that there is a high probability that the area of the polymer film nearest the surface of the electrode will be polymer while at the polymer-electrolyte interface, the coat will be mostly free trimer.

Mount and Thomson have also attempted to discover how these trimer centres link when the electrooxidation is carried over to polymer formation. Studies of the polymerisation of N-methylindole have shown that although no film is formed on the electrode surface, the asymmetric trimer is still one of the major products[56]. However, it was found to be impossible to then link these free trimers to form the polymer. This seems to suggest that in forming the polymer, the free trimers link through the ring nitrogens. In this case a number of secondary linear products were also discovered (mainly dimers and tetramers) and this is attributed to steric effects between the methyl groups hindering the formation of the trimer.

1.3 Overview of Thesis

This thesis is a presentation of the 3 years of research investigating the mechanisms of charge conduction in conducting polymers based on substituted indole. It is hoped that this thesis will show just how powerful the combination of small amplitude perturbation measurements with computer modelling can be in obtaining useful kinetic data. The thesis itself can be split into 3 main sections: background and theory (this chapter along with the following one), experimental (chapter 3) and finally actual experimental results (the remaining chapters). Chapters 4 deals with the results obtained while examining conducting polymer layers formed from indole-5-carboxylic acid. Chapter 5 covers observations on poly(5-cyaniondole) films and chapter 6 covers polymer coats synthesised from the copolymerisation of indole-5-carboxylic acid and 5-cyanoindole monomers. The final chapter, chapter 7, brings together some of the salient points of the thesis in a final conclusion which also includes a discussion of possible further work.

1.4 References

1. V.V. Walatka, M.M. Labes, J.H. Perstein; *Phys. Rev. Lett.*, 1973, **31**, 1139

2. R.L. Green, G.B. Street, L.J. Suter; *Phys. Rev. Lett.*, 1975, **34**, 557

3. C.K. Chiang, C.R. Fincher Jnr., Y.W. Park, A.J. Heeger, H. Shirakawa, E.J. Louis, S.C. Gau, A.G. MacDiarmid; *Phys. Rev. Lett.*, 1977, **39**, 1098

4 A.F. Diaz, K.K. Kanazawa, G.P. Gardini; *J. Chem. Soc. – Chem. Comm.*, 1979, 635

5 P. Kovacic, A. Kyriakis; *J. Am. Chem. Soc.*, 1963, **85**, 454

6 J. Prejza, I. Lundstrom, T. Skotheim; *J. Electrochem. Soc.*, 1981, **128**, 1625

7 E.M. Genies, G. Bidan, A.F. Diaz; *J. Electroanal. Chem.*, 1983, **149**, 101

8 K. Tanaka, T. Shichiri, S. Wang, T. Yamabe; *Synth. Met.*, 1988, **24**, 203

9 A.F. Diaz, J.M. Casquez Vallejo, A. Martinez Duran; *IBM J. Res. Dev.*, 1981, **25**, 42

10 P.N. Bartlett, J.M. Cooper; *J. Electroanal. Chem.*, 1993, **362**, 1

11 B.F.Y. Yon Hin, R.S. Sethi, C.R. Lowe; *Sens. Actuators B*, 1990, **1**, 550

12 D. Bélanger, E. Brassard, G. Fortier; *Anal. Chim. Acta*, 1990, **228**, 311

13 L.D. Couves, S.J. Porter; *Synth. Met.*, 1989, **28**, C761

14 M.B. Saleh, F. Taha, G.S. Aof; *Electroanalysis*, 1995, **7**, 770

15 K.K. Shin, S.K. Pang, H.K. Cheung; *J. Electroanal. Chem.*, 1994, **367**, 115

16 J.N. Barisci, P. Murray, C. Small, G.G. Wallace; *Electroanalysis*, 1996, **8**, 330

17 W. Lu, H. Zhao, G.G. Wallace; *Anal. Chim. Acta*, 1995, **315**, 27

18 P.N. Bartlett, J.W. Gardner, N. Blair, T.C. Pearce, S. Friel; *Analyst*, 1993, **118**, 371

19 R.J. Waltman, A.F. Diaz, J. Bargon; *J. Phys. Chem.*, 1983, **87**, 1459,

20 F. Garnier, G.Tourillon, M. Gazard, J.C. Doubois; *J. Electroanal. Chem.*, 1983, **148**, 299

21 M. Berggren, O. Inganäs, G. Gustafsson, J. Rasmusson, M.R. Andersson, T. Hjertberg, O. Wennerström; *Nature*, 1994, **372**, 444

22 J.W. Gardner, P.N. Bartlett; *Sens. Actuators A*, 1995, **51**, 57

23 P.J. Nigrey, A.G. MacDiarmid, A.J. Heeger; *Mol. Cryst. Liq. Cryst.*, 1982, **83**, 209

24 A.G. MacDiarmid, R.B. Kaner, R.J. Mammone, A.J. Heeger; *J. Phys. Colloq.*, 1983, **C3(6)**, 543

25 R.J. Waltman, A.F. Diaz, J.Bargon; *J. Electrochem. Soc.*, 1984, **131**, 1452

26 R.J. Waltman, J.Bargon; *Can. J. Chem.*, 1986, **64**, 76

27 W.H. Meyer, H. Kiess, B. Binggeli, E. Meier, G. Harbeke; *Synth. Met.*, 1985, **10**, 255

28 T. Skotheim, L.G. Petersson, O Inganäs, I Lundström; *J. Electrochem. Soc.*, 1982, **129**, 1737

29 A.J. Frank, K. Honda; *J. Phys. Chem.*, 1982, **86**, 1933

30 G. Horowitz, F. Garnier; *J. Electrochem. Soc.*, 1985, **132**, 634

31 T. Skotheim, I. Lundström, J. Prejza; *J. Electrochem. Soc.*, 1981, **128**, 1625

32 R. Noufi, A.J. Nozik, J. White, L.F. Warren; *J. Electrochem. Soc.*, 1982, **129**, 2261

33 J. Gardner, P.N. Bartlett; *Nanotechnology*, 1991, **2**, 19

34 R.A. Stonier; *Sampe Journal – Soc. Adv. Mat. Process Engin.*, 1991, **27**, 9

35 P.V. Wright et al., *Adv. Mat. For Optics and Electronics*, 1994, **4**, 253

36 L. Olmedo, P. Hourquebie, F. Jousse; *Handbook of Organic Conducting Polymers*, Vol. 3, John Wiley and Sons Ltd., New York, 1997, 367

37 S.H. Glarum, J.H. Marshall; *J. Phys. Chem.*, 1988, **92**, 4210

38 E.M. Genies, J.M. Pernaut; *J. Electroanal. Chem.*, 1985, **191**, 111

39 J.C. Scott, P. Pfluger, M.T. Krounbi, G.B. Street; *Phys. Rev. B – Cond. Matt.*, 1983, **28**(4), 2140

40 K. Yakushi, L.J. Lauehlan, T.C. Clarke, G.B. Street; *J. Chem. Phys.*, 1983, **79**, 4774

41 W.J. Albery, C.C. Jones; *Faraday Discuss. of the Chemical Soc.*, 1984, **78**, 193

42 W.J. Albery, Z. Chen, B.R. Horrocks, A.R. Mount, P.J. Wilson, D. Bloor, A.T. Monkman, C.M. Elliott; *Faraday Discuss. of the Chemical Soc.*, 1989, **88**, 247

43 F. Genoud, M. Guglielmi, M. Neichstein, E. Genies, M. Slamon; *Phys. Rev. Lett.*, 1985, **55**, 118

44 E.M Genies, M. Lapkowski; *J. Electroanal. Chem.*, 1987, **220**, 67

45 E.M Genies, M. Lapkowski; *J. Electroanal. Chem.*, 1987, **236**, 199

46 A.G. MacDiarmid, J.C. Chiang, A.F. Richter, A.J. Epstein; *Stnth. Met.*, 1987, **18**, 285

47 W.R. Salaneck, R. Eriandson, J. Prezja, I. Lunsdstrom, O. Inganas; *Synth. Met.*, 1983, **5**(2), 125

48 F. Garnier, G. Tourillon, J.Y. Barraud, H. Dexpert; *J. Mat. Sci.*, 1985, **20**(8), 2687

49 G. Tourillon, F. Garnier; *J. Electroanal. Chem.*, 1982, **135**, 173

50 R.J. Waltman, A.F. Diaz; J Bargon, *J. Phys. Chem.*, 1984, **88**, 4343

51 G. Zotti, G. Schiavon, S. Zecchin, A. Berlin, A. Canavesi; *Tetrahedron*, 1996, **52**, 7947

52 J.G. Mackintosh, A.R. Mount; *J. Chem. Soc. Faraday Trans.*, 1994, **90**, 1121

53 J.G. Mackintosh, A.R. Mount, D. Reed; *Mag. Res. Chem.*, 1994, **32**, 559

54 J.G. Mackintosh, C.R. Redpath, A.C. Jones, P.R.R. Langridge-Smith, D. Reed, A.R. Mount; *J. Electroanal. Chem.*, 1994, **375**, 163

55 J.G. Mackintosh, C.R. Redpath, A.C. Jones, P.R.R. Langridge-Smith, A.R. Mount; *J. Electroanal. Chem.*, 1995, **388**, 179

56 A. Mount, A.D. Thomson; *J. Chem. Soc. Faraday Trans.*, 1998, **94**, 553

2. Theory

This chapter will detail the main theoretical ideas used during the course of this work.

2.1. Linear Sweep Voltammetry

The technique of linear sweep voltammetry, and its close relative cyclic voltammetry, is one of the most powerful techniques in the electrochemist's arsenal. Indeed, voltammetry of one form or another is usually the first technique employed by electrochemists when investigating novel systems since it can give a wide range of information. On the qualitative side, voltammetry can show the presence of an electroactive species and identify the role of adsorption and diffusion and give information about the existence of any secondary reactions – both chemical and electrochemical. From a quantitative standpoint, it can, to a first approximation, give kinetic information (though more versatile techniques are available for this).

The actual technique of voltammetry is very simple and is shown in figure 2.1. The potential of the system under examination is held at a value where it is known that no electrochemical activity occurs and is then ramped (either positively or negatively) at a constant rate v_1 to another potential past the area of redox activity E_2. The direction of the ramp is then reversed and the potential is ramped back, usually at the same speed though not always, to either the initial potential E_1 or to an entirely different potential E_3. If the potential sweep is terminated at this point then the technique is termed linear sweep voltammetry (LSV). On the other hand, if the process is repeated for a number of forward and back sweeps the technique becomes cyclic voltammetry (CV) with each sweep from E_1 to E_2 and back being assigned a sweep number (an integer from 1 upwards).

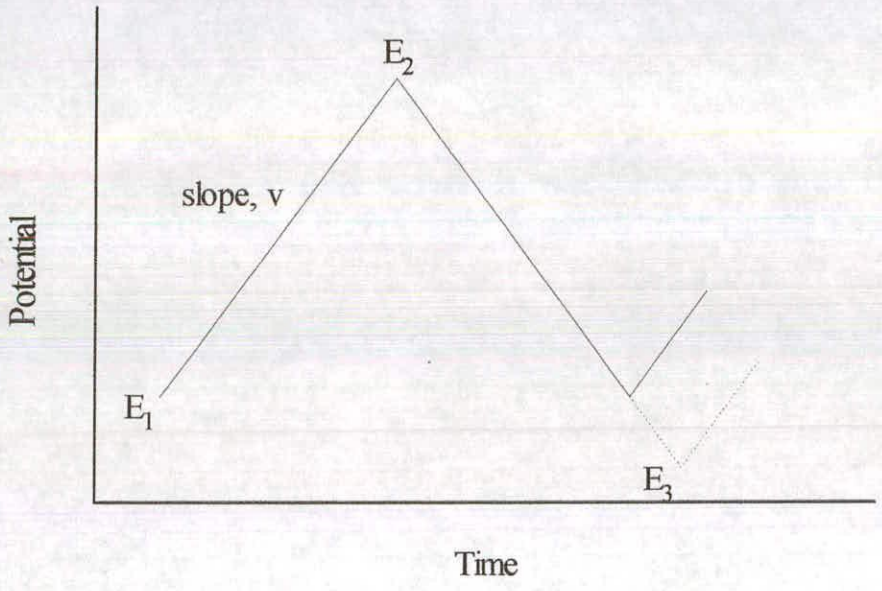

Figure 2.1: Potential-time profile for cyclic voltammetry

In order to understand voltammetry fully it is necessary to consider how the concentration of a redox active species changes as the potential is ramped. The concentration is the important variable since any current

detected at the electrode surface is dependent on the kinetics of the surface reaction and the flux of the electroactive species to the surface. For a stagnant solution, this flux is dependent upon the concentration gradient between the electrode and the bulk solution. If we consider the case where the only active species in solution is a reduced species R which is able to undergo the electron transfer

$$R \longrightarrow O + ne^-$$

Initially, with the applied potential well below the standard redox potential for the above reaction, no reaction occurs and the concentration of R at the electrode surface is constant and equal to the bulk concentration. As the redox potential is approached the electron transfer reaction begins to occur, a current is produced and the concentration of R at the electrode surface is reduced. As the potential is taken more positive, more of the reduced species is oxidised at the electrode surface resulting in a subsequent increase in the current. During this time a concentration gradient starts to extend into the bulk of the solution. In the absence of any form of forced convection, there will, of course, be a slight relaxation of this concentration gradient owing to diffusion of R from the bulk solution. This effect is however offset by the ever increasing potential increasing the rate of reaction at the electrode, in turn reducing the surface concentration further. It can be seen that there will, eventually, be a point where the rate of depletion of R at the electrode surface and the rate of transport from the bulk are equal. This will produce a maximum in the current since any further increase in the electrode reaction rate will cause the depletion zone to extend yet further into the bulk solution. This in turn will create a more extensive depleted region which the fresh R must diffuse through, reducing the rate of species transport to the electrode surface and hence, the current. This creates a peak shape around a characteristic potential E_P for the redox reaction. This maximum (peak) current is sweep rate dependent since

any changes in the timescale of the experiment will affect how quickly and how far the depletion layer extends into the bulk solution. The precise form of this dependence is determined by the nature of the reaction in question; proportional to $v^{1/2}$ for a reaction occurring in solution assuming that the kinetics of the redox process is sufficiently fast that all species reaching the electrode are immediately oxidised/reduced and proportional to v for reactions occurring within films and for all diffusion processes.

Voltammograms can provide a way by which the general nature of a reaction can be easily deduced; whether it is reversible or irreversible. For a reversible system, the peaks are generally sharp with

$$E_P - E_{P/2} = \frac{59}{n}\text{mV}$$

where E_P is the peak potential, $E_{P/2}$ the potential at half peak height and n is the number of electrons involved. The oxidation and reduction peak maxima for a reversible system are of equal current and separated by 59/n mV (Nernstian behaviour). It is also found that for a reversible reaction, there is no variation in the peak position on variation of the sweep rate (i.e. the thermodynamics of the reaction stay the same). For irreversible systems however, the volumetric response is completely different. For such systems, it is also observed that the redox peaks are less sharp than in the reversible case and that

$$E_P - E_{P/2} = \frac{48}{\alpha n}\text{mV}$$

where α is a measure of the irreversibility of the system (=0.5 for a fully reversible redox couple). The peak positions are dependent on the sweep rate of the applied potential and it is found that for a decade change in v, the peak positions will shift by

$$\frac{30}{\alpha n}\text{mV}$$

such that for a positive increase in v, the position of the oxidation peak will change to a more positive potential. This means that, at most sweep rates, the peak separation is no longer 59mV for a one electron redox system. It is interesting however that, as long as both processes are the same (e.g. both in solution) , the variation of peak current with sweep rate is the same – for the case of a solution reaction, for both a reversible and irreversible system, I_{peak} is proportional to $v^{1/2}$.

2.2. Rotating Disc Electrode

In order to obtain more accurate kinetic information, it is necessary to move away from stagnant solutions where random effects caused by diffusion are important and allow the redox system under investigation to reach a steady state. The most common way to achieve this is to impart a forced (and controllable) convection on the system by the use of a rotating disc electrode (RDE).

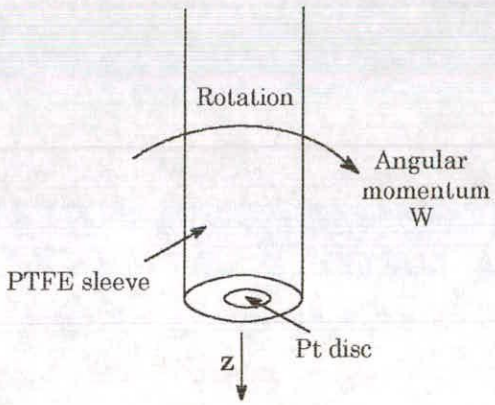

Figure 2.2: The rotating disc electrode (RDE)

The RDE consists of a planar disc electrode (usually of a *noble* metal such as platinum) surrounded by an insulating mantle of PTFE or Teflon

(figure 2.2). This electrode is connected to a motor controller which allows precise control of the electrode rotation speed W. When immersed into a solution containing the redox species in question along with a background electrolyte, this rotation imparts a hydrodynamic flow which effectively sucks solution from the bulk up to the electrode surface (figure 2.3(a)) before throwing it out radially across the electrode's surface (figure 2.3(b)).

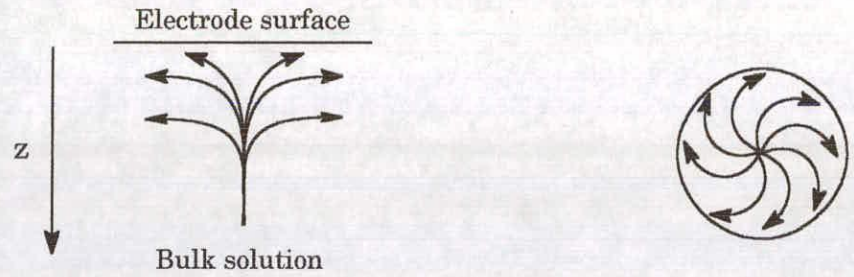

(a) **(b)**

Figure 2.3: Hydrodynamic flow of solution (a) towards the RDE and (b) across the electrode surface

The layer of solution immediately adjacent to the surface of the electrode remains stagnant within the frame of reference normal to the surface of the disc. As a result, movement of the electroactive species is by convection up to this layer (with the concentration of the species at the bulk concentration throughout this well stirred region - figure 2.4) followed by diffusion to the electrode surface. Solution of the convection-diffusion equations gives the thickness of this diffusion layer δ as

$$\delta = 0.63\nu^{1/6}D^{1/3}W^{-1/2}$$

where W is the rotation speed in hertz and ν the kinematic viscosity. Hence it can clearly be seen that the thickness of the diffusion layer (and hence the transport of the electroactive species to the electrode surface) can be very accurately controlled simply by altering the rotation speed of the electrode.

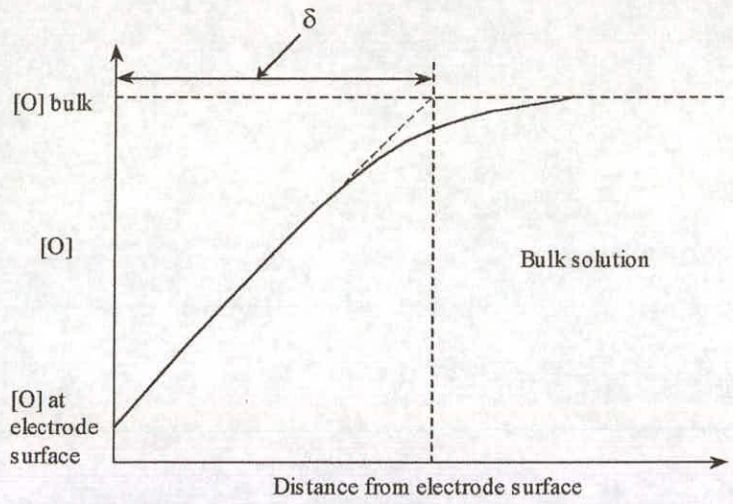

Figure 2.4: Variation of concentration of active species normal electrode surface for a RDE

The use of the rotating disc electrode became more popular after the mid-1940's when it replaced the more commonly used dropping mercury electrode. The main reason for this change in approach was partly due to Levich who, in 1942, showed that the mathematics of the hydrodynamic flow were readily soluble and that the resulting kinetic equations were relatively simple[1].

For a system where the only forms of transport to the electrode is either diffusion or convection (i.e. if there is no migration), the steady state differential equation where the concentration near the electrode surface is independent of time is

$$D\frac{\partial^2 c}{\partial z^2} = v_z \frac{\partial c}{\partial z} \qquad \text{Equation 2.1}$$

where D is the diffusion constant

c is the concentration of the electroactive species

v_z is the velocity component perpendicular to the electrode surface

$$v_z = -0{\cdot}51\omega^{3/2}\nu^{-1/2}z^2$$

z is the perpendicular distance from the electrode surface

Substituting for v_z,

$$\frac{\partial^2 c}{\partial y^2} = -\frac{z^2}{A}\frac{\partial c}{\partial z}$$

where $A = \dfrac{D\omega^{-3/2}\nu^{1/2}}{0.51}$

Integrating this for the boundary conditions where as $z \to \infty$, $c \to c_\infty$ (c_∞ is the bulk concentration) and using Fick's first law of diffusion gives

$$\frac{j}{D} = -\left(\frac{\partial c}{\partial z}\right)_{z=0} = \frac{c_\infty - c_O}{x_D} \qquad \text{Equation 2.2}$$

where c_O is the concentration at z=0 (i.e. the electrode surface)

j is the flux at the electrode surface

$x_D = 0.643\omega^{-1/2}\nu^{1/6}D^{1/2}$

At the surface of the electrode, the rate of the reaction is governed by the electrode kinetics. For the reaction

$$R \longrightarrow O + ne^-$$

this rate is given by

$$k = k_o e^{\left(\frac{\alpha F(E-E^\circ)}{RT}\right)}$$

where k_o is the standard electrochemical rate constant at $E = E^\circ$

α is the electron transfer coefficient

F is the Faraday constant (96,485.6C)

and where, unless otherwise stated, these first order rate constants and all subsequent rate constants have units of cms^{-1} due to the two

dimensional nature of the reaction (since it occurs at the electrode surface).

The flux at the surface of the electrode, assuming that the reaction is irreversible or the potential is sufficiently far from E° so that no back reaction can occur, is given by

$$j = kc_o$$

By substitution of this for c_o into equation 2.2 we can see that

$$-\frac{1}{j} = \frac{1}{kc_\infty} + \frac{1}{k_D c_\infty} \qquad \text{Equation 2.3}$$

where k_D, the first order rate constant describing mass transfer of the electroactive species to the electrode surface, is given by

$$k_D = \frac{D}{x_D}$$

Equation 2.3 has two limiting forms depending on which of the two rate constants is more dominant.

If $k_D c_\infty >> kc_\infty$ then $j = kc_\infty$

In this case, the rate of the charge transfer reaction is slower that the rate of diffusion to the electrode surface and so is rate limiting. Here, only a small amount of the electroactive species reaching the electrode surface will undergo reaction and so the concentration at the electrode surface will be approximately equal to that in the bulk solution.

If $kc_\infty >> k_D c_\infty$ then $j = k_D c_\infty$

Here, the rate of the electrochemical process is very much faster than the rate of diffusion of the reactant to the electrode surface

which is therefore the rate limiting state. Hence the flux is mass transport controlled. The current observed in this case is often termed the mass transport limiting current i_L.

Since, for an oxidation reaction,

$$i = -nFAj$$

where A is the electrode area, the limiting current will be

$$i_L = 1..556nc_\infty FAD^{2/3}W^{1/2}\nu^{-1/6} \qquad \text{Equation 2.4}$$

This equation is known as the Levich equation. By inspection of equation 2.4, a plot of i_L against $W^{1/2}$ (a Levich plot) should be linear.

For more complicated cases where a second, mass transfer independent process occurs prior to electron transfer i.e.

$$R \xrightarrow{k_1} R^* \xrightarrow{k_2} O + ne^-$$

the observed rate constant is

$$\frac{1}{k} = \frac{1}{k_1} + \frac{1}{k_2}$$

where k_1 is the rate constant for the transport independent step. As before, the smaller of these two constants will be for the rate limiting step. In this case, the mass transport limiting current is given by

$$\frac{1}{i_L} = \frac{1}{1.556nFAc_\infty D^{2/3}\nu^{-1/6}W^{1/2}} + \frac{1}{nFAc_\infty k_1} \qquad \text{Equation 2.5}$$

By examination of this equation (a form of the Koutecky-Levich equation) it can be seen that for such a system, a Levich plot would not yield a straight line. However, a plot of i_L^{-1} versus $W^{-1/2}$ will be linear and will have an intercept of $(nFAc_\infty k_1)^{-1}$. This type of plot is termed a Koutecky-Levich plot.

2.3. Ac Impedance

2.3.1. Ac Impedance Spectroscopy

While linear sweep and cyclic voltammetries employ the use of large scale potential changes, ac impedance spectroscopy (also known as electrochemical impedance spectroscopy - EIS) uses small amplitude voltage perturbations to take the system from its equilibrium configuration. Alternating current impedance spectroscopy is an important analytical technique and has a wide range of uses in fields as diverse as building (in the quality control of the concrete used[2,3]) and medicine in areas such as impedance cardiography[4,5] as well as in the area of electrochemistry where, even here, it has a number of different uses such as investigating corrosion processes[6,7,8] and, in the case of this thesis, the characterisation of organic conducting systems[9,10,11]. Impedance spectroscopy has the advantage that the results obtained are relatively easily manipulated using previously prepared simulations and curve fitting techniques to obtain the required data such as system resistances and capacitances. Unfortunately, the use of a small potential perturbation in order to linearise the associated mathematics means that the signal to noise ratio is often poor requiring the need for long averaging procedures. This along with the fact that many impedance apparatus do not have fast Fourier transform (FFT) capability (and so must take discrete readings at each required frequency) imparts a long run-time on the technique requiring that the system under question is static over long time scales. However, work is being carried out to improve the technique including the introduction of computer software for carrying out FFT work[12], enabling non-stagnant systems to be examined, and for automating both the acquisition and analysis of data[13,14,15], reducing the level of error both in the obtaining of the raw ac data and in its manipulation.

Like all forms of spectroscopy, impedance spectroscopy involves perturbing a system from its rest or equilibrium state and observing its response. However, unlike the more common laser spectroscopy, the perturbing energy is in the form of an oscillating potential (often very small to allow simplification of the associating mathematics as well as to prevent the large scale modification of the system in question which may be hard to model accurately) instead of a light pulse and the returning signal is a corresponding oscillating current with a certain magnitude (amplitude) and phase shift as opposed to a characteristic light frequency. These response values are normally combined to give the real (resistive) and imaginary (reactive) impedances of the system under examination (and hence the name of the technique).

In order to fully understand how this technique might be used, it is necessary to consider the response of a number of circuit elements on application of a ac potential of fixed frequency ($V=V_o\sin\omega t$). If the potential is applied to a circuit containing only a resistor R then the response is an oscillating current of magnitude $I=I_o\sin\omega t$ where $I_o = {}^{V_o}\!/_{R}$. Similarly, if the ac potential is applied on top of a dc potential V_{dc}, i.e. $V=V_{dc}+V_o\sin\omega t$, then the current response will be of the form

$$I=I_{dc}+I_o\sin\omega t \qquad \text{Equation 2.6}$$

This is shown in figure 2.5 and from this it can clearly be seen that the applied potential and resulting current are in phase.

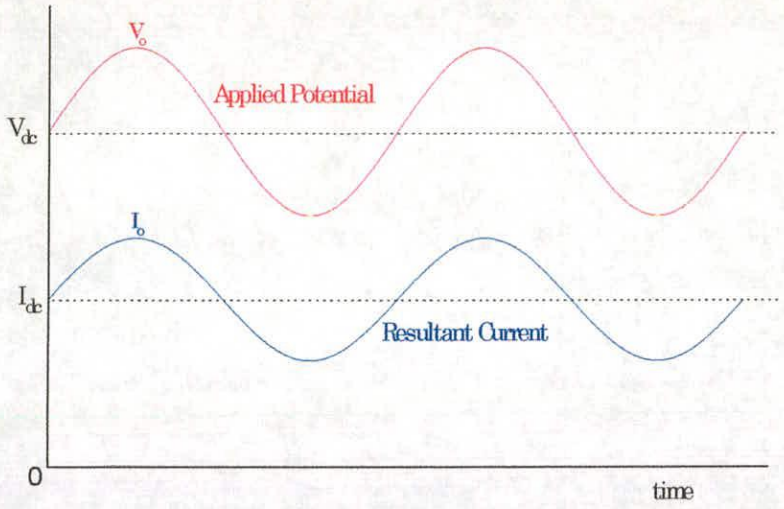

Figure 2.5: Resultant current on application of ac potential to a resistor

If on the other hand, the potential is applied to a capacitor then the capacitor becomes charged. The amount of charge which a capacitor can store, Q, is dependent in the potential applied and the capacitance, C, of the system (which is, in turn, dependent on the geometry of the capacitor) according to the relationship Q=CV. Hence the current will be given by

$$I = \frac{dQ}{dt} = \frac{CdV}{dt}$$

If the applied potential is again $V=V_{dc}+V_o\sin\omega t$ then the current passed will be

$$I=CV_o\cos\omega t \qquad \text{Equation 2.7}$$

This is shown in figure 2.6 along with the applied potential for comparison. From this it can easily be seen that the potential is now 90° out of phase with the applied potential and that the dc component of the current has now been lost.

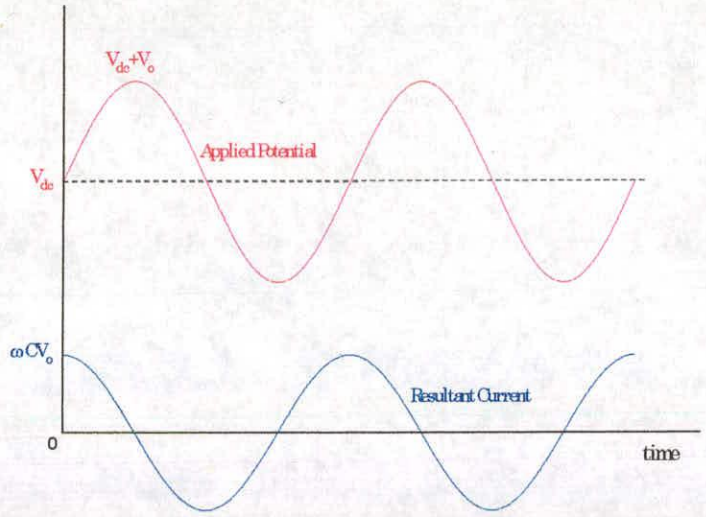

Figure 2.6: Resultant current on application of ac potential to a capacitor

Hence, from this simple example, we have an analytical tool whereby if we had a box containing either a resistor or a capacitor we could correctly identify the contents by simply applying an oscillating potential and measuring the resulting current. Although this is a very simplified example and most electrochemical systems other than reactions at bare electrode surfaces tend to be more complicated, it nonetheless illustrates just how powerful a technique impedance spectroscopy can be.

A typical ac spectrum is usually represented in two distinct ways: either as two graphs showing the variation of the magnitude and phase of the resultant signal with respect to the frequency of the perturbing potential (a Bode plot) or as a plot on a complex plane showing the real (resistive or conductive component) and imaginary (reactive or capacitive component) impedances of the system (a Nyquist plot). The Bode plot has the advantage of showing the frequency dependence of the system while Nyquist plots are generally easier to read since they are usually composed of areas with distinct shape. As an example, a typical Nyquist plot for a conducting polymer (in this case, poly(indole-5-carboxylic acid)

is shown in figure 2.7). This plot shows many of the shapes which are expected in a representative ac spectrum.

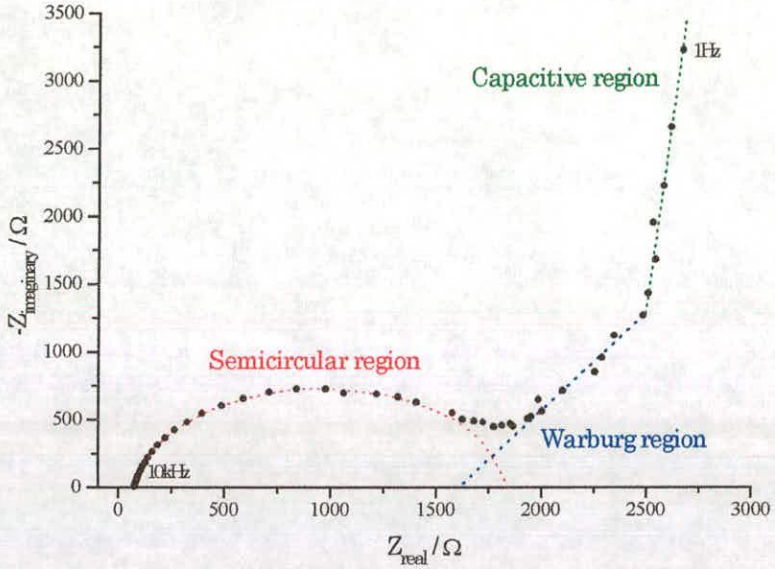

Figure 2.7: Example of an ac spectrum showing the main areas and features

The spectrum can be broken up into three discrete regions. The first region consists of a semicircle. This semicircle corresponds to the existence of a kinetic barrier at either the electrode/polymer or polymer/electrolyte interface (see proceeding section). The semicircle also starts (at high frequency) at a real intercept on the Nyquist plot. This intercept is the value of the solution resistance R_{el}. The semicircle can also be extrapolated again to another real intercept which gives an idea about the magnitude of the kinetic barrier (the charge transfer resistance mentioned in the next section). The maximum height of the semicircle can be used to calculate the capacitance of the double layer at the interface where the kinetic barrier is located. The next visible section is that containing a 'straight' line at 45°. This area is often referred to as a Warburg region and its length gives a measure of the resistance of the

particular system under investigation. The final region of the plot consists of a vertical line. This line is due to the capacitance of the system in question and should, in theory, be at 90° to the real axis. However, it is commonly found that in practice this line has a slight cant. This is customarily ascribed to inhomogeneity within the system[16] (see following section).

In actual experimental use the ac perturbing pulse is usually applied over a dc bias. This dc bias provides a method by which the initial conditions of the system may be set. In work involving conducting polymers, this generally means setting the oxidation state of the system in question. However, in doing this, it is generally necessary to then wait before taking any measurements to allow the system to reach equilibrium. By changing the bias it is possible to investigate the kinetics of a system over a wide range of oxidation states and so obtain a whole family of spectra. By careful examination of these spectra, it is possible to discover if any trends are present and, from this, the identities of the main charge carrying species.

2.3.2. Transmission Lines

In order to fully understand and analyse the data from ac impedance spectroscopy, it is necessary to model the system in question. Probably the most widely used simulation method is comparing the results with the output from an electronic circuit known as a transmission line. A transmission line, so called due to its first use as a model for electric power lines in engineering, is constructed by examining the different components of charge movement within the polymer layer and comparing each with the known physical properties of electronic circuit elements such as resistors, capacitors or inductors. For example, to move an electron though a polymer chain, energy must be supplied to the system. This energy requirement to move electrons (i.e. to produce a current) is very similar to the energy needed to move current through a wire with a finite resistance. Hence, the actual polymer chain can be modelled using a resistor with a finite resistance R_p. A similar argument can be applied for moving ions through an electrolyte solution and through the pores within a polymer film, giving rise to a solution resistance R_{el} and a pore resistance R_x.

These circuit elements can be combined, both physically and (more rigorously) mathematically, to create a transmission line such as the one shown in figure 2.8. This transmission line is commonly used for the simplified case where one of the charge carriers (in this case, ions within the pores of the polymer) is more mobile than the other.

The distributed capacitance C exists due to a need to preserve electroneutrality inside the coat. Hence, movement of electrons through the polymer must be balanced by the movement of counter ions in the pores. This is a similar charge distribution to that found in a parallel plate capacitor and so is thus simulated.

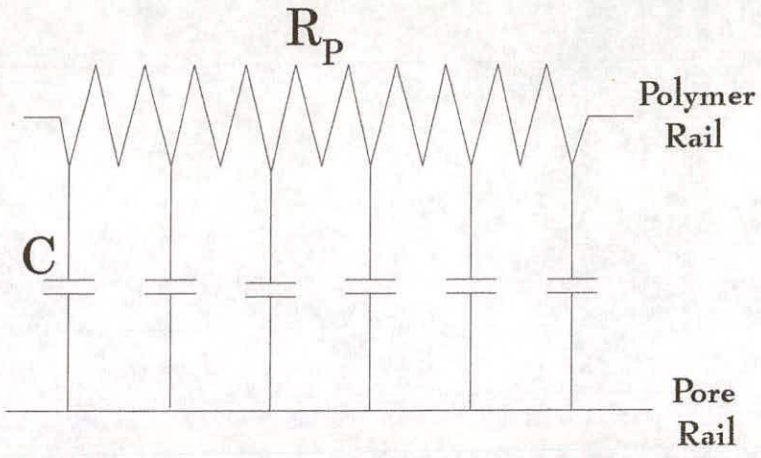

Figure 2.8: Simple transmission line with single resistance R and distributed capacitance C

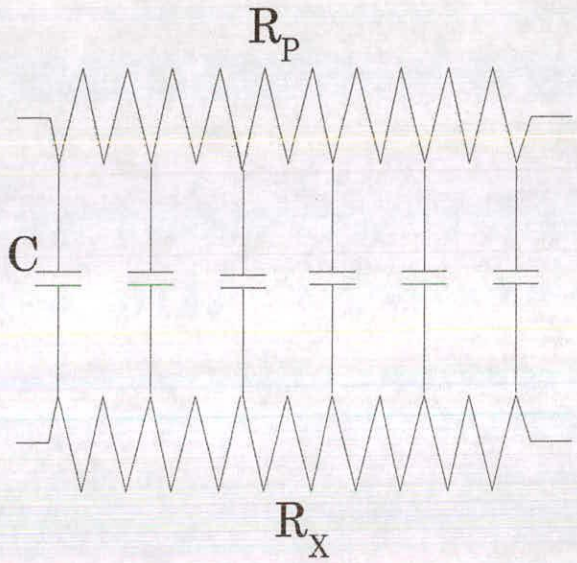

Figure 2.9: Transmission line proposed in the early work of Albery et al. R_P describes the movement of electrons in the polymer coat while R_X the movement of ions in the pores

Work by Albery and Mount[17,18] has shown that the theoretical restriction that one of the charge carriers is so much more mobile than the other that it can be considered to act as a wire with zero resistance is unnecessary. In their early work, they have shown that it is possible to model a system where two charge carriers of approximately equal

mobility are present using a transmission line with two finite resistances (figure 2.9)

Although the use of transmission lines to interpret data from ac impedance spectroscopy experiments involving organic conducting polymers is well established, there still exists a great deal of disagreement as to how the resulting spectra should be interpreted and no clear consensus as to how these circuits should be constructed. Within the field of conducting polymer science, one noticeable area of disagreement is in the actual mathematical nature of the driving potential. Many groups simply assume that, by analogy with electronic circuitry, the potential applied to the system is the cause of any effects seen. In this thesis, the approach of Albery et al will be followed. The mathematics put forward by this group have been well documented elsewhere[18-21], however, the main points and results will be recorded here.

This group has proposed that the charge carriers within the polymer layer are driven by novel potentials[18] which take into account any effects due to diffusion. In this work, the polymer coat is modelled as a series of neutral charge centres A which can be electrochemically oxidised to form a positive charge carrier B^+ (figure 2.10). In this simulation, the resulting positive charge created by this oxidation is balanced by the uptake of a counterion from the bulk electrolyte.

$$A{-}A{-}A{-}A + X^-_{(aq)} \longrightarrow A{-}A{-}\underset{X^-}{B^+}{-}A + e^-$$

Figure 2.10: Model for conducting polymer proposed by Albery et al

Conduction through this matrix occurs via a bimolecular redox exchange reaction by a process known as redox hopping (figure 2.11).

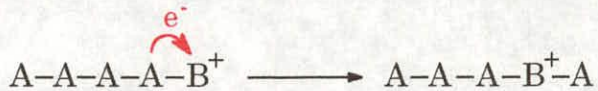

Figure 2.11: Redox hopping mechanism

From this they have shown that the electronic flux through the layer (in the z direction) can be defined by

$$j_{electrons} = D\left[\frac{\partial b}{\partial z} + \left(\frac{ab}{c_t}\right)\frac{F}{RT}\frac{\partial E}{\partial z}\right]$$

where D is the diffusion coefficient for the electrons

a and b are the concentration of A and B respectively

c_t is the total concentration of redox sites in the polymer (i.e. a+b)

E is the applied potential

By inspection, it can be seen that there are two components to the flux. The second term deals with the potential gradient through the coat which is dependent upon the applied potential. In work by most other groups, it is this component which is assumed to be solely responsible for the response of the layer. The first term deals with the flux due to the concentration gradient of oxidised species through the layer due to diffusion of electrons along the polymer backbone. From this Albery and Mount have defined a modified "Nernst potential" E_N (so called due to its similarity to the Nernst equation) which drives the electrons in the polymer backbone

$$E_N = E + \left(\frac{RT}{F}\right)\ln\left(\frac{b}{a}\right) \qquad \text{Equation 2.8}$$

And it is the gradient in this potential which is responsible for driving the flux. It is clear from this equation that it is possible to have a variation in polymer composition throughout the coat but, as long as the potential throughout the film varies and is the Nernst value for the

particular composition, an equilibrium can be established and no current will flow. This is the reason why the applied potential E alone cannot be used.

The ionic flux in the pores is given by

$$j_{counterions} = D\left[\frac{\partial c}{\partial z} \pm \frac{cF}{RT}\frac{\partial E}{\partial z}\right]$$

where c is the concentration of counterions in the pores and the ± allows for differing charge on the counterion. As before, a potential can be defined which controls the movement of counterions within the pores in the film. This modified potential is referred to as the "Donnan potential" E_D due to its similarity to an equation proposed by Donnan to describe the potential at a membrane/electrolyte interface[22]

$$E_D = E - \left(\frac{RT}{F}\right)\ln\left(\frac{c}{s}\right) \qquad \text{Equation 2.9}$$

where E′ is the potential applied to the pores

s is the concentration of counterion in the bulk electrolyte.

It should be noted that this new potential includes a modification caused by the concentration gradient between the bulk electrolyte and the pores in the polymer coat. This correction term, like that in the Nernst potential, is often neglected by other workers in the field.

The extended capacitance C must also be modified to account for these new potentials. As mentioned before, the capacitance is in place to preserve the electroneutrality of the polymer film. It also, however, exists to allow for the existence of a potential difference between the polymer matrix and the pores as proposed by Feldberg[23]. However, as has just been noted, not only may this difference exist, but the potentials experienced by the various areas of the coat may also be different from

the applied potential. This means that the total capacitance of the system must be made up of a combination of the distributed Feldberg capacitance, a capacitance due to the Nernst potential and a capacitance due to the Donnan potential instead of simply considering the distributed double layer capacitance only as several other groups have done. This is perhaps easier to understand by examining figure 2.12.

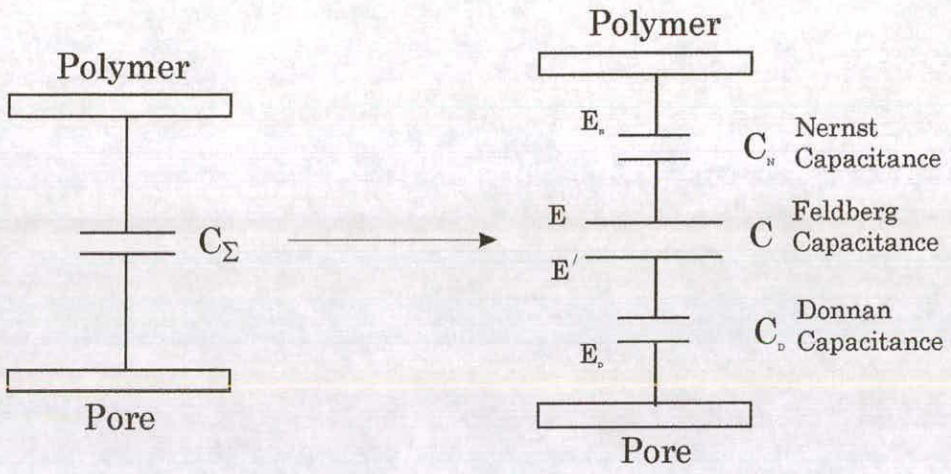

Figure 2.12: Changes to the layer capacitance due to introduction of modified potentials

The total capacitance of the film C_Σ can be given by

$$\frac{1}{C_\Sigma} = \frac{1}{C} + \left(\frac{RT}{ALF^2}\right)\left(\frac{c}{ab}\right) + \left(\frac{RT}{ALF^2}\right)\left(\frac{1}{2s}\right) \qquad \text{Equation 2.10}$$

for the case where there are both ion types present within the coat (i.e. no Donnan exclusion is exhibited) and where the concentration of electrolyte is the same both inside and outside the polymer coat. If this is not the case and complete Donnan exclusion exists i.e. only one type of ion is present then, if only anions are present to balance the charge on the oxidised polymer centres, the capacitance becomes

$$\frac{1}{C_\Sigma} = \frac{1}{C} + \left(\frac{RT}{ALF^2}\right)\left(\frac{c}{ab}\right) + \left(\frac{RT}{ALF^2}\right)\left(\frac{1}{b}\right) \qquad \text{Equation 2.11}$$

In both cases, L is the thickness of the polymer film and A is the area of the surface of the electrode onto which the film is attached.

The first term in equations 10 and 11 is the Feldberg term, the second term is the Nernst term and the third the Donnan term. It is interesting that due to the large surface area of the polymer/pore interface, in practice the Feldberg term, which gives a measure of the double layer charging between the polymer and the pores, is often so large as to be insignificant in the above equation and the capacitive section of the general transmission line simplifies down to figure 2.13. This means that the potential in the polymer and in the pores is the same at any position in the film.

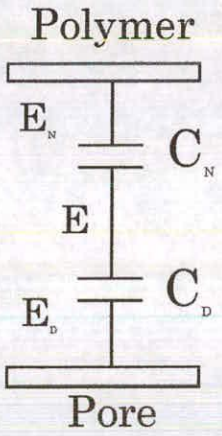

Figure 2.13: Sequence of capacitors used in the general transmission line used for the case where the Feldberg capacitance in insignificant

Once a suitable transmission line has been constructed, it is possible to obtain a theoretical ac impedance spectrum to compare with the experimental results. This is achieved by introducing a small amplitude potential perturbation ΔE into the driving potentials. In practice, this perturbation is applied over a dc bias potential which, as mentioned before, has the effect of setting the system to the required configuration. This gives rise to two effective driving potentials

$$\Delta E_N = \Delta E + \left(\frac{RT}{F}\right)\left(\frac{1}{a}+\frac{1}{b}\right)\Delta b \qquad \text{Equation 2.12}$$

and

$$\Delta E_D = \Delta E - \left(\frac{RT}{F}\right)\Delta c \qquad \text{Equation 2.13}$$

which drive the current through the polymer backbone and the pores of the film. From these, it is possible to obtain the theoretical ac spectrum for the system by taking Laplace transforms. Doing so, gives the theoretical impedance for the classical transmission line as

$$Z = \left(\frac{1}{R_X}+\frac{1}{R_P}\right)^{-1} + \left(\frac{1}{R_X}+\frac{1}{R_P}\right)^{-1} f + \left[\frac{R_X+R_P}{2}+\left(\frac{1}{R_X}+\frac{1}{R_P}\right)^{-1}\right] g$$

Equation 2.14

where

$$f = \frac{[\sinh\theta\cosh\theta - \cos\theta\sin\theta - i(\sinh\theta\cos\theta + \cos\theta\sin\theta)]}{\theta(\sinh^2\theta\cos^2\theta + \cosh^2\theta\sin^2\theta)}$$

$$g = \frac{[\sinh\theta\cosh\theta - \cos\theta\sin\theta - i(\sinh\theta\cosh\theta + \cos\theta\sin\theta)]}{\theta(\sinh^2\theta\cos^2\theta + \cosh^2\theta\sin^2\theta)}$$

and

$$\theta = \sqrt{\frac{[\omega C_\Sigma (R_X + R_P)]}{2}}$$

where ω is the frequency of the ac perturbing pulse (in radians s^{-1}).

At high frequencies, where $\theta \rightarrow \infty$ f and g both tend to zero and so the first term in equation 2.14 dominates. This means that the high frequency intercept, Z_{hf} of the Nyquist plot must give information about the smallest resistance in the transmission line (which dominates the $[1/R_X+1/R_P]^{-1}$ term). However, in reality, the resistance of the electrolyte solution R_{el} also contributes to this intercept i.e.

$$Z_{hf} = R_{el} + \left(\frac{1}{R_X} + \frac{1}{R_P}\right)^{-1} \qquad \text{Equation 2.15}$$

Hence, the current is driven through the solution and the least resistive path through the polymer.

At a frequency determined by the time constant of the distributed capacitance given by

$$\frac{1}{C_{\Sigma}(R_X + R_P)}$$

the overall coat capacitance will begin to charge. This will produce a 45° line (a Warburg region) where

$$-Z_{Im} = Z_{Re} - Z_{hf} = \frac{\left[(R_X + R_P) - 2\left(\frac{1}{R_X} + \frac{1}{R_P}\right)^{-1}\right]}{[2\omega C_{\Sigma}(R_X + R_P)]^{1/2}} \qquad \text{Equation 2.16}$$

until, at very low frequencies, the only process occurring is the charging and discharging of the distributed capacitance through both resistances. When this occurs, a constant real impedance of

$$Z_{Re} = \frac{R_X + R_P}{3} \qquad \text{Equation 2.17}$$

and an imaginary impedance of

$$-Z_{Im} = \frac{1}{\omega C_{\Sigma}} \qquad \text{Equation 2.18}$$

This accounts for the (almost) vertical line seen in some spectra.

If conduction within the polymer itself is indeed by redox hopping, then the resistance will be a minimum when the concentrations of A and B are equal. The polymer resistance (R_P) is given by

$$R_P = \frac{RTL}{AD_P F^2}\left[\frac{1}{a} + \frac{1}{b}\right] \qquad \text{Equation 2.19}$$

where D_P is the diffusion coefficient for movement within the polymer

Turning now to the counterions within the pores of the film, if the concentration of polymer charge in the pores is greater than the bulk electrolyte concentration then there will be a charge imbalance inside the film and a Donnan potential will build up. This causes a large field at the polymer/electrolyte interface to encourage the uptake of the counterion and the expulsion of the coion in order that the coat can be electrically neutral i.e. for a coat whose redox species are positively charged, this will mean that for the electrolyte M^+X^-, this will encourage the displacement of M^+ from the coat and the amassing of X^- within the coat and vice versa. If species A is neutral and B positively charged then when the coat is highly oxidised, the counterion will be an anion and c=b. So,

$$R_X = \frac{LRT}{AF^2}\frac{1}{D_x b} \qquad \text{Equation 2.20}$$

However, if there is no appreciable Donnan exclusion i.e. when c≈s then both counterion and the corresponding electrolyte co-ion will be present in the pores. In this case,

$$R_X = \frac{LRT}{AF^2}\left[\frac{1}{D_X s}+\frac{1}{D_M s}\right] \qquad \text{Equation 2.21}$$

where D_X and D_M are the diffusion coefficients of the X^- and M^+ ions respectively.

Applying these novel potentials and capacitances, Albery et al have attempted to construct a number of transmission lines in order to find the best possible model.

One particular model has been proposed in an attempt to discover what happened in the case of a reduced or lightly oxidised coat where there are two types of charge carrier present within the pore of the film[21] - both

cations and anions. (Previously, models have assumed that there is complete Donnan exclusion preventing one of the ionic charge carriers from entering the coat.) Albery and Mount have modelled using a transmission line where the polymer is a wire of zero resistance and the pores are two separate resistors of finite resistance R_X for anions and R_M for the cations - figure 2.14.

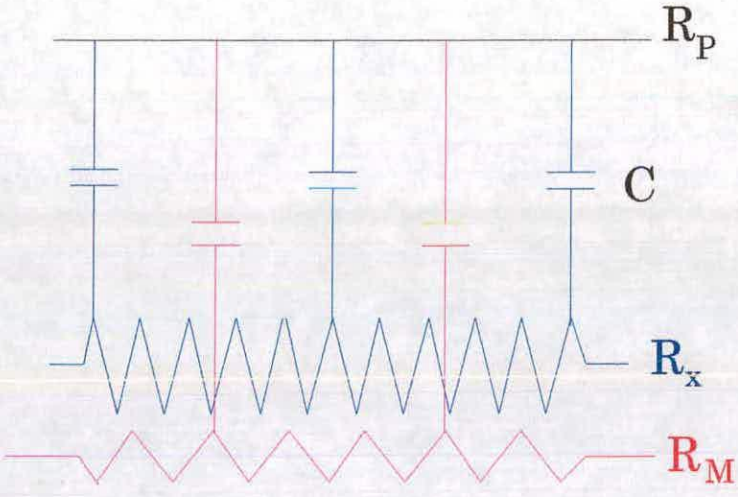

Figure 2.14: Transmission line proposed to model a conducting polymer with two charge carriers in the pores.

They mention that is it entirely feasible for R_P to have a finite resistance but that the mathematics become awe-inspiring. In this work, Albery et al. have found that in general the response of this system to a small potential perturbation is biphasic i.e. on oxidising such a layer further, first the cation is moved (assuming that the cation is the more mobile species). This builds up a field inside the coat between the ions which "drags" the associated anion along and, in some cases, can pull the cation back slightly, giving the impression that the movement of the charge carriers are coupled. This is contradictory to suggestions by Buck[24] who found that, in order to solve the mathematics, he had to impose the condition that the motion of the ions within the layer must be coupled on a microscopic scale without the need for an induced field caused by the

separation of the ions. One by-product of this work by Albery and Mount was the discovery that under certain circumstances, the capacitive region of the ac spectrum in a Nyquist plot was at less that 90°. As has been mentioned previously, this has been generally ascribed to the inhomogeneity of the polymer film. However, since this factor was not considered during the course of the mathematics, Albery and Mount have inadvertently shown that another cause is possible.

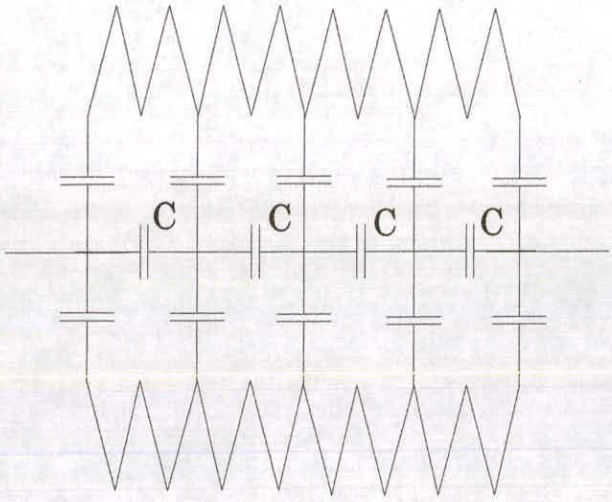

Figure 2.15: Transmission line used by Buck to model cationic and anionic movement in inert polymers and solutions

It is interesting to mention that recent work by Buck[25] has made use of the network analysis program Spice and a transmission line similar to that shown in figure 2.15. The capacitances, C, located along the centre of the circuit allow for the possibility of a potential difference existing between different areas of the polymer film. However, this capacitance would extend through the whole coat and be in series and so, since

$$C_{total} = C/N$$

would be very small. Hence, this capacitance will have a very low time constant for charging. At frequencies over which ac response is generally investigated, these capacitances would all be charged and would, therefore, have a very high impedance and no charge will able to pass

through. In this region, the transmission line would collapse down to the general case proposed by Albery and Mount without the presence of the kinetic barriers at the interface. However, analysis using the Spice program involves the need to limit the transmission line to a finite number of circuit elements and so does not provide the full analytical solution provided by the Albery and Mount approach.

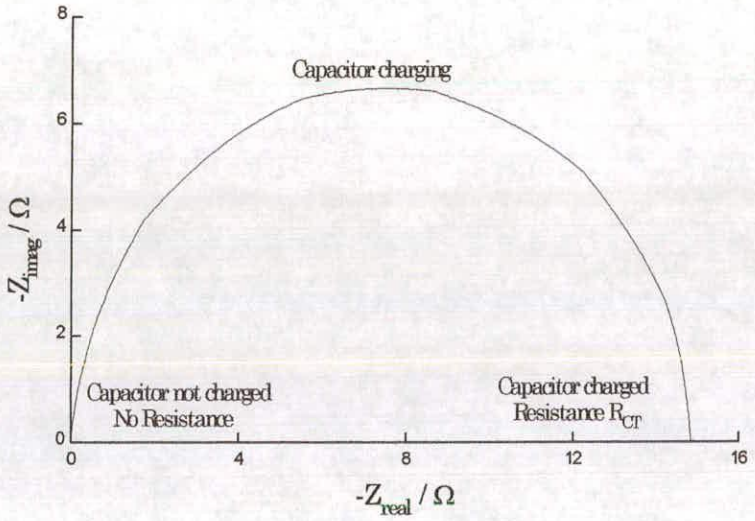

Figure 2.16: Semicircle region seen in some ac spectra of conducting polymers

The models shown previously, figure 2.8 And 2.9, have been used to successfully model ac spectra of poly(vinylferrocene)[19] which, like a number of relatively simple systems show only a 45° Warburg region and a 90° capacitive region. However, not all systems give such a simple Nyquist spectrum. A number of organic polymer systems such as poly(pyrrole)[17] show semicircular regions at high frequencies in their ac spectra, figure 2.16. These semicircular areas can best be modelled using Randles circuit comprising a resistance and capacitance in parallel, figure 2.17

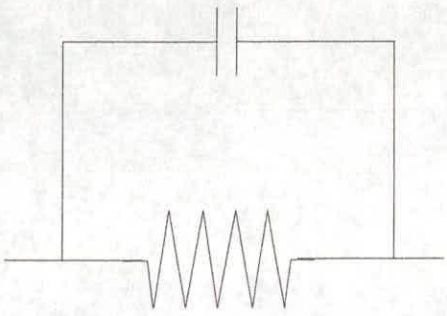

Figure 2.17: Randles circuit element

The nature of this semicircle can easily be accounted for by considering the magnitude of the phase lag of the obtained signal as the frequency of the perturbing signal is altered. At very high frequencies, the charge is carried through the circuit by the rapid charging and discharging of the capacitor. However, this charging/discharging is carried out over such a short time scale that the capacitor does not have time to charge by any significant amount. Hence, the circuit behaves as a wire with no resistance and the resultant signal has no phase lag. At very low frequencies, the capacitor has time to become fully charged and so all of the charge will go through the resistor. This will show as a non-zero intercept on the real axis of the Nyquist plot. In between these two extremes, the capacitor is gradually allowed to charge up. When the frequency of the perturbing signal is the inverse of the CR time constant for the Randles circuit, the phase lag between the perturbing signal and the resultant relaxing signal will be at a maximum. This is shown by a maximum imaginary impedance forming the semicircle. The impedance of this parallel CR circuit is given by

$$Z_{CR} = \frac{R_{K,P} - i\omega C_{DL,P} R_{K,P}^2}{1 + \left(\omega C_{DL,P} R_{K,P}\right)^2} \qquad \text{Equation 2.22}$$

where the subscript K denotes a kinetic barrier, DL the double layer capacitance and P the location of the barrier, in this case at the electrode/polymer interface.

The model proposed by Albery et al. to tackle this problem is shown in figure 2.18[20]. It was initially felt that the presence of the Randles circuit could be due to the redox hopping nature of conduction in some polymer systems where the rate determining step would be the movement of electrons between individual polymer strands. Here, the movement of ions in the pores of the coat was modelled as before with a resistance R_X but the movement of electrons in the polymer was simulated by a wire of zero resistance joined together with a Randles circuit as shown. It should be noted that the distributed capacitance C in figure 2.18 is, in this case, equal to C_iN where N is the number of transmission line segments. However, comparing the output of this model with suitable experimental results showed that a semicircle could not be obtained if more than two of these Randles circuits existed. However, it is unlikely that electronic conduction through any real polymer would take place in so few steps and so this cannot be the origin of the semicircular features. It is more likely, therefor, that these barriers will exist at the interfaces (electrode/polymer and/or polymer/electrolyte) instead. This has allowed the possibility of achieving a good fit to ac data which, like that for polypyrrole, exhibited a semicircle at high frequencies.

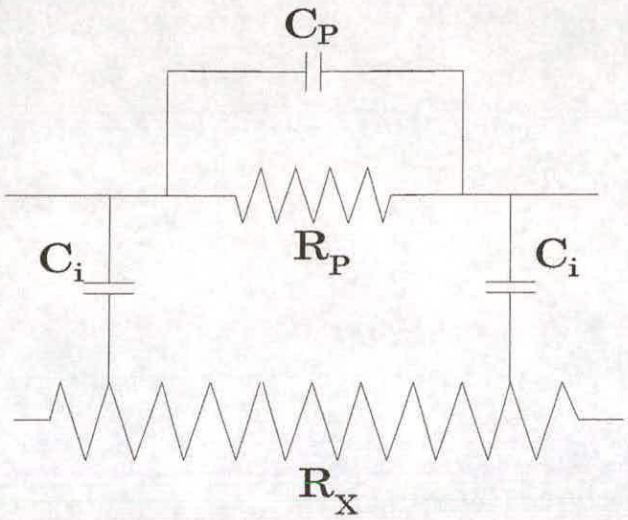

Figure 2.18: Transmission line proposed by Albery et al to model redox hopping in conducting polymers

This barrier has been shown to exist for a number of polymer systems[26,27] and can take a number of different forms such as a kinetic barrier to electron movement from the electrode to the polymer or simply a difference in morphology between the polymer near the electrode surface and the bulk. In modelling this type of system, the resistance R_P in the Randles circuit in figure 2.17 is generally referred to as a charge transfer resistance R_{CT} with an associated double layer capacitance C_{DL}. It has also been found that there can also be a similar kinetic barrier at the polymer/electrolyte interface due to, for example, desolvation of counterion before it can enter the coat. The main difficulty in analysing data using a transmission line incorporating a charge transfer section comes in deciding the exact arrangement of the charge transfer Randles circuit (just which part of the transmission line the capacitance C_{DL} short circuits). One of the main causes of this is that the movement of charge in the charge transfer resistance R_{CT} is driven by either E_N or E_D depending on which interface the barrier is located at whereas C_{DL} is charged by the applied potential E. In the earlier treatments, for a system with a kinetic barrier at one interface only, four possible cases

were thought to exist (two for each interfacial region). The possible cases for a barrier located at the electrode/polymer interface are shown in figure 2.19. Similar circuits exist for a barrier at the polymer electrolyte interface. It should be noted that for ease of mathematics, this work assumed that the less resistive rail could be modelled as a wire. However, this is an unnecessary restriction and, in general, two resistances are required to accurately model the system.

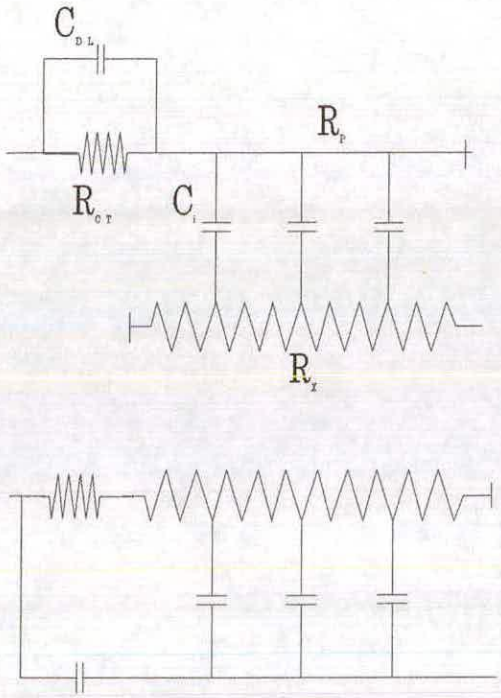

Figure 2.19: The possible circuits for a for a system with a kinetic barrier at the electrode/polymer interface

Initially, in order to tell each case apart, graphical analysis of the ac data was required. However, recent thoughts as to the nature of the capacitance C_Σ as detailed previously have reduced this to only two cases - a barrier at the electrode/polymer interface or at the polymer/electrolyte interface. The fact that the potential in either the polymer or pore rail has to be modified with either C_N or C_D respectively means that the

applied potential must first go through one of these modifying capacitances before being fed into the polymer or pore rail. Once this is achieved, the route that the charge takes will be dependent upon the relative magnitudes of these modifying capacitances. This modification of approach has allowed for a transmission line which, as well as a charge transfer barrier, contains 2 resistance rails both of which have non-zero resistance. For a barrier at the electrode/polymer interface, the transmission line is shown in figure 2.20.

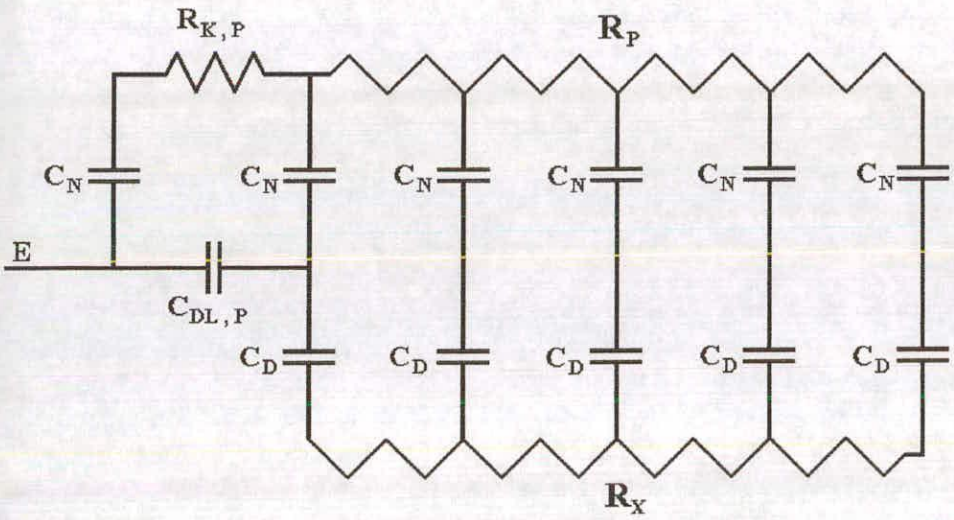

Figure 2.20: Transmission line showing up to date theory for incorporation of a single charge transfer Randles circuit with a negligible Feldberg capacitance

At first, this may seem to be a very complicated system, but by judicious choice of film conditions, it can be easily simplified. The main difficulty in using the circuit shown in figure 2.20 is in mathematically combining the response of both the simple transmission line with the response of the Randles CR circuit. However, if the polymer film is sufficiently thick then the distributed capacitance C_Σ will be very large compared to C_{DL} and CR time constants for the individual circuits will be very different with $C_{DL}R_K << C_\Sigma R_{Pol}$ where C_Σ is the total capacitance of the coat (and so

includes C_N and C_D) and R_{pol} is the resistance of the polymer coat. This means that ac responses of these circuit elements will be separate from one another and no mixing of the signals will occur. Since each response is discrete then the total response will simply be a linear combination of the two signals i.e.

Total impedance response	=	response from the classical transmission line	+	response from the Randles circuit

However, out of all of these possible transmission line circuits, it is the transmission line proposed by Albery and Mount as shown in figure 2.9 improved with the modified capacitance given in figure 2.13 which has the most practical application. It is this general model which is used in this thesis although in a number of cases, it has been extended to include charge transfer Randles circuits at both the electrode/polymer and the polymer/electrolyte as seen in figure 2.21. It is believed that this more general transmission line circuit will be applicable in the simulation of a wide range of polymer systems and provide a very powerful tool in their analysis.

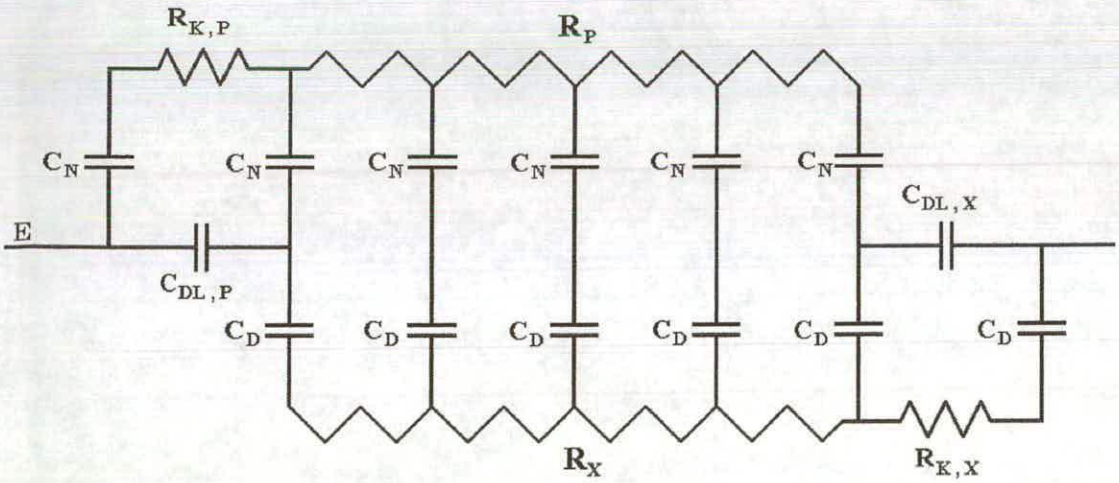

Figure 2.21: General transmission line used to model the polymer impedance data in this thesis

2.3.3. Analysis Of Experimental Results

It is of major importance that, when analysing experimental data, good agreement between observed and calculated values is obtained at all frequencies. In this work, results obtained from ac impedance results were analysed iteratively using a non-linear regression curve fitting package in SigmaPlot, a program developed by Jandel Scientific. This involved inputting the real impedances, Z_{Re}, as positive values and the imaginary impedances, Z_{Im}, as negative values. The program was then instructed to fit the positive values to the equation for Z_{Re} and the negative values to the expression for Z_{Im} as a function of frequency. These equations are dependent on the exact nature of the transmission line used, however, in practice, models containing one charge transfer (CT) circuit only, one CT circuit and one transmission line and two charge transfer circuits and one transmission line were used in that order until a reasonable fit was obtained. (All spectra fitted show the presence of a kinetic barrier and so it was not necessary to fit to a model containing no CT circuit elements). (The functions used in the fitting session are detailed in Appendix A). The goodness of this fit is then found by plotting the experimentally derived values against the calculated values and then carrying out a linear regression on the data. A good fit is then given by a line of gradient one passing through the origin. This method is comparable to other techniques such as comparing experimental and calculated Nyquist plots. However, our method has the advantage that the variation of the real and imaginary impedances with frequency are more clearly shown whereas Nyquist plots show only correlation between the real and imaginary impedances, but not frequency. This method also allows any slight deviations in the fit to be identified. Typical diagnostic plots for a good and poor fit for a poly(indole-5-carboxylic acid) coat are shown in figures 2.22 and 2.23

respectively. The associated Nyquist plots are shown in figure 2.24 for comparison.

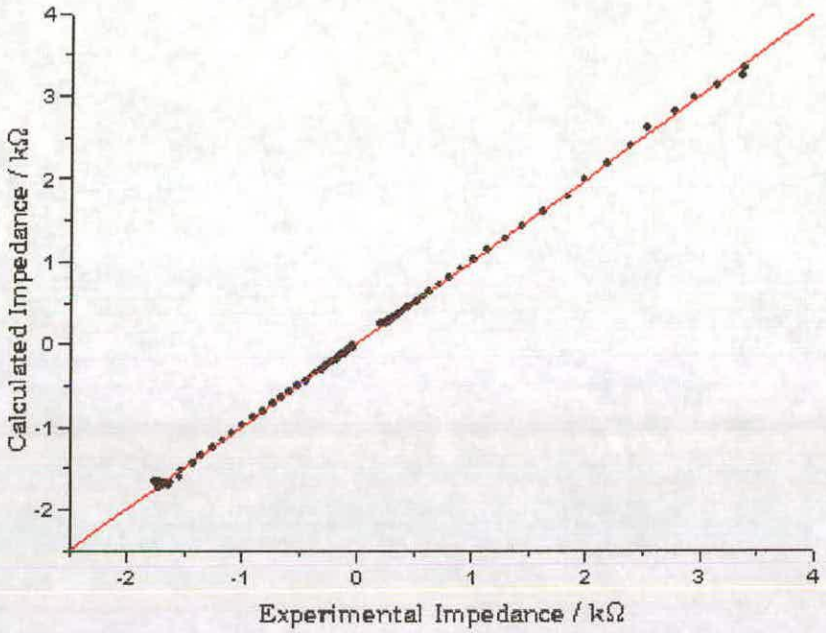

Figure 2.22: Example of a good fit to theory using SigmaPlot
Gradient=0.99969; Intercept=0.00404; Correlation coefficient=0.9997

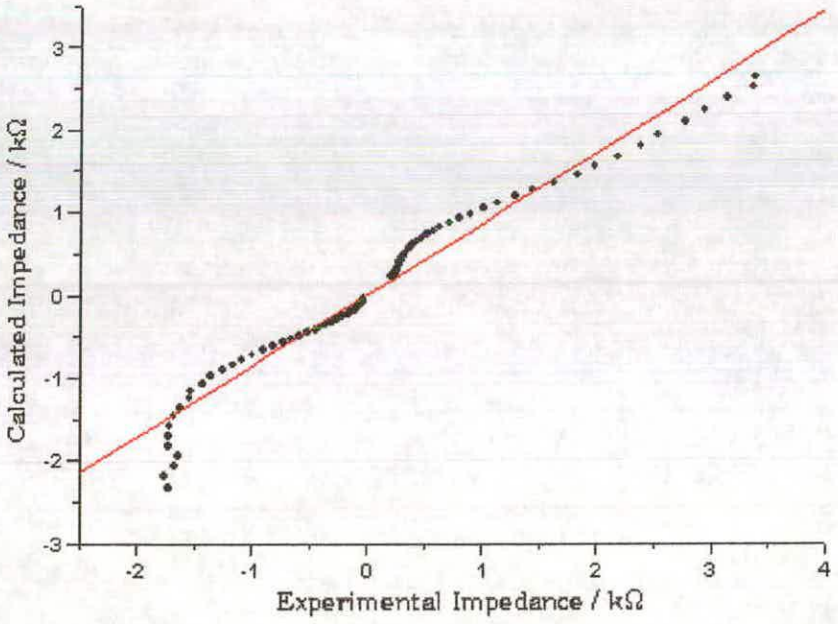

Figure 2.23: Example of a bad fit to theory using SigmaPlot
Gradient=0.85991; Intercept=0.00444; Correlation coefficient=0.9778

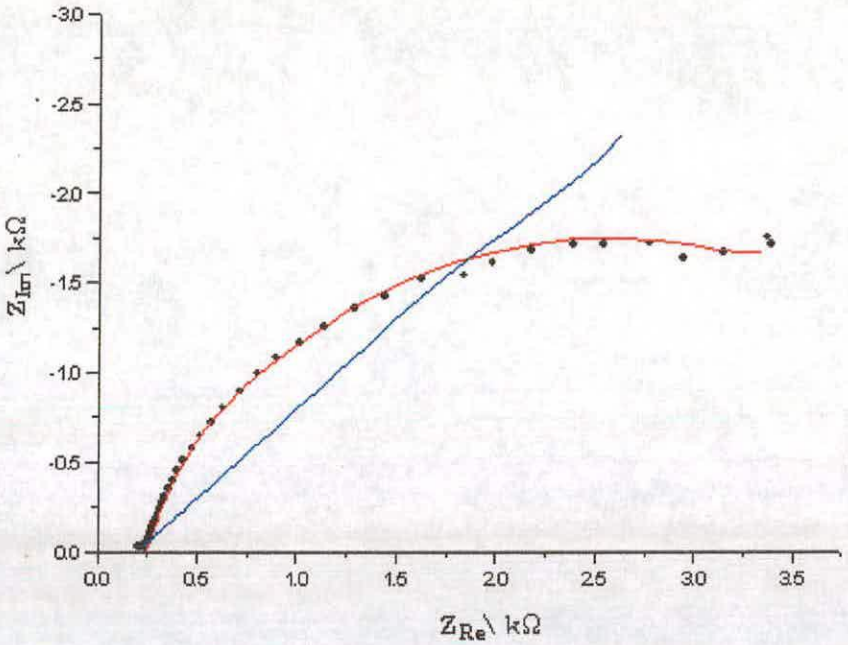

Figure 2.24: Nyquist plots for data shown in figure 2.22 and 2.23

(• Experimental data; — Good fit data; — Poor fit data)

2.4 References

1. V.G. Levich; *Acta Phys. Chim.*, 1942 17, 257

2. W.J. McCarter; *J. Mater. Sci.*, 1996, **31**, 6285

3. P. Gu, P. Xie, J.J. Beaudoin; *Cement, Concrete and Aggregates*, 1995, **17**, 92

4. W.G. Kubicek, J.N. Karnegis, R.P. Patterson, D.A. Witsoe, R.H. Mattson; *Aerospace Med.*, 1966, **37**, 1208

5. M.J. World; *J. Roy. Army Med. Corps*, 1990, **136**, 92

6. V.S. Novitskii, M. Ya. Orishchenko, V.S. Kuzub; *Protection of Metals USSR*, 1987, **23**, 693

7. P. Gu, J.J. Beaudoin; *Adv. In Cement Research*, 1998, **10**, 43

8. S. Magaino; *Electrochim. Acta*, 1997, **42**, 377

9. M.A. Vorotyntsev, L.I. Daikhin, M.D. Levi; *J. Electroanal. Chem.*, 1994, **364**, 37

10. R. Borkowska, M. Siekierski, J. Przyluski; *App. Surface Sci.*, 1996, **92**, 447

11. T. Matencio, V. Mano, M.I. Felisberti, M.A. Depaoli; *Electrochim. Acta*, 1994, **39**, 1393

12. G.S. Popkirov; *Electrochim. Acta*, 1996, **41**, 1023

13. R.L. Zeller, R.F. Savinell; *Corrosion Science*, 1986, **26**, 591

14. G.S. Popkirov, R.N. Schindler; *Electrochim. Acta*, 1994, **39**, 2025

15. S. Bhatnagar, S. Gupta, K. Shahi; *Solid State Ionics*, 1988, **31**, 107

16. A.M. Waller, R.G. Compton; *J. Chem. Soc. Faraday Trans.*, 1989, **85**, 977

17. W.J. Albery, Z. Chen, B.R. Horrocks, A.R. Mount, P.J.Wilson, D. Bloor, A.T. Monkman, C.M. Elliot; *Faraday Discuss. Chem. Soc.*, 1989, **88**, 247

18. W.J. Albery, C.M.Elliot, A.R. Mount; *J. Electroanal. Chem.*, 1990, **288**, 15

19. W.J. Albery, A.R. Mount; *J. Chem. Soc. Faraday Trans.*, 1993, **89**, 327

20. W.J. Albery, A.R. Mount; *J. Electroanal. Chem.*, 1991, **305**, 3

21. W.J. Albery, A.R. Mount; *J. Chem. Soc. Faraday Trans.*, 1993, **89**, 2487

22. F.G. Donnan; *Z. Elektrochem*, 1911, **17**, 572

23. S.W. Feldberg; *J. Am. Chem. Soc.*, 1984, **106**, 4671

24. R.P. Buck, T.R. Brumleve; *J. Electroanal. Chem.*, 1981, **126**, 73

25. R.P. Buck, C. Mundt; *J. Chem. Soc. Faraday Trans.*, 1996, **92**, 4987

26. I. Rubinstein, E. Sabatini, J. Rishpon; *J. Electrochem. Soc.*, 1987, **134**, 3078

27. A.M. Walker, R.G. Compton; *J. Chem. Soc. Faraday Trans I.*, 1989, **85**, 977

3. Experimental

The following chapter details the experimental set-ups used to obtain the results reported in the proceeding chapters.

3.1 Hardware

3.1.1 Standard Electrochemical Equipment

For the early cyclic voltammetry work on indole-5-carboxylic acid, a portable potentiostat (Oxford Electrodes PP2) was used in conjunction with a PPRI Waveform generator (Hi-Tek Instruments) to provide the wave signal. Measurements were recorded on a x-y-t chart recorder (Advance Bryans 60000).

For later work, including pH studies and ring-disc work, the smaller portable unit was replaced with a modular potentiostat/galvanostat with combined waveform generator and voltage sources (Oxford Electrodes).

The potentiostat circuitry is shown in figure 3.1.

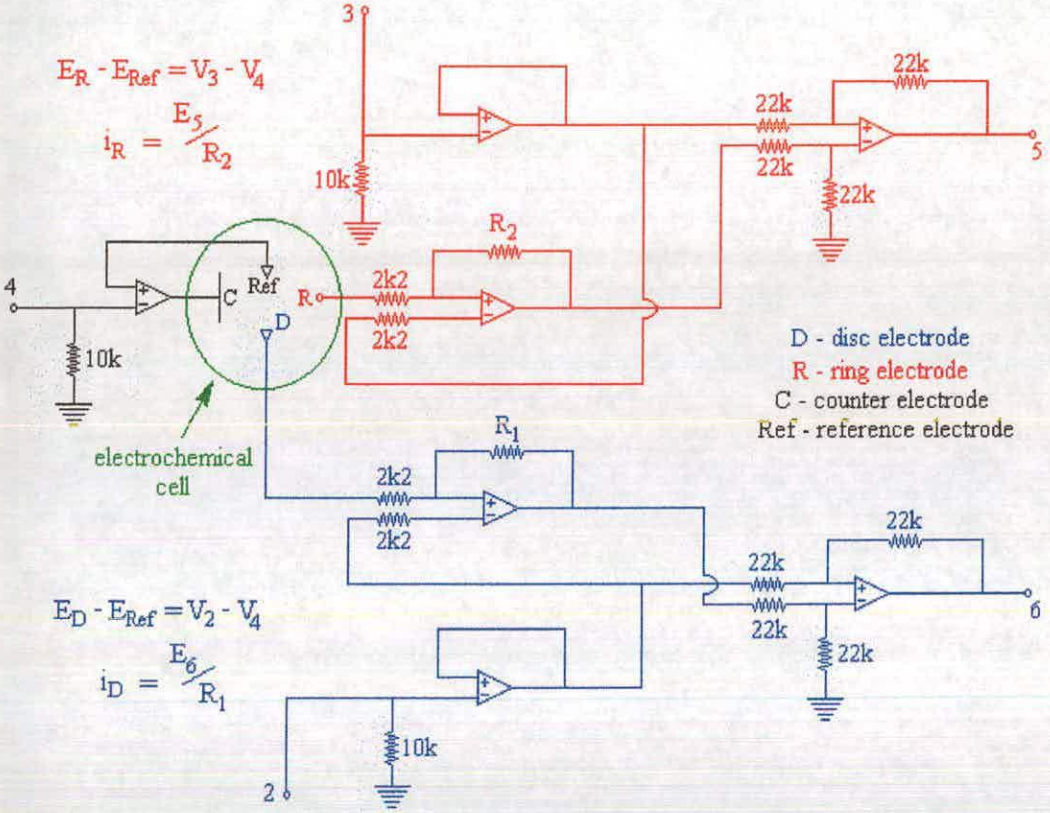

Figure 3.1: Circuit diagram for potentiostat used

For rotating disc and ring-ring disc work, a rotating disc assembly and associating motor controller (both from Oxford Electrodes) were used. Such a set-up has been described fully elsewhere[1]

3.1.2 AC Measurements

A.c. Measurements were taken using an a.c. spectrometer (Sycopel Scientific Ltd. TFA2000A) via a frequency response analyser (Voltech TF2000). The data was collected and stored on a 386MHz laptop computer (Toshiba T1900) running the TFA2000A control software. Data for the spectrometer were saved as an ASCII file and exported for further analysis.

3.1.3 Miscellaneous Equipment

pH measurements were taken using a combination pH probe (Mettler Inlab 405) and displayed using a pH meter (Mettler Delta).

Potentials were measured using a hand held digital volt meter (Radio Spares/Fluke model 75).

During transient studies, the charge passed was recorded using an integrator system constructed in house. A simplified circuit diagram for this apparatus is shown in figure 3.2.

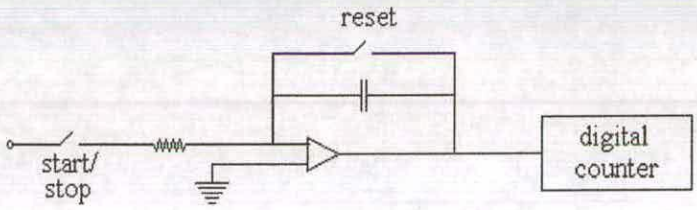

Figure 3.2: Simplified circuit diagram for the charge integrator used

3.1.4 Electrodes

3.1.4.1 Working Electrode

The working electrode for all of the work detailed in this thesis consisted of a platinum disc electrode (Oxford Electrodes) with an area of 0.387cm^2 (diameter of 7.0mm) surrounded by an insulating sheath of PTFE. For the ring disc work, this was altered by the inclusion of a Pt ring (diameter of 8mm) concentric to the disc electrode with a thin layer of PTFE (diameter of 7.5mm) between them.

The working electrodes were cleaned before use with a water slurry of alumina in deionised water on a diamond polishing cloth and then washed thoroughly in deionised water. The working electrode was regularly cleaned further by cycling a number of times past the solvent limits (both anodic and cathodic) in aqueous sulphuric acid (0.1M, Fissons).

3.1.4.2 Counter Electrode

The counter electrode was a piece of platinum gauze with an area of 2cm^2.

The counter electrode was cleaned regularly by immersion in concentrated hydrochloric acid (BDH) and then rinsed with deionised water followed by heating until red hot in a micro-Bunsen burner.

3.1.4.3 Reference Electrodes

The reference electrode used for the non-aqueous studies was an Ag / Ag^+ electrode constructed in-house. The electrode comprised of a silver wire dipping into a solution of 0.01M silver perchlorate (99%, Aldrich) in background electrolyte.

This electrode has a potential of +0.437V with respect to the saturated calomel electrode and +0.681V compared to the normal hydrogen electrode. All non-aqueous potentials quoted in the following chapters are given with respect to this electrode.

For aqueous work, a saturated calomel electrode (SCE, Russell Electrodes) was employed.

3.2 Chemicals

Unless otherwise stated, all chemicals reported were of AnalaR grade or equivalent.

3.2.1 Indole Derivatives

Indole-5-carboxylic acid (99%, Aldrich) was recrystallised twice from deionised water and dried in an oven at 130°C for three days before use. 5-cyanoindole (99%, Aldrich) was recrystallised from ethanol (Prolabo) and dried *in vacuo*.

3.2.2 Electrolytes

The main electrolyte used in this series of investigations, was 0.1M lithium perchlorate (Aldrich 99%+ and Fisons 99%) in acetonitrile (Prolabo). The lithium perchlorate was dried *in vacuo* for two days prior to use while the acetonitrile was used as received.

Other non-aqueous electrolytes used were sodium perchlorate (Fluka), Tetraethylammonium perchlorate (Fluka), Tetraethylammonium tetrafluoroborate (Fluka), Tetraethylammonium hexafluorophosphate (Fluka). All were used as received in the production of 0.1M solutions, unless otherwise stated, in acetonitrile.

For non-aqueous work, potassium chloride (99.5%, Prolabo) was used as received and made up as a 0.1M solution in deionised water (from a Millipore Milli-ro 15 system)

3.2.3 Other Chemicals

Ferrocene (Fluka) and argon gas (BOC) were used as received.

3.3 Experimental Technique

3.3.1 Electrochemical polymerisation

Indole-5-carboxylic acid (I5CA) was polymerised onto a polished platinum disc electrode by application of a potential of +1.46V to a solution of I5CA (100mM unless otherwise stated) in background electrolyte (0.1M $LiClO_4$ in acetonitrile) until a film of required thickness was obtained. While the potential was applied, the electrode was rotated at 4Hz. From previous work[2] this was deemed to give a good, reproducible film with a high proportion of the I5CA trimer.

5-cyanoindole (5CI) was polymerised from a solution in background electrolyte (100mM unless otherwise stated) at an oxidising potential of +1.64V. Again, during electropolymerisation, the working electrode was rotated at 4Hz to give a polymer coat with reproducible morphology.

The I5CA/5CI copolymers were deposited under similar conditions with the application of a potential of +1.64V. This ensured that both monomer species underwent electrooxidation under mass transport limited conditions. In all cases, the total concentration of monomer present was 100mM.

In all cases, the time taken for polymerisation was kept constant at 20 seconds. This enabled the growth of a film approximately 2000 monolayers thick. During all electropolymerisation processes, the reproducibility of coat production was verified by examination of the constant current-time transients taken as the films were deposited.

3.3.2 Cyclic Voltammetry

Cyclic voltammograms were taken using a potentiostat (Oxford Electrodes) and the standard 3 electrode assembly. Hardcopy was obtained using the x-y-t chart recorder. Before cycling, the electrolyte solution used was degassed using argon. The argon was first passed through a flask of acetonitrile to prevent evaporation of the supporting electrolyte solution.

3.3.3 Ac Impedance Spectroscopy

All ac spectra were taken using the TFA2000A and the standard 3 electrode assembly. The applied sinusoidal perturbation was set to 10mV and spectra were taken in the 10kHz to 1Hz or 10kHz to 0.1Hz frequency ranges. The experiments were carried out in various background electrolytes (all 0.1M in concentration unless otherwise stated). Before any ac measurements, the electrolyte solution was thoroughly degassed by bubbling argon saturated with acetonitrile through it for 20 minutes to remove any oxygen dissolved in the solution. Argon was then passed over the surface of the reaction vessel to prevent any reintroduction of oxygen during the experiment.

3.3.4 pH Studies

For investigation of the pH responses of the various coats, the polymer films were first prepared in a non-aqueous background electrolyte (0.1M $LiClO_4$ in MeCN) and then transferred gradually into an aqueous electrolyte (0.1M KCl in deionised water) to prevent the build-up of

osmotic pressure in the coat. If this procedure was not followed, the polymer film became detached from the electrode surface. The polymer modified working electrode was then placed into pure, fresh aqueous electrolyte and the solution made acidic (pH3) by the gradual addition of 1M HCl. The film potential was measured with respect to the standard calomel electrode by buffering the outputs before sending them to the subtractor of the Oxford Electrodes modular potentiostat. The pH of the system was progressively made more alkaline by addition of KOH, while rotating the working electrode at 2Hz to ensure pH equilibrium, to the electrolyte. After allowing some time for equilibrium to be reached, the potential was then measured with respect to the SCE. The amount of alkali added was reduced both in concentration and amount as pH7 was neared. During the experiment, care was taken that the solution pH stayed within the limits of pH3 to pH9 outside of which it was observed that the indole films became soluble and dissolved from the surface of the electrode.

3.3.5 Charge Studies and Chronoamperometry

The polymer under investigation was deposited onto a disc electrode and the total charge passed during the polymerisation process obtained from the integrator. The coat potential was then switched between a reducing (-400mV) and oxidising (250mV) potential and the charge passed on application of each pulse, as well as the resultant transient, recorded.

3.3.6 Rotating Disc Studies

The kinetics of charge conduction were studied by examining the rate of charge transfer (i.e. current) from a well known redox system through a film of the polymer in question deposited onto the surface of a disc working electrode. The redox species used for this was ferrocene (in non-aqueous solution with background electrolyte). The potential across the film was held at a potential suitable to ensure that the redox reaction was under mass transport control and the current at a series of rotation speeds recorded as a current-time trace on the chart recorder. These values were then subjected to Levich and Koutecky-Levich analysis and the results plotted.

3.4 References

1 A.R. Mount; *PhD. Thesis*, Imperial College, London, 1987

2 J.G. Mackintosh, A.R. Mount; *J. Chem. Soc. – Faraday Trans.*, 1994, **90**, 1121

4. Indole-5-Carboxylic Acid

4.1 Introduction

Reports have suggested that indole-5-carboxylic acid has a possible use as a fast pH sensor. However, studies have shown that cycling the coat between its oxidised and reduced states dramatically alters its voltammetric response. Initially, these results were considered to be simply a product of coat degradation However, observations have shown this to be a real effect caused by the changing oxidation state. This change could seriously affect the response of an indole-based sensor and so must be fully understood. Ac impedance has been used to probe this change.

It is hoped that poly(indole-5-carboxylic acid) will provide a useful standard with which to model other polymer systems which undergo a similar change from hydrophobic to hydrophilic behaviour.

4.2 Cyclic Voltammetry

A large amount of work has been carried out previously on the cyclic voltammetry of indole-5-carboxylic acid films. However, most of the work done up until now has been over short time scales and/or using relatively fast scan speeds[1,2]. However, working at slow scan speeds allows the cyclic voltammetry to have a time scale similar to that of the ac experiments. Initial cyclic voltammograms recorded directly after the deposition of the polymer film are similar to that shown in figure 4.1.

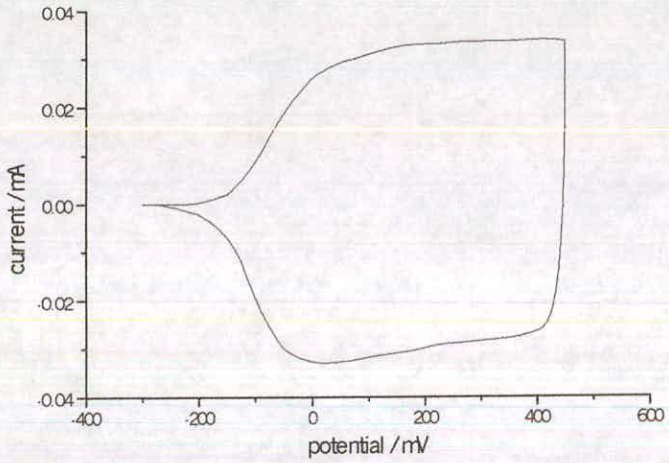

Figure 4.1: CV of poly(indole-5-carboxylic acid) taken after film deposition onto electrode surface. Scan speed = 2½mVs^{-1}

The CV shows two distinct regions. At low potentials, there is essentially no current visible. At more positive potentials, the CV displays a wide almost featureless envelope indicative of the presence of a constant capacitance (a pseudo-capacitance). This CV displays neither the sharply peaked features expected from a reversible system nor the widely spaced peaks diagnostic of an irreversible system. The complete lack of redox features seems to indicate that the polymer layer is not behaving as a

reversible one electron system expected from other work[1,2] but is instead behaving as if it were a metal electrode with a large surface area. The high pseudo-capacitance seen of the voltammogram suggests that, more accurately, the polymer acts as a porous metal containing a large concentration of charge species.

After continuous slow cycling over a number of days, the capacitive envelope still exists but redox peaks begin to appear, figure 4.2.

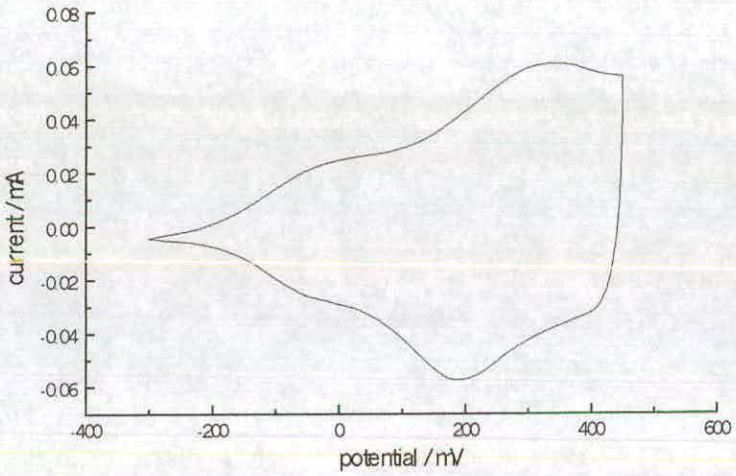

Figure 4.2: CV of poly(indole-5-carboxylic acid) after cycling for a number of days. Scan speed = 2½mVs^{-1}

After repeated slow cycling over a long time scale (of the order of 2-3 weeks), redox features appear and the capacitive envelope drops, figure 4.3.

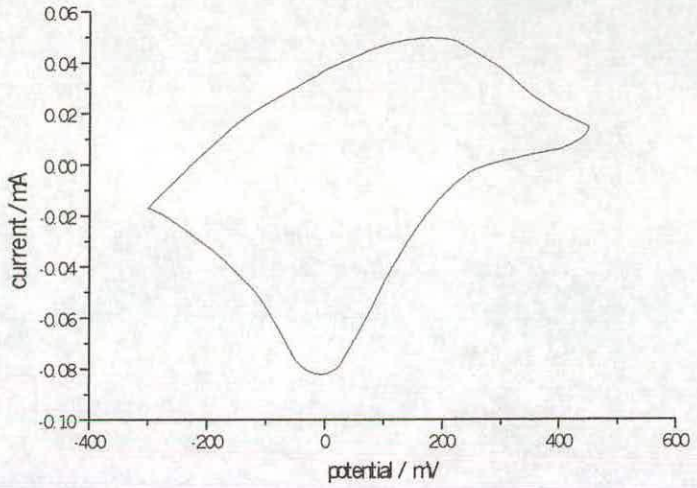

Figure 4.3: CV of poly(indole-5-carboxylic acid) after extensive cycling.
Scan speed = 2½mVs^{-1}

This represents a major change in the behaviour of the coat on a timescale consistent with solid state diffusion and could be ascribed to a change in the coat morphology. The rate of this change has been found to increase proportionally with the time spent at high positive potentials (greater than 300 mV) and is chemically irreversible, at least in a comparable timescale to the change from its initial state.

This altered form of the coat has been found to exhibit a cation sensitivity. Studies have been carried out changing the nature of the cation in the electrolyte. The result of this investigation is shown in figure 4.5 and 4.6.

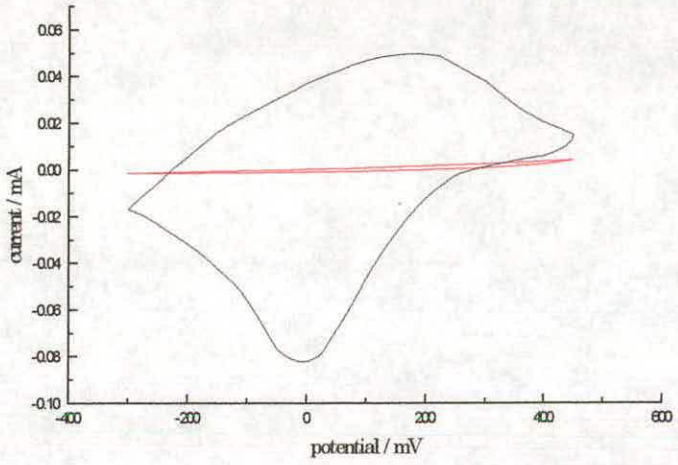

Figure 4.5: CVs of poly(I5CA) before and immediately after transfer to 0.1M $NaClO_4$ in acetonitrile. (— $LiClO_4$; — $NaClO_4$)

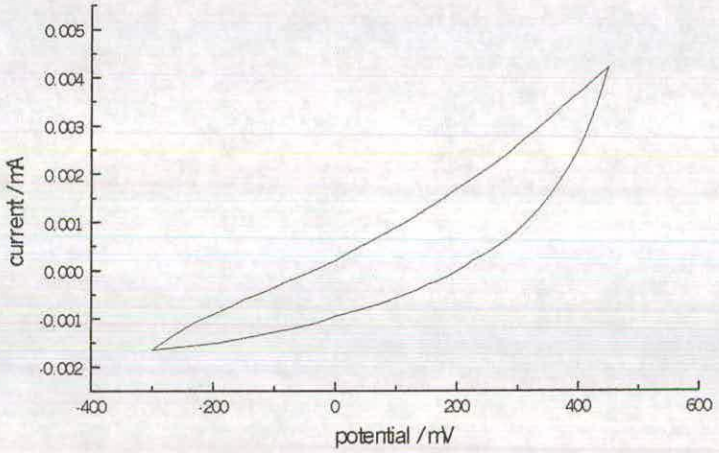

Figure 4.6: Enlarged view of CV taken in 0.1M $NaClO_4$, immediately after transfer from $LiClO_4$

It can be clearly seen that increasing the size of the cation initially removes any redox characteristics. From this it can be concluded that the redox peaks observed for this polymer film involve the incorporation of cation into the coat and its subsequent expulsion. Increasing the cation

size prevents this incorporation due to the limited size of the pores within the film. It is interesting to note that repeated cycling in $NaClO_4$ causes these peaks to reappear though with a much reduced current compared to the 0.1M $LiClO_4$ case, figure 4.7, which could be due to the relaxation of the coat structure and the resultant widening of the polymer pores.

CVs have also been recorded in various concentrations of $LiClO_4$ in acetonitrile. These are reproduced in figure 4.8. These results seem to bear out the previous conclusions as to the cause of the redox peaks. It seems sensible that as the concentration of cation in the bulk electrolyte increases, the level of incorporation/expulsion from the coat will increase (leading to an increase in the peak current). It is interesting that in figure 4.8 the reduction peak is more sensitive to the concentration of electrolyte than the oxidation peak. This is consistent with the redox process being

$$(In_3^+(COOH)_2(COO^-))_{(s)} + Li^+ + e^- \rightarrow (In_3(COOH)_2(COOLi))_{(s)}$$

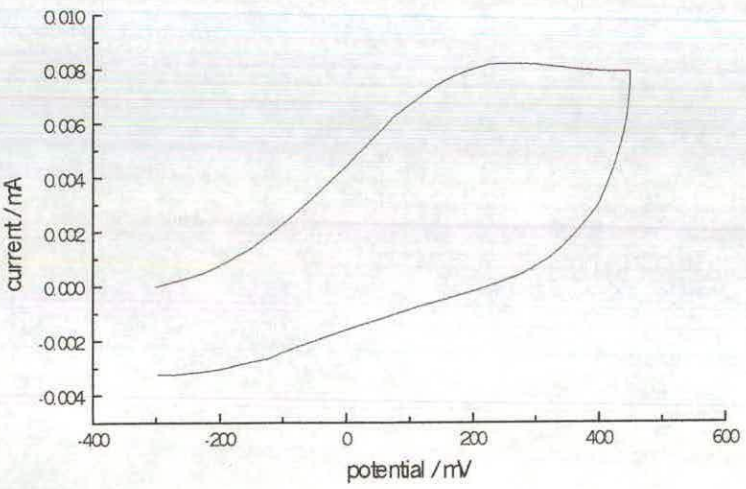

Figure 4.7: CV of poly(I5CA) after cycling in 0.1M $NaClO_4$

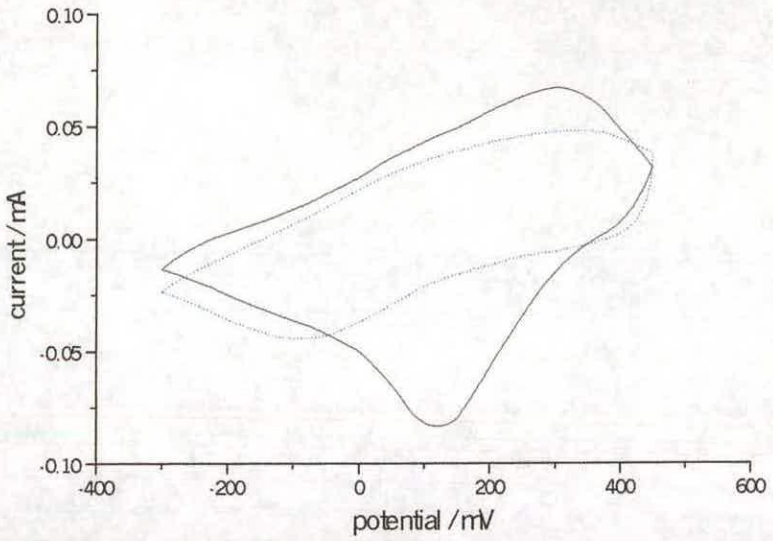

Figure 4.8: CVs of poly(indole-5-carboxylic acid) in differing concentrations of $LiClO_4$. (— $0.5moldm^{-3}$, ----- $0.1moldm^{-3}$)

4.3 Ac Impedance Spectroscopy

4.3.1 Qualitative analysis

The ac response of the polymer film is very interesting. Ac spectra for a fully reduced, uncycled coat show only a real resistance along with a capacitance. This is indicative of the polymer film behaving like a bare metal surface which only has a small resistance and a capacitance. As the potential is increased to a more positive value, the ac spectrum stays reasonably constant until a positive potential is applied. When this point is reached, the spectrum changes to show the presence of a semi-circle, indicating the existence of a charge transfer barrier, the size of which increases with potential. The fact that the barrier increases with increasing potential indicates that it is due to movement of ions into the layer. This means that this barrier is probably at the polymer/electrolyte

interface and is caused by the incorporation/removal of positive ions into the coat. The exact cause of this barrier might be removal of the solvation shell from the ion or possibly the actual insertion of the ion into the polymer film. Work by Albery and Mount[3] has shown that, mathematically and kinetically, the process of insertion is more important than the removal process. This would seem to suggest that the kinetic barrier is due to cation insertion from the electrolyte at the polymer interface. Due to the highly conducting nature of the film in its reduced form and the fact that no evidence of a transmission line is seen in the spectra (no line at 45°), it would seem that this process only operates at the very edge of the polymer film and that, due to the metal-like fast electron transfer through to the electrode, the potential drop is all at the electrolyte interface to increase the rate of ion transfer. Typical spectra for an uncycled poly(I5CA) layer are shown in figures 4.8 to 4.10. These spectra were taken at -100mV (reduced), figure 4.8; 200mV (moderately oxidised), figure 4.9, and 400mV (fully oxidised), figure 4.10, respectively.

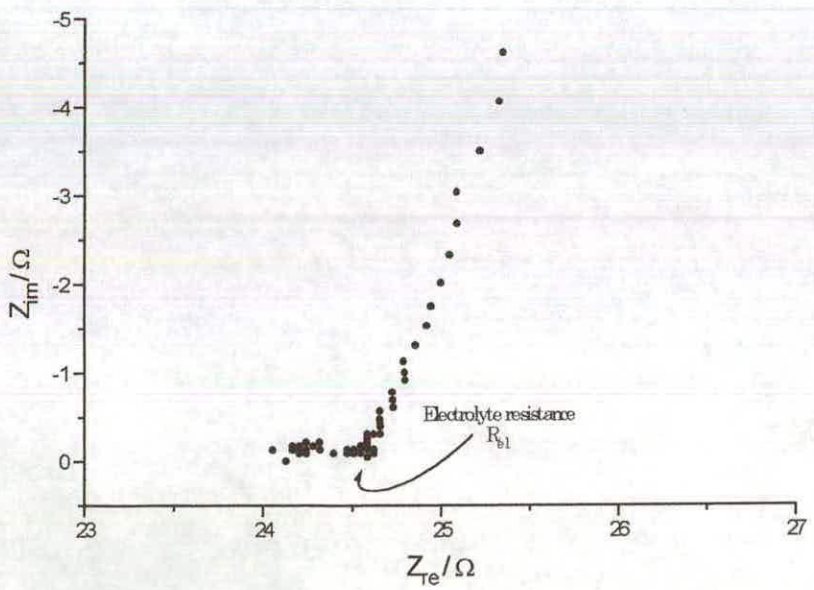

Figure 4.8: Ac spectrum of uncycled poly(I5CA) film taken at -100mV

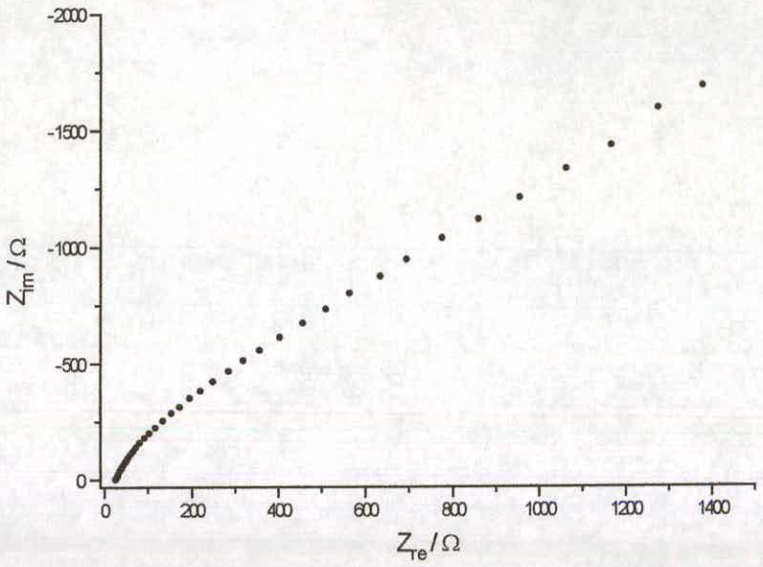

Figure 4.9: Ac spectrum of uncycled poly(I5CA) film taken at 300mV

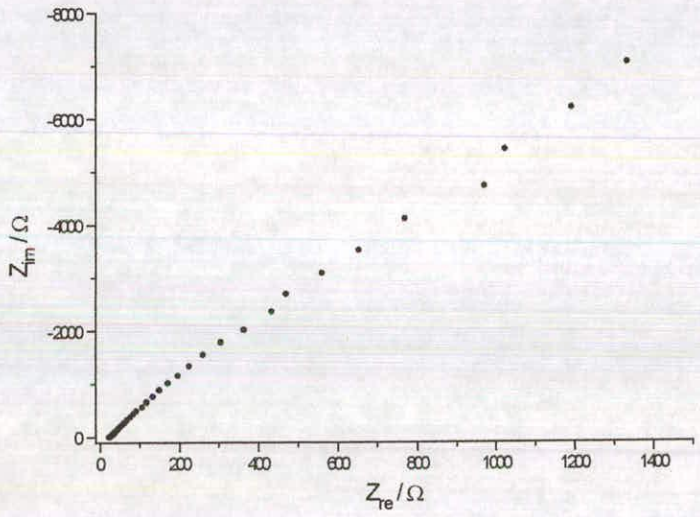

Figure 4.10: Ac spectrum of uncycled poly(I5CA) film taken at 500mV

After thorough cycling between its oxidised and reduced forms, the ac response changes quite considerably. Most noticeably, the earlier metallic behaviour disappears to be replaced by a charge transfer barrier at negative potentials. This barrier is seen to initially decrease (figure

4.11) to a minimum before increasing once more (figure 4.12). This could either be due to a loss of the coat's permselectivity in that both ion types present (cation and anion) are important in conduction or, more likely, the barrier is caused by electronic motion in the polymer backbone at the electrode/polymer interface. This would be consistent with redox hopping through the barrier where the lowest resistance would occur when there are equal numbers of oxidised and reduced species when the coat is half oxidised. The charge transfer barrier at positive potentials is also much smaller than previously observed. This suggests that the incorporation of cations into the coat is much easier than in the uncycled case. This ties in well with the theory that cycling causes the coat to change morphology to a more open structure which allows the free incorporation of ions. It is also possible that this increase in the ion transfer kinetics is due to the fact that the coat also becomes well solvated and so is well bathed in electrolyte and there is no need for cation incorporation at the interface. Typical spectra for such a coat are shown in figures 4.11 and 4.12.

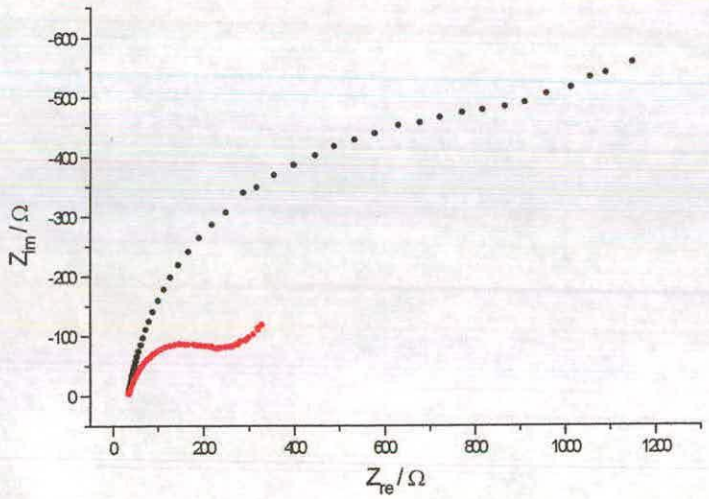

Figure 4.11: Ac spectra of cycled poly(I5CA) to show the decrease in the kinetic barrier at negative potentials (• -300mV, • -200mV)

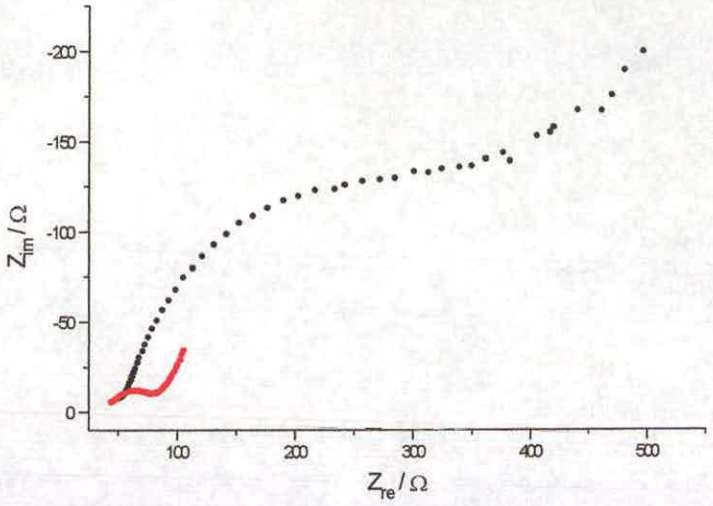

Figure 4.12: Ac spectra of cycled poly(I5CA) to show the increase in the kinetic barrier at positive potentials (• 300mV, • 200mV)

A similar trend in the value of the kinetic barrier is seen if the film is immersed in 0.08M $LiClO_4$ or in 0.04M $LiClO_4$.

On transfer to a solution with 0.1M $NaClO_4$ as the background electrolyte, the charge transfer resistance increases by, on average, a factor of 10 relating the difficulty faced in injecting the larger cation into the film, figure 4.13. This is in complete agreement with results from cyclic voltammetry detailed previously. This new barrier is large enough to swamp the electronic resistance seen in the heavily cycled $LiClO_4$ case. This provides evidence that the barrier is due to the actual insertion of the cation, not due to the desolvation step. If the latter was the case, the barrier would be less for Na^+ than for Li^+ due to the smaller solvation shell of the sodium ion. It is thought that the increase of this barrier is due to the fact that the larger Na^+ ions are unable to fit into the pores of the coat until the structure relaxes further and allows the pores to open more. If this is indeed the case then it seems obvious that cycling the coat on transfer from $LiClO_4$ to $NaClO_4$ will eject any Li^+ ions present in

the coat before a sufficient field will build up to force the incorporation of the new cation. It is thought that this accounts for the dramatic drop in redox activity seen using cyclic voltammetry.

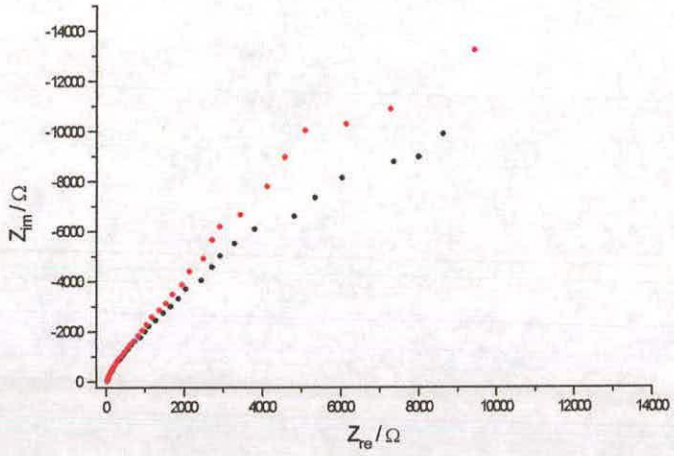

Figure 4.13: Ac spectra of poly(I5CA) taken in 0.1M $NaClO_4$ (• -300mV, • -200mV)

4.3.2 Quantitative analysis

A number of ac spectra obtained were modelled using the transmission line shown in figure 2.21 and mathematically fitted using an iterative curve fitting program.

For the uncycled system, the low signal to noise ratio meant that it was difficult to obtain any meaningful fits. However, from simple theory, the capacitance of the coat can be found from equation 4.1

$$-Z_{im} = \frac{1}{2\pi f C_{obs}} \qquad \text{Equation 4.1}$$

where f is the frequency (in hertz) of the oscillating perturbation. From this, it has been found that the capacitance of the coat is approximately constant with dc potential at a value of 32±2mF. This value is much

larger than a normal double layer capacitance with is generally of the order of tens of microFarads. This would seem to say that this capacitance must be due to an extended double layer through the whole of the coat i.e. the Feldberg capacitance. However, from equation 2.11 we would expect that the total capacitance would have three contributions with the major contributing factor being the smallest of the three. This means that the terms from the Nernst and Donnan capacitances (C_N and C_D), which will both be potential dependent, must be very large, or else that charge is driven through the layer by the applied field and not by any concentration gradient. This accounts for the square envelope seen in the voltammogram of the as formed coat (figure 4.1). This and the impedance data which show that initially the coat behaves as a metal with fast electron through its structure gives an idea of the initial structure of the polymer. It has already been proposed that the polymerisation reaction for indole-5-carboxylic acid involves the adsorption and cyclisation of monomer on a previously deposited film. It seems very likely that this cyclisation will result in planar trimer units arranged in stacks with extensive π delocalisation. This means that conduction in the polymer backbone cannot occur by redox hopping and must be described by band theory. This hypothesis seems to be borne out by xray powder diffraction studies which show a graphite-like spacing between the trimer centres. This delocalisation will result in fast electronic communication through these stacks and therefore a low electronic resistance. This is verified by the constant current observed in the current-time transient for the electropolymerisation reaction. It is assumed that the counter anion will be similarly stacked in channels between the trimer "wires". These anion stacks will be a finite distance from the trimer centres with no means of direct communication (by for example any solvent) resulting in a distributed Feldberg capacitance C.

On the other hand, good fits were obtained for spectra taken for heavily cycled systems which had undergone a change in morphology to a more open film. Figure 4.14 to 4.16 show a number of the fits achieved. For the sake of presentation, the remaining figures showing the goodness of fit can be found in appendix B. All show gradients close to one and good correlation coefficients. This fact provides good evidence as to the viability of the transmission line model proposed by Albery and Mount. The values obtained from the fitting sessions were then plotted against potential and compared to theory. It is interesting to note that although, in the main, the ac spectra contained a single semicircular region, the data did not fit well to a transmission line containing one kinetic barrier. However, good fits were obtained using a transmission line with a barrier at each interface. This seems to suggest that the semicircular features were actually the combination of two semicircles, each with a different time constant, making it possible to resolve each one.

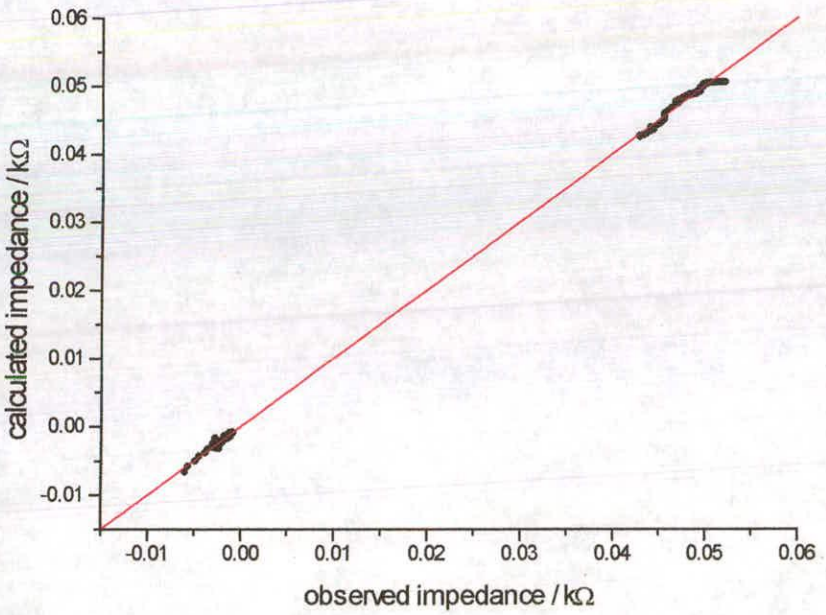

Figure 4.14: Fit plot for a cycled poly(I5CA) layer at -200mV in $LiClO_4$ Gradient = 0.9939; Intercept = 0.0003; Correlation coefficient = 0.9995

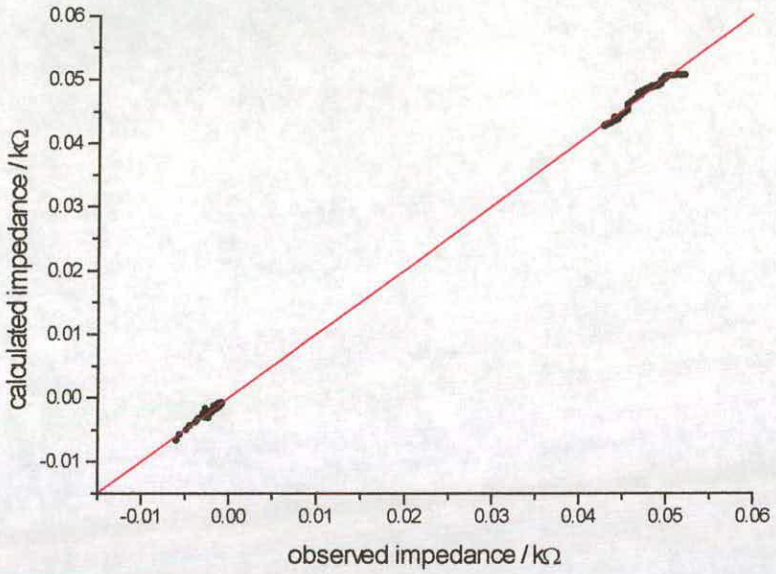

Figure 4.15: Fit plot for a cycled poly(I5CA) layer at 0mV in $LiClO_4$
Gradient = 1.0016; Intercept = 0.0001; Correlation coefficient = 0.9998

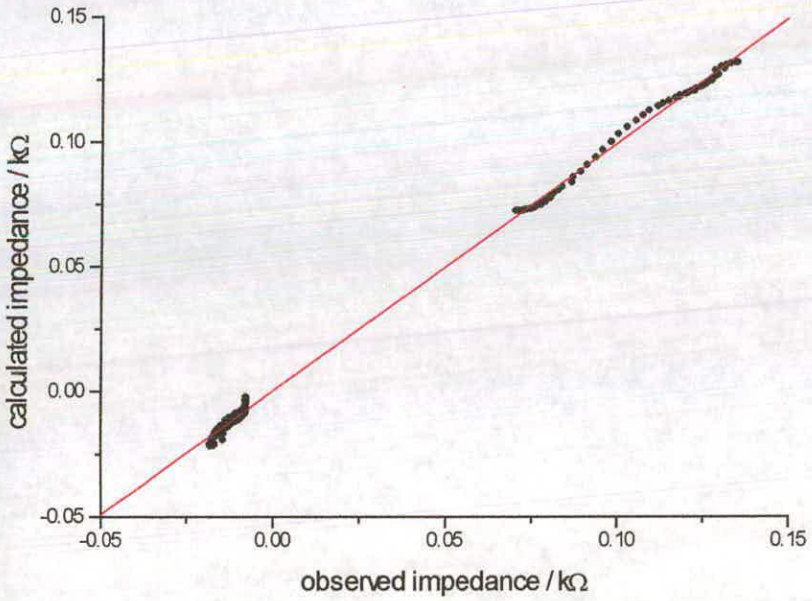

Figure 4.16: Fit plot for a cycled poly(I5CA) layer at 200mV in $LiClO_4$
Gradient = 0.9919; Intercept = 0.0003; Correlation coefficient = 0.9994

A graph of capacitance against potential is shown in figure 4.17. The theoretical fits were obtained using from equation 4.2.

$$\frac{1}{C_\Sigma} = \left(\frac{RT}{ALF^2}\right)\left(\frac{c}{ab}\right) + \left(\frac{RT}{ALF^2}\right)\cdot\frac{1}{2s} \qquad \text{Equation 4.2}$$

It should be noted that the above equation has one important difference to equation 2.10 in that the term for the distributed Feldberg capacitance has been neglected. It is interesting that, with this correction, good fits are obtained for data from ac studies from 0.1M and 0.08M $LiClO_4$. This fact is significant for two reasons. The first reason is that it backs up claims by Albery et al. that, in the case of a one electron redox reaction where $C_N, C_D << C$, the capacitance proposed by Feldberg is so large as to be insignificant when taken into consideration with the new proposed Donnan and Nernst capacitances. The second significance, and possibly the most important one, is that for this equation to apply, there must be an ionic concentration of 2s within the film. For this to occur, there can be no Donnan exclusion present within the polymer film. This means that the coat must be well solvated which is consistent with the idea that during cycling, the coat opens up, allowing solvent and electrolyte to enter until, eventually, all of the coat is accessible.

As mentioned previously, the fitted results from a cycled I5CA layer also show the existence of two barriers as discussed previously. Figure 4.18 shows the variation of both charge transfer barriers with potential. A number of important observations can be gleaned by examination of this figure.

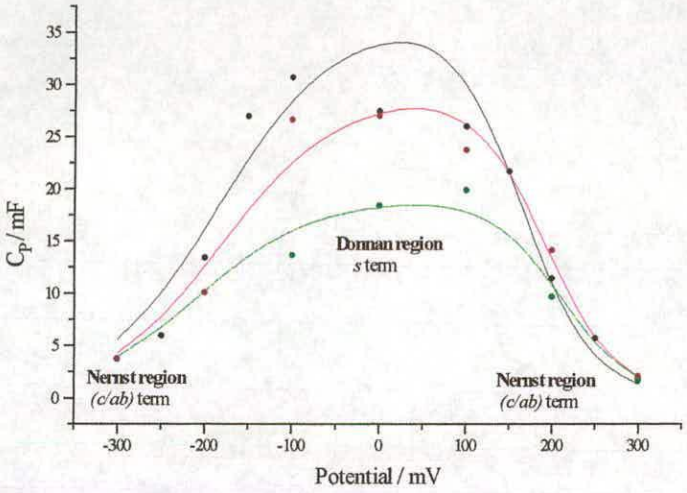

Figure 4.17: Plot of C_P values along with their theoretical fits (given by the solid lines). • 0.1M $LiClO_4$, • 0.08M $LiClO_4$, • 0.04M $LiClO_4$

Firstly, the barrier at the polymer/electrolyte interface, $R_{K,X}$, is approximately constant and shows little concentration dependence except at very low frequencies. This is entirely consistent with the absence of any Donnan exclusion and a coat which is well solvated and liberally bathed with electrolyte. It interesting to see that the barrier increases at low electrolyte concentrations. This indicates that, even in a well solvated system, at low enough concentrations, the insertion process is still important while at higher concentrations, enough ions are present that the limiting factor in the insertion kinetics is the size of the pores and the rate of insertion approaches a constant value.

Secondly, the kinetic barrier at the electrode/polymer interface, $R_{K,P}$, can be seen to go through a minimum. This is consistent with the barrier existing over the first few layers of the polymer. This "bowl" can be fitted using equation 4.3.

$$R_{K,P} = R_o e^{\frac{-\alpha_{ox} nF(E-E^\circ)}{RT}} + R_o e^{\frac{(1-\alpha_{ox}) nF(E-E^\circ)}{RT}} \qquad \text{Equation 4.3}$$

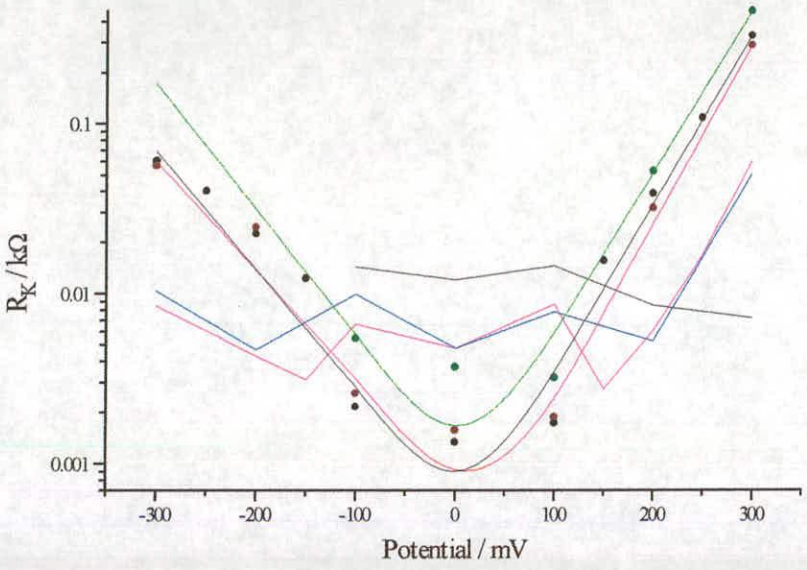

Figure 4.18: Plot of variation of charge transfer resistances at both the electrode/polymer interface (• 0.1M $LiClO_4$, • 0.08M $LiClO_4$, • 0.04M $LiClO_4$) and polymer/electrolyte interface (— 0.1M $LiClO_4$, — 0.08M $LiClO_4$, — 0.04M $LiClO_4$). The values of the electrode/polymer resistance are shown along with their fits to theory (given by the solid lines of the same colour as the points)

Iterative fitting of the $R_{K,P}$ values gives an estimate of α_{ox} of 0.38±0.02 and E^o, the standard redox potential of the polymer at the electrode surface, of 0.04±0.01V for all concentrations. The fact that E^o is concentration independent, along with the symmetrical nature of the bowl, provides yet greater evidence as to the absence of any Donnan exclusion within this coat. The fact that the experimental data for $R_{K,P}$ fits the theory so well with the potential being equal to the total applied potential indicates that all of the potential drop, or at least the largest percentage of it, must occur over the charge transfer barrier at the electrode/polymer interface. If this is indeed the case then it would seem probable that as this barrier becomes less important, the degree of fit will

become worse since less potential is dropped at the interface and more is dropped across the bulk polymer. This, indeed, seems to be the case as it can clearly be seen that the fit to theory at approximately half oxidation is much poorer than for the fully oxidised/reduced polymer. It is interesting to see that at the edges of the bowl the $R_{K,P}$ values show almost direct overlap with no concentration dependence. This is to be expected since at these potentials all of the potential drop is at the electrode/polymer interface and there is no ion involvement. The exact cause of the slight deviation from theory at –200mV to –300mV is currently unknown though it is thought to be due to secondary processes such as reduction of dissolved O_2.

It is interesting to note that that the location of the more dominant barrier changes from the electrode/polymer interface to the polymer electrolyte interface at potentials near the standard redox potential.

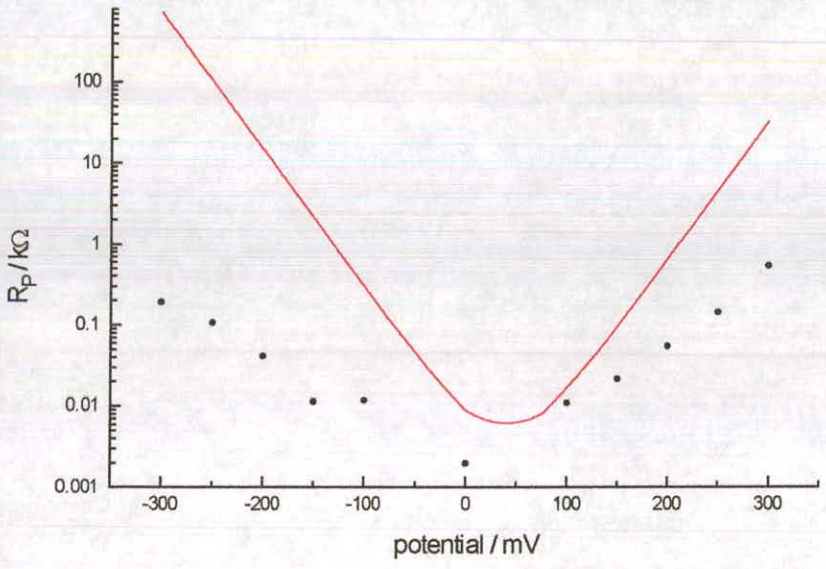

Figure 4.19: Variation of R_P for film in 0.10M $LiClO_4$. The straight line shows the theoretical variation for Nernstian behaviour (—)

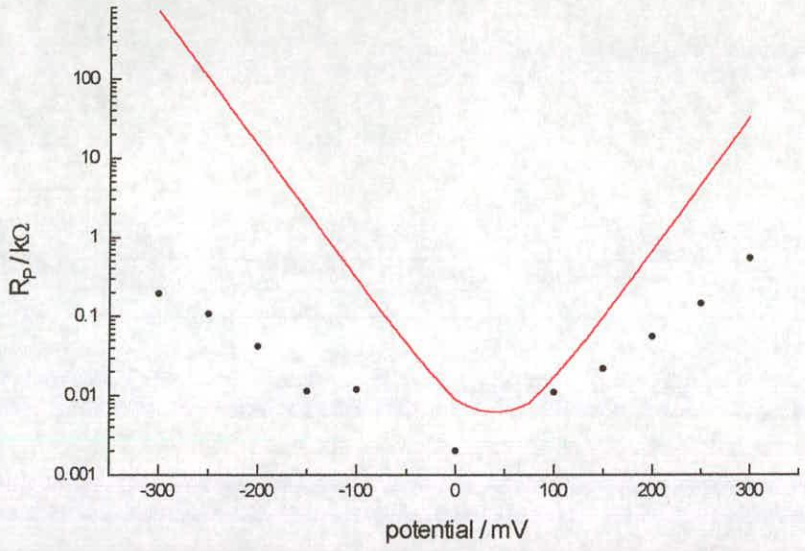

Figure 4.20: Variation of R_P for film in 0.08M $LiClO_4$. The straight line shows the theoretical variation for Nernstian behaviour (—)

The values of R_P also go through a minimum consistent with a redox hopping conduction mechanism. It is interesting, however, that the resulting bowls are much wider that those for $R_{K,P}$. This suggests that very little potential drop occurs across the bulk of the polymer film (and so must occur over the electrode/polymer interface, agreeing with the earlier observation for $R_{K,P}$). The variation of R_P with potential for poly(I5CA) in 0.1M and 0.08M $LiClO_4$ is shown in figures 4.19 and 4.20. If the potential drop was indeed taking place over the bulk of the polymer film then the movement of electrons would obey the Nernst equation

$$E = E^{o} + \frac{RT}{F} \ln \frac{b}{a}$$

$$\Rightarrow \frac{b}{a} = e^{\frac{F(E-E^{o})}{RT}}$$

Now, $a+b=c$ so, using $\frac{a}{a}=1$,

$$\frac{a}{c}=\frac{1}{1+e^{\frac{F(E-E^\circ)}{RT}}}$$

and

$$\frac{b}{c}=1-\frac{a}{c}=1-\frac{1}{1+e^{\frac{F(E-E^\circ)}{RT}}}$$

So,

$$\frac{ab}{c}=c\frac{ab}{c^2}$$

$$=c\frac{e^{\frac{F(E-E^\circ)}{RT}}}{\left(1+e^{\frac{F(E-E^\circ)}{RT}}\right)^2}$$

$$=c\frac{e^{\frac{-F(E-E^\circ)}{RT}}}{\left(1+e^{\frac{-F(E-E^\circ)}{RT}}\right)^2}, \text{ for computational purposes}$$

Now, $R\propto\frac{c}{ab}$ so

$$R=A\frac{\left(1+e^{\frac{-F(E-E^\circ)}{RT}}\right)^2}{e^{\frac{-F(E-E^\circ)}{RT}}}$$

where A is a constant of proportionality incorporating the concentration and is equal to ¼R_P at E° (i.e. the minimum R_P value at the base of the bowl). Curves showing the Nernstian variation or R_P with potential are also shown in figures 4.19 (A=0.0013) and 4.20 (A=0.0015) for comparison.

In theory, it should be possible to use the difference between the experimentally derived values and these theoretical curves to quantify the degree of potential drop occurring over the bulk film and so obtain a correction curve for the $R_{K,P}$ values in figure 4.19, hence improving the fit. In practice, however, this has been found to be difficult due to the ambiguity in the location of the minimum resistance in each bowl. Although little use could be made of the values of R_P to correct $R_{K,P}$, the R_P values were used to calculate the c/ab terms required to obtain the theoretical fits to C_P shown in figure 4.17. The good fits obtained show that both R_P and C_Σ must, independently, give very similar values of c/ab, demonstrating the power of the technique. This also shows that it is possible to determine the redox composition of the polymer film.

4.4 Charge studies

This idea of the coat gradually opening up to ions and becoming more accessible to complete oxidation and reduction has been investigated by observing the change in the charge of the coat as the film is taken from its reduced state to its oxidised form. Mount et al have proposed that the polymerisation of indole-5-carboxylic acid involves the loss of between 7 and 9 electrons[1] per trimer unit and hence the redox charge available should be between one seventh and one ninth of the charge passed during the polymerisation process. Figure 4.21 shows the typical current-time transients for the first two pulses from such an experiment. The charge passed during a number of pulses is recorded in table 4.1.

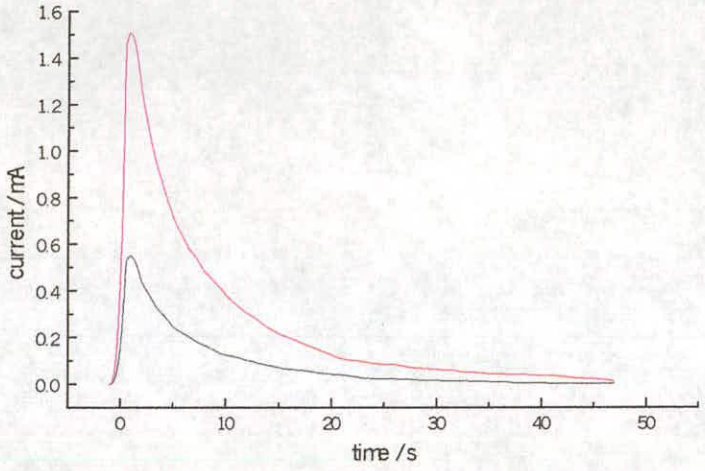

Figure 4.21: I-t transients recorded on pulsing poly(I5CA) film from – 400mV to 250mV. (—— 1st pulse, — 2nd pulse)

Pulse Number	Charge Passed / mC
1	4
2	13
3	15
4	14
5	16
6 +	15
polymerisation charge	135

Table 4.1: Charge passed on pulsing poly(I5CA) coat from –400mV to 250mV

The current spike caused by the first pulse is thought to be due to the charging of a distributed double layer at the polymer/electrolyte interface, with the rest of the coat behaving as a fast charge transfer system. However, as the coat is pulsed alternately between its reduced and

oxidised states, the coat will open and more solvent/electrolyte will be able to enter. This will have two effects: the first is that the increase in the concentration of electrolyte species within the coat will increase the distributed capacitance to the detriment of the fast electron conduction through the layer to the electrode. Secondly, due to the presence of the electrolyte inside the coat, the Nernst and Donnan capacitances will begin to charge. Both of these effects will increase the capacitance of the coat and hence the amount of charge accessible. As the pulsing continues, it is thought that the coat opens up even more, making these previous arguments all the more valid. Eventually, after a number of switching pulses, the coat will become fully open and all of the redox charge will be available. It is interesting to see that, in this case, the total accessible charge obtained after a number of such pulses is one ninth of the polymerisation charge as predicted from theory.

4.5 Rotating Disc Work

Rotating disc studies were carried out on cycled and uncycled poly(indole-5-carboxylic acid) films. The results obtained were subjected to Koutecky-Levich analysis and the resulting plots shown in figures 4.22 for the uncycled film and 4.23 for the extensively cycled polymer.

The plot for the uncycled film (figure 4.22) shows, within experimental error (approximately 5%) very little potential dependence in the intercept with almost direct overlap of the linear regression lines. This suggests that the layer is behaving as a metal with the redox reaction taking place at the surface. Hence, the redox composition of the polymer/electrolyte interface has no real influence on the redox reaction process. The fact that the y intercept of the plots is not the origin shows that the coat does

not exhibit simple Levich behaviour and that, before electron transfer can occur, another process, probably absorption onto the surface of the film, must take place. The fact that the intercept is constant shows that the redox state of the adsorption site is unimportant.

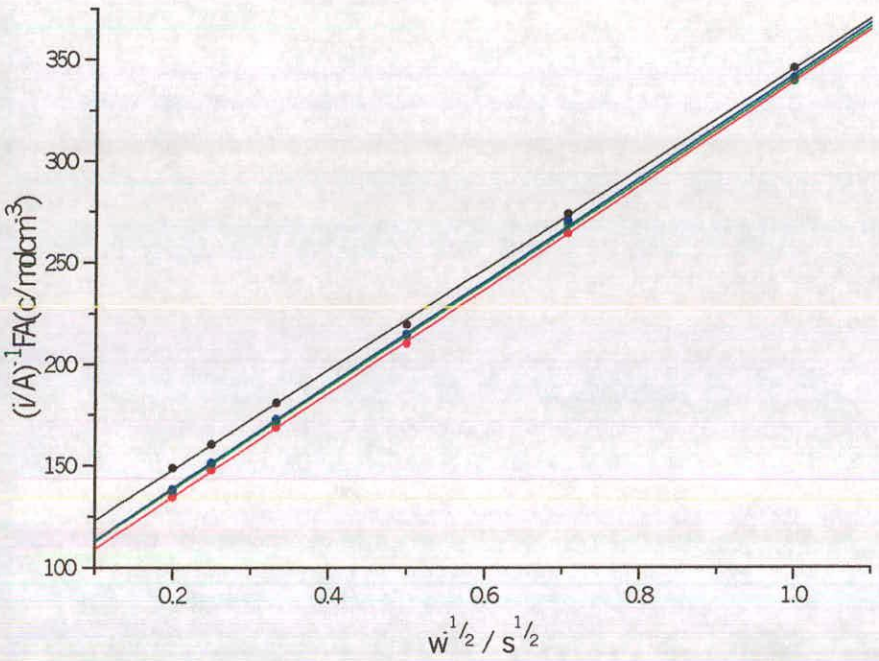

Figure 4.22: Koutecky-Levich plot for an as formed poly(I5CA) film. The intercepts are given in table 4.2
(• 200mV, • 300mV, • 400mV, • 500mV)

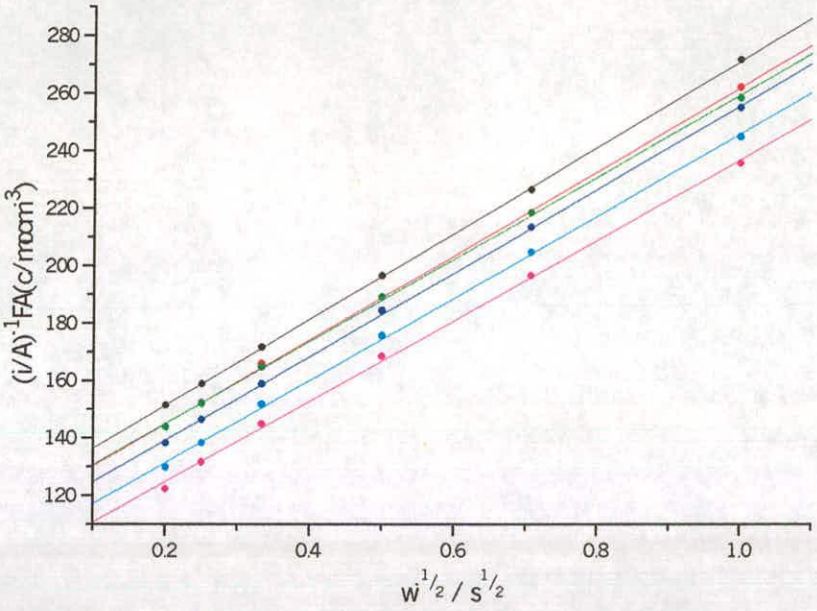

Figure 4.23: Koutecky-Levich plot for a cycled poly(I5CA) film. The intercepts are given in table 4.2 (• 200mV, • 300mV, • 400mV, • 500mV, • 600mV, • 700mV)

Potential / mV	Intercept for uncycled layer / $CA^{-1}cm^{-1}$	Intercept for cycled layer / $CA^{-1}cm^{-1}$
200	98.616	121.556
300	83.412	115.816
400	87.503	116.621
500	87.941	110.243
600	-	102.951
700	-	96.841

Table 4.2: Table of intercepts from the Koutecky-Levich plots shown in figures 4.22 and 4.23

On the other hand, while the Koutecky-Levich plot for the cycled case also shows non-zero intercepts, it is obvious that, in this case, the

intercepts show a potential dependence with the higher potential plots having the lower intercept. This indicates that, in this case, the redox nature of the absorption site and its immediate neighbours is very important. As expected, suitable sites for redox reaction are those in the oxidised state and so, the more oxidised the coat is, the greater the chance that ferrocene will be adsorbed onto one of those sites. This type of behaviour would be expected if there are localised oxidised trimer centres and conduction in the coat was via redox hopping. It is very interesting that the intercept for the fully oxidised cycled film (i.e. at 500mV) is approximately the same as the intercept obtained for the uncycled polymer showing that the uncycled coat behaves as though all of the trimer centres are fully oxidised with fast electron transfer to the electrode surface.

4.6 pH Studies

The potential use of poly(indole-5-carboxylic acid) as a fast pH sensor was first advocated by Bartlett in 1992[4]. However, for a use as a commercially viable and effective sensor, the polymer must give a stable and reproducible signal over a wide timescale. The results presented in this chapter, unfortunately, show that the morphology of the polymer film is not stable, but changes over a number of weeks. It is therefore important to see how, if at all, this morphology change affects the pH response of the coat.

Previous work has shown that the slope of a plot of potential against pH deviates from the ideal Nernstian slope of 59mV at approximately pH5.5, which is within the reported range for the pK_a of the carboxylic acid group of from 4.7[5] to 5.55[2]. However, much of the work has not raised

the pH of the system above pH7 due to the loss of the film into the solution. In the course of this work, the polymer's response over a wider pH range was investigated.

The response of an uncycled coat is shown in figure 4.24 and shows the break from Nernstian behaviour at approximately pH 5.5 observed by other workers. It is interesting, however, that after the break (at approximately pH9) the response become almost Nernstian once more.

The first Nernstian slope has been found to be attributed to a one electron one proton loss involving the proton of one of the imide groups on the trimer centre according to the reaction

$$In_3H(COOH)_3 \longrightarrow In_3(COOH)_3 + H^+ + e^-$$

The region showing non-Nernstian behaviour is thought to be due to a switch in the mechanics of the coat response from a simple 1 electron 1 proton loss (which would give the expected 59mV gradient) to a redox process which, overall, does not involve the loss of a proton. Since this break region is well within the pK_a range for the indole-5-carboxylic acid monomer, it is likely that this process involves the movement of a proton from one of the imide groups onto a now deprotonated carboxylic acid moiety (i.e. onto a carboxylate anion).

$$In_3H(COOH)_2(COO^-) \longrightarrow [In_3(COOH)_3] + e^-$$

In theory, this mechanism should give rise to a region with zero gradient. Inspection of figure 4.24 shows, however, that this is clearly not the case. This break from the theory is probably due to the presence of a range of different trimer –COOH environments, and hence a range of pK_a values, at the electrolyte boundary of the polymer layer. This will cause the

boundary between the proton loss mechanism and the non-proton loss mechanism to become less well defined.

The final Nernstian area is due again to a one proton one electron step involving the loss of a proton located on the imide group i.e.

$$\left[In_3H(COOH)_2(COO^-)\right] \longrightarrow \left[In_3(COOH)_2(COO^-)\right] + H^+ + e^-$$

At pH>10, it is thought that all of the carboxylic acid groups on the trimer become deprotonated, increasing the solubility of the film, and the polymer dissolves off the electrode surface.

The pH response from an extensively cycled coat is shown in figure 4.25 and, for the sake of easy comparison, with the figure 4.24 overlaid in figure 4.26. It can be seen that the response for the cycled system is essentially the same as for the uncycled case but with two noticeable differences. The first break is similar to that found by Pickup for poly(3-methylpyrrole-4-carboxylic acid)[6] and has also been seen for poly(indole-5-carboxylic acid) by Bartlett[2]. Although the exact cause of this is unknown at the moment, it is thought that it might be due to the further protonation of the imide groups within the trimer centres due to the highly acidic conditions. It does however, give a good indication that the coat is different when compared to the uncycled case.

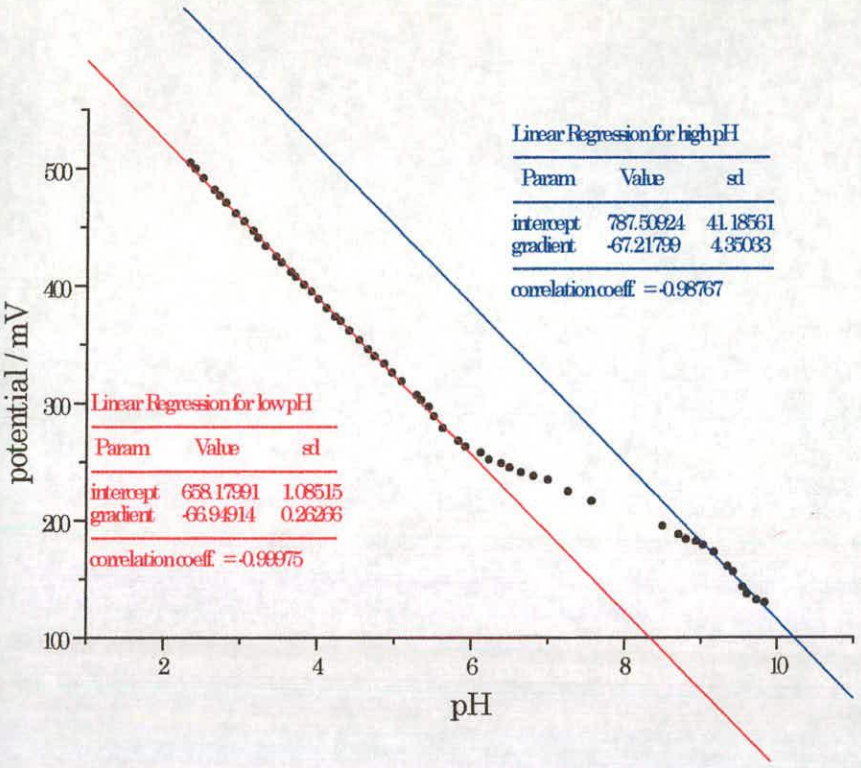

Figure 4.24: pH response for uncycled poly(I5CA) film

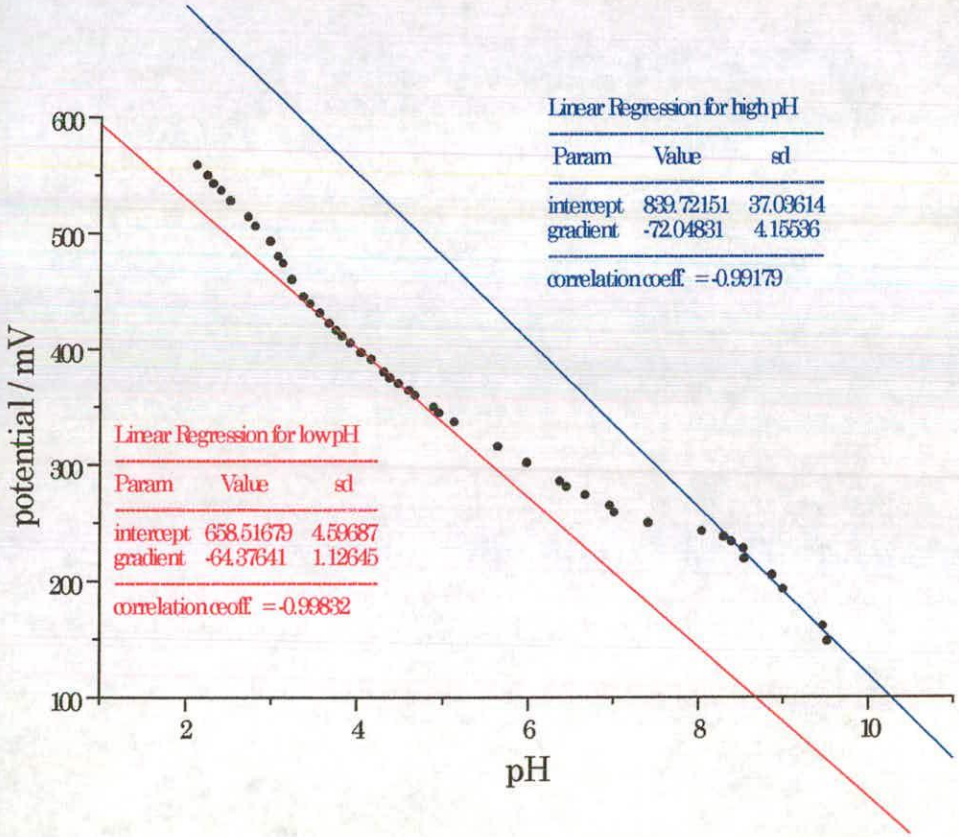

Figure 4.25: pH response for a cycled poly(I5CA) film

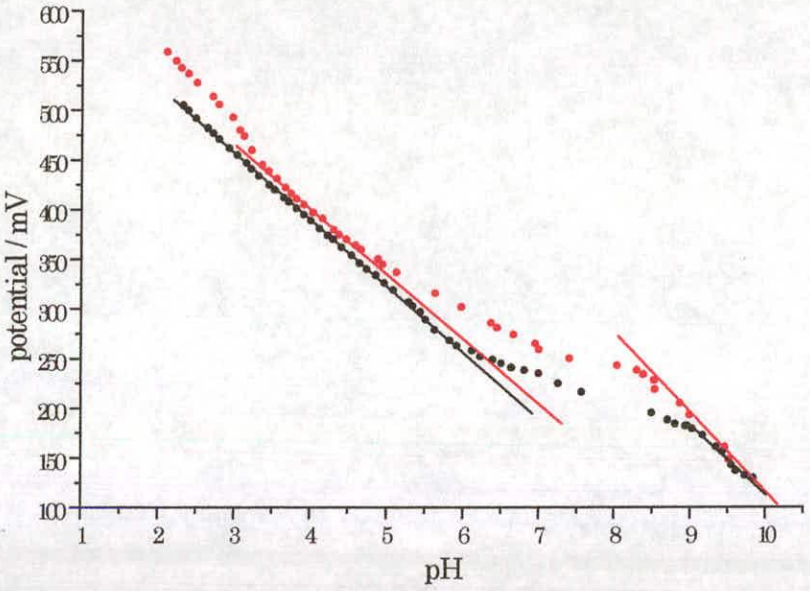

Figure 4.26: Overlay of figures 4.22 and 4.23. (• uncycled coat, • cycled film). The straight lines represent the 'Nernstian regions'

Probably the most striking difference between the uncycled and heavily cycled coats, however, is in the 'non-Nernstian' region. It can clearly be seen from figure 4.26 that this 'break region' is much wider in the cycled than in the uncycled case. It should be noted that due to the different nature of the solvents used (acetonitrile and water), the characteristics of the coat in water cannot, with all certainty, be said to be same as in acetonitrile. It is, however, probable that a coat that is cycled in a non-polar solvent until it has an open (less compact) structure will stay relatively open on transfer to a polar system and so be more accessible to solvent on transfer. This open structure will allow more electrolyte to enter the coat and so will create a greater number of redox active trimer centres with a wider range of pH environments. However, since the coat is more open (and hence more solvent/electrolyte is present in the pores), the cycled case will experience more pH environments than the uncycled case, causing a much wider non-Nernstian region.

It is, however, interesting that this change in morphology has not caused a change in the energy, and therefore the standard potential, of the redox system. This can clearly be seen in figure 4.26 by the fact that the gradients of the Nernstian regions for both the uncycled and cycled cases are approximately the same. If there was a change in the energy of the system, one would expect that there would be a Gaussian distribution of E° which would lower the gradient of the Nernstian regions[7].

4.7 Summary

From the results presented in this chapter, it is obvious that polymer films prepared from indole-5-carboxylic acid undergo a significant change on continuous switching between the reduced and oxidised forms over a time scale of a number of weeks.

Initial cyclic voltammograms and ac spectra show that immediately after deposition, the polymer layer behaves as though it were metallic. One possible explanation for this is that the trimer centres deposit on the electrode surface as stacks. Such stacking has been suggested by x-ray powder diffraction[8] which shows that the freshly deposited polymer has peaks which are consistent with graphite-like spacings between the trimer centres. This stacking would exhibit a great deal of π delocalisation which would allow fast electronic conduction through the coat. This would account both for the lack of redox peaks on the CV and for the initial ac spectra showing only the presence of a real resistance and a capacitance at low potentials. If this is indeed the case then any redox activity would occur at the electrolyte interface only and should be independent of potential. Such behaviour is indeed observed using a rotating disc electrode and Koutecky-Levich analysis of the data. At

potentials above 300mV, a semicircular feature is seen in the ac spectra which increases with potential. This is indicative of the presence of a kinetic barrier to cation insertion at the polymer/electrolyte interface. The fact that this barrier is seen to increase on changing to a cation which is larger when unsolvated shows that the rate determining step must be the insertion of the naked ion into the polymer pores and not desolvation.

After cycling between the polymer's oxidised and reduced forms, the cyclic voltammograms begin to show the presence of redox behaviour. The redox peak heights are found to be dependent on the cation species present. It is found that on changing to a larger cation, the peaks vanish and are observed to grow in on further cycling. This provides strong evidence that the redox peaks must, in some way, be due to the presence of the cation within the layer.

After further, extensive, cycling, it is found that the redox peaks become more prominent and become invariant, both in height and position, with further cycling (i.e. reach steady state). Ac analysis shows that the location of the dominant kinetic barrier to charge conduction changes from being solely at the polymer/electrolyte interface and is now at the electrode/polymer interface at low and high potentials and at the polymer/electrolyte interface at potentials around the redox potential for the trimer film. It is thought that the appearance of a barrier at the electrode/polymer interface is due to a restructuring of the polymer coat to allow the ingress of ions/solvent, which causes buckling of the trimer stacks. This causes an overall change in the electronic conduction mechanism to the slower redox hopping process and creates difficulty in injecting/ejecting electrons into/out of the coat. The switch to redox hopping has been confirmed by rotating disc work. The barrier at the polymer/electrolyte interface is found to be constant with respect to

changes in the applied potential. This behaviour suggests that the coat already contains a high concentration of (cat)ions and there is no Donnan field present at the polymer electrolyte interface. This is confirmed by the fact that the "size" of this barrier is independent of concentration except at very low concentrations. These observations are consistent with the polymer film becoming more open and lyophilic with electrolyte within the pores.

Charge studies show that very little redox charge within the coat is accessible upon initial polymerisation while, after cycling, the charge expected from theory is available. This, along with the ac and cyclic voltammetry results, suggests that the as-formed polymer film is very compact with little solvent/electrolyte contained within. However, with cycling, and, hence, the insertion of cations, gradually more and more of the redox charge becomes accessible. This observation agrees with the hypothesis that the polymer film becomes less compact and more accessible to solvent/electrolyte on switching from its oxidised to its reduced state. These observations are further verified by comparison of the pH responses of the polymer film in its as formed and cycled states.

4.8 References

1 J.G. Mackintosh; *PhD. Thesis*, University of Edinburgh, 1995

2 P.N. Bartlett, D.H. Dawson, J. Farrington; *J. Chem. Soc. Faraday Trans.*, 1992, **88**, 2685

3 W.J. Albery, A.R. Mount; *Electroactive Polymer Electrochemistry, Part 1: Fundamentals*, edited by M.E.G. Lyons, Plenum Press, New York, 1994, 443

4 P.N. Bartlett, J. Farrington; *Bulletin of Electrochem.*, 1992, **8**, 208

5 M. Krishnamurthy, H.K. Sinha, S.K. Dogra; *J. Luminescence*, 1986, **35**, 343

6 P.G. Pickup; *J. Electroanal. Chem.*, 1987, **225**, 273

7 W.J. Albery, M.G. Boutelle, P.J. Colby, A.R. Hillman; *J. Anal. Chem.*, 1982, **133**, 135

8 A.R. Mount, A. Harrison; *Personal communications*, 1995

5. 5-Cyanoindole

5.1 Cyclic Voltammetry

The linear sweep voltammograms for poly(5-cyanoindole) show very little change with time except for a slight reduction in size initially due to loss of the layer to the electrolyte solution. The initial voltammograms show the existence of redox peaks though these are superimposed over a wide background envelope. However, unlike the case in the previous chapter, this envelope is not found to decrease with cycling. A typical voltammogram is shown in figure 5.1.

The cation dependence of the coat was investigated. It was found that there was very little change in the redox activity of the film on transferring it from 0.1M $LiClO_4$ to 0.1M tetraethylammonium (TEA) perchlorate. The existence and location of the redox peaks both stayed constant though the peak sizes reduced slightly. This is shown in figure 5.2.

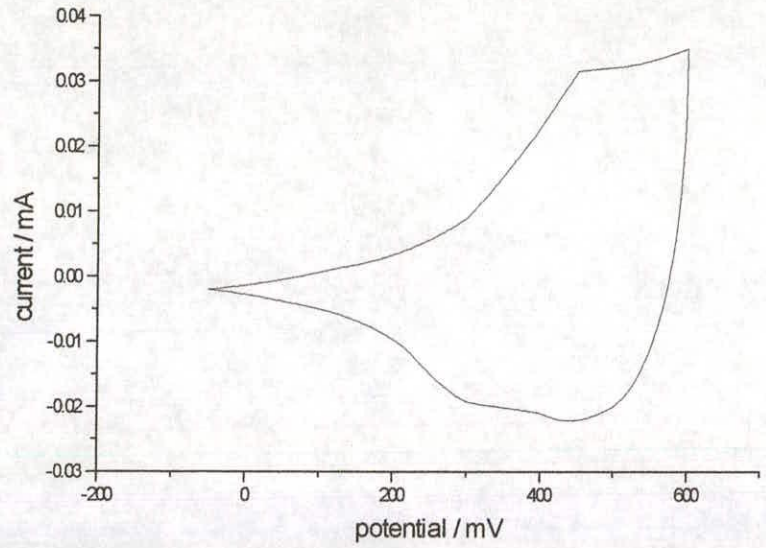

Figure 5.1: Steady state voltammogram of poly(5-cyanoindole) in 0.1M $LiClO_4$

Scan speed = $2mVs^{-1}$

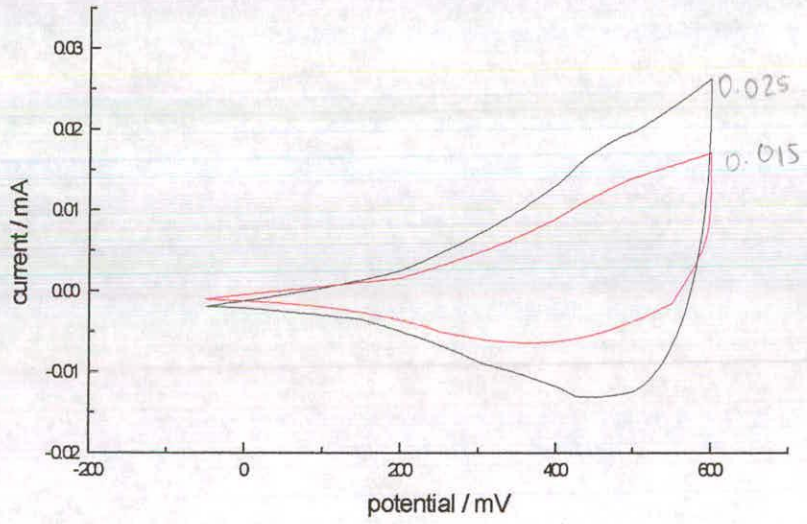

Figure 5.2: Steady state voltammograms of poly(5-cyanoindole) in 0.1M $LiClO_4$ (—) and 0.1M $(TEA)ClO_4$ (—)

Scan speed = $2mVs^{-1}$

One the other hand, when the identity of the anion was changed, there was a large change in the voltammogram. Figure 5.3 Shows voltammograms taken in 0.1M (TEA)ClO_4 and 0.1M (TEA)PF_6. From these it can be seen that there is a large decrease in the overall charge as well as the disappearance of the redox features. This is consistent with results from other workers[1]. No peaks were found to appear after further cycling in (TEA)PF_6.

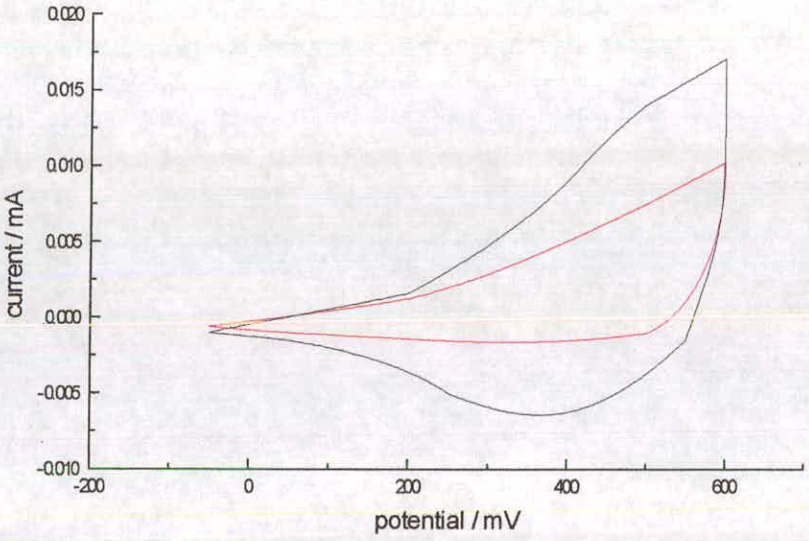

Figure 5.3: Steady state voltammograms of poly(5CI) in 0.1M (TEA)ClO_4 (——) and 0.1M (TEA)PF_6 (—)
Scan speed = $2mVs^{-1}$

Further evidence of the insensitivity of the polymer film to cation can be seen in figure 5.4 - on going from 0.1M $LiClO_4$ to 0.1M $NaClO_4$ there is little change in the voltammetric response.

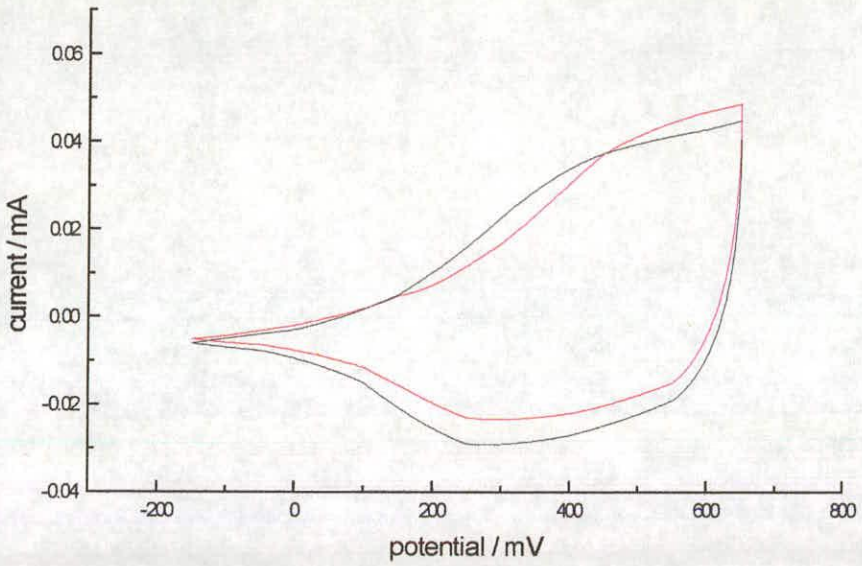

Figure 5.4: Steady state voltammograms of poly(5CI) in 0.1M $LiClO_4$ (—) and 0.1M $NaClO_4$ (—)
Scan speed = $5mVs^{-1}$

5.2 Ac Impedance Spectroscopy

5.2.1 Qualitative Analysis

As would be expected from the cyclic voltammograms, the ac spectra obtained from an as-formed polymer film are very similar to those for a film which has undergone extensive cycling. Typical spectra are shown in figure 5.5. Examination of these spectra show the existence of what appears to be a semicircular feature which decreases as the potential is increased. This could be explained by the presence of a kinetic barrier to anion injection at the polymer/electrolyte interface.

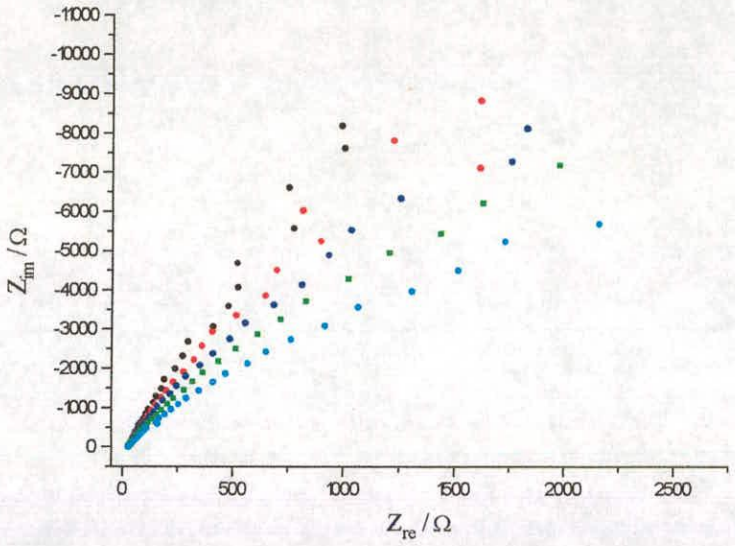

Figure 5.5: Ac spectra of poly(5CI) in 0.1M $LiClO_4$
(• -100mV, • 100mV, • 200mV, • 300mV, • 400mV)

On changing the background electrolyte to 0.1M tetraethylammonium perchlorate however, a very interesting change in the ac spectra (figure 5.6) is observed. Probably the most striking feature now is that the semicircle found at negative potentials seems to be very much smaller than those at positive potentials. If this feature were due to the presence of a kinetic barrier, this trend suggests that, at these potentials, cation insertion has become an important factor. This is reasonable since at these potentials it is likely that a Donnan field will exist which will favour the insertion of cations over anions. It is expected that the much larger tetraethylammonium ion will display a much larger kinetic resistance to insertion than the lithium cation. However, this is not found to be the case and, in fact, the opposite is true. This could suggest that the barrier is not due to the actual insertion into the layer but probably due to the desolvation of the cation beforehand – TEA^+, being the larger cation, should have the smaller solvation shell. The spectra at positive potentials show very little variation with oxidation state. This

seems to show that anion insertion is no longer such a dominant factor in the coat's conduction. It is possible that the coat is well solvated in a manner similar to the cycled poly(indole-5-carboxylic acid) film discussed previously.

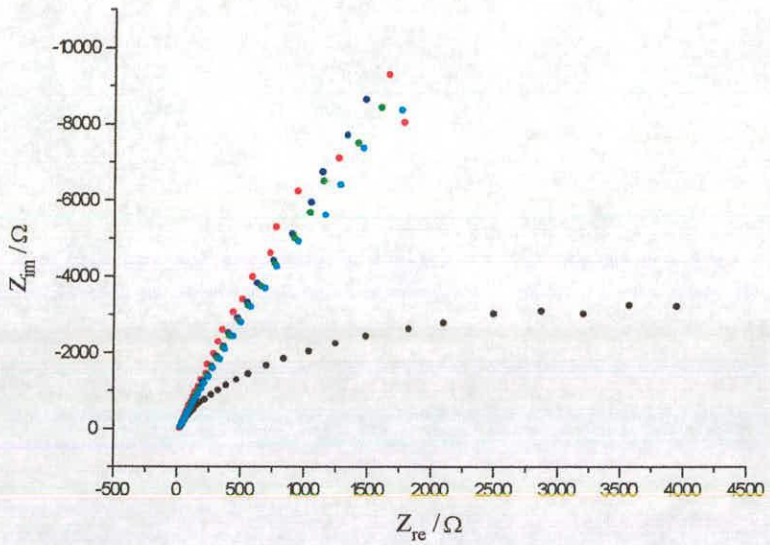

Figure 5.6: Ac spectra of poly(5CI) in 0.1M $TEAClO_4$
(• -100mV, • 100mV, • 200mV, • 300mV, • 400mV)

On transferring the modified electrode to 0.1M tetraethylammonium hexafluorophosphate, the spectra (figure 5.7) taken at positive potentials show an increase in the size of the semicircular region. This behaviour would be expected if these features were indeed due to the insertion of anions into the coat. However, the spectra taken at negative potentials also show an increase in the semicircular region when compared to the $TEAClO_4$ spectra. If this response was due to the kinetics of cation insertion then it would be expected that no appreciable change would be seen in the ac impedance spectra. Thus, this observation is not consistent with the kinetic barrier explanation. One possible reason for this behaviour could be that at the electrolyte concentrations used, the electrolyte salt cannot be said to be at infinite dilution with no

interactions occurring between the ions, but, instead, a degree of aggregation will occur with the cations having a "shell" of anions and vice versa. If this occurs then it would be expected that a slight dependence on anion type would be seen in the cation insertion kinetics due to the interaction of cations and anions in solution. However, this effect seems too large to be explained in this manner.

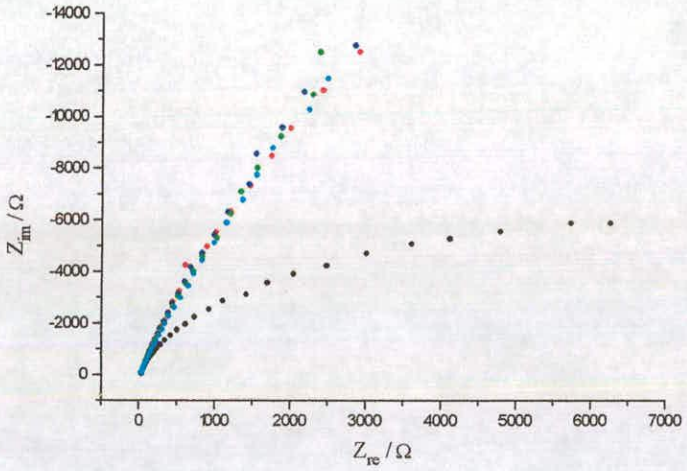

Figure 5.7: Ac spectra of poly(5CI) in 0.1M $TEAPF_6$
(• -100mV, • 100mV, • 200mV, • 300mV, • 400mV)

5.2.2 Quantitative Analysis

The spectra discussed in the last section clearly show the difficulties encountered in trying to obtain meaningful information about a particular system under study by qualitative analysis. This is because such analysis only makes use of the imaginary and real components of the data (i.e. the "shape" of the Nyquist plot) and does not use the frequency at which the data was taken in assessing the fit. Hence there is a need for an accurate method to extract physical parameters without the need for extensive hand waving. After fitting the spectra obtained to

a transmission line with a single charge transfer circuit, the trends in the spectra are more clearly seen.

Initial examination of the charge transfer resistance values for the cycled layer in 0.1M $LiClO_4$ (figure 5.8) show what, on first glance, appears to be a trend very similar to that seen for a poly(indole-5-carboxylic acid) film after extensive cycling. In that particular case, the behaviour of the kinetic resistance was explained by invoking a barrier at the electrode/polymer interface as the rate limiting charge transfer step at low and high potentials (the "walls" of the bowl) and a barrier to ion insertion at the polymer/electrolyte interface as the most resistive step at intermediate potentials (the flat "bottom" of the bowl). It is tempting to attribute the response seen for poly(5-cyanoindole) to a similar process. However, the comparison of this plot with the kinetic barriers observed for 0.1M $TEACLO_4$ and $TEAPF_6$ (figure 5.9) show that, in fact, this is not the case.

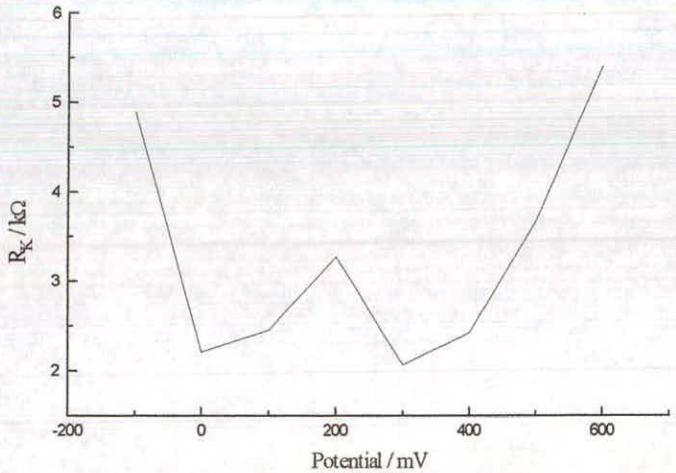

Figure 5.8: Variation of the kinetic barrier of poly(5CI) with potential in 0.1M $LiClO_4$

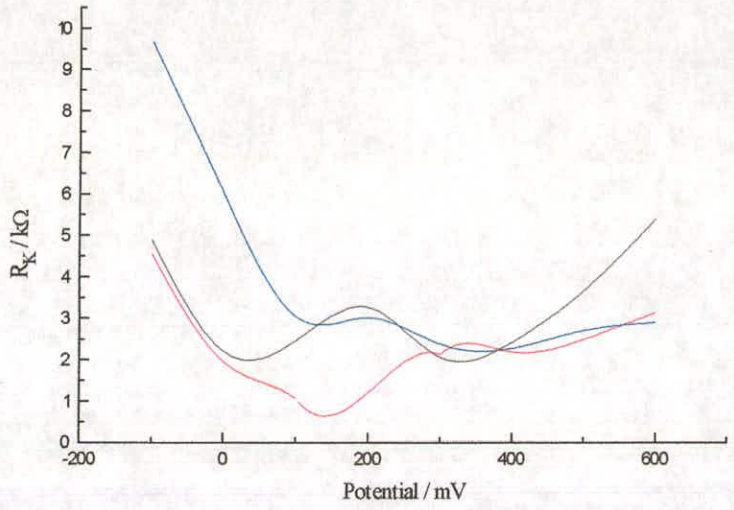

Figure 5.9: Variation of the kinetic barrier of poly(5CI) with potential (— 0.1M $LiClO_4$, — 0.1M $TEAClO_4$, — 0.1M $TEAPF_6$)

Examination of figure 5.9 shows a number of interesting features. The first is that, with the exception of the slight fluctuation around 150mV, the R_K values for $LiClO_4$ and $TEAClO_4$ show good agreement. This is to be expected if the redox behaviour of the coat indeed has a strong anion dependence, as can be inferred from the cyclic voltammograms. Also, as is to be expected, there is an increase in the R_K values on moving to a PF_6^- solution, though this only occurs at negative potentials. However, the difference in the sizes of the ClO_4^- and PF_6^- ions is too small, of the order of 0.1Å^2, to fully explain this large increase in R_K. It is more likely that the increase is caused either by a change in the thermodynamics of the insertion process or by a change in the shape of the anion. It is very interesting that the ion behaviour in the low potential region is entirely at odds with what is deduced by qualitative analysis. This provides clear evidence of the need for full and effective qualitative analysis of ac data. What is strange, however, is that it is only at these low potentials that any difference between the ClO_4 and PF_6 responses is seen. One possible

reason for this is that at higher potentials, the kinetic barrier to insertion is no longer due to desolvation. (It would be expected that the rate of ion desolvation would be potential dependent - in this case, increasing the potential applied to the coat would increase the driving force for anion insertion and, hence, would increase the rate of anion desolvation.) It is, instead, quite possible that the rate determining process for ion insertion is some other (potential independent) process at these more oxidising potentials such as the reorientation of the actual polymer strands to allow for the introduction of the anion. This process would be potential independent as well as being unaffected by the size of the anion present. From figure 5.9 it can be seen that, at least over the limited range of anion sizes used, this is so.

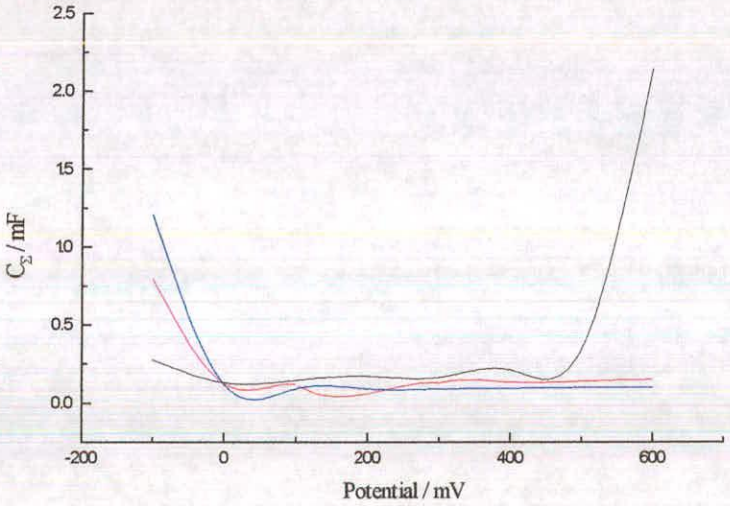

Figure 5.10: Plot showing the behaviour of the polymer capacitance, C_Σ, of a poly(5CI) film on varying the applied potential (— 0.1M $LiClO_4$, — 0.1M $TEAClO_4$, — 0.1M $TEAPF_6$)

Further confirmation of this hypothesis seems to come from both the behaviour of the polymer capacitance (figure 5.10) and the double layer capacitance (figure 5.11). Probably the most important feature of both of these plots is the actual values – the values of C_{DL} and C_Σ are, within

experimental error, equal and both have values which are consistent with a double layer capacitance. For this to be possible, C_Σ must only exist over a very small area of the polymer film and so only a small amount of the polymer must be accessible to solvent/electrolyte. The values for C_Σ, given by

$$\frac{1}{C_\Sigma} = \frac{1}{C} + \frac{1}{C_N} + \frac{1}{C_D}$$

are approximately constant with potential and show little fluctuation with anion size, again consistent with a polymer film with poor anion accessibility since

$$\frac{1}{C} >> \frac{1}{C_N}, \frac{1}{C_D}$$

which implies that C, the distributed capacitance of the coat, must be the smallest of the three terms. It is interesting, however, that the small fluctuations with anion size are consistent with what would be expected in that the results from the electrolyte with the smallest ions (both cations and anions) i.e. $LiClO_4$ has the largest capacitance while the electrolyte with the largest ions ($TEAPF_6$) has the smallest capacitance. Examination of figure 5.11 show two distinct anomalies: one at –100mV for $TEAClO_4$ and $TEAPF_6$ and on at 600mV for $LiClO_4$. It is possible that these are due to cation and anion insertion respectively with an increase in the solvation of the film leading to an increase in the Donnan and, especially, the Feldberg capacitances. However, this seems physically unlikely, especially since this is no similar large increase at 600mV for the other perchlorate salt ($TEAClO_4$). The more probable explanation is experimental error although the goodness of the fits for these values are comparable to that at any other potential/anion type combination (see Appendix C). It should, however, be pointed out that that these "large" increases in the polymer capacitance are very small when compared to the total capacitance available to the system. This maximum capacitance

is taken to be equal to the maximum capacitance obtained for a similarly produced (i.e. similar amount of charge passed during polymerisation) poly(indole-5-carboxylic acid) layer (figure 4.17). In this case, the film capacitances are approximately 2.5% of the maximum capacitance shown by a fully solvated poly(indole-5-carboxylic acid) coat. Also, it should be noted that when fitting the ac spectra, the C_Σ parameter has very little effect on any of the other values and so, little error should be introduced into the other fit parameters as a result of errors in C_Σ.

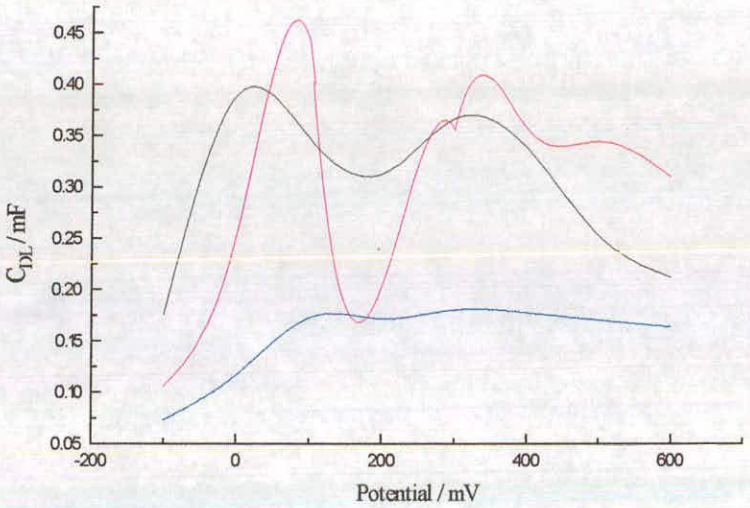

Figure 5.11: Plot showing potential dependence of the double layer capacitance, C_{DL}, for poly(5CI)
(— 0.1M $LiClO_4$, — 0.1M $TEAClO_4$, — 0.1M $TEAPF_6$)

The behaviour of the double layer capacitance seems to be a random variation around 0.3mF for $LiClO_4$ and $TEAClO_4$ with the values for $TEAPF_6$ on average a factor of 2 smaller than for the other electrolytes. One possible explanation for this is that the shape of the PF_6 anion prevents it from approaching the film as close as the ClO_4 anion is able to. This could cause a decrease in the capacitance since

$$C \propto \frac{1}{d}$$

where d is the distance between the charges (ions). However, the values are all of the same order of magnitude (within a factor of 2) and are of a value which is consistent with a double layer capacitance.

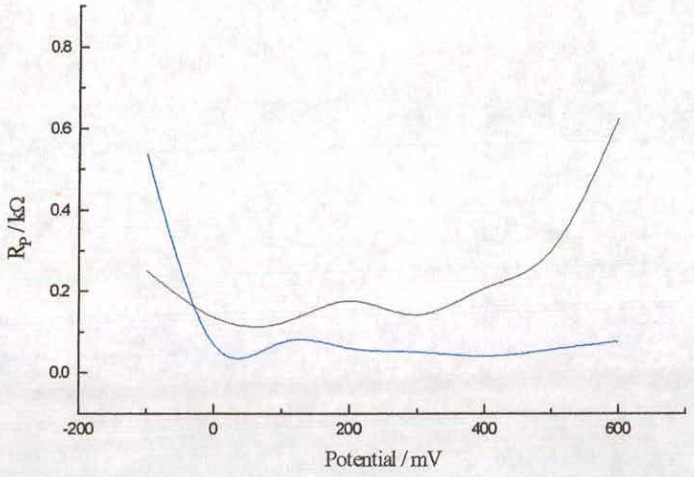

Figure 5.12: Plot showing the effect of variation in the applied potential on the actual resistance of a poly(5CI) film
(— 0.1M $LiClO_4$, — 0.1M $TEAPF_6$)

The values obtained for the observed polymer resistance show some very interesting behaviour. The values of R_P for 0.1M $TEAPF_6$ show a decrease with potential. This is entirely consistent with anion movement being the rate limiting step in conduction through the polymer film. The values for 0.1M $LiClO_4$ also show a rise at negative potentials. Although this rise could also be attributed to random scatter around a mean value, it is smaller than that observed for $TEAPF_6$ which is, again, consistent with anion movement being rate limiting. The sharp increase at high potentials seen for $LiClO_4$ can be attributed to an error since a similar (and equally physically inexplicable) rise is seen in the polymer capacitance (figure 5.10) at this potential. Probably the most startling fact about the values obtained for the resistance of the polymer film is their actual size (or lack of it). It would be expected that, due to the

relative sizes of the interfacical and bulk polymer regions, the values of R_P should, on the whole, be much larger than that of R_K. However, comparison of the R_P values (figure 5.12) and the R_K values (figure 5.9) show that, on average, the R_K values are a factor of 10 greater than the R_P values. The only plausible explanation for this is that this anion rate limiting process must only occur over a very small region of the polymer coat. This is entirely consistent with earlier observations that the coat is very compact and any redox behaviour occurs only in a small area at the electrolyte edge. The rest of the coat then exhibits very fast electron conduction similar to that shown by a fresh poly(indole-5-carboxylic acid) film which shows very little film resistance prior to cycling. This hypothesis is confirmed by the fact that the real intercept of the Nyquist plots is constant for each electrolyte used. This clearly shows that the resistance of the second conduction rail (i.e. that for the actual polymer strands) is so small as to be immeasurable. This is reasonable since the electropolymerisation and subsequent coupling mechanisms are similar so there is no reason to suspect that simply changing a side group for one of approximately equal size would prevent the polymer from being electrodeposited in stacks. A further verification of this is that constant current-time transients are always recorded on electropolymerisation of 5-cyanoindole signifying that the layer must have a constant resistance no matter the what the thickness. For this to be the case, then any coat resistance must be extremely small. This would, as before, mean that the polymer film will behave as a metal with fast electron conduction though the bulk. This argument is further verified by the fact that there is very little variation in the value of R_P with potential. This suggests that the conduction mechanism within the polymer is not electron hopping and so must be described by band theory, not by a localised redox model. This is consistent with the C_Σ data. The fact that the R_P values are also relatively constant (within experimental error) on changing the size of

the electrolyte anion gives good evidence that there is very little change in the polymer conduction mechanism (and so no gross morphology change) on cycling in supporting salts.

5.3 Charge Studies

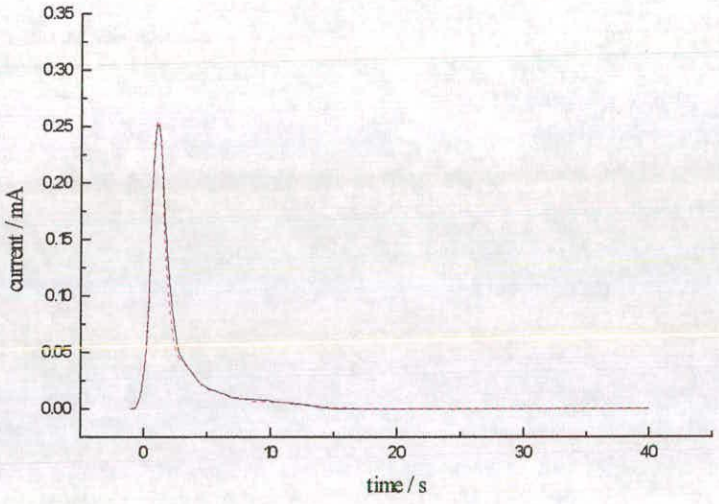

Figure 5.13: I-t transients recorded on pulsing poly(5CI) film from -125 to 475mV. (—— 1st pulse, --- 5th pulse)

The level of charge available to the polymer film on continuous cycling/pulsing between the oxidised and reduced states was monitored for 5-cyanoindole. Unlike the previous indole system, within the confines of experimental fluctuations, no change was noted in the amount of charge passed on repeated pulsing from a negative potential to a positive one. This can clearly be seen on examination of the current-time transients shown in figure 5.13. This behaviour confirms that there is little change in the coat on extensive switching between its reduced and oxidised states with little of the coat available for redox use. It is unfortunate that, in the case of the poly(5-cyanoindole) films studied,

even though, on average, more than 160mC was passed during polymerisation, the redox charge obtained during these experiments was too small to be measured using the equipment available. However, integrating under the current time transients gives a charge of 0.55mC passed during the first pulse and 0.53mC passed during the fifth. By comparing these values with the total available redox charge i.e.

$$\frac{160}{9} = 17.78\text{mC}$$

then it seems that, on average, only 3.0% of the total charge is accessed (compared with a fully solvated poly(indole-5-carboxylic acid) coat). It can reasonably be assumed, therefore, that only approximately 3% of the polymer film is used to provide the redox characteristics observed.

5.4 pH Studies

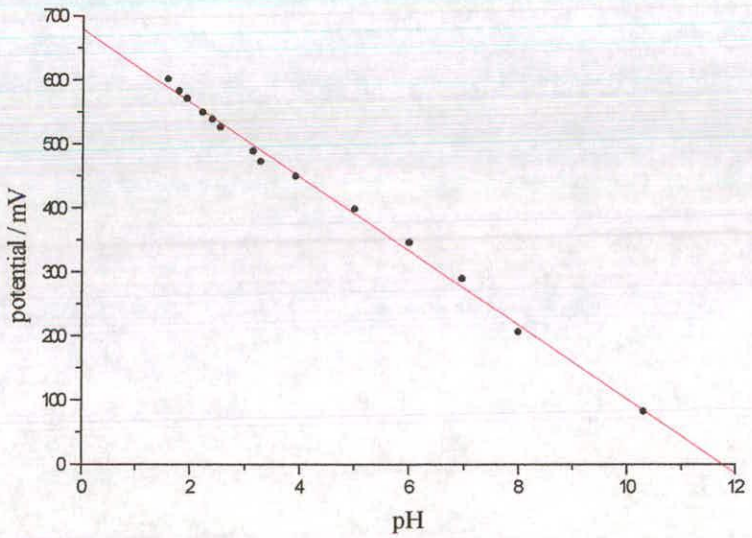

Figure 5.14: pH response of an as formed poly(5-cyanoindole) film

The following pH investigation was undertaken by other members of the Edinburgh Electrochemistry Group[3] and are reported here for completeness. A plot of potential against pH for a poly(5-cyanoindole) is shown in figure 5.14. It is very clear from the plot that there is a good linear dependence between the two variables with the line of best fit having a gradient of -57±5mV. This is entirely consistent with a response involving the removal of a single electron and proton. Like poly(indole-5-carboxylic acid), this proton is thought to come from one of the imide groups located on the trimer centre.

$$In_3H(COOH)_3 \longrightarrow In_3(COOH)_3 + H^+ + e^-$$

It has been found that after cycling, no appreciable difference is observed in the pH response of the system. This is entirely consistent with earlier thoughts that continuous switching of the polymer film between its oxidised and reduced forms has no effect in its electronic or physical nature. However, since there is no break region as there was in the case of poly(indole-5-carboxylic acid), it would be much more difficult to probe this system using this method anyway.

5.5 Summary

The results for cyclic voltammetry indicate that coats formed from 5-cyanoindole show redox behaviour with depends markedly on anion type and a slight dependence on cation type. On using a background electrolyte with a large anion and cation, the cyclic voltammogram shows an absence of redox features which do not reappear on further cycling. The amount of charge under the cyclic voltammograms is very much lower than expected considering the level of charge passed during electropolymerisation. This suggests that the capacitance of the coat is very much lower than, for example, a similarly polymerised poly(indole-5-

carboxylic acid) coat. This is consistent with only part of the polymer film being electroactive. Unlike the previous case of poly(indole-5-carboxylic acid), the CV in 0.1M $LiClO_4$ shows no change on extensive cycling, even after a number of weeks. This indicates that there is little change in the electrochemistry with time. Hence, unlike poly(I5CA), it can be implied that there is no gross morphological change.

Although, initially, the ac spectra obtained appear confusing to analyse from the Nyquist plots, fitting them using the transmission line developed during this thesis allows meaningful parameters to be extracted due to the use of the extra variable of frequency. These fitted values provide film capacitances which are approximately 2.5% of the maximum capacitance found for a fully solvated poly(indole-5-carboxylic acid) coat. This agrees well with results from chronoamperometry which shows that, constantly, only around 3% of the total redox charge is available. This clearly demonstrates the powerful nature of this technique. The fact that the fitted values of C_Σ are very similar to the double layer capacitance at the interface, C_{DL}, provides further proof that this capacitance must only be due to a small amount of the polymer film. It is interesting that the Feldberg capacitance appears to be smaller than the Nernst or Donnan capacitances. This is consistent with the results for an uncycled poly(indole-5-carboxylic acid) film which exhibits metallic like conduction and shows little redox oxidation/reduction. This is only to be expected since the electropolymerisation of indole-5-carboxylic acid and 5-cyanoindole follow similar mechanisms and show constant current-time transients during electrodeposition. Thus the discovery that both films are very conducting when first formed comes as no surprise.

The fitted values for resistance show, as expected from the cyclic voltammograms, that (at least at low potentials) anion insertion into the coat is the dominant factor in charge conduction, possibly due to the need

to initially remove the solvent shell from the ion before actual insertion into the film can occur. However, at higher potentials, although anion insertion is still the dominant process, the rate becomes potential independent and could be due, instead, to the rate determining step becoming the reorientation of the individual polymer strands to accommodate the anions.

The values for the observed polymer resistance show a potential dependence consistent with anion movement being the rate limiting step in the conduction. The values obtained are striking in their low magnitude suggesting that conduction though the actual polymer film must be fast and that the redox active anion insertion/removal region is small. This behaviour is similar to that seen for a freshly deposited poly(indole-5-carboxylic acid) coat which has not undergone any cycling. The fact that the Nyquist plots have a common real intercept (within experimental error) also suggests that conduction through the actual polymer backbone is extremely fast.

It is very interesting that the small cation dependence observed in the voltammograms is not shown in the fitted ac impedance data. However, this is not a great surprise since voltammetry involves large scale changes to the redox composition of the film and so can create large fields within the film. At high scan speeds, this can cause, for example, the intake of cation into the film as opposed to the ejection of anion (depending on the relative ease of each process). Impedance spectroscopy however only involves small perturbations from equilibrium and so these large fields do not come into play. It is interesting, however, that the cation dependence is seen at such low scan speeds. A slight cation dependence is seen on qualitative analysis of the ac Nyquist plots. However, the fitted data show that this apparent dependence is an

artefact of the change in shape of the Nyquist graphs. This is most probably due to the behaviour of the system being more of a mixed response from a transmission line with a frequency distinct charge transfer Randles circuit. This "mixing" of the individual responses cannot be seen by simply examining the real and imaginary impedances, but is very clear if the frequency relationship is considered. This clearly demonstrates the effectiveness of the analytical approach over the simplistic qualitative analysis.

The pH results give very little information with the exception that there is very little change in the film's response on cycling. Unlike the previous case, there is no break region and the response is Nernstian over a wide pH range.

5.6 References

1 A.D. Thomson; *PhD. Thesis*, University of Edinburgh, 1997

2 R.O. Gould; *Personal communications*, 1998

3 J.G. Mackintosh; *PhD. Thesis*, University of Edinburgh, 1995

6. Copolymers

6.1 Introduction

The copolymerisation of indole-5-carboxylic acid (I5CA) and 5-cyanoindole (5CI) has already been examined[1]. Previous work has focussed on the mechanism by which the electropolymerisation occurs along with the structural characterisation of the resultant film with no work examining the mechanism of charge conduction through this novel polymer coat. However, armed with fresh knowledge of how homogeneous films of either poly(indole-5-carboxylic acid) or poly(5-cyanoindole) conduct, it seems a logical step to next examine the subsequent behaviour where these monomers are mixed within a polymer film.

Work by MacKintosh et al. has shown that for equal concentrations of I5CA and 5CI and at an oxidising potential large enough to cause the mass transport controlled oxidation of both monomer species (+1.64V), a limiting current was observed which was approximately twice that for a

potential where only one monomer (I5CA), present at that concentration, would oxidise (+1.46V). The current-time transient for copolymerisation was found to show a current which was constant with time. Working from a simple model where the monomer species undergoes rapid oxidation followed by adsorption onto the electrode surface before any linking takes place, they suggest that this shows that the oxidation/adsorption of each monomer species must be equally likely under these high potential conditions. Assuming full monolayer coverage of the reacting monomer, this means that the proportion of adsorbed radical cation would be dependent on the ratio of the monomer concentrations at the electrode surface i.e.

$$\theta_{I5CA} = (1 - \theta_{5CI}) = \frac{c_{o,I5CA}}{c_{o,I5CA} + c_{o,5CI}} \qquad \text{Equation 6.1}$$

where $c_{o,I5CA}$ and $c_{o,5CI}$ are the surface concentrations of indole-5-carboxylic acid and 5-cyanoindole respectively and θ is the surface coverage of each species. Now, for the case where mass transport is not the limiting factor (i.e. where limiting currents are measured), the concentration of monomer species at the surface is equal to the bulk concentration and so equation 6.1 becomes

$$\theta_{I5CA} = (1 - \theta_{5CI}) = \frac{c_{\infty,I5CA}}{c_{\infty,I5CA} + c_{\infty,5CI}} \qquad \text{Equation 6.2}$$

where the c_{∞} terms represent the bulk concentrations of the individual monomer species.

Following the model proposed for the other indole systems where trimer formation results from the coupling of three neighbouring radical cations adsorbed onto the surface of an electrode and, since there will be a statistically random distribution of these cations, the coupling process should result in 4 separate trimer forms (figure 6.1).

Since the formation of a new trimer centre is required for further adsorption and reaction of three more monomer species on that particular site, the coupling rate for film formation is given by

$$\text{Rate} = (k_{I5CA}^3)\theta_{I5CA}^3 + 3(k_{I5CA}^2 k_{5CI})\theta_{I5CA}^2\theta_{5CI} + 3(k_{I5CA}k_{5CI}^2)\theta_{I5CA}\theta_{5CI}^2 + (k_{5CI}^3)\theta_{5CI}^3$$

where k_{I5CA} and k_{5CI} are the rate constants for the coupling of the I5CA and 5CI cations respectively. The first term in the above equation represents the formation of the pure I5CA trimer (figure 6.1(a)), the last the formation of the pure 5CI trimer (figure 6.1(d)) and the second and third terms the formation of the (2xI5CA, 1x5CI) trimer (figure 6.1(b)) and the (1xI5CA, 2x5CI) trimer (figure 6.1(c)) respectively of which each have three geometric isomers. It would therefore be expected that the ratio of these trimer units present in a coat formed from equal concentrations of the monomer would be 1:3:3:1 for (3xI5CA):(2xI5CA, 1x5CI):(1xI5CA, 2x5CI):(3x5CI). It is reassuring that this distribution is seen in mass spectrometric data[1]. It is therefore possible, by replacing the θ terms with the respective concentration ratios, to calculate the fractions of each trimer present in the coat by simply evaluating each of these terms

Hence, in a 50:50 I5CA:5CI film there will be:

For the pure 15CA trimer,

$$Fraction = \theta_{I5CA}^3 = (0.5)^3 = 0.125 \equiv 12.5\%$$

For the cotrimer comprising of (1x5CI, 2xI5CA),

$$Fraction = 3\theta_{I5CA}^2\theta_{5CI} = 3(0.5)^2(0.5) = 0.375 \equiv 37.5\%$$

For the cotrimer containing (2x5CI, 1xI5CA),

$$Fraction = 3\theta_{I5CA}\theta_{5CI}^2 = 3(0.5)(0.5)^2 = 0.375 \equiv 37.5\%$$

For the pure 5CI trimer,

$$Fraction = \theta_{5CI}^3 = (0.5)^3 = 0.125 \equiv 12.5\%$$

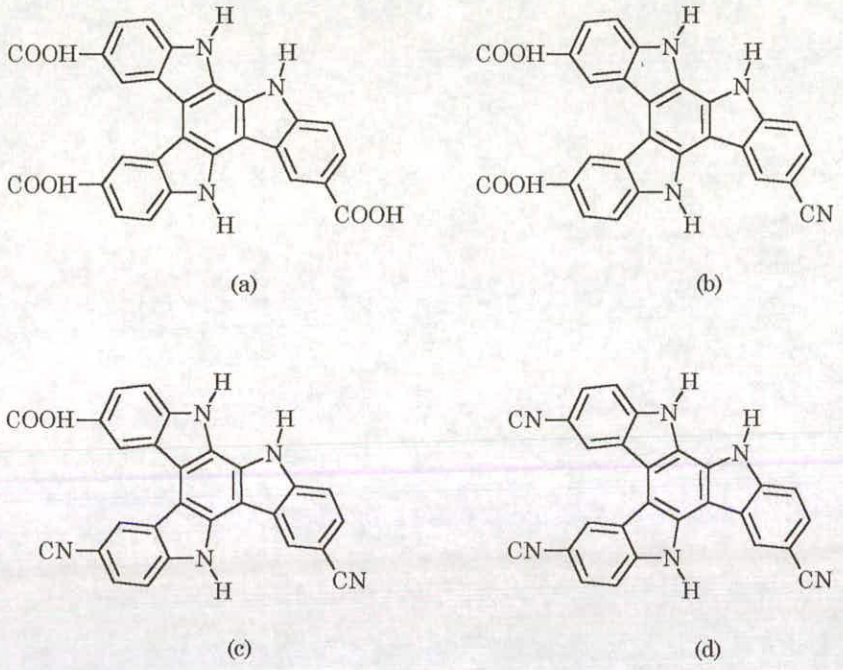

Figure 6.1: Structures of the possible trimer centres obtained from copolymerisation of I5CA and 5CI. It should be noted that structures (b) and (c) each have three geometric isomers

From the previous sections, it has been found that polymer films formed from indole-5-carboxylic acid and 5-cyanoindole have redox characteristics which are cation and anion dependent respectively. It is, however, not known how these dependencies will manifest themselves in a film where, unlike systems previously studied[2], no islands containing only one particular monomer species exist and where, instead, there is a random distribution of trimers within the polymer coat. It is hoped that, when fully understood, this type of copolymer will give rise a useful model for polymers containing dual functionality (in this case the -COOH and -CN groups) in an extremely intimate mixture. It is also hoped that examination of this system will provide some idea as to the effects (if any) on the use of transmission lines to model polymer films which contained a distribution of E° values.

6.2 Cyclic Voltammetry

All of the cyclic voltammetry data presented in this chapter are taken from studies of a copolymer electrodeposited from a 50:50 I5CA:5CI monomer solution.

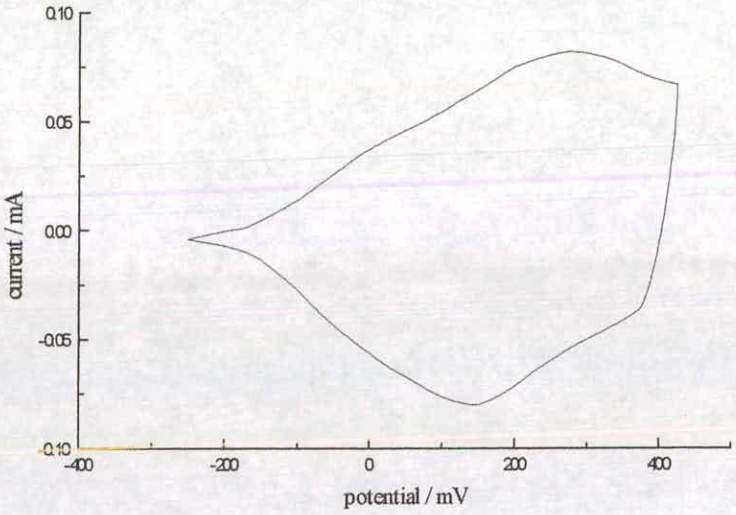

Figure 6.2: CV of the 50:50 I5CA:5CI copolymer in 0.1M $LiClO_4$ immediately after the production of the film. Scan speed = $2mVs^{-1}$

The initial cyclic voltammogram taken in 0.1M $LiClO_4$ (figure 6.2) is surprisingly similar to that obtained for a pure indole-5-carboxylic acid coat after moderate cycling. This suggests that the polymer, when formed, is relatively open and well solvated. The similarity to the I5CA CV also indicates that the coat exhibits very little –CN influence i.e. initially, the polymer film behaves as if it is simply a poly(I5CA) layer with no evidence for the presence of the 5-cyanoindole groups.

On further cycling, the peak present on the CV are seen to increase by approximately 50% (figure 6.3) possibly due to the ingress of ions on cycling in a manner similar to that seen in a poly(I5CA) film. It can also

be seen that both peaks shift slightly to more negative potentials. This indicates that with the oxidation process is becoming easier, the reduction step is becoming more difficult. Again this is consistent with observations from poly(indole-5-carboxylic acid).

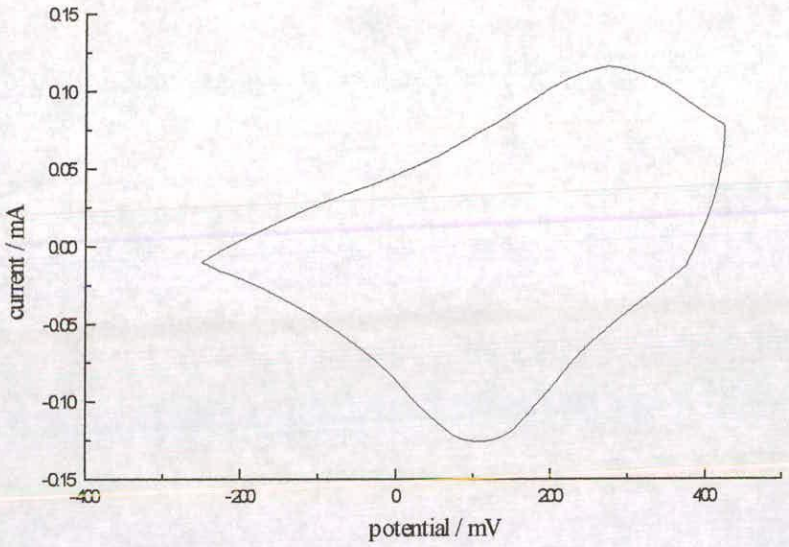

Figure 6.3: CV of a 50:50 copolymer after further cycling in 0.1M $LiClO_4$
Scan speed = $2mVs^{-1}$

On transferring the polymer modified electrode into 0.1M $TEAClO_4$ (figure 6.4), the charge under the CV is seen to drop by a considerable amount. The reduction peak is found to move by over 300mV to a much more negative potential while the oxidation peak stays approximately in the same place. This suggests that the reduction process is kinetically controlled and is possible due to cation insertion into the layer – the larger cation would be harder to incorporate.

The opposite change is seen on transferring the film to 0.1M $TEAPF_6$ (figure 6.5). As before, the total charge under the CV decreases, however, on this occasion, it is the oxidation peak that moves to more negative

potentials while the reduction peak stays in the same place. This suggests that it is now the oxidation process that exhibits kinetic control. One possible explanation for this behaviour is that the change in the oxidation peak must be due to anion while the change in the reduction peak is due to cation i.e. we are beginning to see evidence of both poly(indole-5-carboxylic acid) and poly(5cyanoindole) behaviour. Hence, the film seems to show both a cation dependence (at negative potentials) and an anion process (at high positive potentials).

If this film is once more immersed into 0.1M $LiClO_4$ solution then it is found that the peaks quickly (during the course of a single scan) reappear in approximately the same position and with approximately the same peak currents (figure 6.6). This provides very convincing evidence that any changes in the redox charge within the coat must be due to the changes in the cation/anion size/type and not due to any gross underlying morphological modifications.

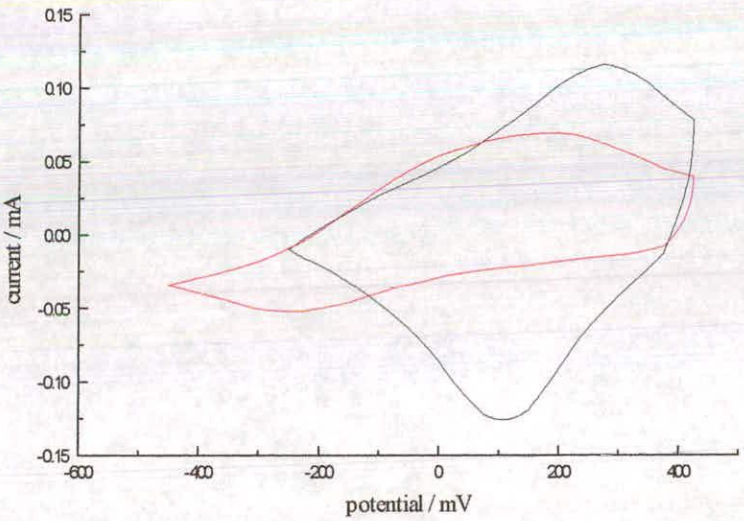

Figure 6.4: Steady state CVs of a 50:50 I5CA:5CI copolymer layer
(—— 0.1M $LiClO_4$, —— 0.1M $TEAClO_4$)
Scan Speed = $2mVs^{-1}$

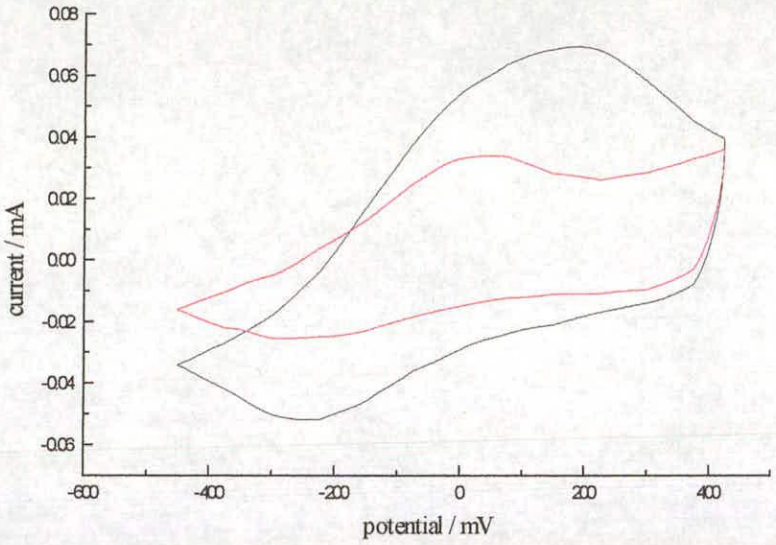

Figure 6.5: Steady state CVs of copolymer layer (—— 0.1M $TEAClO_4$, —— 0.1M $TEAPF_6$) Scan speed = $2mVs^{-1}$

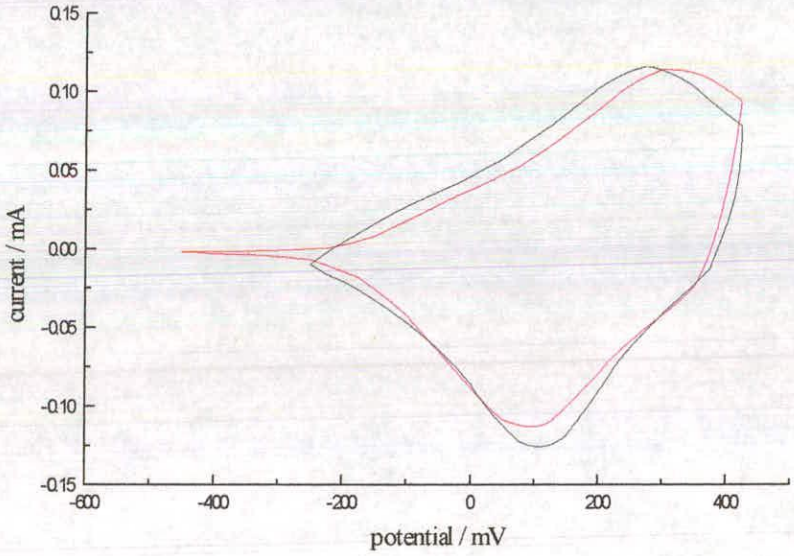

Figure 6.6: Steady state CVs of copolymer in 0.1M $LiClO_4$ showing the voltammograms taken before (——) and after (——) alteration of the electrolyte. Scan speed = $2mV^{-1}$

6.3 Ac Impedance Spectroscopy

The ac spectra obtained for a 50:50 I5CA:5CI copolymer are very difficult to analyse by examination of the Nyquist plots and require fitting before any meaningful results can be obtained. It is found that most fit well to a transmission line with a single charge transfer Randles circuit in series (see appendix D for fits).

A number of the low potential spectra, could not, however, be fitted. At these potentials, a very strange feature is seen. This anomaly seems to comprise of the latter half of a semicircle and has been attributed to the presence of small pinholes within the coat which can be used to short circuit the film at very high frequencies. Normally, the frequencies at which this effect takes place are outwith the range used. However, for this particular layer, this behaviour is seen for all electrolytes used where the layer impedance is very small. Thankfully, as the magnitude of the impedances measured increases, thie effect of this decreases. Those spectra which could be fitted, however, have provided some very interesting results.

The values of the kinetic barrier resistance (R_K) for a cycled copolymer film in various background electrolytes are shown in figure 6.7. It can clearly be seen that, on the whole, the kinetic barrier for all electrolytes increases with potential. It is quite possible that this behaviour is part of a "bowl" similar to that shown for a cycled poly(indole-5-carboxylic acid) layer (figure 4.18) but, examining the trends, it is more likely that it is due to a barrier to cation insertion. This cation dependent behaviour is to be expected since the CV is similar to that for a moderately cycled poly(I5CA) film. It would therefore be anticipated that the copolymer film would show a cation dependence as poly(I5CA) coat does. It is

interesting that the values of R_K above 400mV for $LiClO_4$ and $TEAClO_4$ are very similar. This seems to bear out the hypothesis that at potentials this positive, the cyano groups are oxidised and the anion dependence seen in poly(5CI) becomes apparent. On moving to $TEAPF_6$, this kinetic barrier at high potentials increases compared to the $LiClO_4$ and $TEAClO_4$ values. This is consistent with the kinetic barrier being due to anion insertion due to the effect of the oxidised (3x5CI) trimer. However, the difference in ion size between the perchlorate and hexafluorophosphate anions is, again, too small to account for such a large increase in R_K. This is similar to the behaviour of a pure poly(5-cyanoindole) film at low potentials (figure 5.9) and, again, is probably due to a difference in ion shape or a difference in the thermodynamics of the insertion process.

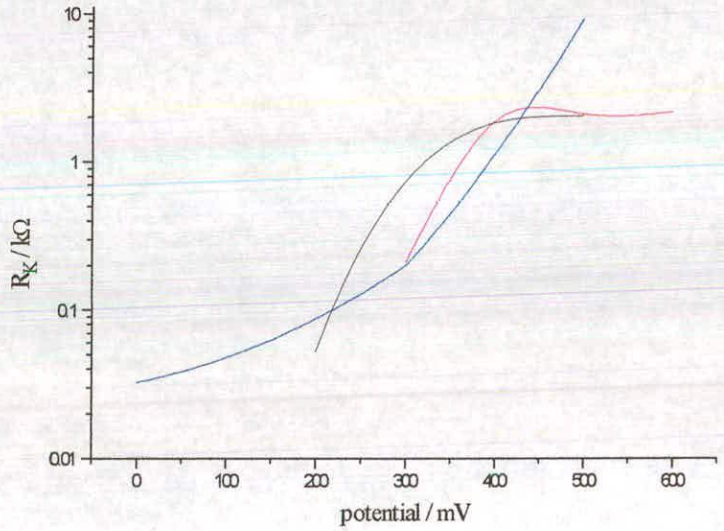

Figure 6.7: Variation of the kinetic charge transfer resistance with potential (—— 0.1M $LiClO_4$, —— 0.1M $TEAClO_4$, —— 0.1M $TEAPF_6$)

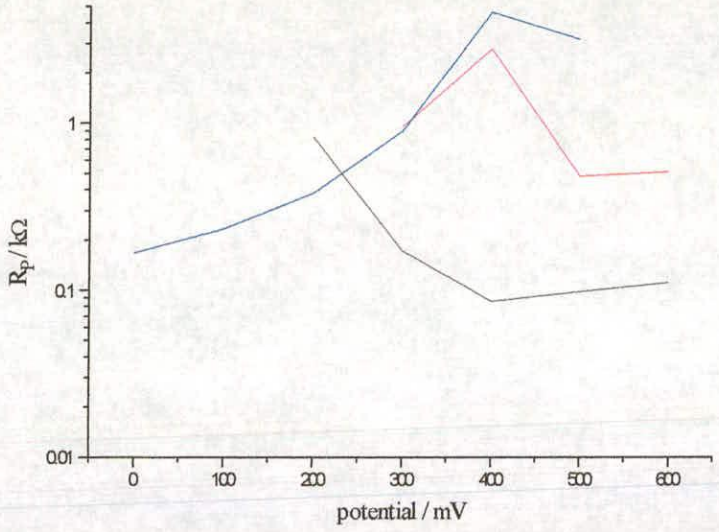

Figure 6.8: Plot showing potential dependence of the resistance of the bulk polymer, R_P

(— 0.1M $LiClO_4$, — 0.1M $TEAClO_4$, — 0.1M $TEAPF_6$)

The resistance of the actual polymer film shows some very interesting behaviour. Figure 6.8 shows the variation of R_P with potential. The polymer resistance in 0.1M $LiClO_4$ seems to go through a very shallow minimum at approximately 400mV though the width of this bowl appears to be very narrow. It is more likely that this resistance minimum is due to a statistical fluctuation in the polymer resistance and that, instead, the resistance values simple show a decrease with increasing potential. This behaviour is characteristic of a rate limiting step in the conduction due to anion movement. The magnitude of this resistance is very small (as are all of the values of R_P obtained from the spectral fits). This seems to indicate that this rate limiting step must only occur over a very small region of the polymer film. However, the presence of large redox peaks in the voltammograms and the C_Σ values reported later in this chapter both provide evidence that all of the polymer film is accessible. Therefore, the more plausible explanation for these low resistances is that the film is

very conducting over its entire bulk. The values of R_P obtained in a background electrolyte of 0.1M $TEAClO_4$ are slightly larger than those for $LiClO_4$ and could also show a slight decrease with increasing potential. However, due to the small number of fits obtained for spectra in this electrolyte and the amount of scatter in the data obtained, it is difficult to say with certainty if this is indeed the actual trend or if, in this case, R_P is actually independent of potential and we are seeing a statistical distribution of values around a mean. If the film is then transferred into 0.1M $TEAPF_6$, then the trend in the data changes and the R_P values show an increase with potential. This indicates that the dominant process in the coat conduction is now cation movement. It is possible that the slight drop in R_P at high potentials is a real and is due to the build-up of anion in the layer which acts as a secondary conduction pathway and so causes a slight decrease in the film resistance.

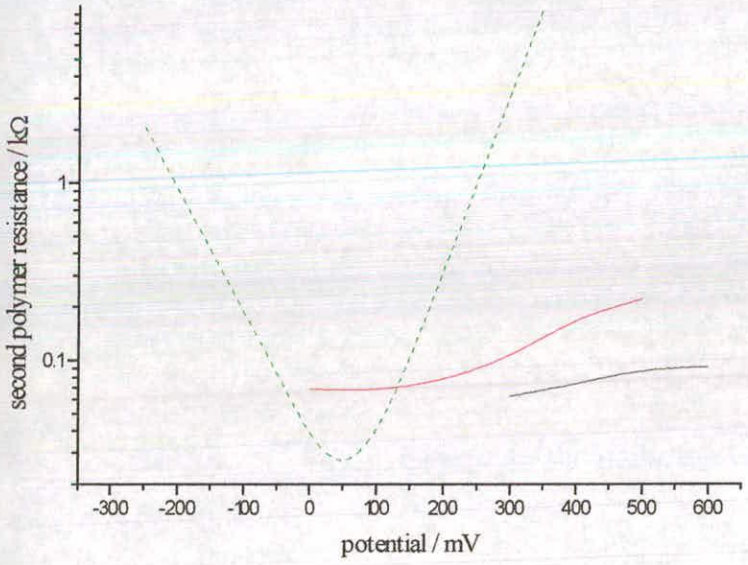

Figure 6.9: Plot of second polymer (electronic) resistance for 0.1M $TEAClO_4$ (——) and 0.1M $TEAPF_6$ (——). The dotted line (---) shows the repositioned fit obtained for poly(I5CA) in 0.1M $LiClO_4$ for comparison of shape

Although quantitative analysis of the Nyquist plots proved to be difficult, they do show one interesting fact. As mentioned previously, the real intercept of the Nyquist plot provides a value for the resistance of the electrolyte solution. It should, therefore, for a given cell arrangement, be constant. However, close examination of the Nyquist spectra for 0.1M $TEAClO_4$ and $TEAPF_6$ show that this is not the case. Instead, the intercepts are seen to increase with potential. The cause for this is that there is a second polymer resistance which must also be taken into consideration. The value of this second resistance can easily be obtained by subtracting the true solution resistances for these electrolytes from the observed ones. The trends in these values with potential are shown in figure 6.9 along with the theoretical fit to $R_{K,P}$ for poly(indole-5-carboxlyic acid) in 0.1M $LiClO_4$. It should be noted that the location of this fit has been altered from figure 4.18 to enable a better comparison of the shape of the plots. As expected, these second polymer resistance values increase with potential and are thought to be due to electron conduction through the polymer backbone (since R_P has already been assigned to ion motion though the pores). Although difficult to observe for the $TEAClO_4$ data due to the small number of spectra fitted, comparison with the fit obtained for poly(indole-5-carboxylic acid) shows that the copolymer bowls are much wider than those seen for poly(I5CA). There are two possible reasons for this: 1. there is a distribution of E° within the coat due to the presence of the different trimer centres and 2. very little of the potential is dropped over the bulk of the polymer coat due to the large kinetic barrier at the polymer/electrolyte interface. It is, however, impossible to assess the relative contributions of these two factors. Again, these values are small and are consistent with fast conduction through the polymer film.

One interesting result from both the R_K and R_P values obtained from ac studies which should be noted is that the resistances obtained for the copolymer in 0.1M $TEAClO_4$ and 0.1M $TEAPF_6$ show good agreement at 300mV and gradually worse agreement as the potential is increased (table 6.1). It is possible that this is just down to chance, however, it is also possible that this is caused by the fact that at 300mV, the cyano groups are not oxidised and so the film shows some cation dependence probably due to the presence of the reduced form of one of the cotrimers containing a carboxylic acid group. However, as the potential is increased, the (3x5CI) trimer will become oxidised and the anion dependence observed in poly(5-cyanoidole) will be observed.

	Potential / mV	
	300	500
R_P in 0.1M $TEAClO_4$ / kΩ	0.95	0.51
R_P in 0.1M $TEAPF_6$ / kΩ	0.90	3.18
R_K in 0.1M $TEAClO_4$ / kΩ	0.21	2.11
R_K in 0.1M $TEAPF_6$ / kΩ	.020	9.27

Table 6.1: Comparison of resistances of 50:50 copolymer in 0.1M $TEAClO_4$ and $TEAPF_6$ showing similarities at 300mV

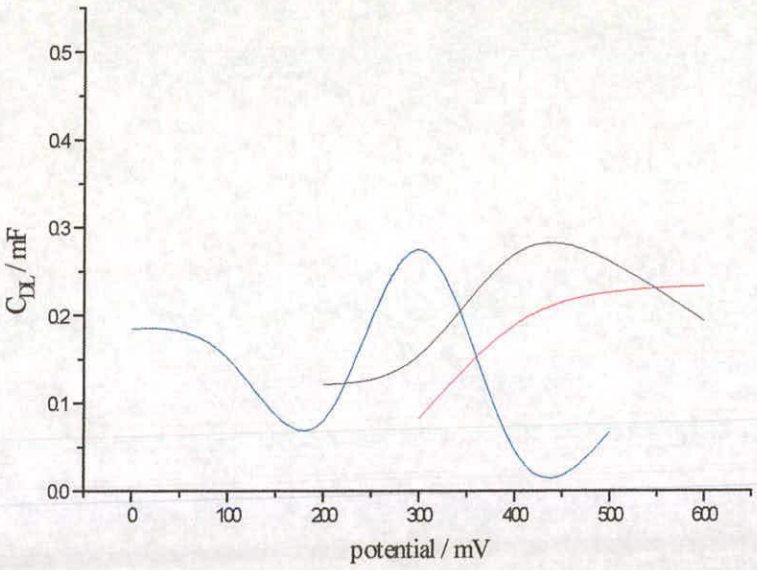

Figure 6.10: Variation of the double layer capacitance, C_{DL}, with potential.
(—— 0.1M $LiClO_4$, —— 0.1M $TEAClO_4$, —— 0.1M $TEAPF_6$)

Turning now to the coat capacitances, it is very reassuring that the values of the interfacial double layer capacitance, C_{DL}, (figure 6.10) are approximately constant and are of the magnitude expected for the results from the pure polymer layers (i.e. around 0.1-0.2mF). Although there appears to be a relatively large spread in the C_{DL} values, these values do not have much effect on the other parameters obtained.

The trends in the C_{Σ} data (figure 6.11) are of much more interest than those of C_{DL}. All of the polymer capacitances are seen to decrease with potential in a manner similar to that seen for poly(indole-5-carboxylic acid) and also have values with are similar to that of fully cycled poly(I5CA) films. This suggests that the capacitance is due to cations in the film. However, previous studies on poly(I5CA) have shown that it is unable to accept the insertion of very large ions. Therefore, somehow,

copolymerising indole-5-carboxylic acid with 5-cyanoindole has allowed the previously impossible ingress of a large, organic cation to take place. The fact that the values of C_Σ for the copolymer are of similar magnitude to that for poly(indole-5-carboxylic acid) is good evidence that the coat has a similar open structure with all sites accessible unlike polymer films of pure poly(5-cyaniondole).

The fact that the data, with the exception of the values for $TEAClO_4$ which consists of only a few points, show lower slopes (i.e. a wider shape) than that for poly(I5CA) is consistent with the trend in the polymer resistance (obtained from the change in the electrolyte resistance). The cause of this has already been discussed.

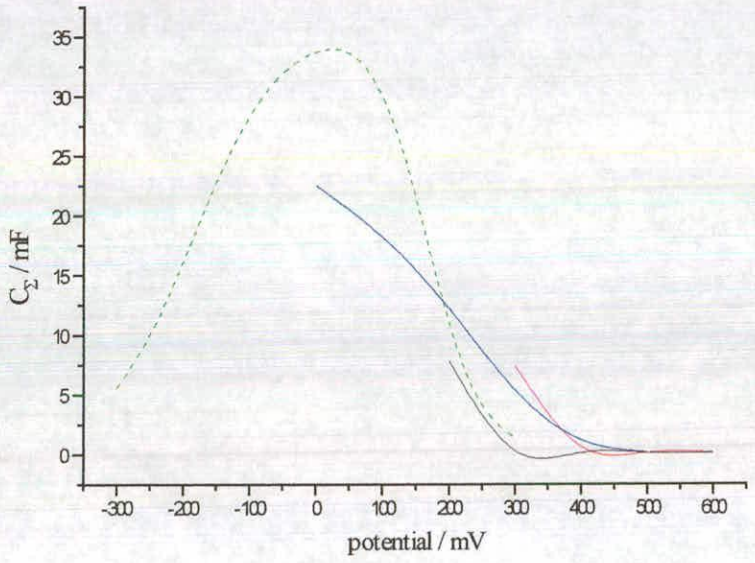

Figure 6.11: Plot of variation of coat capacitance, C_Σ, with potential for a 50:50 copolymer film.
(—— 0.1M $LiClO_4$, —— 0.1M $TEAClO_4$, —— 0.1M $TEAPF_6$,
---fit for poly(I5CA) in 0.1M $LiClO_4$)

6.4 pH Studies

The pH response of a 50:50 I5CA:5CI film has already been well studied[3]. However, studies observing the pH response of films with monomer ratios of 1:9 (I5CA:5CI) and 4:6 have been carried out and yield interesting results.

Following same system used in section 6.1, the percentage of each possible trimer species in the layer has been calculated:

in a 1:9 I5CA:5CI film there will be:

For the pure 15CA trimer,

$$Fraction = \theta_{I5CA}^3 = (0.1)^3 = 0.001 \equiv 0.1\%$$

For the cotrimer comprising of (1x5CI, 2xI5CA),

$$Fraction = 3\theta_{I5CA}^2\theta_{5CI} = 3(0.1)^2(0.9) = 0.027 \equiv 2.7\%$$

For the cotrimer containing (2x5CI, 1xI5CA),

$$Fraction = 3\theta_{I5CA}\theta_{5CI}^2 = 3(0.1)(0.9)^2 = 0.243 \equiv 24.3\%$$

For the pure 5CI trimer,

$$Fraction = \theta_{5CI}^3 = (0.9)^3 = 0.729 \equiv 72.9\%$$

and, in a 4:6 I5CA:5CI film there will be:

For the pure 15CA trimer,

$$Fraction = \theta_{I5CA}^3 = (0.4)^3 = 0.064 \equiv 6.4\%$$

For the cotrimer comprising of (1x5CI, 2xI5CA),

$$Fraction = 3\theta_{I5CA}^2\theta_{5CI} = 3(0.4)^2(0.6) = 0.288 \equiv 28.8\%$$

For the cotrimer containing (2x5CI, 1xI5CA),

$$Fraction = 3\theta_{I5CA}\theta_{5CI}^2 = 3(0.4)(0.6)^2 = 0.432 \equiv 43.2\%$$

For the pure 5CI trimer,

$$Fraction = \theta_{5CI}^3 = (0.6)^3 = 0.216 \equiv 21.6\%$$

The pH responses of both copolymer films are shown if figure 6.12. As expected, the film responses lie between that of poly(I5CA) and poly(5CI).

It is very interesting that, initially, both films display very similar responses with very similar gradients. It would be expected that, for a redox hopping polymer, due to the heterogeneous nature of the polymer films and the different relative compositions of each layer, the variation of E° caused by the different E° values for the four trimer compositions will be different. Hence, due to a modified Nernst equation which takes into account the (Gaussian) spread of E°, the gradients of the pH responses would be expected to be different. In work by Albery et al.[4] this modification takes the form of an α term (equation 6.3)

$$E = E^\circ + \frac{RT}{\alpha nF} \ln \frac{[oxidised\_species]}{[reduced\_species]} \qquad \text{Equation 6.3}$$

where

$$\alpha = -\frac{1}{nP} \ln \left[\frac{\pi^{1/2}}{\int_{-\infty}^{+\infty} \frac{\exp(-\xi^2 \Delta P^2) d\Delta P}{1 + \exp(n\Delta P - nP)}} - 1 \right]$$

and

$$P = \frac{(E - E^\circ)F}{RT}$$

$$\Delta P = \frac{(E^\circ - \overline{E}^\circ)F}{RT}$$

and where $\overline{E}^\circ$ in the average standard potential and ξ describes the spread of the Gaussian distribution. It would also be expected that the gradients of these initial Nernstian regions should also be very different to those of the pure poly(I5CA) and poly(5CI) films. The observation that this is not the case is good evidence that charge transport in the bulk of the coat is not due to redox hopping.

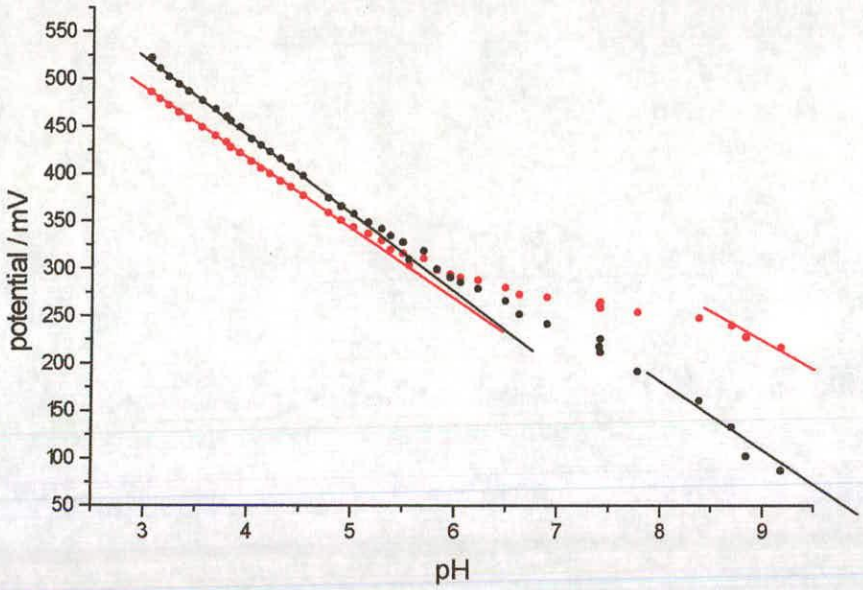

Figure 6.12: pH responses of the 1:9 (•) and 4:6 (•) I5CA:5CI copolymers. (The straight lines show the approximate location of the Nernstian regions)

Although the Nernstian areas are very similar, there is, however, a very obvious difference between the break areas. As mentioned previously, these break areas are thought to be due to the transfer of a proton from the imide group to a deprotonated carboxylic acid site on the trimer centre on electron transfer and, therefore, they should provide a means to determine, at least qualitatively, the level of COOH groups with in the polymer film.

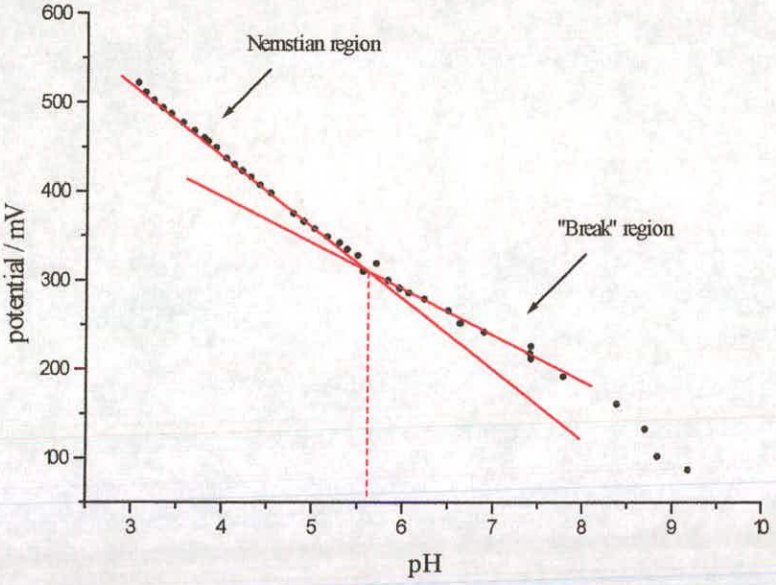

Figure 6.13: pH response of 10:90 copolymer film showing break from Nernstian behaviour at pH 5.62

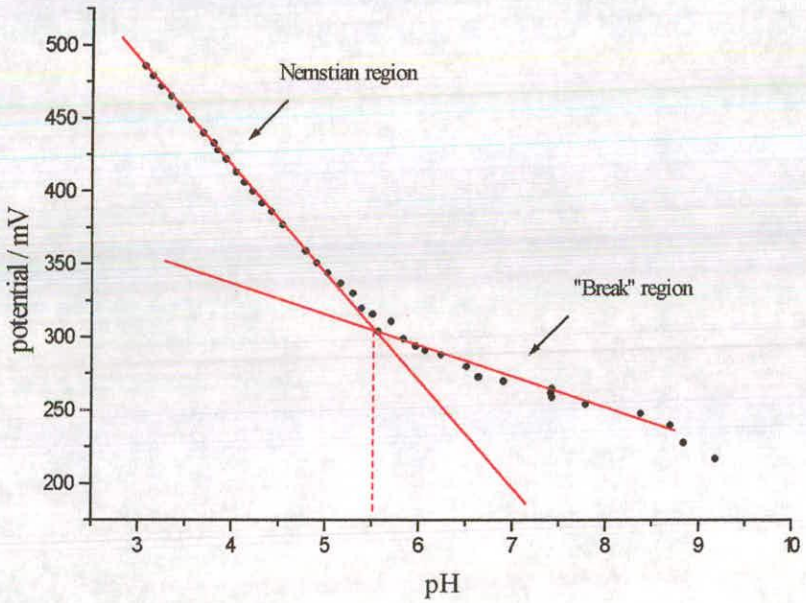

Figure 6.14: pH response of 40:60 copolymer showing break from Nernstian behaviour at pH 5.52

It is reassuring that the pH at which this break from Nernstian behaviour occurs is the same for both copolymer compositions (shown clearly in figures 6.13 and 6.14). If, indeed, the break is caused by the deprotonation of a carboxylic acid group then, due to the stabilisation of the resultant carboxylate anion by the two electron withdrawing –CN groups, it would be expected that the trimer consisting of (1xI5CA, 2x5CI) would have the lowest pK_a. Since both copolymer compositions have such trimer groups in reasonably large quantities (even in the 10:90 film, approximately 25% of the coat comprises of such trimers) it is only logical that the breaks will occur at the same location

It can be seen in figure 6.12, 6.13 and 6.14 (though most clearly in figure 6.12) that the break region for the 40:60 copolymer is much wider than that for the 10:90 copolymer. Again, this is entirely to be expected. The 40:60 copolymer comprises of a greater percentage of trimers containing (2xI5CA, 1x5CI) and (3xI5CA). Following the same argument as above, the pK_a values for these trimer units will be progressively greater than that of the (1xI5CA, 2x5CI) cotrimer. The spread of pK_a values leads to the break region extending over a wider pH range. On the other hand, the 10:90 copolymer consists mainly of the (3x5CI) and (1xI5CA, 2x5CI) trimers and so does not experience such a wide range in the pK_a values.

6.5 Summary

Initial cyclic voltammograms taken for a 50:50 indole-5-carboxylic acid:5-cyanoindole copolymer in 0.1M $LiClO_4$ exhibit both the behaviour shown by poly(I5CA) and poly(5CI). At high positive potentials, where the (3x5CI) trimer is oxidised, the polymer film displays an anion dependence

while at lower potentials, where the I5CA containing trimers and cotrimers are reduced, a cation dependence is found.

Ac data shows the presence of a considerable barrier to cation insertion at the polymer/electrolyte interface consistent with results for poly(I5CA). However, at high potentials, an anion dependency is observed. This is consistent with the polymer film becoming anion dependent at high potentials due to the oxidation of the (3x5CI) trimer resulting in the build up of a slight (positive) Donnan field. However, the anion dependence is too large to be accounted for by simply considering anion size. This interesting discovery could be caused by the different shapes of the anions used in the investigation or could be due to a change in the thermodynamics of the anion insertion process.

The values of the corresponding (double layer) capacitance, although showing extreme fluctuations, are all of the expected magnitude (0.1-0.3mF) for a double layer.

The coat capacitance shows behaviour similar to that seen in poly(I5CA) suggesting that the capacitance is in part due to the concentration of cations within the coat. However, studies of pure poly(I5CA) have suggested that the coat is unable to accept the entry of such large cations even when fully solvated. It seems sensible to suggest that the inclusion of the 5-cyanoindole species into the polymer film has altered the thermodynamics of the coat in some way as to allow the ingress of such a large, organic cation. The values of C_{Σ} obtained indicate that the film, when cycled, has a much more open structure than that of a pure poly(5CI) film which is expected and that all of the trimer sites are accessible.

The resistance of the bulk polymer is found to have of two separate components, one the resistance of the ions within the pores and the other the electronic resistance of the polymer backbone. Results from the pure trimers have shown only one of these resistances to be important. The electronic resistance is found to go through a minimum consistent with a redox hopping mechanism. The actual magnitude of this resistance suggests that this process is very fast. The width of the resistance "bowl" is much wider than that found at the poly(I5CA) electrode/polymer interface. This is due to the presence of a distribution of redox potentials in the coat (due to the presence of the different trimer species) and/or due to there being little potential drop across the bulk of the polymer (with most of the drop occurring at the polymer/electrolyte interface). The resistance of the ions in the polymer layer indicates that the nature of the background electrolyte used determines which ion type is important in conduction.

pH studies on 10:90 and 40:60 copolymer compositions have shown that the length of the break from Nernstian behaviour seen in poly(I5CA) and due to the intratrimer transfer of a imide proton to a deprotonated carboxylic acid group can be correlated with the proportion of the different indole-5-carboxylic acid containing trimer centres (and hence the pK_a of the trimer centre) within the film. The location at which this break occurs is found to be constant for the compositions studied and represents the loss of an acid proton from a carboxylic acid group in a (1xI5CA, 2x5CI) cotrimer.

6.6 References

1 J.G. MacKintosh, S.J. Wright, P.R.R. Langridge-Smith, A.R. Mount; *J. Chem. Soc. Faraday Trans.*, 1996, **92**, 4109

2 X.M. Ren, P.G. Pickup; *Electrochim. Acta*, 1996, **41**, 1877

3 J.G. Mackintosh; *PhD. Thesis*, University of Edinburgh, 1995

4 W.J. Albery, M.G. Boutelle, P.J. Colby, A.R. Hillman; *J. Electroanal. Chem.*, 1982, **133**, 135

7. Conclusion

From the results presented in this thesis, two things seem obvious. On a chemical front, the simple change in the functionalisation of a 5-substituted indole monomer leads to great changes in the behaviour and conduction mechanism of the associated polymer film. From an analytical viewpoint, this thesis shows the powerful nature of the model proposed by Albery and Mount to simulate charge conduction within conducting polymers in that it can be used to obtain values and trends which are physically viable from such diverse systems, even when the spectra obtained are, at first sight, confusing. Probably the most powerful aspect of this approach is that, unlike the scheme proposed by Buck, Brumleve and Barker[1] (the BBB model), the Albery and Mount model does not require the truncation of the equivalent circuit in order to obtain a numerical approximation of the necessary differential equations and so provides a "purer" analytical solution.

Films produced from a monomer solution of indole-5-carboxylic acid show initial behaviour consistent with a very conducting film with very little

electrochemical behaviour. This agrees with chronoamperometry taken during electropolymerisation. This high conduction is most likely due to the extensive delocalisation of π-electrons through planar stacks of deposited trimer centres. When initially formed, the polymer layer displays a kinetic barrier to cation insertion which has been assigned to the physical insertion of cations. These films show a gross morphological change on cycling. This change, which is thought to be due to the reorientation of the polymer strands which opens the coat and allows the ingress of cations. This reorientation is believed to buckle the trimer stacks and remove the π-delocalisation causing the dominant conduction mechanism in the film to change to redox hopping. This change from a compact structure allows the film to become more lyophilic, with more solvent and electrolyte entering the layer, and the dominant kinetic barrier changes from cation insertion at the polymer/electrolyte interface to electron insertion at the electrode/polymer interface. These observations are backed up by potential step chronoamperometry and pH measurements which all indicate that the coat becomes more open and accessible to ion incorporation on extensive switching between its oxidised and reduced states.

In complete contrast, coats of similar thickness formed from 5-cyanoindole show no gross morphological changes on redox switching. The redox behaviour of such films are observed to exhibit a strong anion dependence as opposed to a cation dependence shown by poly(indole-5-carboxylic acid) layers. Poly(5CI) films do show a cation dependence in cyclic voltammetry though only very slight. As in the previous case, the coat is believed to be deposited in a compact form with very little of the film accessible to such things as electrolyte and solvent. In fact, chronoamperometry and ac impedance data suggest that in the films studied, only approximately 3% of the film is electroactive. The rest of

the film it believed to exhibit fast conduction similar to that for poly(I5CA) films with extensive π-delocalisation. A kinetic barrier to anion insertion exists at the polymer/electrolyte interface as expected though the rate determining step for this barrier is seen to change at high potentials from the actual insertion of the anion to the reorientation of the local area of the film to accommodate the ion.

Although the conduction in poly(5-cyanoindole) is relatively well understood, a little further work may be useful. It would be interesting to see if it is possible to create a more open poly(5-cyanoindole) coat for example by polymerising with larger anions present in the background electrolyte in the hope to buckle the trimer stacks and allow redox hopping to occur. Such behaviour has been seen for poly(5-cyanoindole) polymerised in 0.1M $TEAClO_4$ in acetonitrile from conductivity measurements by Zotti et al[2]. However, this work has also shown that, interestingly, poly(5-cyanoindole) films show no conduction, i.e. are insulating, in their fully oxidised and reduced states. At this time, it is not known is this observation is due to limitations in the equipment (i.e. a large, but not infinite, polymer resistance which gave rise to a current to small to detect) or due to the fact that the investigation was carried out in aqueous media. It would be useful, therefore, to repeat such an investigation using ac impedance to see if any concurrence could be observed. It is also interesting that the potential at which Zotti observed maximum conduction is what would be expected given the results for poly(indole-5-carboxylic acid) detailed in this thesis if the difference in the polymerisation potentials between poly(I5CA) and poly(5CI) are taken into account along with the correction required by Zotti's use of a saturated calomel electrode.

Recent work at Edinburgh University[3] has also shown that modification of other polymerisation variables (such as monomer concentration and degree of forced convection) can have an effect on the degree of

compactness of the coat structure. This group has found that for poly(I5CA) there is a correlation between that degree to which the coat is open when deposited and the proportion of polymer present in the film. In fact, it has been observed that indole-5-carboxylic acid films which contain primarily polymer (as opposed to trimer) show cyclic voltammograms consistent with an open film within 10 cycles instead of 10s of days/100s of cycles. It is expected that a similar correlation will be observed for poly(5CI) films.

It is obvious that the vastly different behaviour shown by polymer films formed from indole-5-carboxylic acid and 5-cyanoindole must be due to the different functional groups present. However, the reason for this difference is not immediately obvious and requires consideration of the effects of fields induced during voltammetry. In the case of a poly(indole-5-carboxylic acid), the film, as previously discussed in chapter 1, is deposited in its oxidised form with an associated counterion (in this case a perchlorate anion) from the background electrolyte to preserve electroneutrality. On reducing the coat, the polymer becomes neutral. However, the anions cause the coat to become negatively charged and some (probably those close to the electrolyte interface) are ejected to reduce this effect. On re-oxidising the film, the polymer again becomes positively charged, however some of the counteranions have been lost to the bulk solution. There is, therefore, a deficiency in the countercharge and a field builds up to reduce this. This (Donnan) field can do this in one of two ways: it can either encourage the uptake of negative ions from the electrolyte or it can cause the ejection of positive ions (protons from the carboxylic acid groups) from the coat. Due to the size of the perchlorate anion and the acid nature of the –COOH groups, it is likely that this field assisted deprotonation will occur in preference to anion ingress. Hence, the coat will become less positive than before. On reducing the film, the carboxylate anions will create a slight field at the

interface which will drag cations into the coat from the bulk electrolyte. This process is especially important when the cation is Li^+ since it is known that the carboxylate anion has a strong affinity for lithium with which it form an ion-pair like complex (hence there is a strong thermodynamic driving force for the incorporation of this cation). This will distort the polymer film due to the different shape/size of the ion and cause it to become more accessible to solvent and electrolyte (i.e. essentially, the position of the interface will move into the film). Continuous oxidising and reducing will repeat this process of field assisted deprotonation and cation incorporation followed by coat opening until the whole coat is accessible to solvent and electrolyte ions.

On the other hand, poly(5-cyanoindole), although initially similar, being deposited in its oxidised form with a perchlorate anion (again to preserve electroneutrality), has no easily pathway to lessen the positive charge present on reduction and subsequent re-oxidation. It must, therefore, reincorporate the previously ejected anion in order to keep the coat electrically neutral. There is, consequently, no need for the coat to distort (the same ion goes in that comes out) and so the film does not become more open and accessible to solvent/electrolyte.

The copolymer formed from indole-5-carboxylic acid and 5-cyanoindole yields very interesting results. Put in its simplest terms, the polymer behaves both like a poly(I5CA) and a poly(5CI) film. At potentials where the indole-5-carboxlic acid groups are reduced, a cation dependence is observed while at potentials where the 5-cyanoindole species are oxidised, an anion dependence is noted. This is to be expected considering the charge on the indole-5-carboxylic acid species (neutral when oxidised, negative when reduced) and the 5-cyanoindole species (neutral when reduced, positive when oxidised). The anion dependence observed cannot simply be explained away as a difference in anion size since the anions

used have the same radii (to within 0.1Å). However, it seems that the perchlorate ion is easier to insert into the film than the hexafluorophosphate ion. It is possible that this may be due not to the size of the anion, but instead to its shape although more work would have to be carried out using different electrolytes with a wide range of anion size to confirm this. What is, however, interesting is that the exact nature of the dependence shown in the ion resistance of the polymer is dependent on the nature of the electrolyte used. If a small cation (such as Li^+) is used with a large anion (e.g. ClO_4^-) then the resultant film shows an anion dependence in its conduction mechanism while if the opposite is true i.e. large cation and small anion then a cation dependence is noted. This suggests that both types of ions play an important role in the conduction mechanism however, further study is required to see if this is also the case at negative potentials where, in the case of this thesis, physical parameters could not be obtained from ac spectra. One very interesting discovery is that copolymerisation of the two monomer species allows the uptake of the TEA^+ cation which would not normally be able to be inserted into either coat in their pure states. It seems possible that copolymerisation creates a more open structure on polymerisation (and the CVs seem to suggest that this is the case). However, it is obvious that cation insertion into the coat is not simply related just to ion size since the copolymer coats appear to have a greater kinetic barrier to ion insertion but can also readily incorporate the large TEA^+ cation. It is possible, therefore, that the presence of the –CN groups in the copolymer encourages the ingress of the organic tetraethylammonium ion. It would be very interesting to study the degree of TEA^+ uptake in copolymer films with differing proportions of indole-5-carboxylic acid incorporated. It would also be interesting to see if this effect could be seen for other, perhaps non-organic, large cations.

It is interesting that, although initial CV's of the copolymer are very similar to those of poly(indole-5-carboxylic acid), the steady state CV shows some differences. It is possible that this difference shows that the copolymer film does not become as accessible to ion ingress as a poly(I5CA) film does. However, this fact does not seem to be borne out by the ac data which show that the copolymer coat capacitance, C_{Σ}, is of an order of magnitude similar to that for poly(I5CA) although slightly lower at its maximum. Assuming that this opening up of the film is due to film reorientation to allow the inclusion of cations (in this case, Li^+) it is possible that the presence of at least one –CN group on a number of the trimer units lowers the thermodynamic driving force causing the formation of the carboxylate anion/lithium cation ion pair i.e. fewer Li^+ ions are incorporated into the coat and so there is less reorientation and slightly less opening of the coat structure. This, however, is purely an assumption since such a result could be due to a number of other factors including the fact the film may be slightly thinner. It would, therefore, be interesting to examine the amount of charge accessed during successive switching between the oxidised and reduced forms of the copolymer in a manner similar to that carried out for the pure polymer coats. It would also be helpful to examine this charge as a function of coat composition to establish the effect of the –CN groups on the (rate of) opening of the coat structure.

It is also interesting to note that unlike the pure poly(I5CA) and poly(5CI) films, ac data for the 50:50 copolymer show that both transmission line rails describing conduction within the actual polymer are important i.e. the resistance of the ions in the polymer pores is of a similar magnitude to the electronic resistance (in the pure cases, one of these resistances in much lower than the other). It would interesting to examine the behaviour to see if it was a real effect and, if so, if it is composition

dependent (i.e. if it where due to one particular monomer species or simply a general result of the copolymerisation).

The results obtained from pH measurements reaffirm previous work as to the nature of the "break region" (i.e. the region where the slope becomes less than Nernstian) seen for poly(I5CA) at above pH4. pH studies of the copolymer has shown that as the percentage of I5CA in the film increases, the width of the break region increases, giving further evidence that this break is due to the transfer of an imide proton to the deprotonated trimer carboxylic acid group. The location of the initial break from Nernstian behaviour can be correlated with the pK_a values of the acid centres on the trimer.

The pH results detailed in this report have also shown that the suggestion by Bartlett[4] that poly(indole-5-carboxylic acid) may have a possible application as a fast pH sensor is flawed due to the changeable nature of the coat morphology upon polymerisation. In fact work in Edinburgh has noted that the time taken to cycle to a fully open structure (and so the initial degree of "openness") is variable, even for films polymerised under identical conditions. This has been attributed to the statistically random nature of the very first monolayer deposited onto the electrode surface and on to which subsequent polymer layers are adsorbed. This variation in the compactness of the film will give rise to a subsequent variation in the rest potential of the polymer at a given pH, making the calibration of any associated hardware difficult. Results seem to suggest that poly(5-cyanoindole), the rest potential of which exhibits a more linear dependence upon pH, would be more applicable to this role (though it is expected that the degree of compactness of such films can, under certain conditions, change). It seems obvious that the applicability of such films as pH sensors offers a lot of scope for further study.

The analytical method used to obtain physical parameters from the ac spectra recorded has proved to be a very powerful technique and has shown itself able to analyse data from systems with very varied characteristics; from the relatively simple poly(pyrrole)[5] and poly(vinylferrocene)[6] systems to the more widely variable indole based systems detailed in this thesis. However, as shown by the results from the I5CA/5CI copolymer, this approach is only as good as the data used. It can therefore quantify both the reliability of the ac data obtained as well as the accuracy of the hardware used.

7.1 References

1 R.P. Buck, T.R. Brumleve; *J. Electroanal. Chem.*, 1981, **126**, 73

2 G. Zotti, S. Zecchin, G. Schiavon, R. Seraglia, A. Berlin, A. Canavesi; *Chem. Mater.*, 1994, **6**, 1742

3 P. Jennings; *Personal communications*, 1998

4 P.N. Bartlett, J. Farrington; *Bulletin of Electrochem.*, 1992, **8**, 208

5 W.J. Albery, C.M.Elliot, A.R. Mount; *J. Electroanal. Chem.*, 1990, **288**, 15

6 W.J. Albery, A.R. Mount; *J. Chem. Soc. Faraday Trans.*, 1993, **89**, 327

Appendix A –
Ac Impedance Fitting Routines

The following programs within this appendix are listing of the curve fitting functions used with the iterative fitting suite of SigmaPlot (Jandel Scientific) to obtain physically useful data from the ac spectra recorded during the course of this PhD. The programs are mathematical simulations of the transmission lines shown in figures 2.17, 2.20 and 2.21 respectively. It should be noted that after fitting, all of the capacitance values were divided by 2π to obtain the values in units of milliFarads.

A.1 Model With One Kinetic Barrier And No Polymer Transmission Line

See figure 2.17 for transmission line

[Parameters]
RK = 0.7
CK = 0.06
[Variables]
Z = col(6)
W = col(5)
WW = 1/Abs(col(6))
[Equations]
RE = 0.1
U = W*RK*CK
E = 1 + U**2
R = RE + RK/E
I = -RK*U/E
F = if(Z>0,R,I)

fit F to Z with weight WW

Key

RK = charge transfer resistance, R_{CT}

CK = double layer capacitance, C_{DL}

RE = solution resistance, R_{el}

Z = experimental impedance, Z_{re} and Z_{Im} (in kΩ)

W = frequency of the perturbing potential (in Hz)

Impedance Equations:

$$Z_{Re} = R_{el} + \frac{R_{CT}}{1+(\omega R_{CT} C_{DL})^2}$$

$$Z_{Im} = -\frac{R_{CT}(\omega R_{CT} C_{DL})}{1+(\omega R_{CT} C_{DL})^2}$$

A.2 Model With One Kinetic Barrier And A Polymer Transmission Line

See figure 2.20 for transmission line

```
[Parameters]
RK = 2.608
RP = .5
CK = 0.118
CP = 43
[Variables]
Z = col(6)
W = col(5)
P = Abs(col(6))
WW = 1/Abs(col(6))
[Equations]
RE=0.112
TT = W*RP*CP/2
T = sqrt(TT)
SH = sinh(T)
CH = cosh(T)
S = sin(T)
C = cos(T)
D = 2*T*(SH**2*C**2 + CH**2*S**2)
SCH = SH*CH
SC = S*C
U = W*RK*CK
E = 1 + U**2
R = RE + RK/E + RP*(SCH - SC)/D
I = -RK*U/E - RP*(SCH + SC)/D
F = if(Z>0,R,I)

fit F to Z with weight WW
```

Key

RK = charge transfer resistance, R_K

RP = resistance of the polymer transmission line, R_P or R_X

CK = double layer capacitance, C_{DL}

CP = capacitance of polymer film, C_Σ (includes C, C_N and C_D)

RE = solution resistance, R_{el}

Z = experimental impedance, Z_{re} and Z_{Im} (in kΩ)

W = frequency of the perturbing potential (in Hz)

Impedance Equations:

$$Z_{Re} = R_{el} + \frac{R_K}{1+(\omega R_K C_{DL})^2} + \frac{R_P(\sinh\theta\cosh\theta - \sin\theta\cos\theta)}{2\theta(\sinh^2\theta\cos^2\theta + \cosh^2\theta\sin^2\theta)}$$

$$Z_{Im} = -\frac{R_K(\omega R_K C_{DL})}{1+(\omega R_K C_{DL})^2} - \frac{R_P(\sinh\theta\cosh\theta + \sin\theta\cos\theta)}{2\theta(\sinh^2\theta\cos^2\theta + \cosh^2\theta\sin^2\theta)}$$

where $$\theta = \sqrt{\frac{\omega R_P C_P}{2}}$$

A.3 Model With Two Kinetic Barriers And A Polymer Transmission Line

See figure 2.21 for transmission line

```
[Parameters]
RX = 1
RK = 2.608
RP = .5
CDL = 0.118
CP = 43
[Variables]
Z = col(6)
W = col(5)
P = Abs(col(6))
WW = 1/Abs(col(6))
[Equations]
RE=0.112
TT = W*RP*CP/2
T = sqrt(TT)
SH = sinh(T)
CH = cosh(T)
S = sin(T)
C = cos(T)
D = 2*T*(SH**2*C**2 + CH**2*S**2)
SCH = SH*CH
SC = S*C
U = W*RK*CDL
V = W*RX*CDL
E = 1 + U**2
G = 1 + V**2
R = RE + RK/E + RX/G + RP*(SCH - SC)/D
I = -RK*U/E - RX*V/G - RP*(SCH + SC)/D
F = if(Z>0,R,I)

fit F to Z with weight WW
```

Key

RX = charge transfer resistance at electrolyte interface, $R_{K,X}$

RK = charge transfer resistance at electrode interface, $R_{K,P}$

RP = resistance of the polymer transmission line, R_P or R_X

CK = double layer capacitance, C_{DL}

CP = capacitance of polymer film, C_Σ (includes C, C_N and C_D)

RE = solution resistance, R_{el}

Z = experimental impedance, Z_{re} and Z_{Im} (in kΩ)

W = frequency of the perturbing potential (in Hz)

Impedance Equations:

$$Z_{Re} = R_{el} + \frac{R_{K,P}}{1+(\omega R_{K,P} C_{DL})^2} + \frac{R_{K,X}}{1+(\omega R_{K,X} C_{DL})^2} + \frac{R_P(\sinh\theta\cosh\theta - \sin\theta\cos\theta)}{2\theta(\sinh^2\theta\cos^2\theta + \cosh^2\theta\sin^2\theta)}$$

$$Z_{Im} = -\frac{R_{K,P}(\omega R_{K,P} C_{DL})}{1+(\omega R_{K,P} C_{DL})^2} - \frac{R_{K,X}(\omega R_{K,X} C_{DL})}{1+(\omega R_{K,X} C_{DL})^2} - \frac{R_P(\sinh\theta\cosh\theta + \sin\theta\cos\theta)}{2\theta(\sinh^2\theta\cos^2\theta + \cosh^2\theta\sin^2\theta)}$$

where $$\theta = \sqrt{\frac{\omega R_P C_P}{2}}$$

Appendix B –

Ac Impedance Fits For Chapter 4

The following graphs contained within this appendix show the results obtained when fitting the ac impedance spectra for poly(indole-5-carboxylic acid) to theory. Unless otherwise stated, the fitting program used is that detailed in appendix A.3.

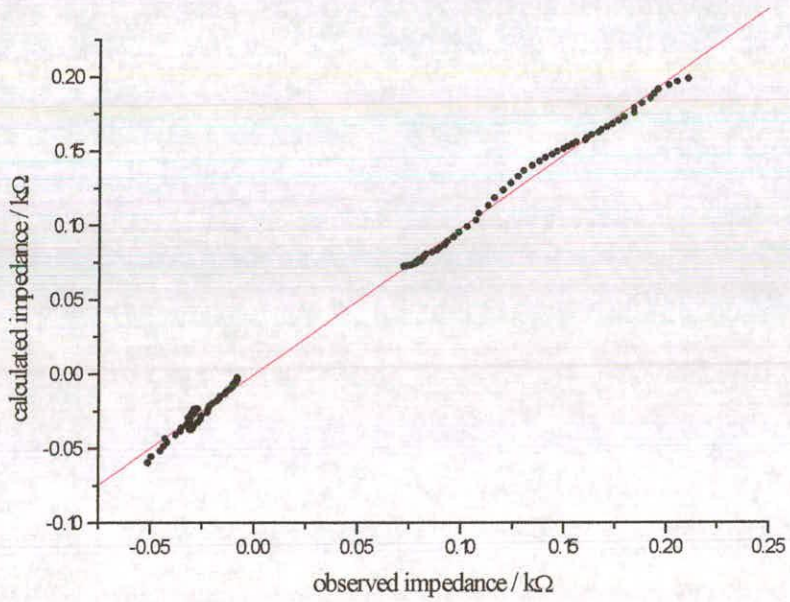

Figure B.1: Fit for cycled poly(I5CA) layer at -300mV in 0.1M $LiClO_4$
Gradient = 0.9882; Intercept = -0.0002; Correlation coefficient = 0.9989

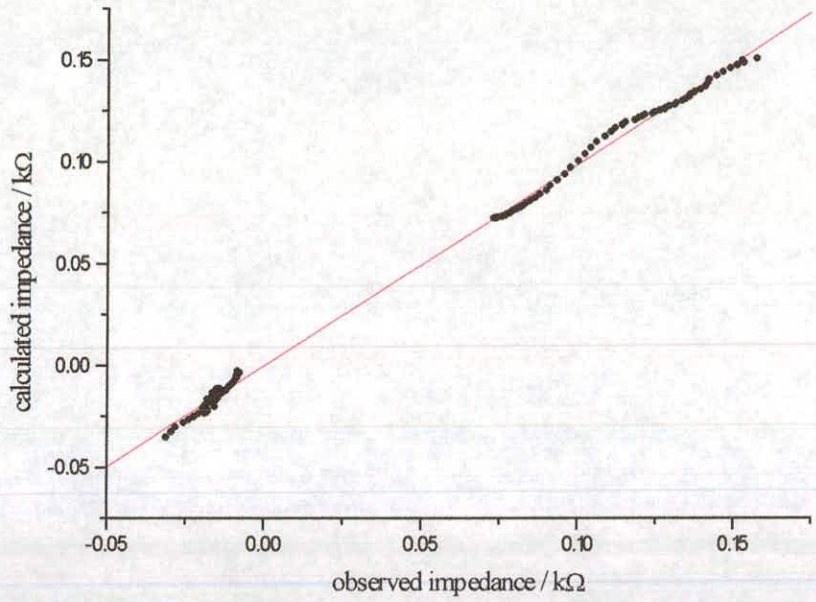

Figure B.2: Fit for cycled poly(I5CA) layer at -250mV in 0.1M $LiClO_4$
Gradient = 0.9890; Intercept = 0.0000; Correlation coefficient = 0.9991

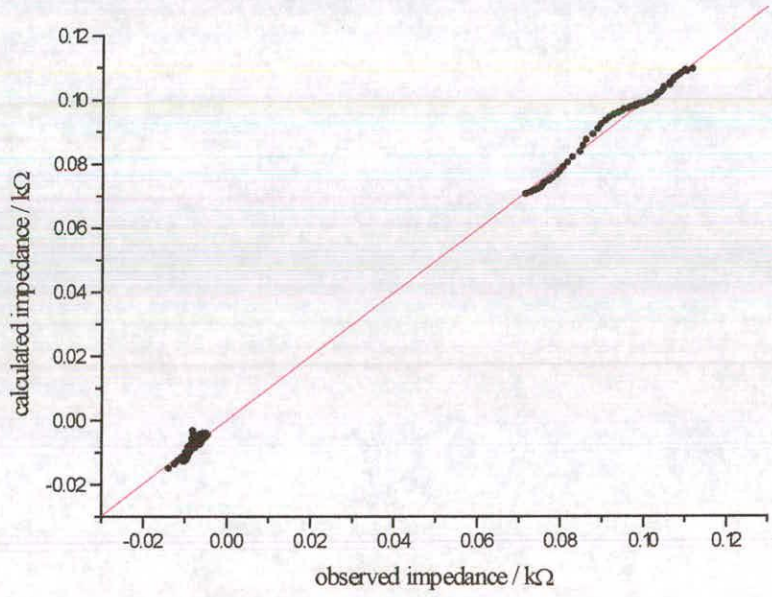

Figure B.3: Fit for cycled poly(I5CA) layer at -200mV in 0.1M $LiClO_4$
Gradient = 0.9939; Intercept = 0.0003; Correlation coefficient = 0.9995

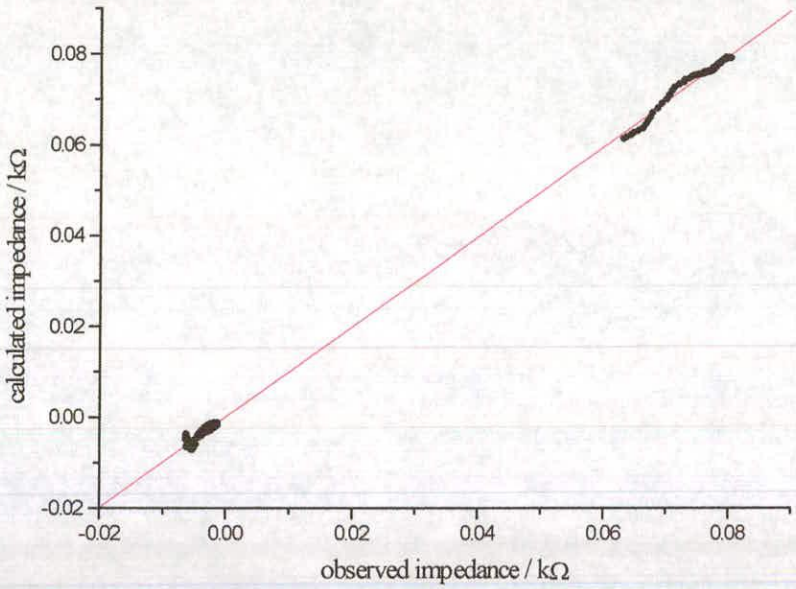

Figure B.4: Fit for cycled poly(I5CA) layer at -150mV in 0.1M $LiClO_4$
Gradient = 0.9928; Intercept = 0.0001; Correlation coefficient = 0.9997

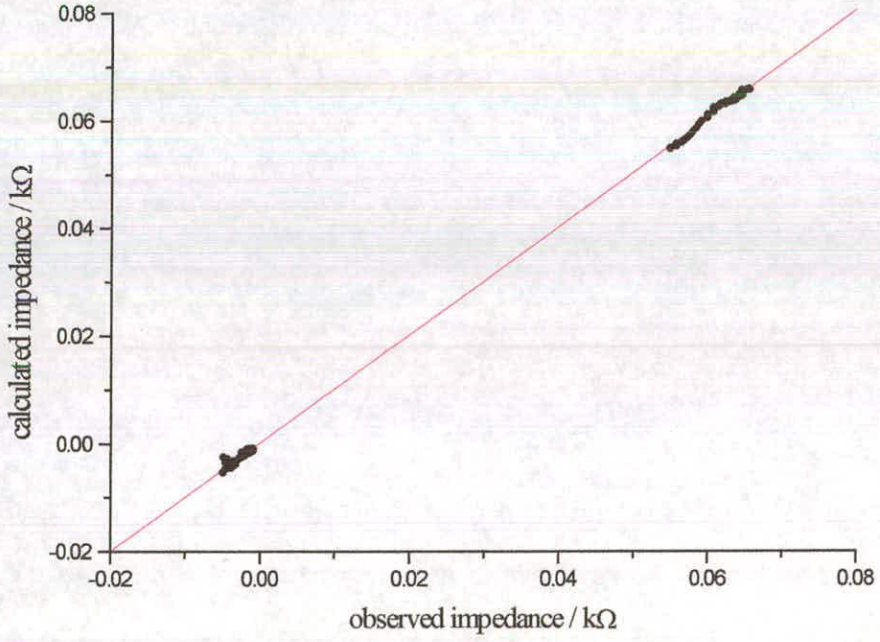

Figure B.5: Fit for cycled poly(I5CA) layer at -100mV in 0.1M $LiClO_4$
Gradient = 1.0073; Intercept = 0.0002; Correlation coefficient = 0.9999

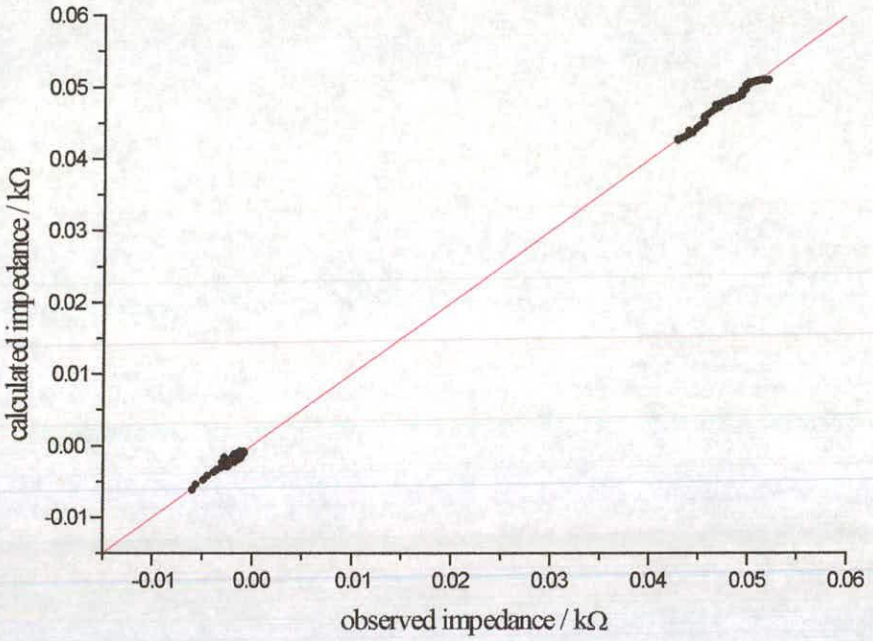

Figure B.6: Fit for cycled poly(I5CA) layer at 0mV in 0.1M $LiClO_4$
Gradient = 0.9980; Intercept = 0.0001; Correlation coefficient = 0.9999

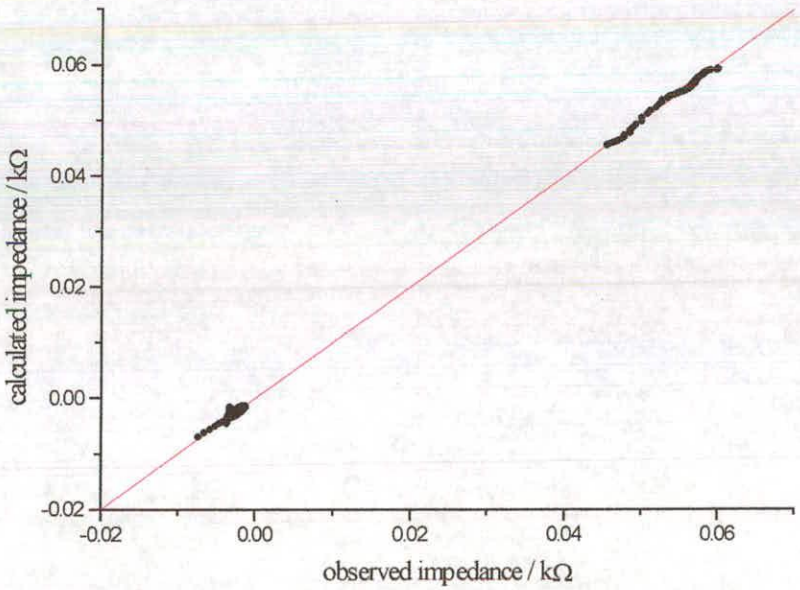

Figure B.7: Fit for cycled poly(I5CA) layer at 100mV in 0.1M $LiClO_4$
Gradient = 0.9987; Intercept = 0.0000; Correlation coefficient = 0.9999

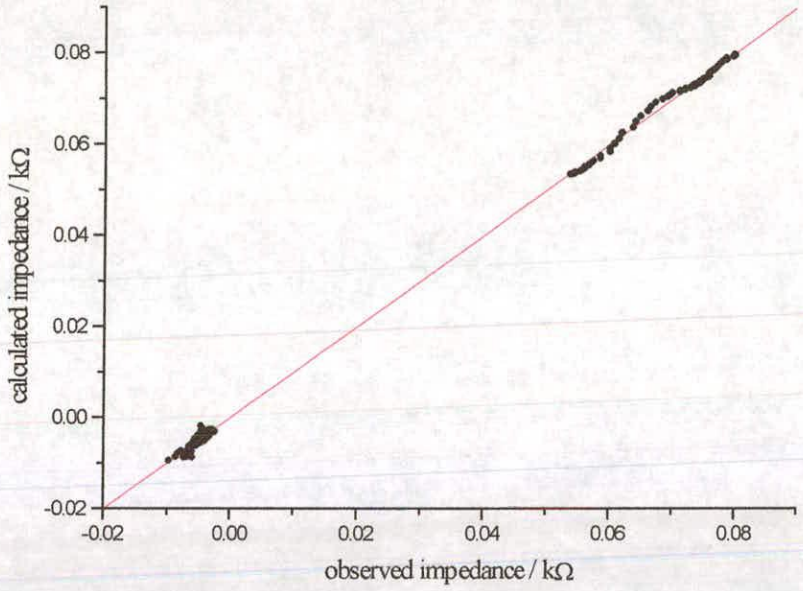

Figure B.8: Fit for cycled poly(I5CA) layer at 150mV in 0.1M $LiClO_4$
Gradient = 0.9980; Intercept = -0.0001; Correlation coefficient = 0.9997

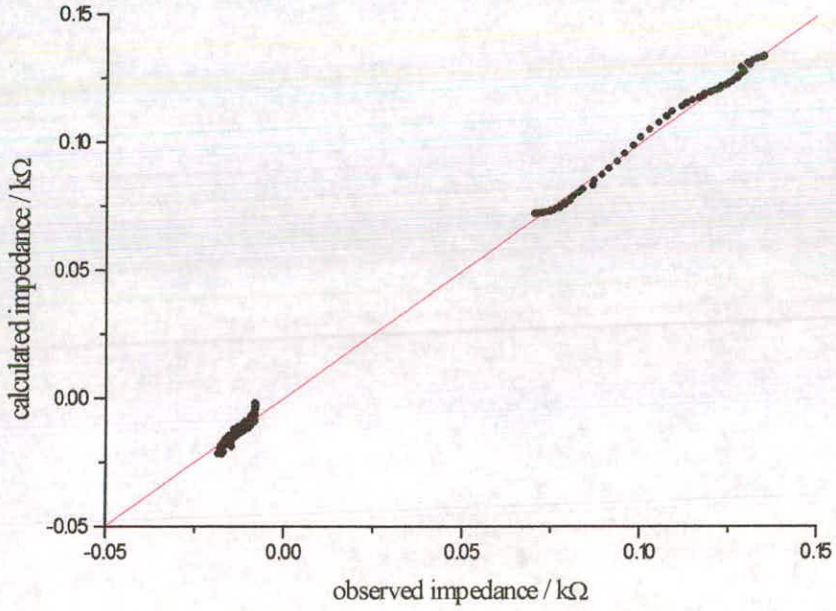

Figure B.9: Fit for cycled poly(I5CA) layer at 200mV in 0.1M $LiClO_4$
Gradient = 0.9949; Intercept = 0.0001; Correlation coefficient = 0.9994

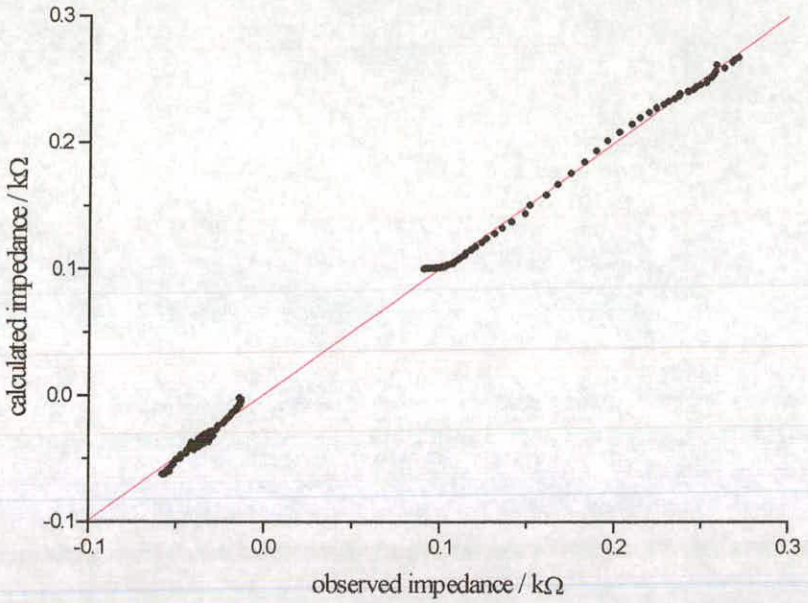

Figure B.10: Fit for cycled poly(I5CA) layer at 250mV in 0.1M $LiClO_4$
Gradient = 0.9951; Intercept = 0.0010; Correlation coefficient = 0.9993

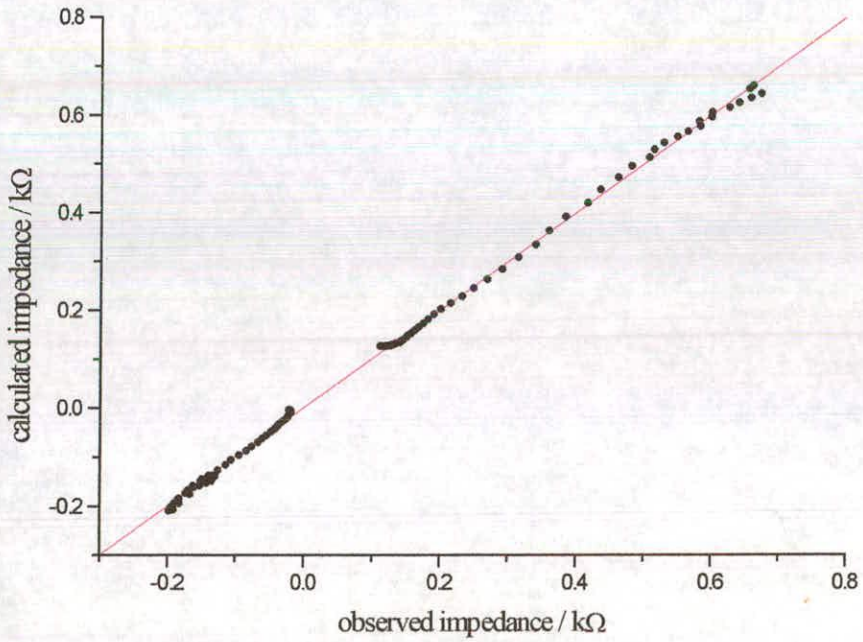

Figure B.11: Fit for cycled poly(I5CA) layer at 300mV in 0.1M $LiClO_4$
Gradient = 0.9977; Intercept = 0.0010; Correlation coefficient = 0.9995

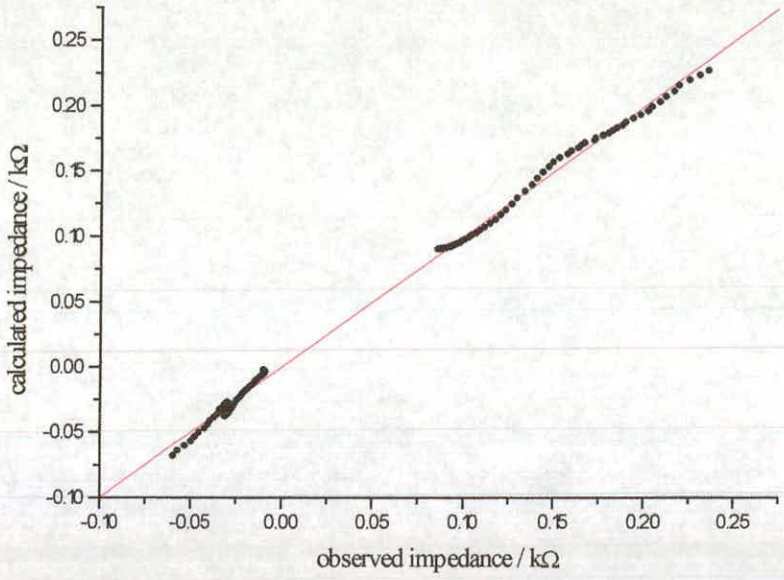

Figure B.12: Fit for cycled poly(I5CA) layer at -300mV in 0.08M $LiClO_4$

Gradient = 0.9972; Intercept = 0.0001; Correlation coefficient = 0.9990

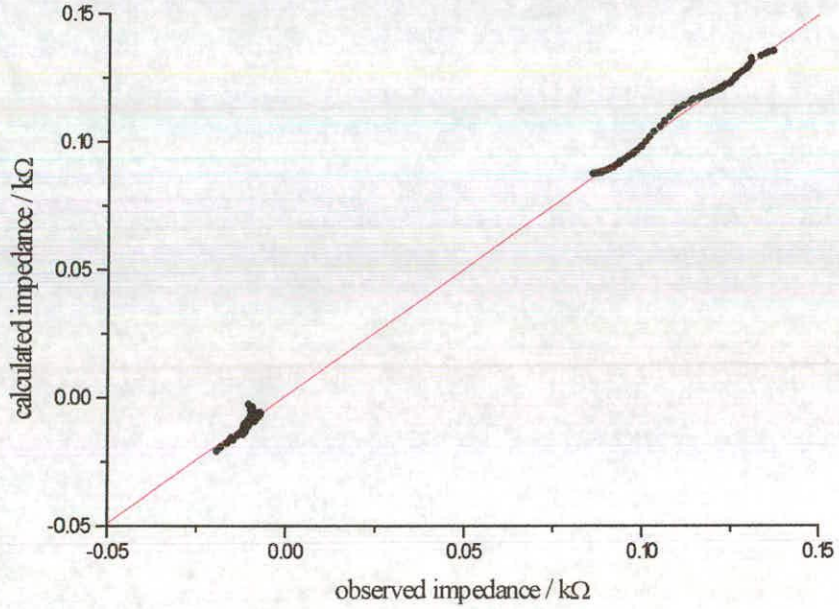

Figure B.13: Fit for cycled poly(I5CA) layer at

-200mV in 0.08M $LiClO_4$

Gradient = 0.9922; Intercept = 0.0009; Correlation coefficient = 0.9995

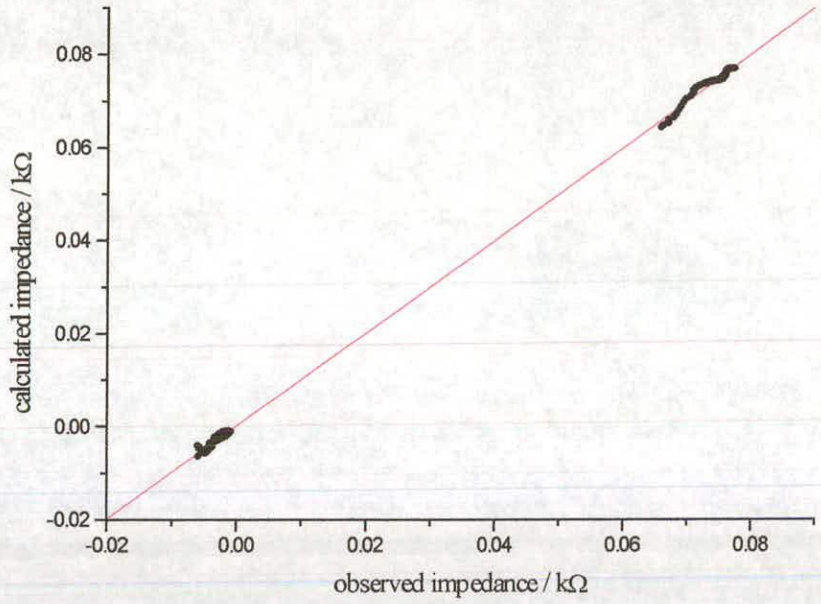

Figure B.14: Fit for cycled poly(I5CA) layer at -100mV in 0.08M $LiClO_4$

Gradient = 0.9964; Intercept = 0.0002; Correlation coefficient = 0.9999

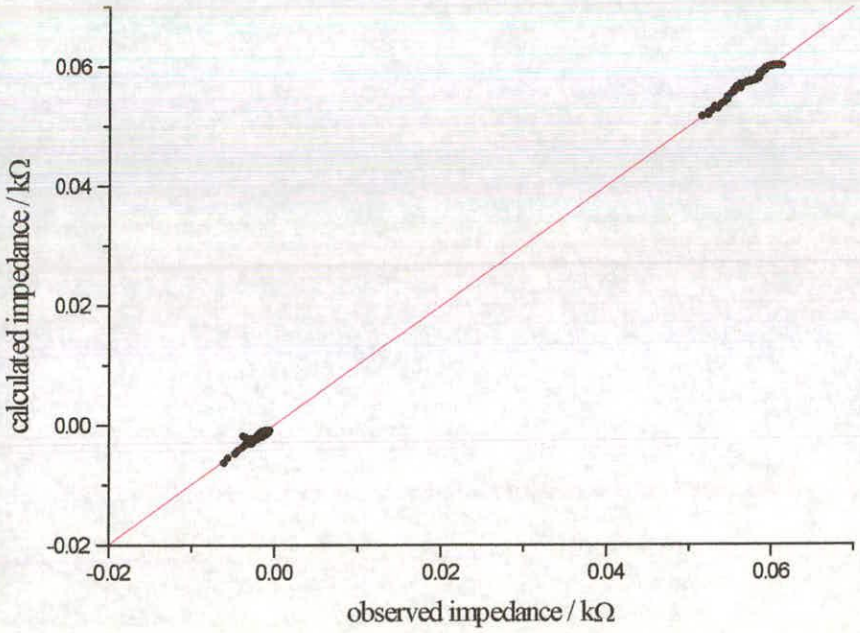

Figure B.15: Fit for cycled poly(I5CA) layer at 0mV in 0.08M $LiClO_4$

Gradient = 0.9980; Intercept = 0.0002; Correlation coefficient = 0.9999

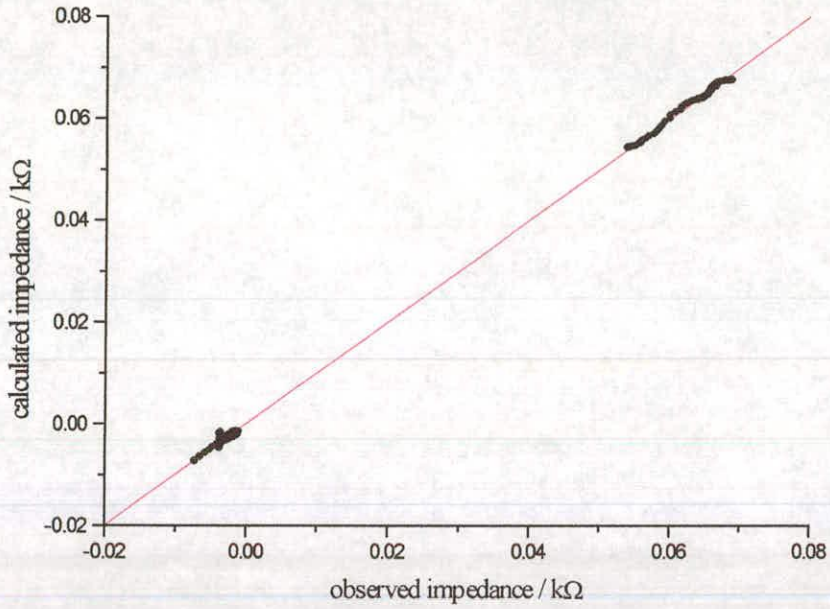

Figure B.16: Fit for cycled poly(I5CA) layer at 100mV in 0.08M $LiClO_4$

Gradient = 0.9979; Intercept = 0.0002; Correlation coefficient = 0.9999

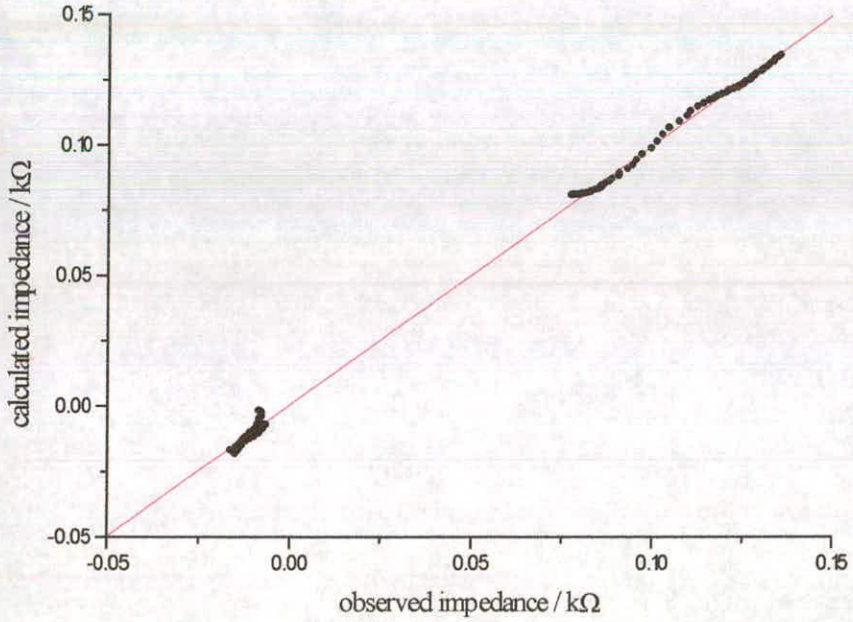

Figure B.17: Fit for cycled poly(I5CA) layer at 200mV in 0.08M $LiClO_4$

Gradient = 0.9959; Intercept = 0.0004; Correlation coefficient = 0.9995

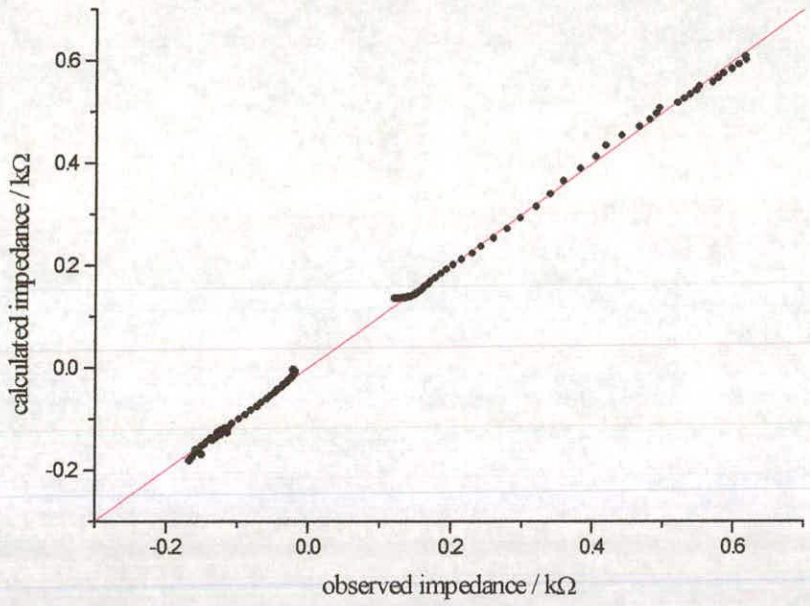

Figure B.18: Fit for cycled poly(I5CA) layer at 300mV in 0.08M $LiClO_4$

Gradient = 0.9976; Intercept = 0.0010; Correlation coefficient = 0.9994

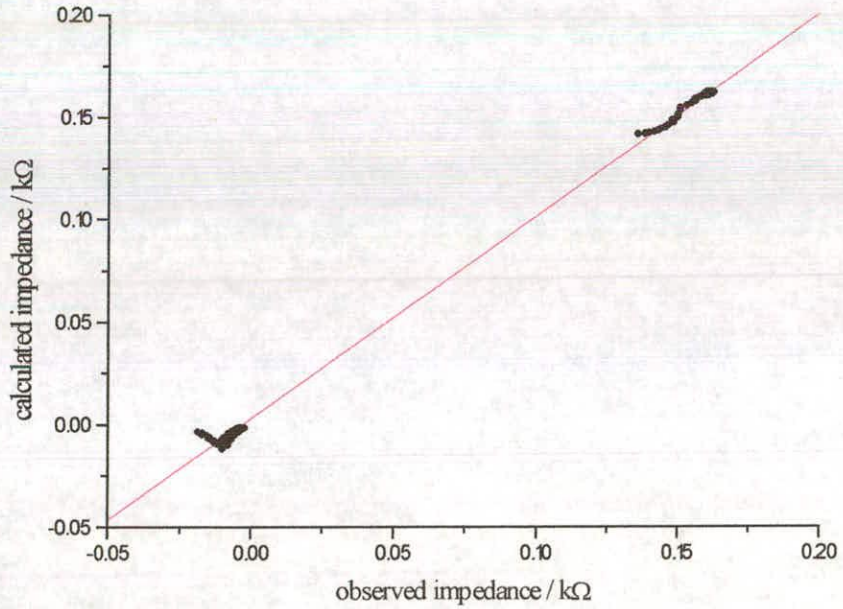

Figure B.19: Fit for cycled poly(I5CA) layer at -100mV in 0.04M $LiClO_4$

Gradient = 0.9863; Intercept = 0.0031; Correlation coefficient = 0.9995

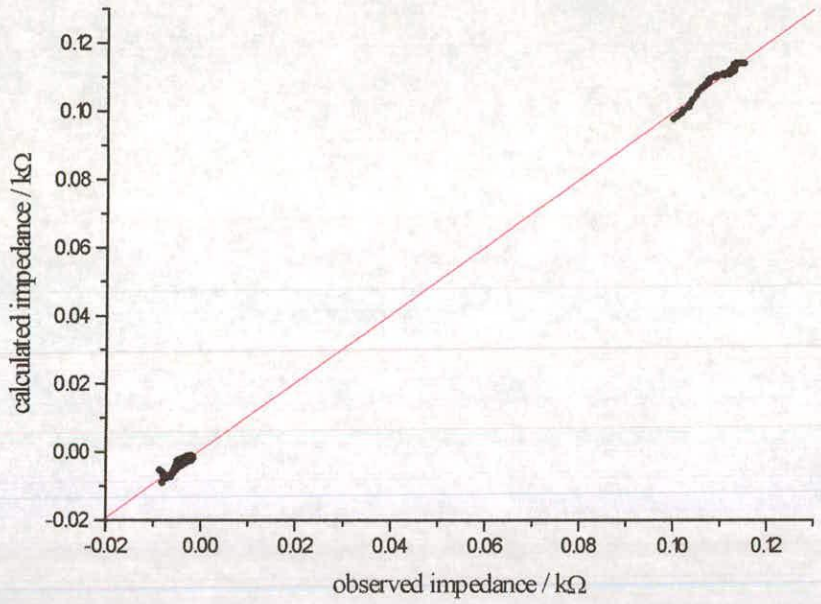

Figure B.20: Fit for cycled poly(I5CA) layer at 0mV in 0.04M $LiClO_4$

Gradient = 0.9937; Intercept = 0.0007; Correlation coefficient = 0.9999

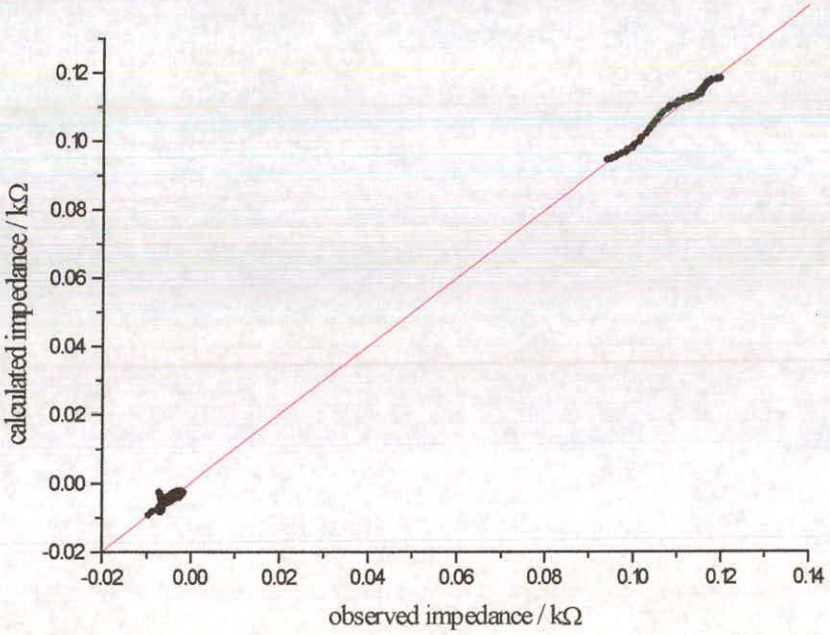

Figure B.21: Fit for cycled poly(I5CA) layer at

100mV in 0.04M $LiClO_4$

Gradient = 0.9968; Intercept = 0.0003; Correlation coefficient = 0.9998

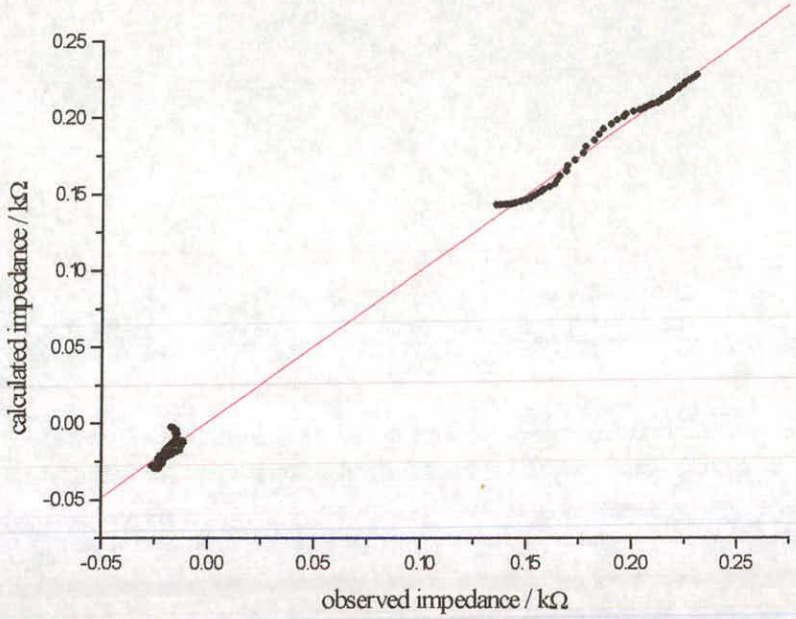

Figure B.22: Fit for cycled poly(I5CA) layer at 200mV in 0.04M $LiClO_4$

Gradient = 0.9921; Intercept = 0.0012; Correlation coefficient = 0.9991

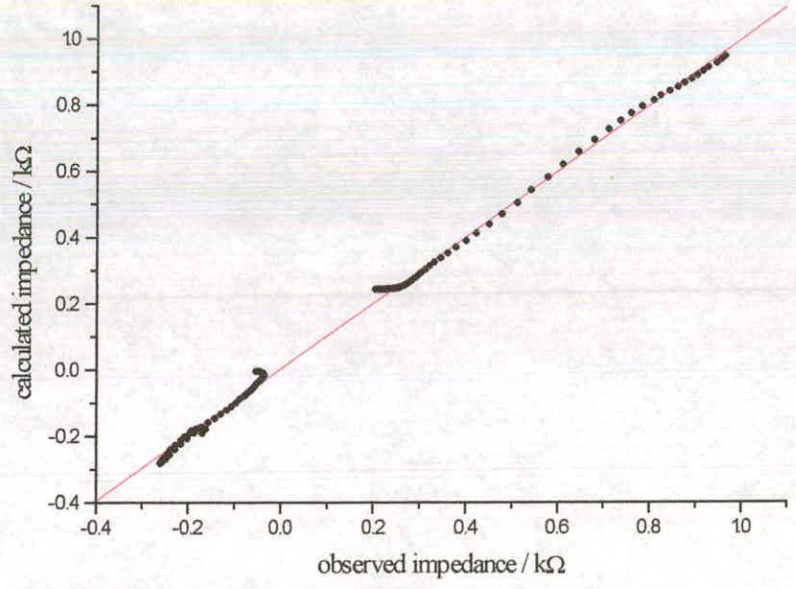

Figure B.23: Fit for cycled poly(I5CA) layer at 300mV in 0.04M $LiClO_4$

Gradient = 0.9942; Intercept = 0.0038; Correlation coefficient = 0.9990

Appendix C –

Ac Impedance Fits For Chapter 5

The following graphs contained within this appendix show the results obtained when fitting the ac impedance spectra for poly(5-cyanoindole) to theory. Unless otherwise stated, the fitting program used is that detailed in appendix A.2.

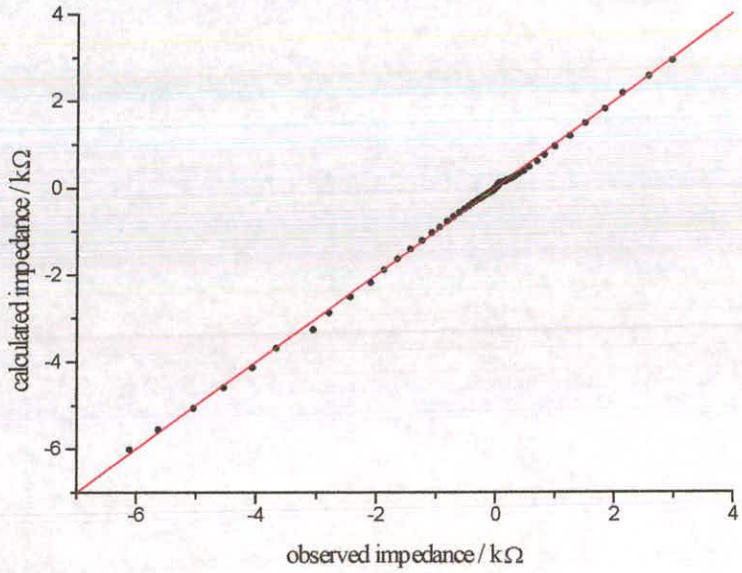

Figure B.1: Fit for uncycled poly(5CI) layer at -100mV in 0.1M $LiClO_4$
Gradient = 1.0001; Intercept = 0.0058; Correlation coefficient = 0.9995

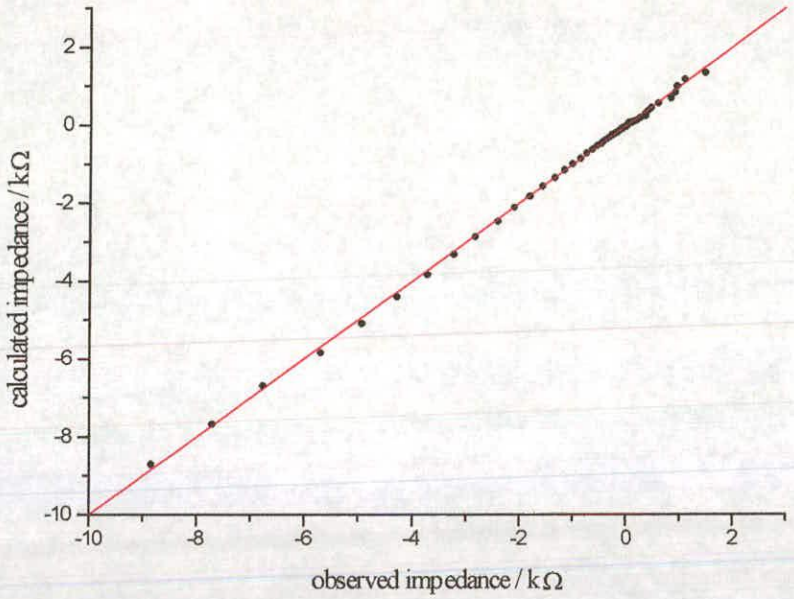

Figure B.2: Fit for uncycled poly(5CI) layer at 0mV in 0.1M $LiClO_4$
Gradient = 1.0000; Intercept = 0.0036; Correlation coefficient = 0.9996

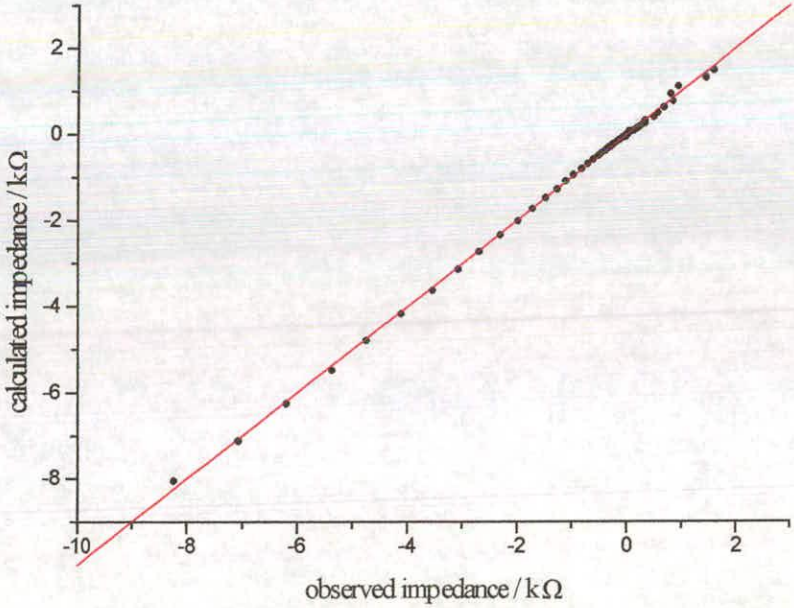

Figure B.3: Fit for uncycled poly(5CI) layer at 100mV in 0.1M $LiClO_4$
Gradient = 1.0001; Intercept = 0.0047; Correlation coefficient = 0.9996

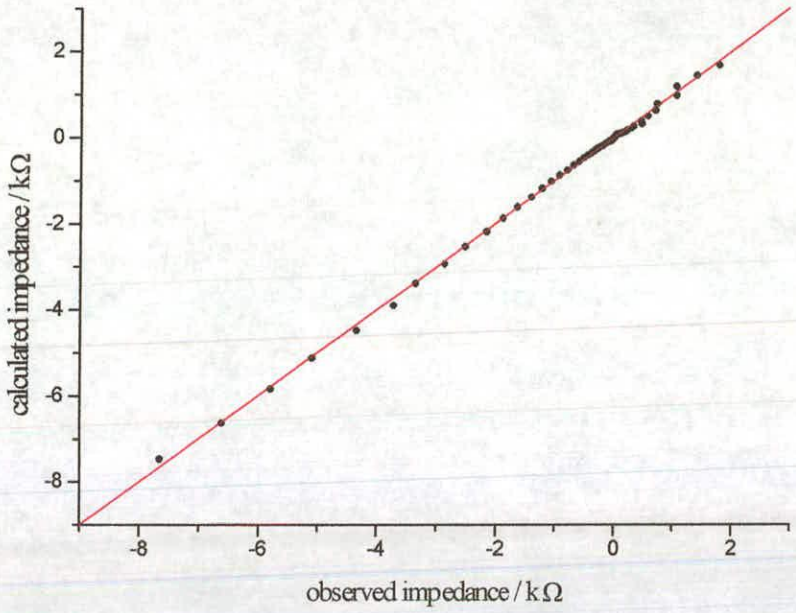

Figure B.4: Fit for uncycled poly(5CI) layer at 200mV in 0.1M $LiClO_4$
Gradient = 1.0002; Intercept = 0.0056; Correlation coefficient = 0.9995

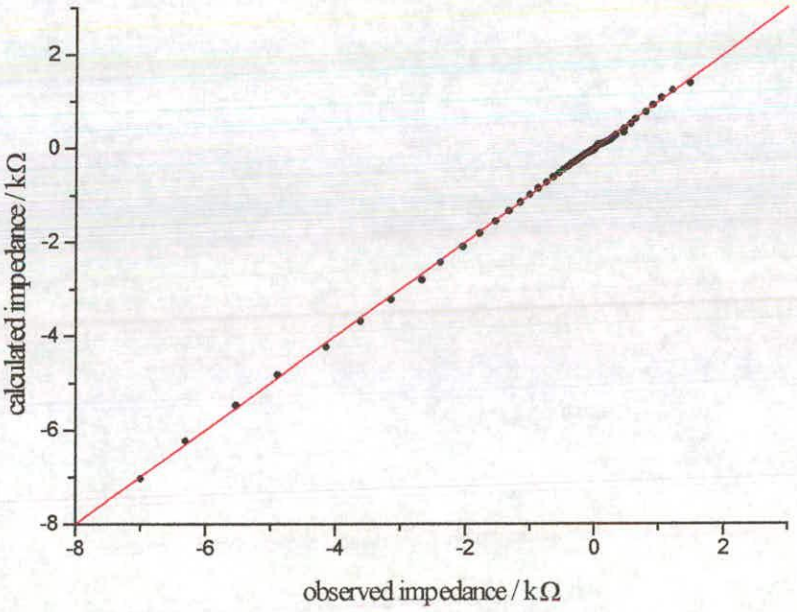

Figure B.5: Fit for uncycled poly(5CI) layer at 300mV in 0.1M $LiClO_4$
Gradient = 1.0004; Intercept = 0.0047; Correlation coefficient = 0.9997

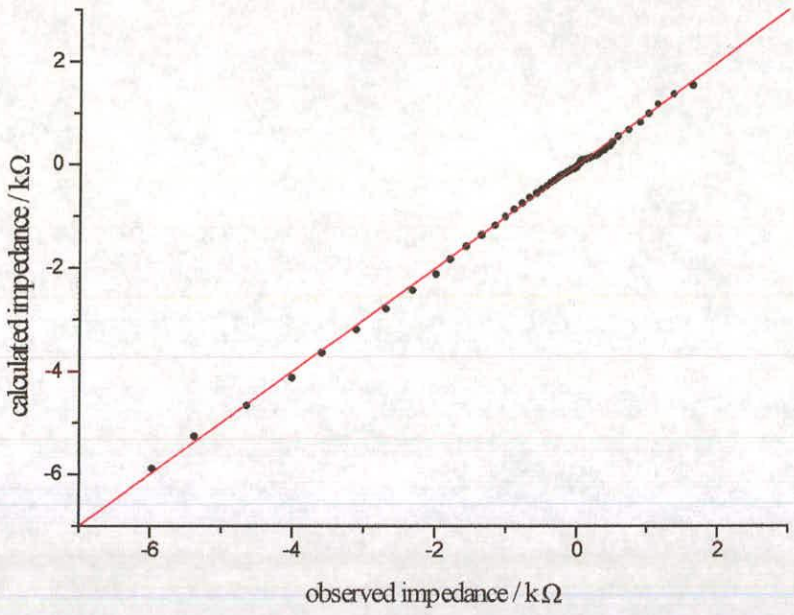

Figure B.6: Fit for uncycled poly(5CI) layer at 400mV in 0.1M $LiClO_4$
Gradient = 1.0002; Intercept = 0.0053; Correlation coefficient = 0.9994

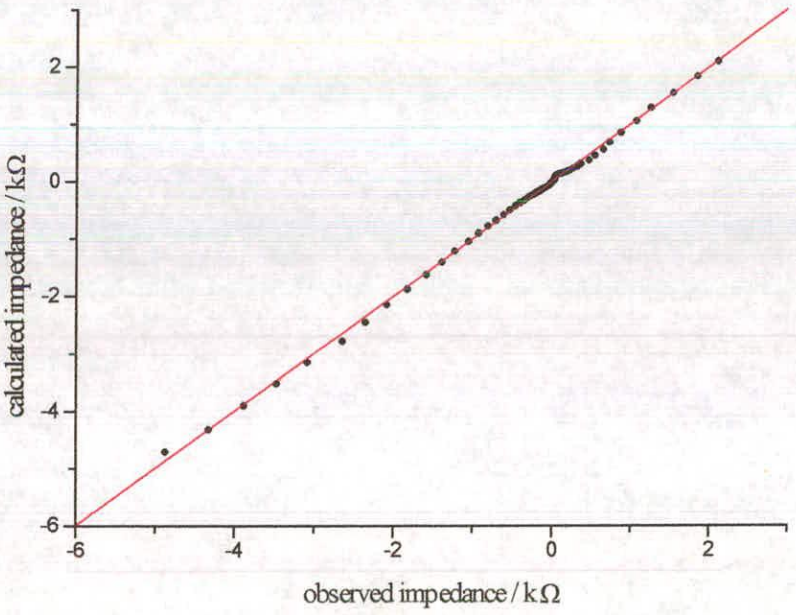

Figure B.7: Fit for uncycled poly(5CI) layer at 500mV in 0.1M $LiClO_4$
Gradient = 0.9999; Intercept = 0.0052; Correlation coefficient = 0.9993

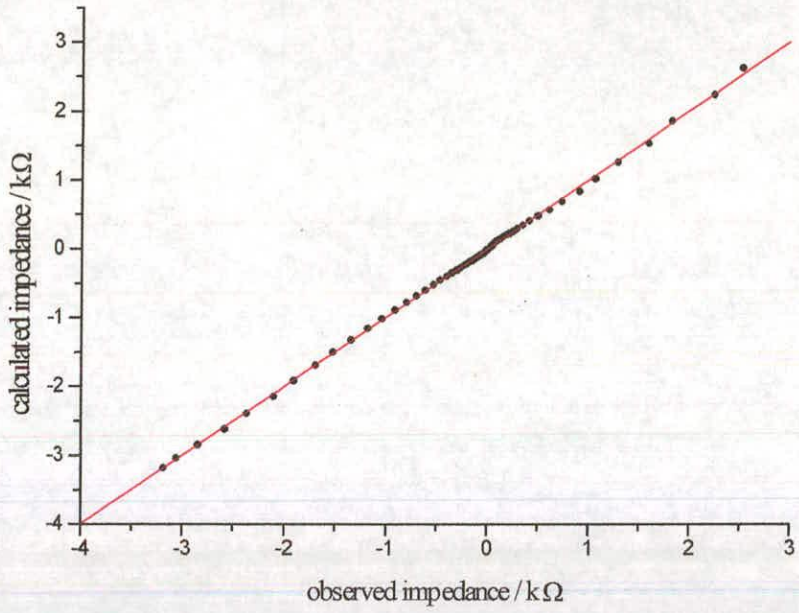

Figure B.8: Fit for uncycled poly(5CI) layer at 600mV in 0.1M $LiClO_4$
Gradient = 1.0012; Intercept = 0.0090; Correlation coefficient = 0.9997

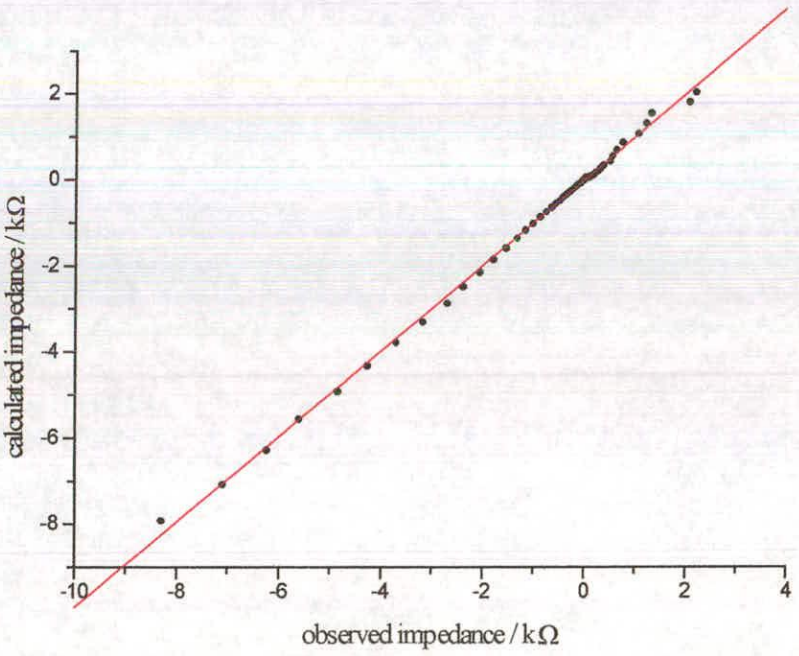

Figure B.9: Fit for cycled poly(5CI) layer at 0mV in 0.1M $LiClO_4$
Gradient = 0.9932; Intercept = -0.0022; Correlation coefficient = 0.9992

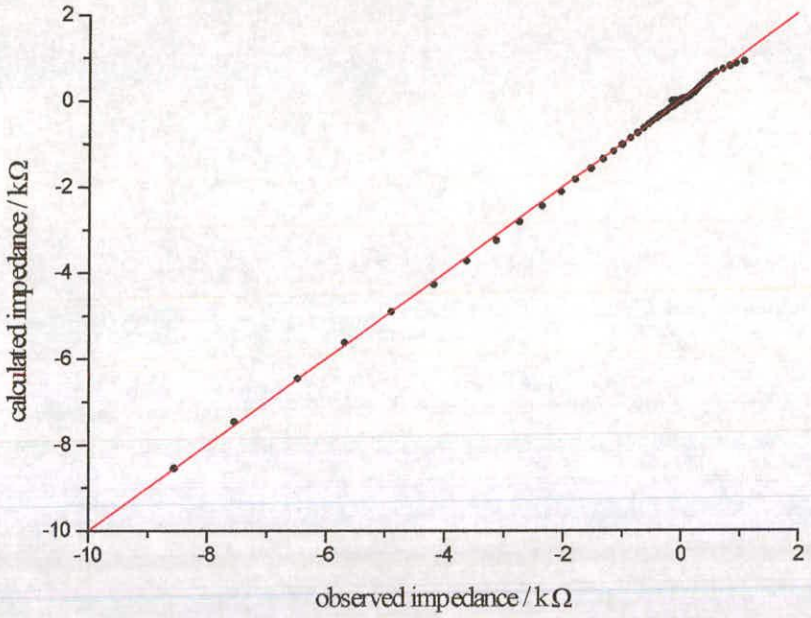

Figure B.10: Fit for cycled poly(5CI) layer at 100mV in 0.1M $LiClO_4$
Gradient = 1.0024; Intercept = 0.0205; Correlation coefficient = 0.9995

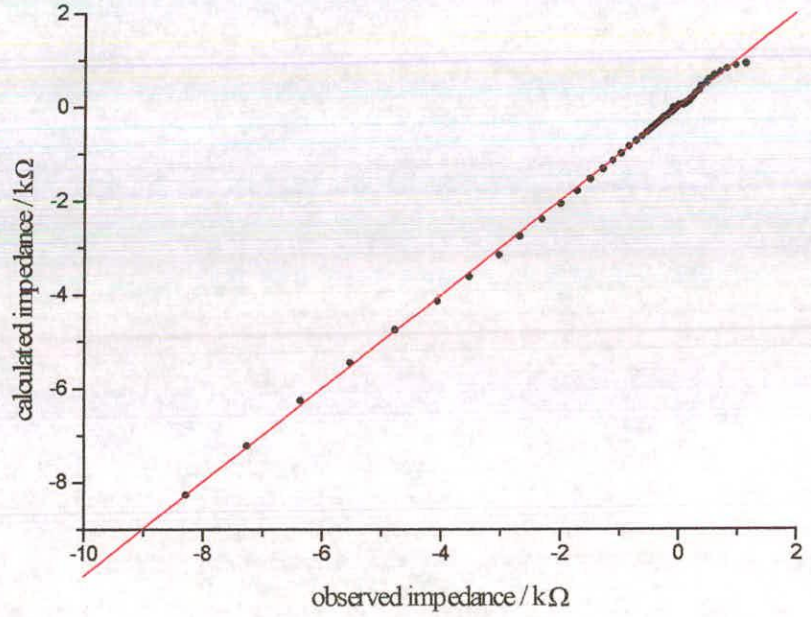

Figure B.11: Fit for cycled poly(5CI) layer at 200mV in 0.1M $LiClO_4$
Gradient = 0.9980; Intercept = 0.0037; Correlation coefficient = 0.9996

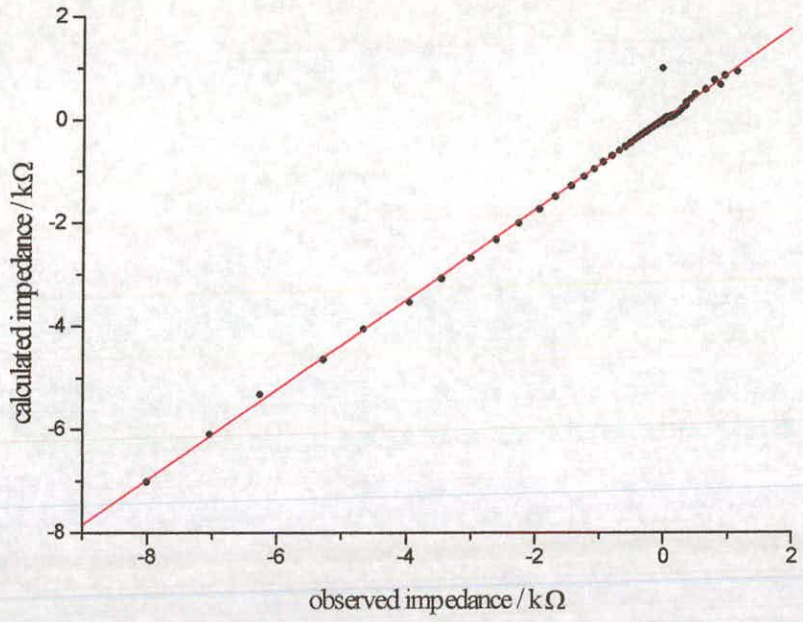

Figure B.12: Fit for cycled poly(5CI) layer at 300mV in 0.1M $LiClO_4$
Gradient = 0.8732; Intercept = 0.0145; Correlation coefficient = 0.9971

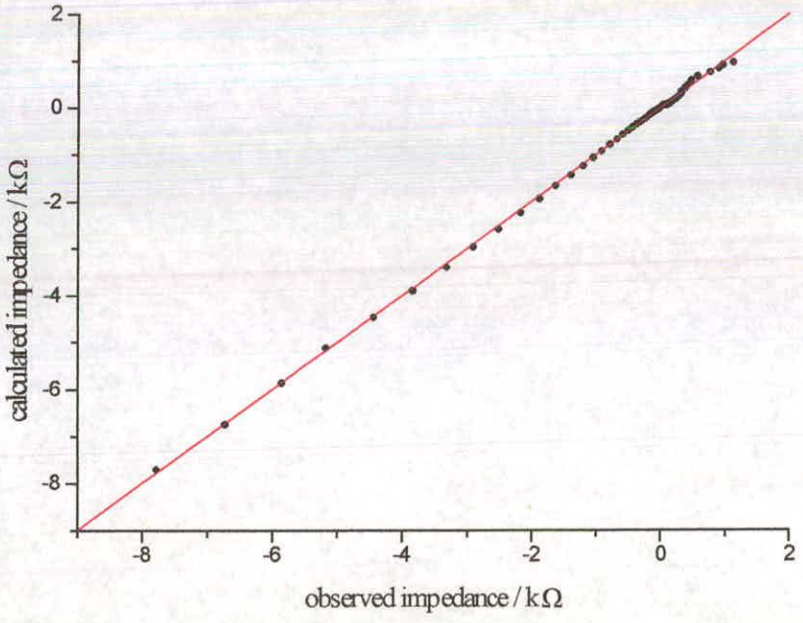

Figure B.13: Fit for cycled poly(5CI) layer at 400mV in 0.1M $LiClO_4$
Gradient = 0.9996; Intercept = 0.0018; Correlation coefficient = 0.9997

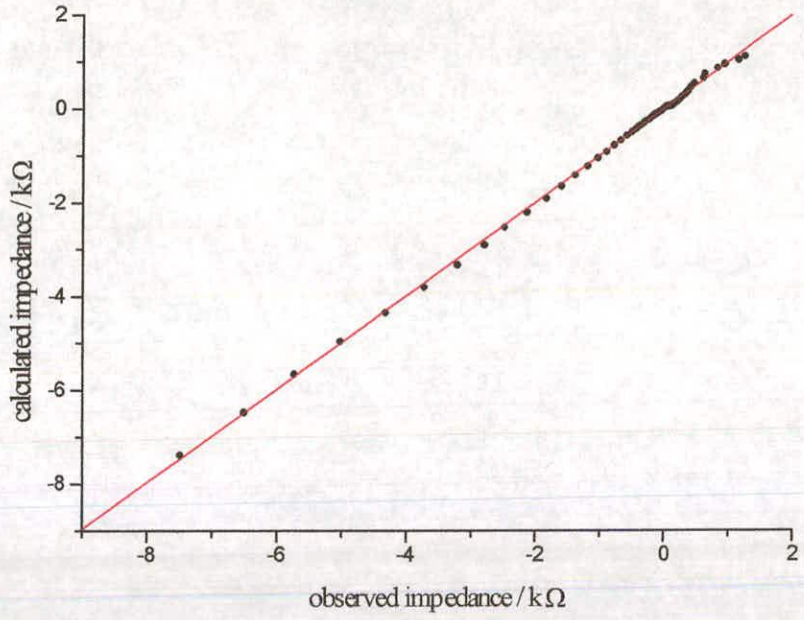

Figure B.14: Fit for cycled poly(5CI) layer at 500mV in 0.1M $LiClO_4$
Gradient = 0.9966; Intercept = 0.0005; Correlation coefficient = 0.9996

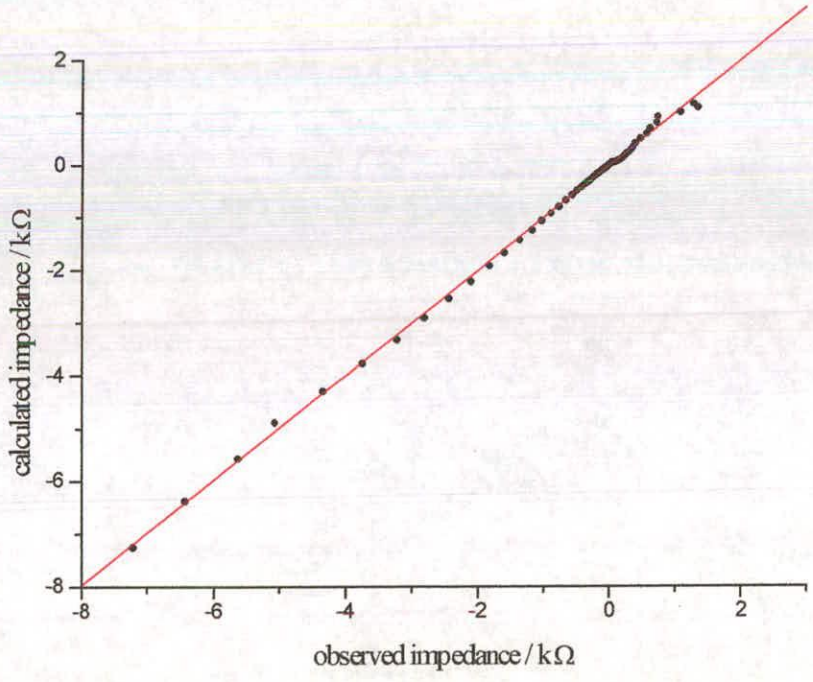

Figure B.15: Fit for cycled poly(5CI) layer at 600mV in 0.1M $LiClO_4$
Gradient = 0.9962; Intercept = -0.0002; Correlation coefficient = 0.9994

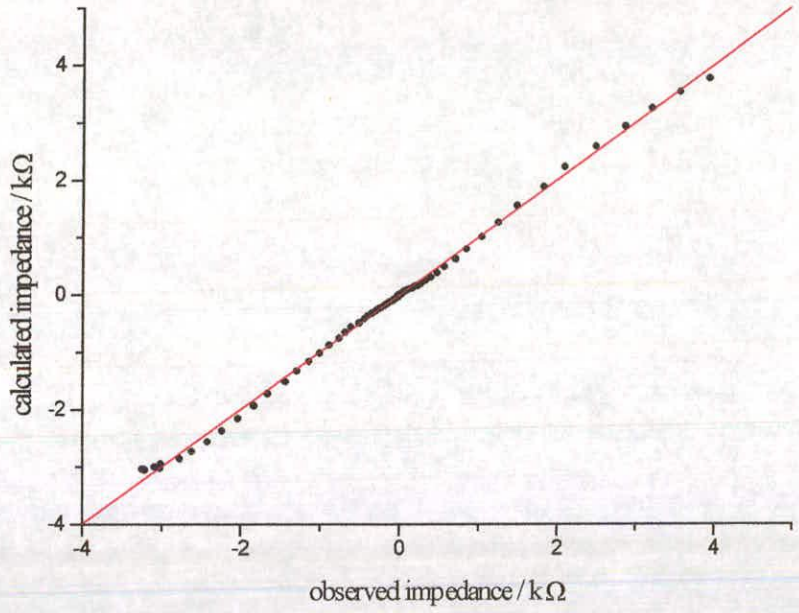

Figure B.16: Fit for cycled poly(5CI) layer at -100mV in 0.1M $TEAClO_4$
Gradient = 0.9995; Intercept = 0.0047; Correlation coefficient = 0.9991

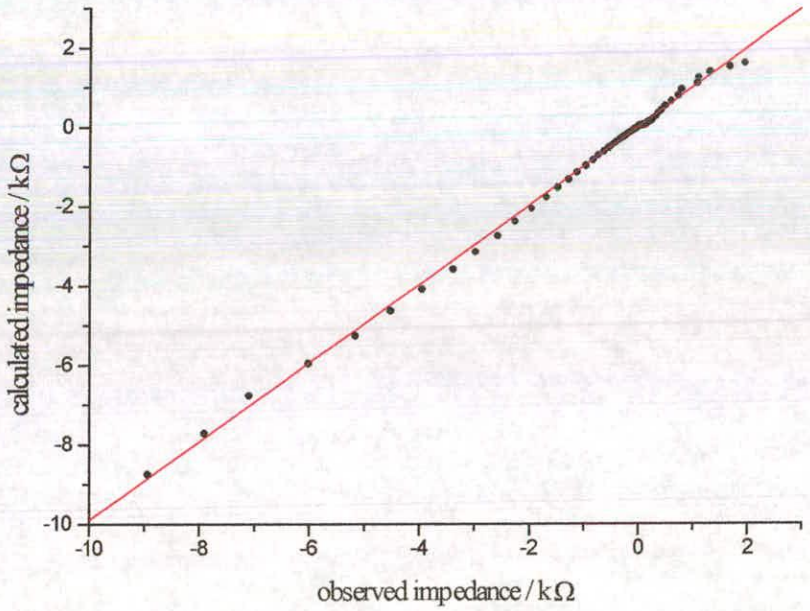

Figure B.17: Fit for cycled poly(5CI) layer at 0mV in 0.1M $TEAClO_4$
Gradient = 0.9891; Intercept = -0.0062; Correlation coefficient = 0.9991

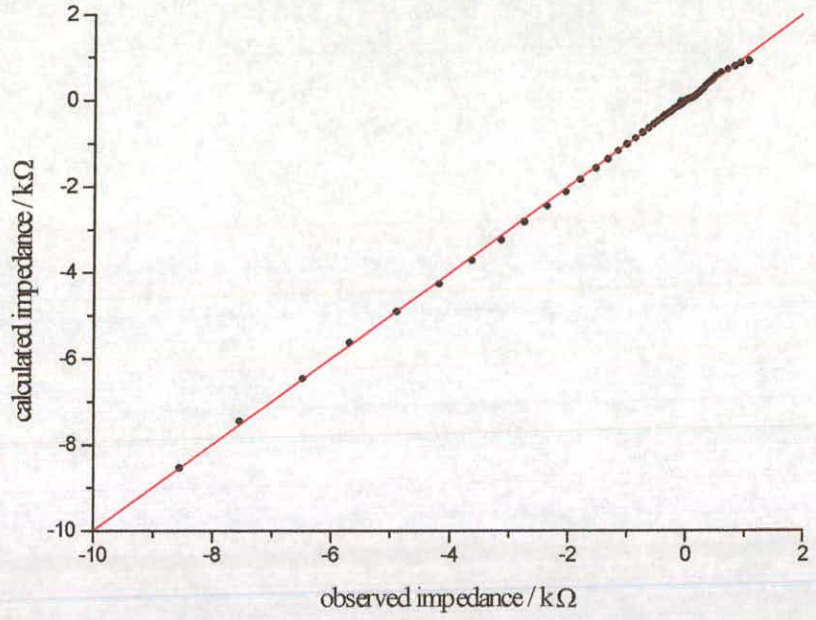

Figure B.18: Fit for cycled poly(5CI) layer at 100mV in 0.1M $TEAClO_4$

Gradient = 0.9992; Intercept = 0.0056; Correlation coefficient = 0.9998

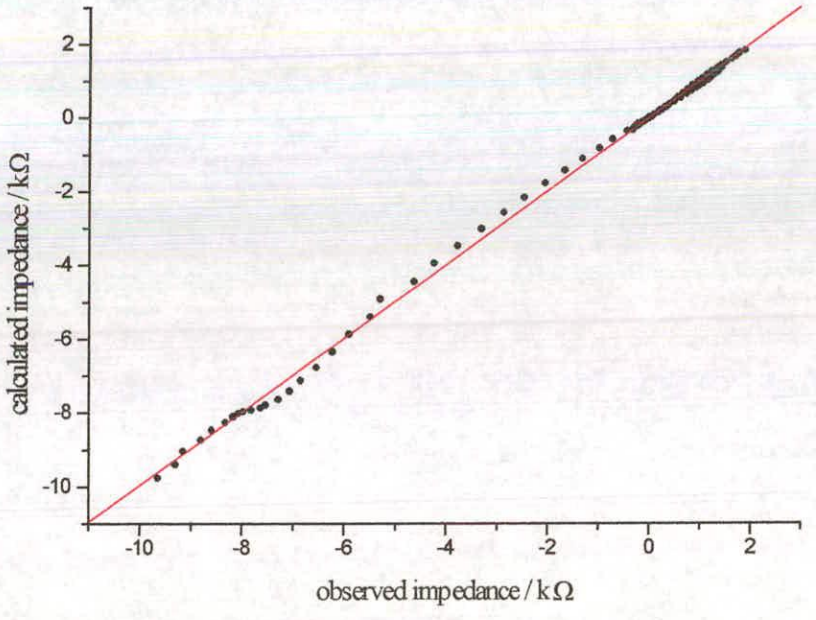

Figure B.19: Fit for cycled poly(5CI) layer at 200mV in 0.1M $TEAClO_4$

Gradient = 0.9992; Intercept = 0.0056; Correlation coefficient = 0.9998

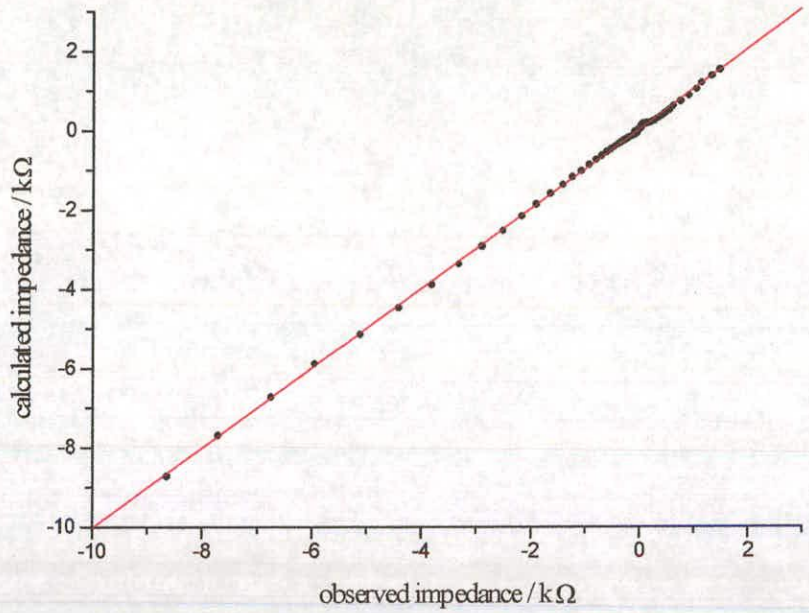

Figure B.20: Fit for cycled poly(5CI) layer at 300mV in 0.1M $TEAClO_4$

Gradient = 0.9973; Intercept = 0.0083; Correlation coefficient = 0.9993

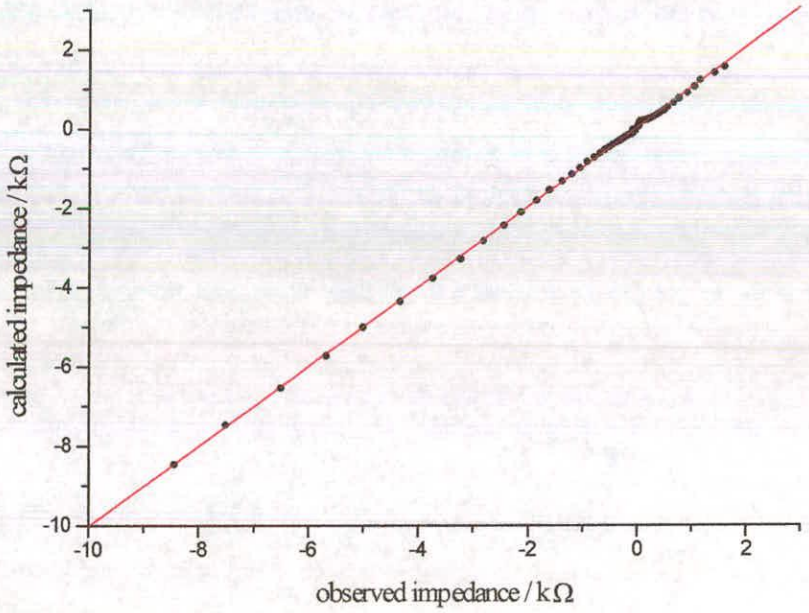

Figure B.21: Fit for cycled poly(5CI) layer at 400mV in 0.1M $TEAClO_4$

Gradient = 1.0055; Intercept = 0.0364; Correlation coefficient = 0.9996

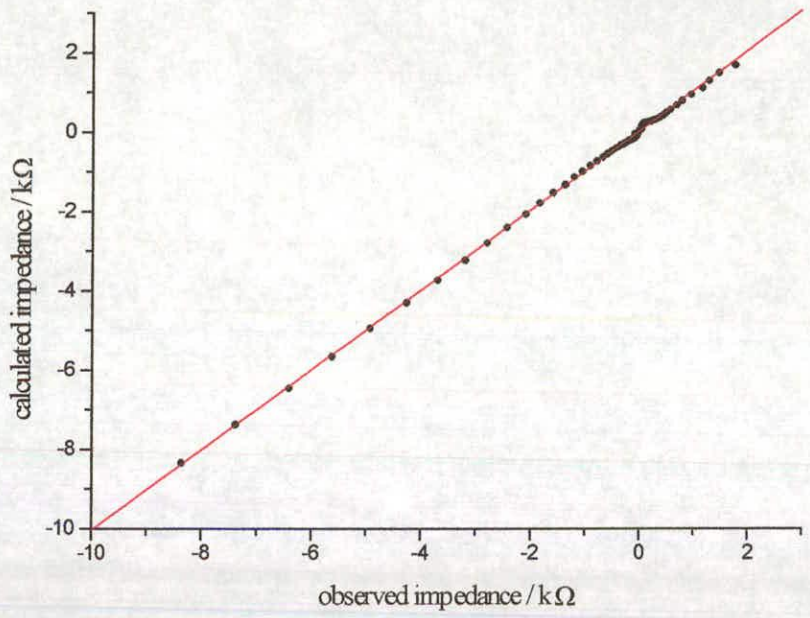

Figure B.22: Fit for cycled poly(5CI) layer at 500mV in 0.1M $TEAClO_4$
Gradient = 1.0068; Intercept = 0.0430; Correlation coefficient = 0.9994

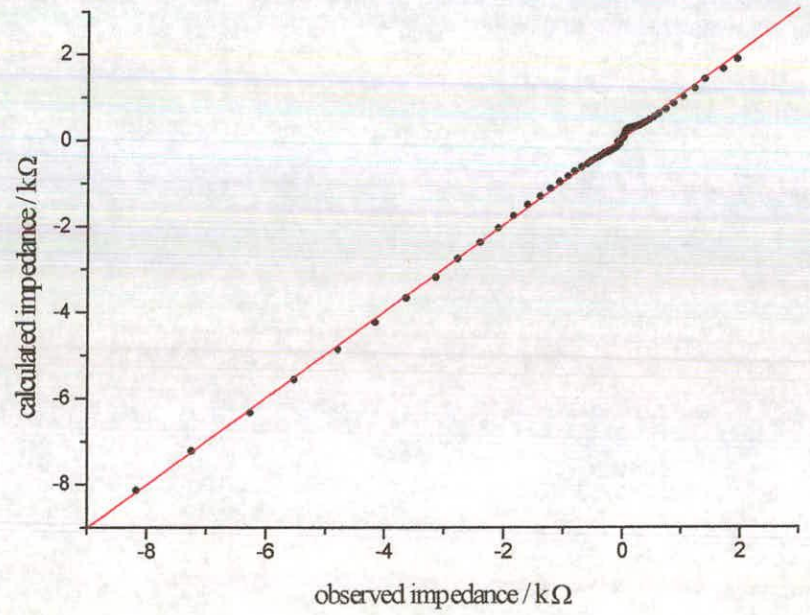

Figure B.23: Fit for cycled poly(5CI) layer at 600mV in 0.1M $TEAClO_4$
Gradient = 1.0073; Intercept = 0.0491; Correlation coefficient = 0.9991

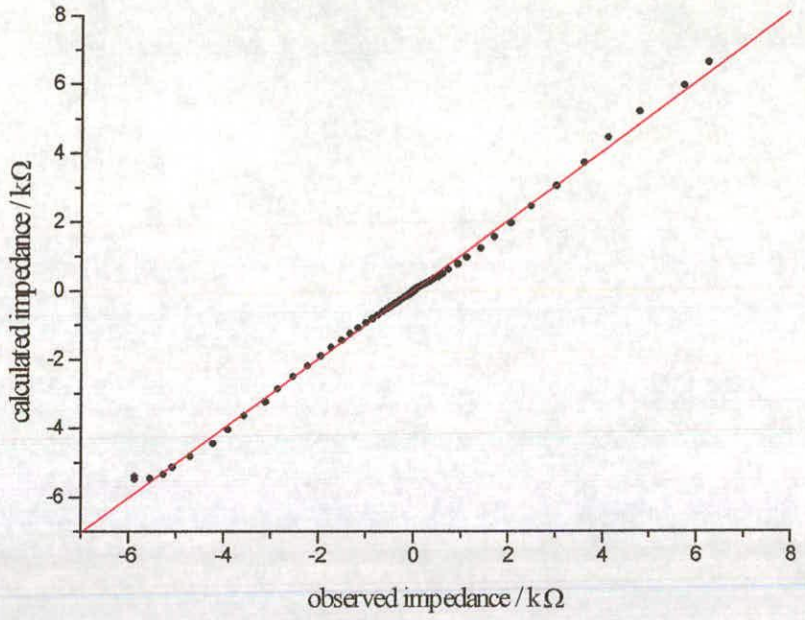

Figure B.24: Fit for cycled poly(5CI) layer at -100mV in 0.1M $TEAPF_6$

Gradient = 1.0083; Intercept = 0.0217; Correlation coefficient = 0.9986

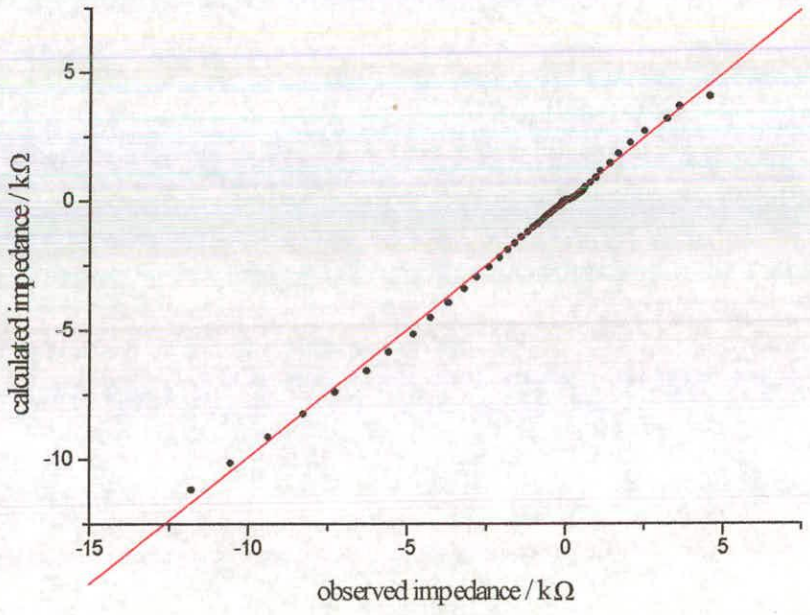

Figure B.25: Fit for cycled poly(5CI) layer at 0mV in 0.1M $TEAPF_6$

Gradient = 0.9881; Intercept = -0.0095; Correlation coefficient = 0.9988

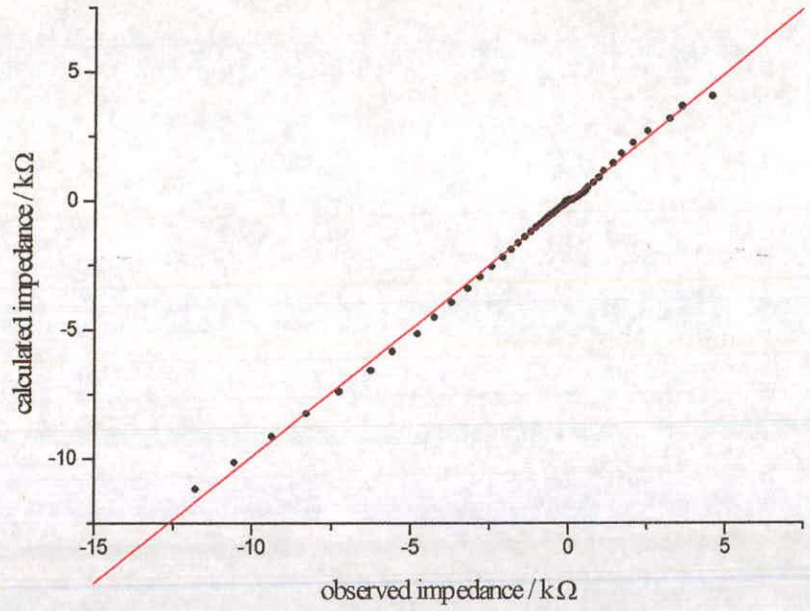

Figure B.26: Fit for cycled poly(5CI) layer at 100mV in 0.1M $TEAPF_6$
Gradient = 0.9934; Intercept = -0.0038; Correlation coefficient = 0.9993

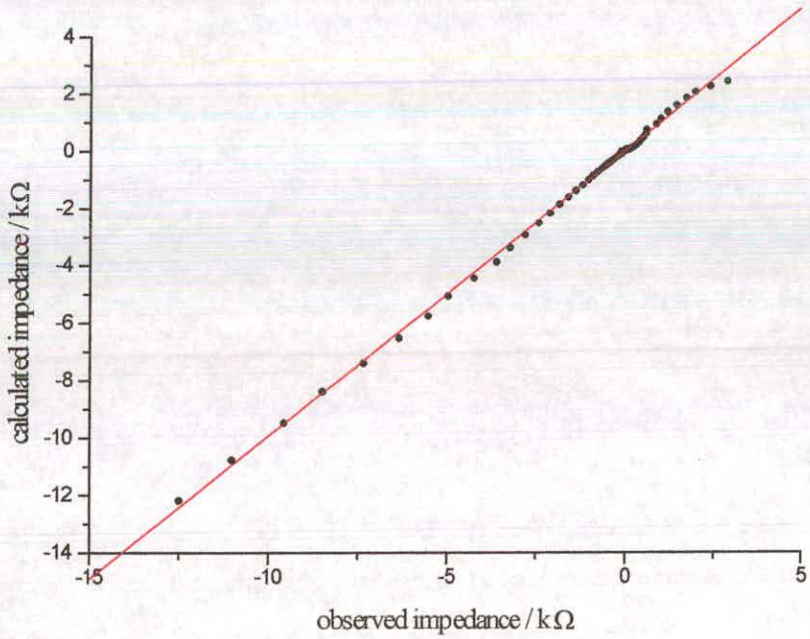

Figure B.27: Fit for cycled poly(5CI) layer at 200mV in 0.1M $TEAPF_6$
Gradient = 0.9932; Intercept = -0.0042; Correlation coefficient = 0.9993

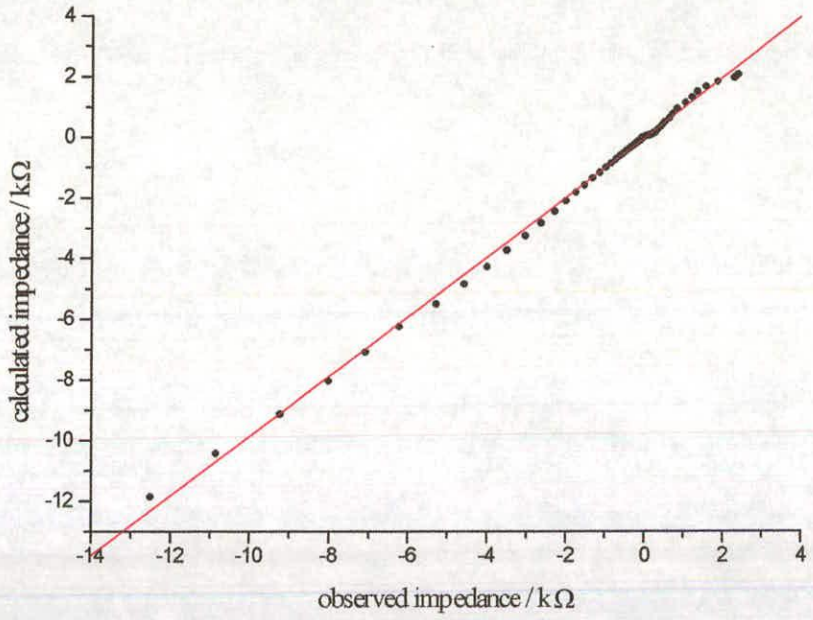

Figure B.28: Fit for cycled poly(5CI) layer at 300mV in 0.1M $TEAPF_6$
Gradient = 0.9843; Intercept = -0.0127; Correlation coefficient = 0.9990

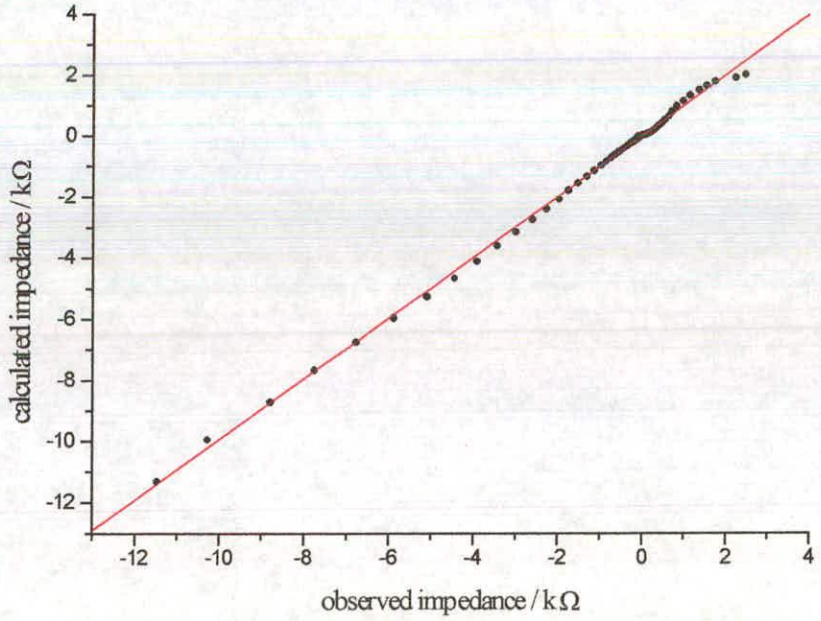

Figure B.29: Fit for cycled poly(5CI) layer at 400mV in 0.1M $TEAPF_6$
Gradient = 0.9920; Intercept = -0.0060; Correlation coefficient = 0.9992

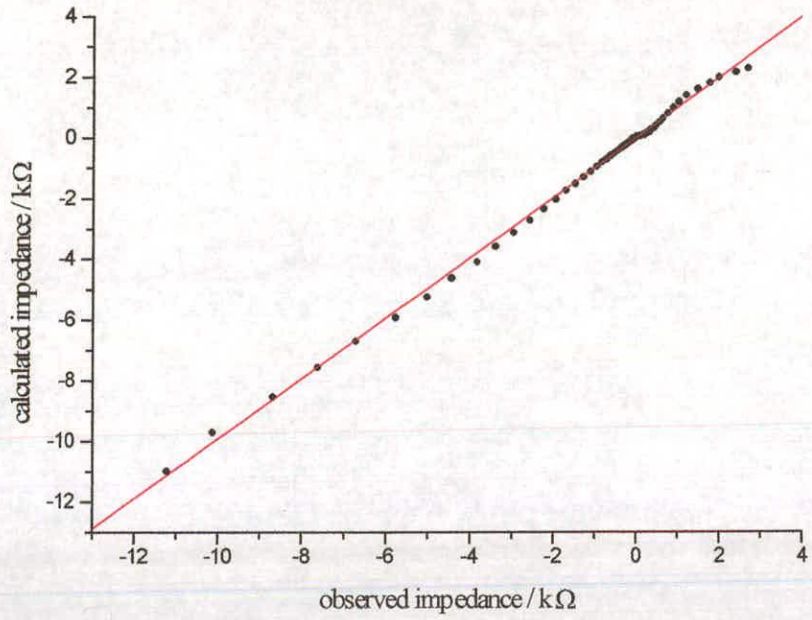

Figure B.30: Fit for cycled poly(5CI) layer at 500mV in 0.1M $TEAPF_6$
Gradient = 0.9899; Intercept = -0.0066; Correlation coefficient = 0.9991

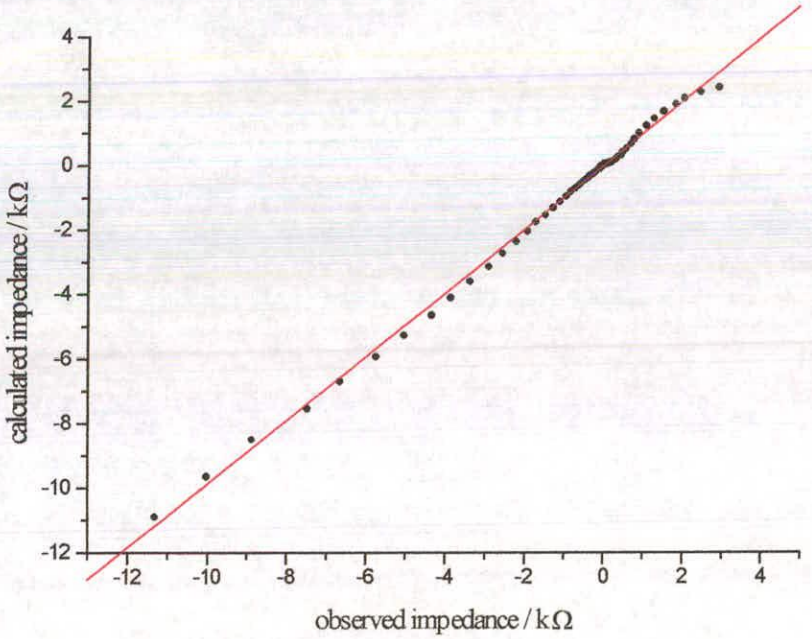

Figure B.31: Fit for cycled poly(5CI) layer at 600mV in 0.1M $TEAPF_6$
Gradient =0.9861; Intercept = -0.0109; Correlation coefficient = 0.9988

Appendix D –

Ac Impedance Fits For Chapter 6

The following graphs contained within this appendix show the results obtained when fitting the ac impedance spectra for a 50:50 I5CA:5CI copolymer to theory. Unless otherwise stated, the fitting program used is that detailed in appendix A.2.

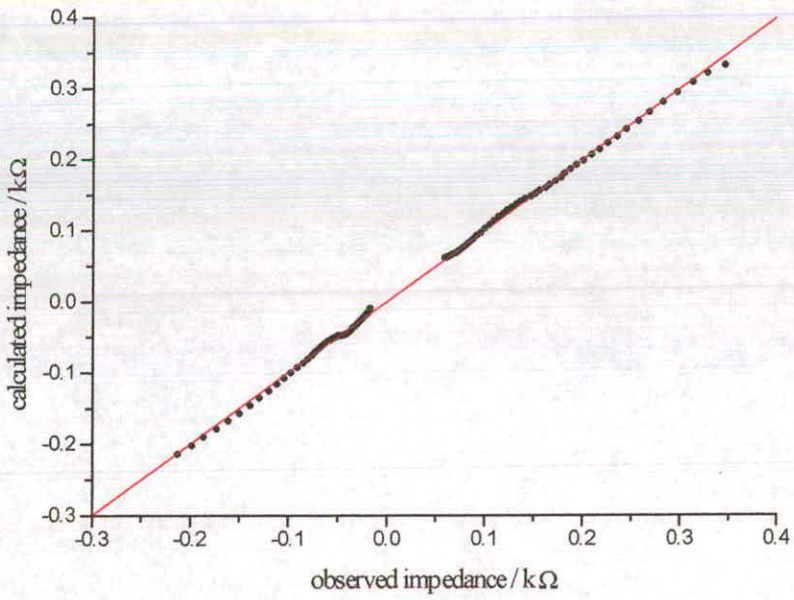

Figure B.1: Fit plot for cycled copolymer layer at 200mV in 0.1M $LiClO_4$
Gradient = 0.9980; Intercept = 0.0004; Correlation coefficient = 0.9996

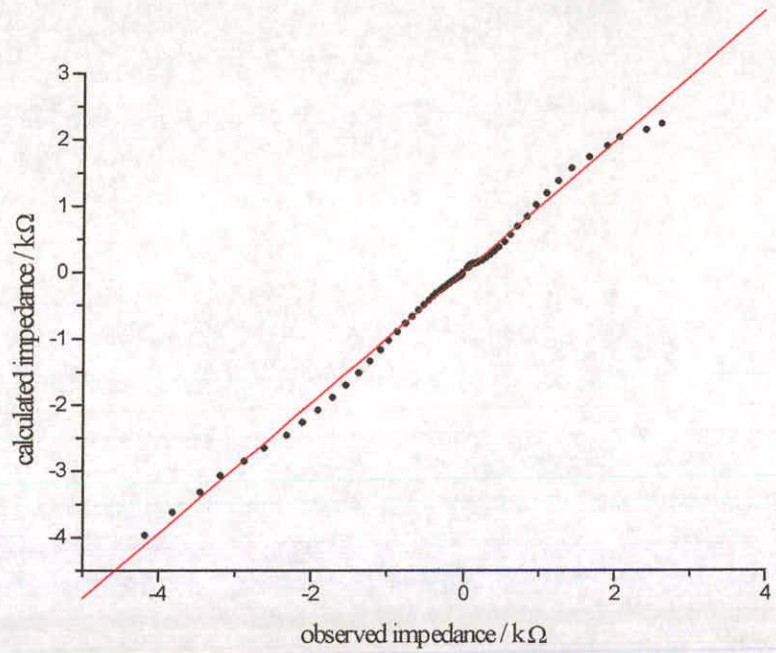

Figure B.2: Fit plot for cycled copolymer layer at 300mV in 0.1M $LiClO_4$

Gradient = 0.9842; Intercept = -0.0026; Correlation coefficient = 0.9976

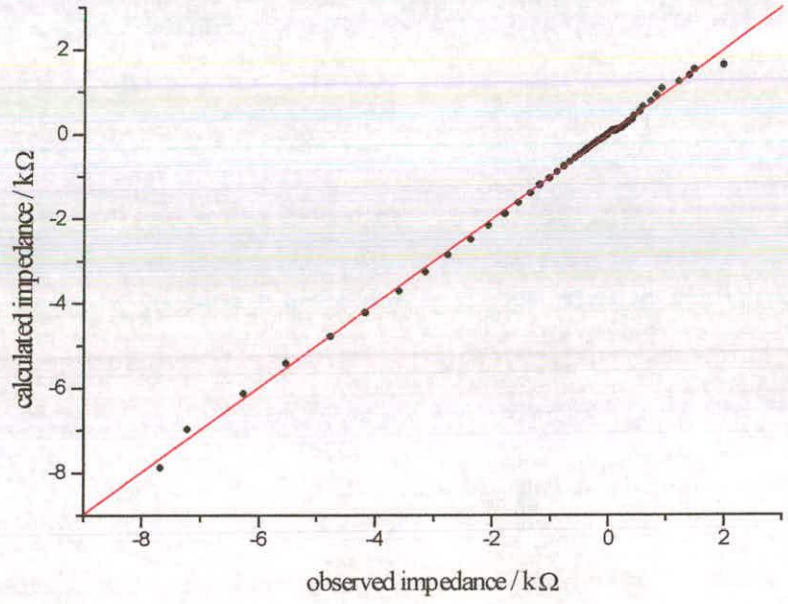

Figure B.3: Fit plot for cycled copolymer layer at 400mV in 0.1M $LiClO_4$

Gradient = 0.9975; Intercept = 0.0022; Correlation coefficient = 0.9992

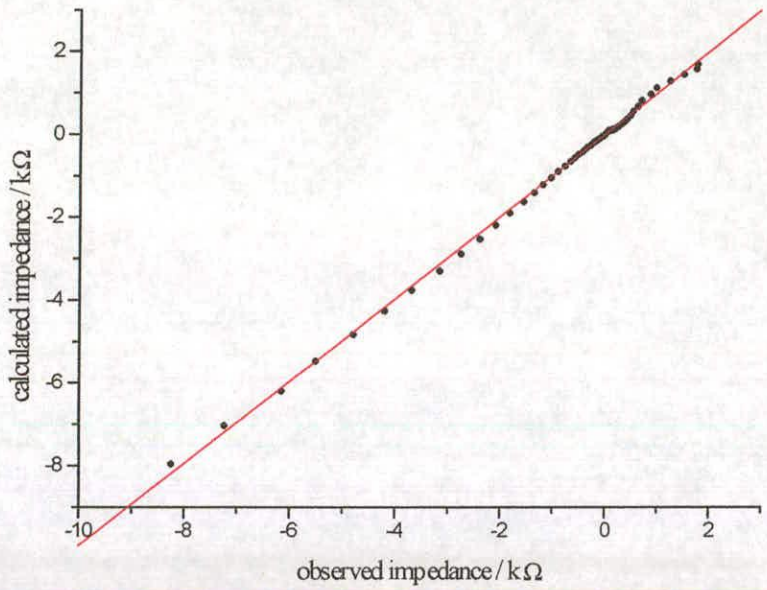

Figure B.4: Fit plot for cycled copolymer layer at 500mV in 0.1M $LiClO_4$

Gradient = 0.9927; Intercept = -0.0009; Correlation coefficient = 0.9994

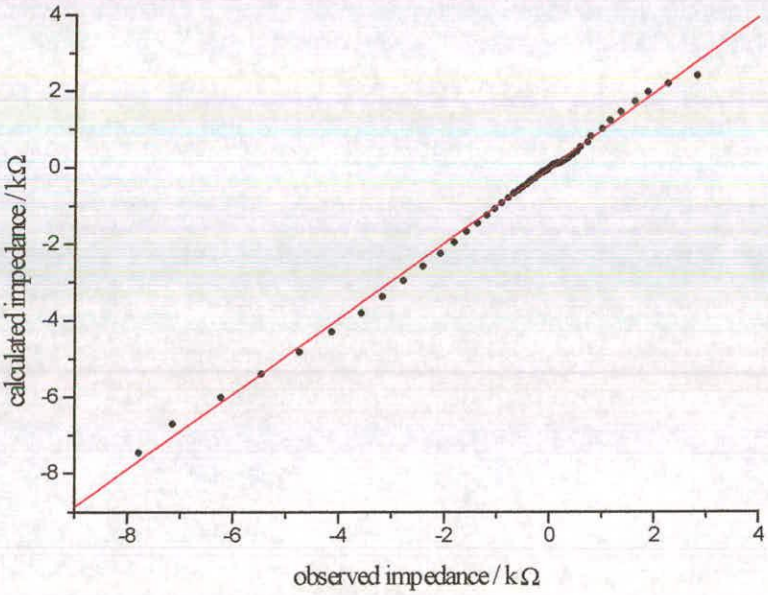

Figure B.5: Fit plot for cycled copolymer layer at 600mV in 0.1M $LiClO_4$

Gradient = 0.9850; Intercept = -0.0053; Correlation coefficient = 0.9986

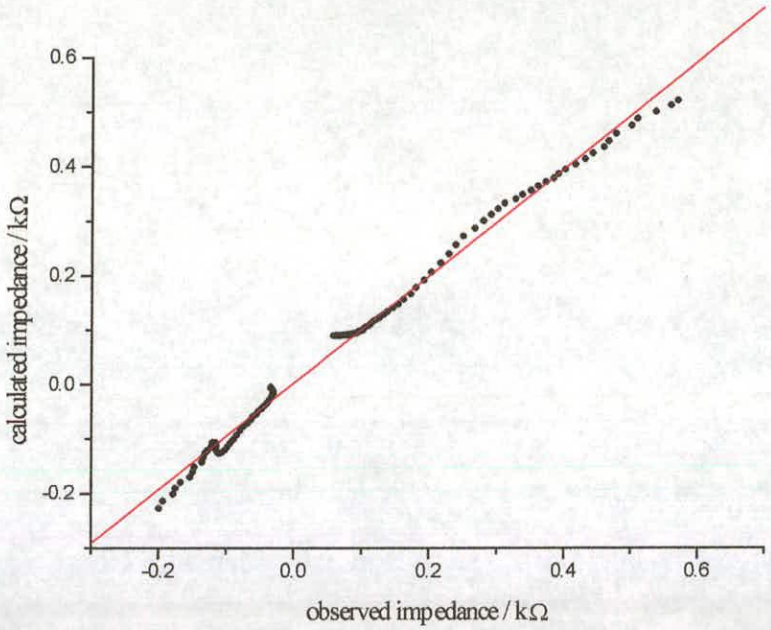

Figure B.6: Fit plot for cycled copolymer layer at 300mV in 0.1M $TEAClO_4$

Gradient = 0.9816; Intercept = 0.0036; Correlation coefficient = 0.9970

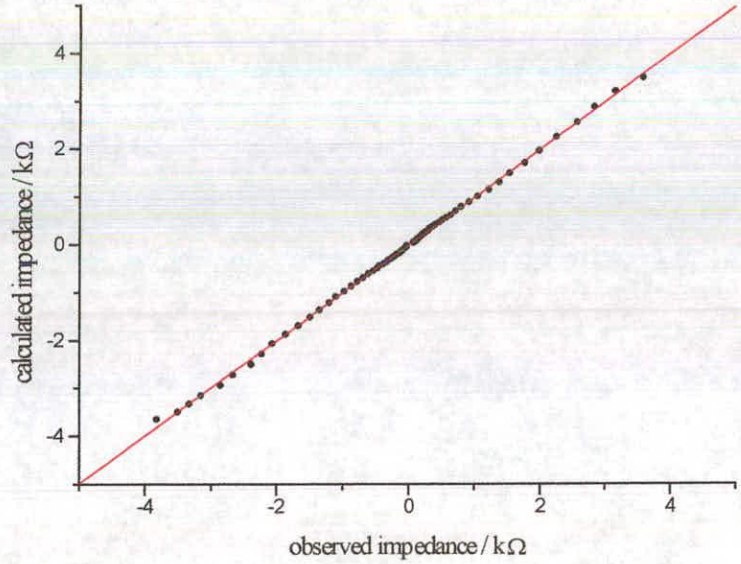

Figure B.7: Fit plot for cycled copolymer layer at 400mV in 0.1M $TEAClO_4$

Gradient = 0.9959; Intercept = -0.0066; Correlation coefficient = 0.9997

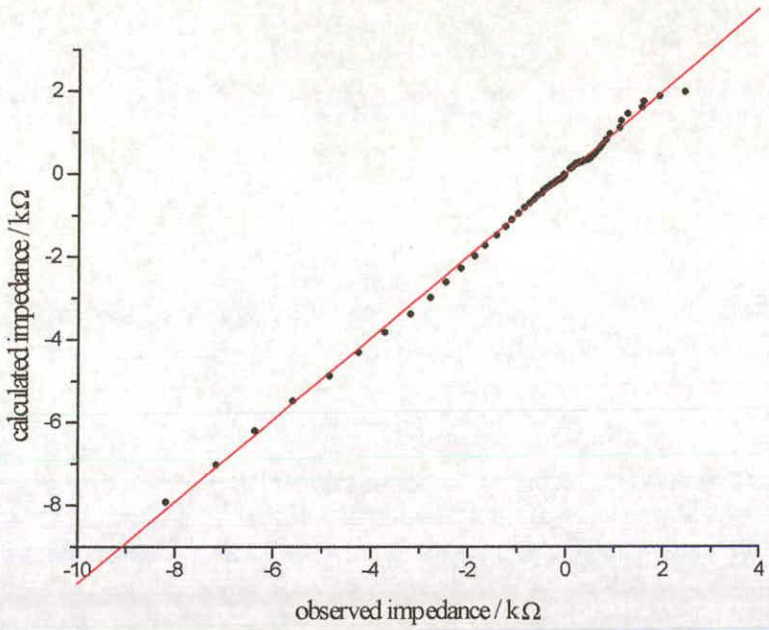

Figure B.8: Fit plot for cycled copolymer layer at 500mV in 0.1M $TEAClO_4$

Gradient = 0.9907; Intercept = 0.0099; Correlation coefficient = 0.9988

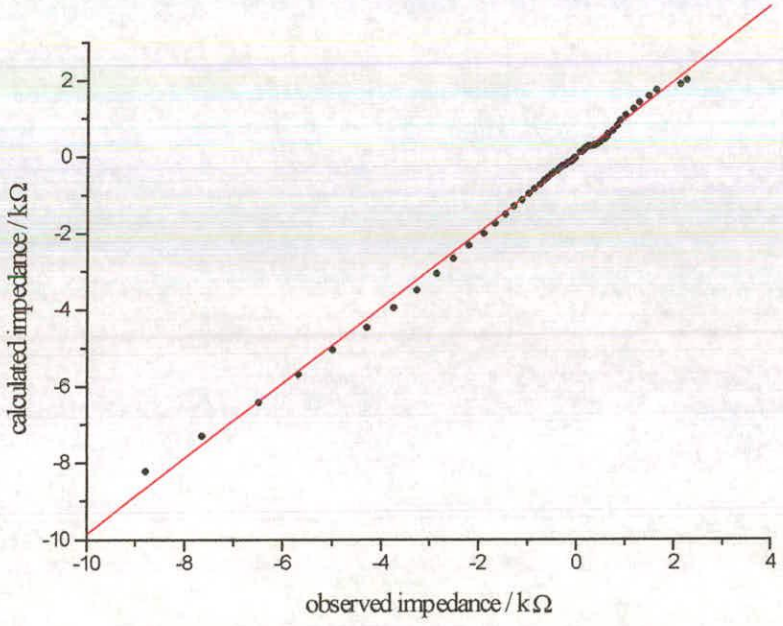

Figure B.9: Fit plot for cycled copolymer layer at 600mV in 0.1M $TEAClO_4$

Gradient = 0.9849; Intercept = 0.0068; Correlation coefficient = 0.9986

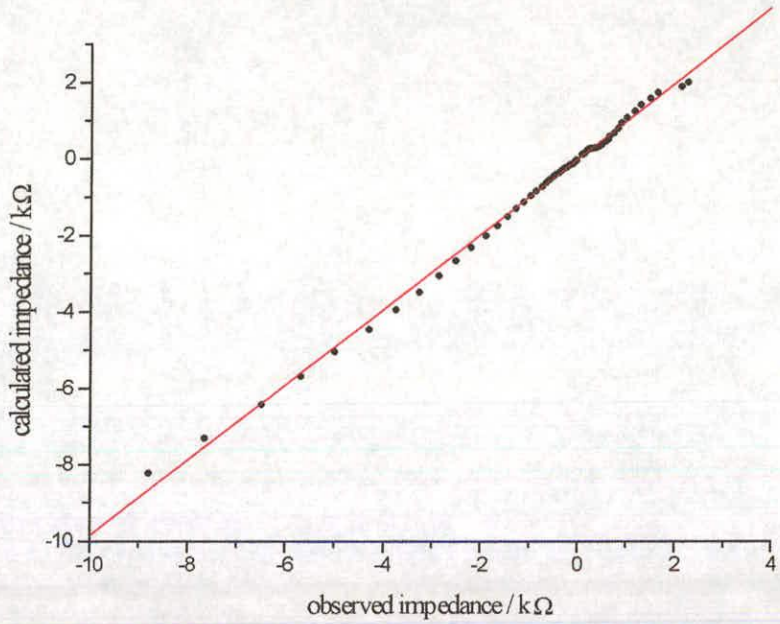

Figure B.10: Fit plot for cycled copolymer layer at 0mV in 0.1M $TEAPF_6$

Gradient = 1.0054; Intercept = 0.0009; Correlation coefficient = 0.9997

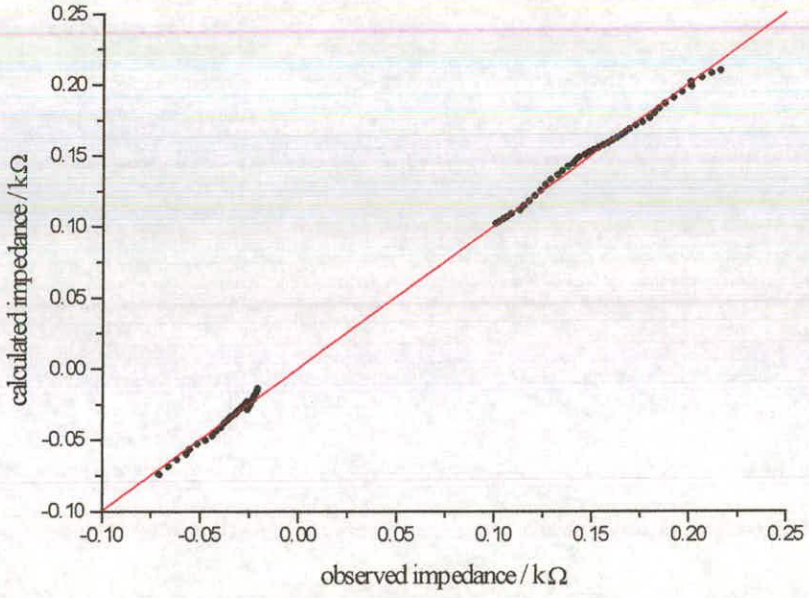

Figure B.11: Fit plot for cycled copolymer layer at 100mV in 0.1M $TEAPF_6$

Gradient = 1.0016; Intercept = 0.0007; Correlation coefficient = 0.9996

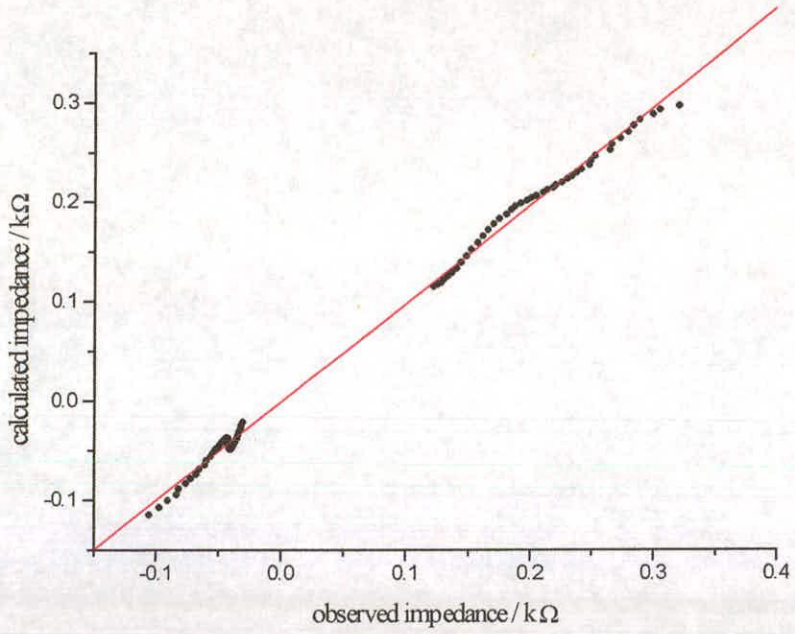

Figure B.12: Fit plot for cycled copolymer layer at 200mV in 0.1M $TEAPF_6$

Gradient = 0.9877; Intercept = -0.0012; Correlation coefficient = 0.9989

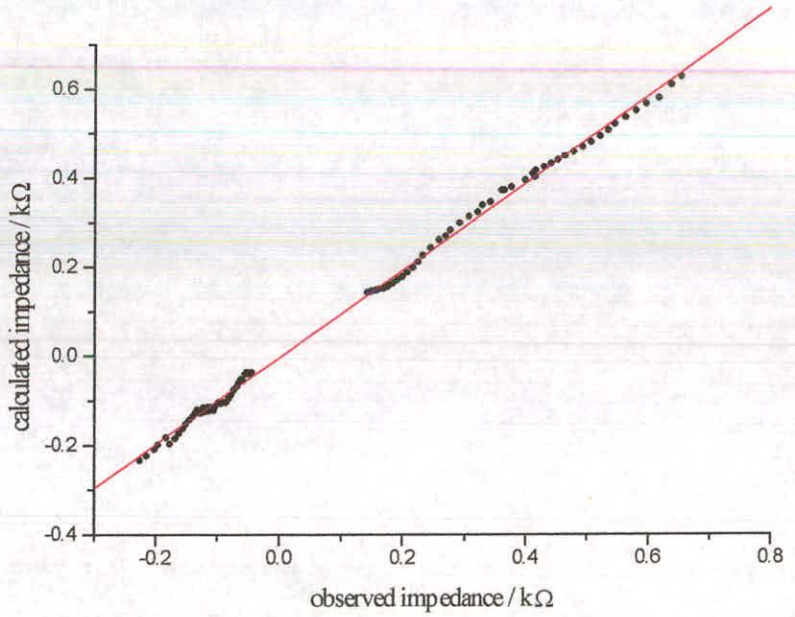

Figure B.13: Fit plot for cycled copolymer layer at 300mV in 0.1M $TEAPF_6$

Gradient = 0.9779; Intercept = -0.0029; Correlation coefficient = 0.9991

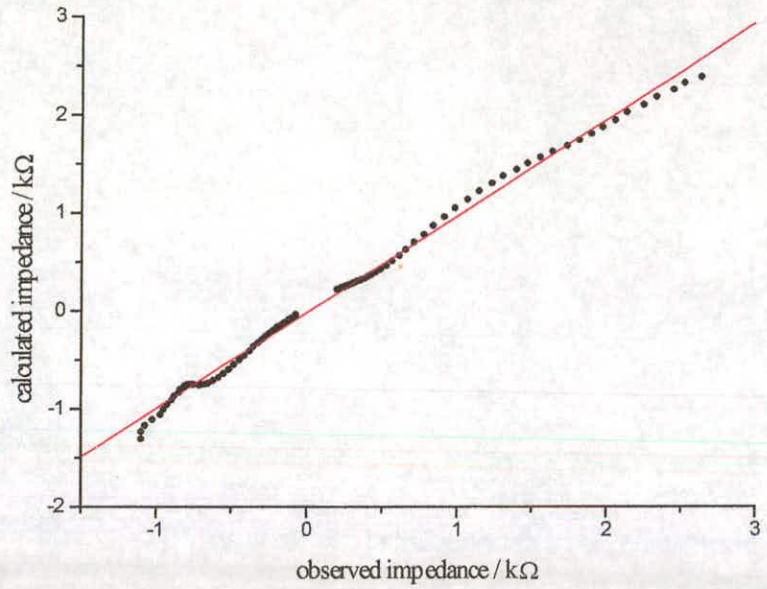

Figure B.14: Fit plot for cycled copolymer layer at 400mV in 0.1M $TEAPF_6$

Gradient = 0.9823; Intercept = -0.0160; Correlation coefficient = 0.9978

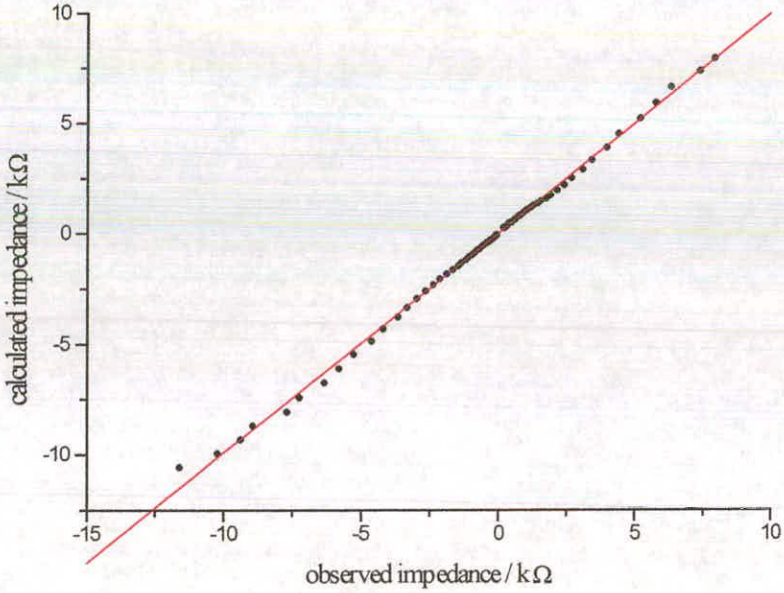

Figure B.15: Fit plot for cycled copolymer layer at 500mV in 0.1M $TEAPF_6$

Gradient = 0.9938; Intercept = 0.0327; Correlation coefficient = 0.9989